University of Reading
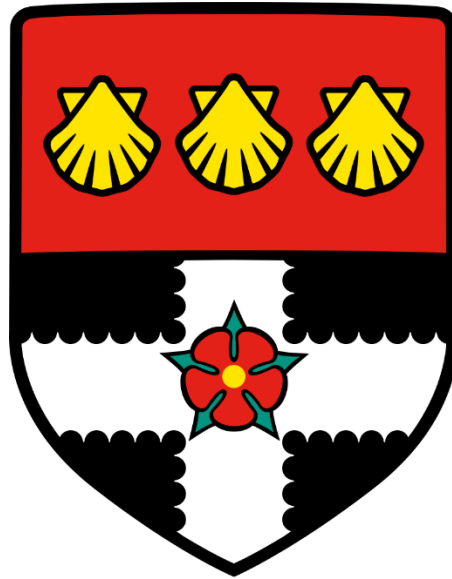
Department of Meteorology

Improving the Simulation of Carbonaceous Aerosol in HadGEM3-UKCA

James Mollard

A thesis submitted for the degree of Doctor of Philosophy

March 2017

Declaration: I confirm that this is my own work and the use of all material from other sources has been properly and fully acknowledged.

Signed _____

James Mollard

Abstract

The effects of aerosols on the climate system are a major source of uncertainty in past and future simulations of climate. The role played by carbonaceous aerosols is particularly uncertain. Black carbon, which absorbs shortwave radiation, exerts a positive radiative forcing of the climate system, warming the Earth. This warming is offset by co-emitted organic carbon, which scatters shortwave radiation back to space. However, a subset of organic carbon aerosols, called brown carbon, may be absorbing, further complicating the issue. Carbonaceous aerosols also influence cloud formation and properties, potentially contributing an additional cooling of Earth's surface temperatures.

This work aims at improving the simulation of carbonaceous aerosols in the UK Met Office's HadGEM3-UKCA model with the GLOMAP-mode aerosol scheme. That model does not always compare well with regional multi-variable observations, often underestimating surface concentrations and aerosol optical depth. Although single scattering albedo, a measure of aerosol absorption, is well replicated in biomass burning regions, it is overestimated in regions where fossil- and bio-fuel emissions are dominant. To improve the comparison, we propose a range of changes to modelled carbonaceous aerosol emissions, refractive index and density. An analysis of the sensitivity of the model to these changes shows that emissions alone cannot be responsible for the discrepancies between observations and models. The analysis also shows that while the black carbon mass absorption coefficient needs to be high in fossil fuel combustion regions, black carbon absorption must be reduced in biomass burning areas to leave room for brown carbon absorption.

A selected combination of changes leads to improvements in the simulation of carbonaceous aerosols in most regions compared with observations. Those improvements do not however lead to a significant change in the total aerosol effective radiative forcing, but reduces the contribution of aerosol-radiation interactions. Using an internally-mixed aerosol scheme means that changes in one aerosol species affects the simulation of other aerosol types. Therefore, aerosol model improvements require an integrated consideration of all aerosol species.

Acknowledgements

Firstly, I would like to thank my supervisors, Dr Nicolas Bellouin, Professor Ellie Highwood and Dr Ben Johnson, for what I'm sure to them has felt like a very long and trying three years! This project would not be half as good if it wasn't for your enthusiasm, commitment, and dedication to squeezing every ounce of potential out of me. I would also like to thank my monitoring committee, Dr Christine Chiu and Dr Joy Singarayer. You've helped ensure this project has stayed on track, and made sure my understanding was watertight with your probing questions in meetings. Many thanks to you all.

I'd also like to thank the staff in the department, particularly the admin staff, who have organised meetings, travel and bookings, and the post-docs of Lyle 3, especially Dr Laura Wilcox, for being both an official strategy guide on surviving a PhD, and a fountain of knowledge on climate and aerosol. A further special thanks to those who also continually bought in biscuits, prosecco and home-baked goods!

To my fellow ~~sufferers~~ PhD students in the Department, my many thanks for the much-needed Friday drinks, rugby trips, and support required to get this far. A PhD may seem like an eternity, but it is over much too soon. And for those of you in Lyle 3, my thanks for making the eternity feel like only 2 weeks. My eternal gratitude for putting up with me this long.

I'd also like to thank and acknowledge the funding support I have received throughout my PhD, specifically from the natural environment research council (award 1366124) and from my CASE industrial partnership with the UK Met Office.

A special thank you also must go to my many teachers throughout the years, through school, college and university, who have unknowingly given me the tools and pushed me along to make the choices that have led me to be here, writing this sentence. For all the knowledge you have given me, thank you.

My final thanks go to my family and friends. In particular, my parents, who can now stop nagging me to get a proper job; my sister, who makes me look like the better child; and my fiancée Lizzie, who has been by my side throughout, and ensured that my bad days still remain better than most.

Contents

Contents

x

1. Chapter 1: Introduction

1.1 Introduction

Climate change is considered by scientists to be one of the largest issues that humanity has faced in its history (Mann, 2009; McMichael et al., 2006). The average global surface temperature is rising at an unprecedented rate, and changes to weather patterns across the world are likely to affect millions of people (Trenberth, 2011; Stocker et al., 2013). The effects of climate change are also predicted to bring abrupt changes to almost all earth systems, including vegetation, sea ice and atmospheric dynamics (Walther et al., 2002; Willis & Bhagwat, 2009; Woollings & Blackburn, 2012). Economic modelling suggests that the global economy could suffer by as much as $24 trillion dollars (Dietz et al., 2016). Secondary effects of a changing climate include changes to disease distribution, changes or losses of sensitive ecosystems and effects on the ability of agriculture and farming to produce food (Hoegh-Guldberg & Bruno, 2010; Morton, 2007; Rohr et al., 2011). Studies focusing on both the detection of a shift in climate, and attributing a cause to the change shows that anthropogenic actions are the primary causes for our changing climate (Myhre et al., 2013), regardless of any misgivings from public or political figures.

The understanding of our current climate is based on a mixture of real world observations, scientific theory, and simulations of previous events run through mathematical weather and climate models. These computational representations of the climate attempt to replicate the physics, dynamics and chemistry of the atmospheric system as closely as possible, and can be used as an experimental sandbox for scientists to examine and analyse. Climate models can be altered in any way the user chooses, allowing theories to be tested, which cannot be done in the real world. This includes experiments looking at the effect and sensitivity of individual components of the Earth system to changes in the emission of gases and particles from both human and natural sources (Hansen et al., 1981). Climate models have also been used to provide backing to theories that greenhouse gas increases must be responsible for rising temperatures (Myhre et al., 2013), as previously suggested by Hansen et al. (1981), and to

evaluate the effectiveness of international policies relating to anthropogenic emissions (Morgenstern et al., 2008).

Climate models are continuously compared to observations to determine whether they can accurately represent the real world (Collins et al., 2008; O'Connor et al., 2014). These can be used to highlight both errors in the climate model from missing effects, such as missing aerosols to explain mid-20th century cooling (Thompson et al., 2008, Lee et al., 2011), and errors in how currently modelled processes are represented (Kipling et al., 2013). Climate models have evolved significantly since the first mathematical models were made over 100 years ago (Arrhenius, 1896), as a result of continued comparisons with observations, resulting in refined processes and parameters. Further increases in complexity can also be modelled today due to the increase in modern computing power. It should however be noted that climate model uncertainties are not the only uncertainties affecting projections of future climate. Uncertainties also occur from internal variability and scenario uncertainties (Hawkins & Sutton, 2009).

1.2 Aerosols

One of the largest modelling uncertainties are those related to aerosols (Boucher et al., 2013). This uncertainty can be reduced through improving both scientific understanding and continued comparisons with new observations. Aerosols are small particles of matter, which are suspended in the atmosphere. The majority of aerosols are too small to be seen by the human eye, unless they are present in large concentrations, resulting in haze. Primary aerosols are emitted directly in the aerosol phase and have diameters in the range of a few micrometres. Secondary aerosols condense and nucleate from precursor gases in the atmosphere, and typically have diameters of a few nanometres. Both types of aerosol grow as they age through further condensation of gases and coagulation with other aerosols (Bond et al., 2013a). Aerosols typically have a lifetime of a few days in the troposphere, with larger and more soluble aerosols having shorter lifetimes due to the combined effect of gravitational settling and removal via cloud growth and precipitation. However, aerosols which are injected into the stratosphere can remain in the atmosphere for much longer, as the removal processes are significantly lower (Deshler, 2008).

Chapter 1: Introduction

Atmospheric aerosols have several effects on the climate system and the environment. All aerosols interact with radiation, either scattering or absorbing the shortwave radiation from the sun (Boucher et al., 2013).This alters the reflectivity of the Earth, termed the planetary albedo. Changes to the albedo lead to changes in the radiation balance at the top of the atmosphere. These can not only affect climate, but also have short term affects which affect weather, requiring aerosols to be included in numerical weather prediction models (Mulcahy et al., 2014). Figure 1-1 shows different aerosol-radiation interactions and their effects. Scattering aerosols increase the planetary albedo, which reduces the amount of radiation reaching the surface of the Earth (a). Decreasing the energy at the surface reduces surface and atmospheric temperatures, which cool the planet (b). On the other hand, absorbing aerosols reduce the amount of shortwave radiation both reaching the surface and the amount reflected into space (c). These aerosols then re-radiate the energy at a longer wavelength, which warms the atmosphere and contributes to global warming (d).

Aerosol-radiation interactions
Scattering aerosols
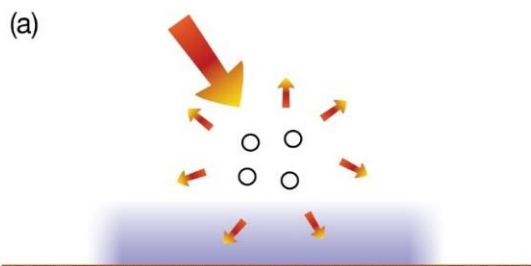
(a) Aerosols scatter solar radiation. Less solar radiation reaches the surface, which leads to a localised cooling.
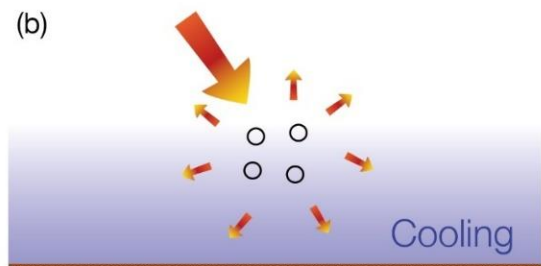
(b) Cooling. The atmospheric circulation and mixing processes spread the cooling regionally and in the vertical.

Absorbing aerosols
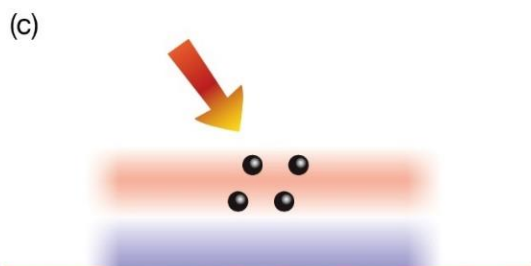
(c) Aerosols absorb solar radiation. This heats the aerosol layer but the surface, which receives less solar radiation, can cool locally.
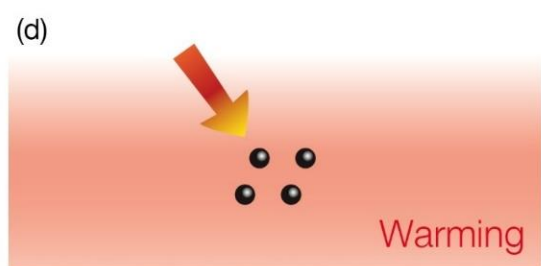
(d) Warming. At the larger scale there is a net warming of the surface and atmosphere because the atmospheric circulation and mixing processes redistribute the thermal energy.

Figure 1-1 - The difference in direct radiative effects, or aerosol-radiation interactions (RFari) from scattering and absorbing aerosols in the atmosphere. Figure taken from Boucher et al., 2013*, Figure 7.23*

Aerosols also have strong interactions with clouds, or Aerosol-Cloud Interactions. These processes are shown in Figure 1-2. Under the small super-saturations encountered in the atmosphere, cloud droplets only form when they have a nucleus for water vapour to condense on. The nuclei are termed Cloud Condensation Nuclei (CCN). Soluble aerosols, such as sulphates, salts and nitrates, make excellent CCN. The initial effect of an increase in soluble aerosols in clouds is an increase in the number of CCN in a cloud-developing region. By increasing the number of CCN available, greater numbers of droplets can form, assuming that the liquid water content remains constant (Twomey, 1977). An increase in the number of drops means that there is less water in each droplet, giving the droplets a smaller size than had they developed without aerosol. Clouds with more droplets are brighter, and so they reflect more shortwave radiation back to space, exerting a negative radiative forcing. This is now called the radiative forcing of aerosol-cloud interactions (RFaci), but has also been termed the first-indirect effect, or cloud albedo effect in previous IPCC reports.
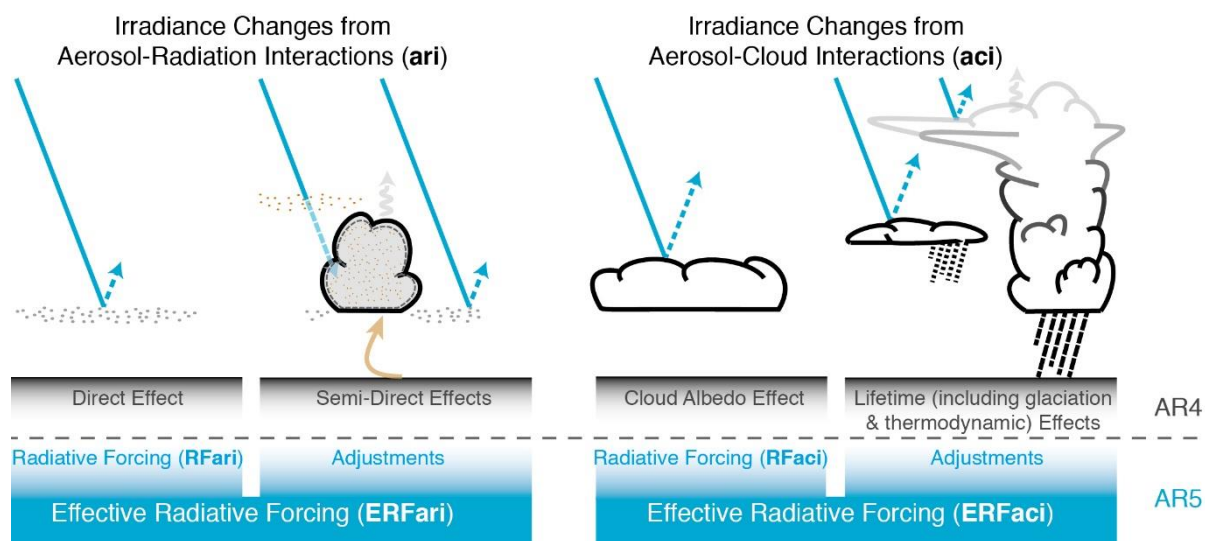
Figure 1-2 - Schematic showing the effect on irradiance from aerosol-radiation interactions and aerosol-cloud interactions, with new and old terminology for comparison. The blue arrows depict solar radiation, the grey arrows terrestrial radiation and the brown arrow symbolizes the importance of couplings between the surface and the cloud layer for rapid adjustments. Taken from Boucher et al., 2013, Figure 7.3.

Aerosols also exert further effects on clouds, most resulting from the smaller droplets produced. These can lead to both a positive and negative radiative forcing, depending upon the conditions of the atmosphere. Whilst literature released prior to the last IPCC assessment

report characterised a range of different changes called second indirect effects, the most recent report states that these effects are either unproven, or are impossible to disentangle. Therefore, in the most recent IPCC report, these adjustments are added to the radiative forcing to define the effective radiative forcing (ERF) (Myhre et al., 2013).

Issues relating to aerosols are not limited to radiative effects and clouds changes. Aerosols also effect air quality, and have considerable implications for air quality policy. In particular, aerosols of just below 2.5 micrometres in diameter (termed Particulate Matter, or PM2.5), have been shown to have significant impacts on human health when inhaled (Brunekreef & Forsberg, 2005). Figure 1-3 shows the increase in mortality compared with the level of PM2.5 seen the day before from an epidemiology study in New England, USA. Increases in these particles are also shown to be detrimental not just to the respiratory systems, but are also linked to increases in heart disease and cancer. Globally, PM2.5 is thought to cause nearly 3.4 million premature deaths a year (Lelieveld et al., 2015; Zhang et al., 2017). In many countries, legislation has been introduced to reduce the amount of PM2.5, particularly in urban areas where there are significant numbers of people. This has been achieved through making transport more efficient, the banning of burning in certain areas, and applying particle filters on both vehicles and industries (Wolff & Perry, 2010).
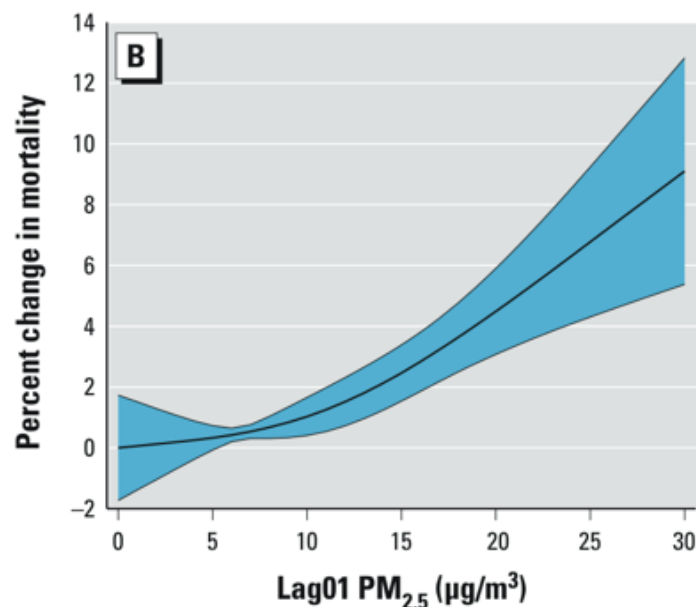
Figure 1-3 - Change in mortality as a function of Particulate Matter (PM2.5) concentrations from the previous day in New England, USA. Shaded areas indicate a 95% confidence interval. Taken from Shi et al., 2016

1.3 Carbonaceous Aerosols

Definitions

Carbonaceous Aerosols (CA) are aerosols whose composition is mostly carbon, mixed with varying amounts of other organic matter (Bond et al., 2013). A large, but uncertain fraction of these aerosols come from primary and secondary formation following the incomplete combustion of carbon-based fuels, such as fossil fuels, biofuels or biomass burning (Lamarque et al., 2010). Further sources of CA come from biogenic sources, such as aerosols emitted from plants, fungi and oceans, and from precursor-gases that condense into aerosols. Sources such as pollen are omitted from most definitions of CA, including for the most recent IPCC report (Boucher et al., 2013). Similarly, dust which contains carbon is also excluded from the definition of CA.

Even with those exclusions, the term carbonaceous aerosol encompasses aerosols which have a large range of characteristics so CA can be further characterised by either the level of carbon contained, or their thermal and optical properties (Bond et al., 2013). Figure 1-4 summarises the different definitions used to define subsets of carbonaceous aerosols, with comparisons between definitions. The two most common definitions which are used to split carbonaceous aerosols are Black Carbon (BC) and Organic Carbon (OC). However, several alternative definitions exist, many based on the methods of measurements or properties when emitted. BC defines carbonaceous aerosols that are entirely composed of carbon, and are black in colour. This definition of BC is also sometimes called Elemental Carbon (EC). However, there are several deviations on the definition of BC used in literature. Refractory Black Carbon (rBC) is defined as carbon-based aerosols that reach incandescence at a given temperature. This means that some BC is not contained within measurements of rBC (Lack et al., 2014).

OC refers to carbonaceous aerosols that contain both carbon and other organic molecules, such as oxygen and hydrogen. Often masses of OC are given as mass of carbon within the aerosols (Bond et al., 2013), and the term organic aerosols (OA) or organic matter (OM) is used to define the full mass of the particles. OC can also be further split into primary organic aerosol (POA) and secondary organic aerosol (SOA). OC can also be split into two further categories, absorbing OC, commonly called Brown Carbon (BrC), and non-absorbing OC. BrC

is also sometimes referred to as partially absorbing carbonaceous aerosol, as it only absorbs radiation strongly at wavelengths lower than 800 nm (Andreae & Gelencsér, 2006; Lack et al., 2012; Saleh et al., 2013; Saleh et al., 2014). BrC can be emitted from various sources, and can vary in the percentage of carbon composition. Light Absorbing Carbon (LAC) is another definition which is commonly used, and is the carbonaceous aerosol that absorbs radiation and so can be defined as BC + BrC (Bond & Bergstrom, 2006).

Definitions	Organic Carbon	Elemental Carbon	Light Absorbing Carbon	Refractory Black Carbon	Primary Organic Aerosol
Black Carbon		✓	✓	Greater than 80% of mass	
Brown Carbon	✓		✓		✓
Non-Absorbing Organic Carbon	✓				✓

Decreasing Carbon Content ↓

Figure 1-4 - Summary of differing carbonaceous aerosol terminology used in literature, adapted from Bond & Bergstrom (2006) and using values from Schwarz et al., (2010)

BC aerosols are absorbing, reducing the planetary albedo, warming the atmosphere. Figure 1-5 shows the radiative forcing of individual gas and aerosols species, as calculated for the IPCC 5th Assessment Report. BC alone is considered to have the 3rd largest positive radiative forcing after CO_2 and Methane (Myhre et al., 2013). The models on which the IPCC report relies upon consider OC to be a purely scattering aerosol, and so has a negative radiative forcing slightly lower in magnitude than sulphate. The effect of biomass burning emissions of both BC and OC are of similar magnitudes but opposite sign, so effectively cancel the radiative forcing of each other out on a global basis. However, the positive forcing of BC from fossil fuel is much stronger than the negative radiative forcing of OC from fossil fuels, implying a global positive forcing for all CA.

Sources

BC emissions total approximately 8 Tg yr^{-1} in the present day, although this value fluctuates on a yearly basis (Lamarque et al., 2010). **Error! Reference source not found.** shows the contribution of different

Components of Radiative Forcing
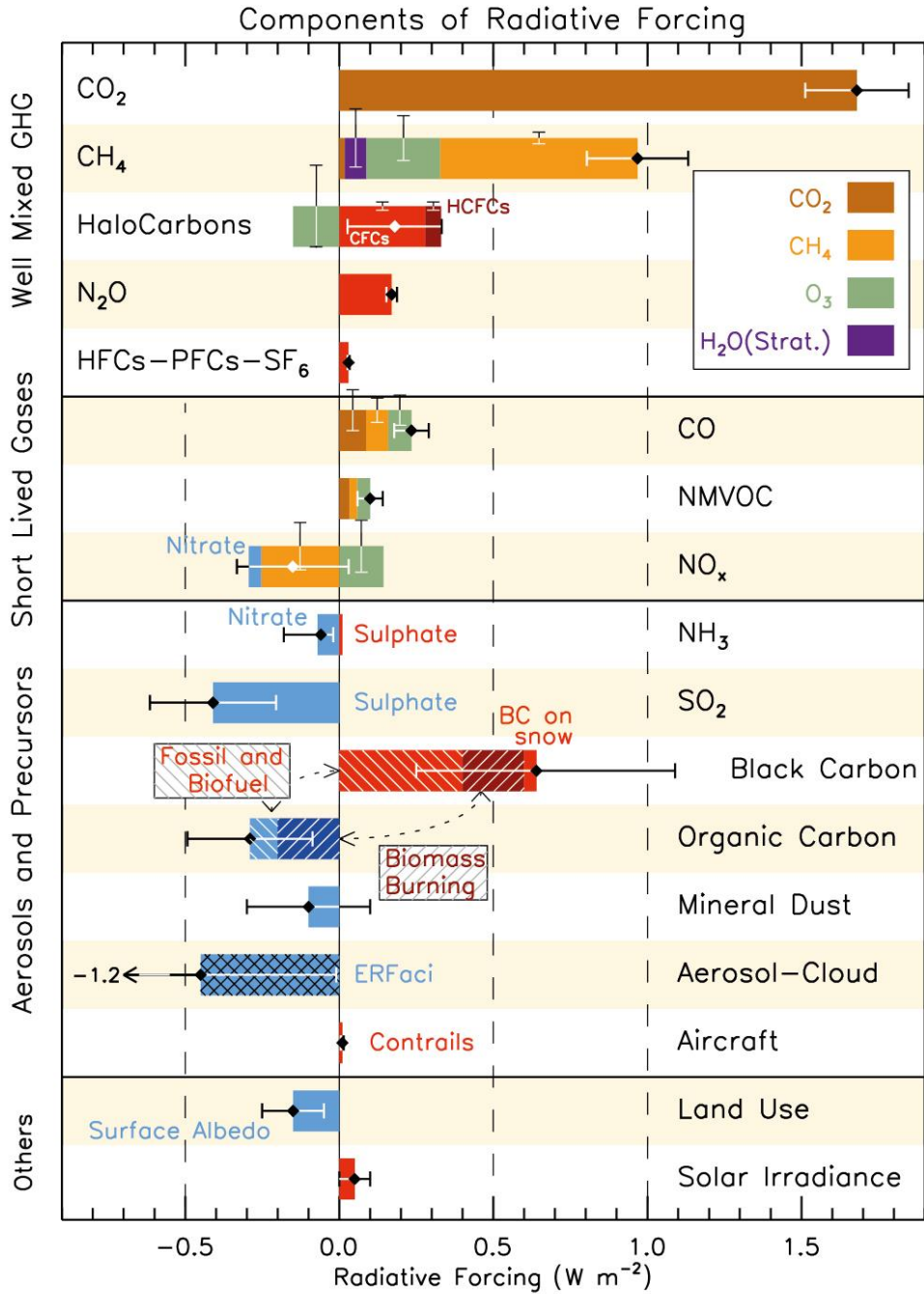
Figure 1-5 - Radiative forcing due to changes in various atmospheric components since pre-industrial age (1850), including aerosols. According to the assessment, BC is the third highest radiative forcing after methane and CO2. Organic carbon exerts a negative radiative forcing. Figure taken from Myhre et al., 2013 *Figure 8.17*

sectors to BC and primary OC emissions. Most BC emissions are from anthropogenic fossil fuel burning in various sectors, with about 35% coming from open biomass burning. Primary OC emissions total somewhere between 20 – 70 Tg[C] yr^{-1} , depending on which literature is

believed (Bond et al., 2013a). OC also varies depending on the year. Nearly 75% of primary OC aerosol comes from open biomass burning (Bond et al., 2004; Streets et al., 2004; Lamarque et al., 2010). This means that in biomass burning regions such as South America, Central Africa and South East Asia, the level of CA is largely dependent on the time of year. Biogenic emissions can contribute to OC as particles are condensed from isoprene and monoterpene emissions. Isoprene and monoterpene have emissions of up to 700 Tg[C] yr^{-1}, which can result in between 50 – 380 Tg[C] yr^{-1} of secondary organic aerosol through the nucleation of particles or condensation of gases onto pre-existing aerosol (Spracklen et al., 2011; Boucher et al., 2013) . The distribution of emissions of CA are also highly regionally dependent. Figure 1-6 shows the spatial distribution of total BC emissions for 2006, based upon ECLIPSE (Evaluating the Climate and Air Quality Impacts of Short-lived Pollutants) and GFED (Global Fire Emissions Database) version 3.1 emission datasets (Randerson et al., 2013; Stohl et al., 2013). Large urban settlements and areas of large annual biomass burning activity have the largest emissions over the year. It should be noted that emission estimates have large uncertainties, which can be of a similar magnitude to the emissions (Chow et al., 2010).
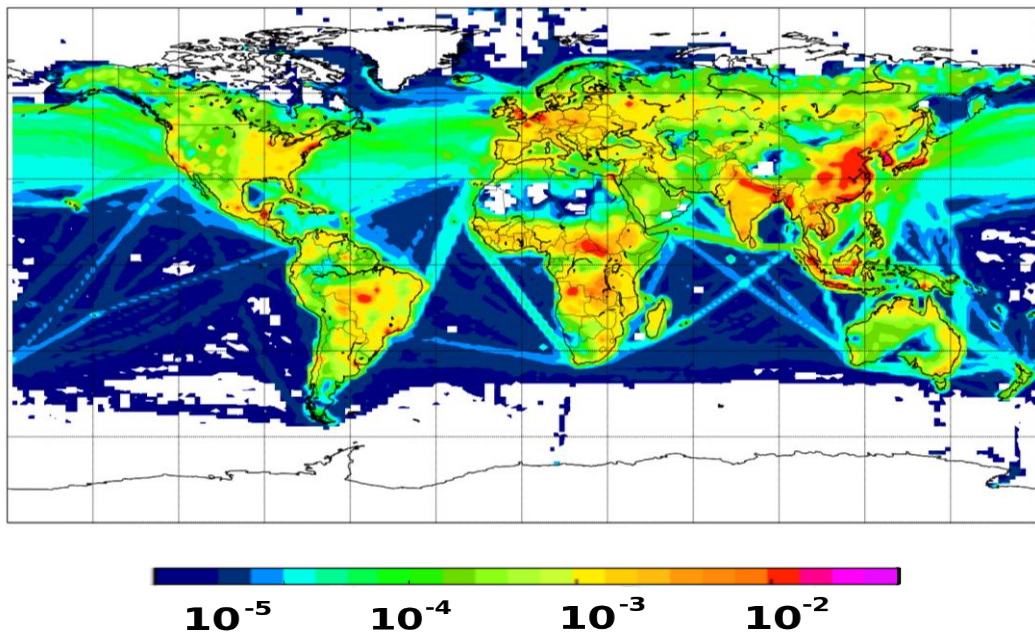
Figure 1-6 -Total combined annual emissions of black carbon for 2006 in Tg/gridbox/year, taken from the ECLIPSE fossil fuel and biofuel and GFED3.1 biomass burning (Randerson et al. 2013) *datasets*

Physical Properties

The properties of CA emissions are very dependent on the source. Freshly emitted BC consist of small spherical particles around 0.001 – 0.01 μm in diameter, that coagulate together to form irregularly shaped chains of aerosol, and are made entirely of carbon particles (Pósfai et al., 1999). Figure 1-7 shows the chain-like structure of BC, and how it compares with sulphate particles. The long chain-like particles of BC which form initially are gradually compressed by coagulation with other species. The compression of these chains also leads to an increase in the density of the particle, with the density of BC chains being dependent on the structural arrangement of the individual particles (Bond & Bergstrom, 2006). Kondo et al. (2011) and Schkolnik et al. (2007) quote that pure BC graphite has a density of between 1.9 and 2.1 g cm^{-3}, however, as combined BC aerosols have small air pockets due to the chained structure, the density is considered to be less than pure graphite.

 OC is emitted at a similar size, but also contains organic materials, in varying percentages. The aging processes of CA are complex and currently only partially understood through the use of sparse observations in differently-aged plumes (Schwarz et al., 2008). Both BC and OC are insoluble when emitted, but are quickly mixed with other co-emitted species such as sulphate (Lee, 2002), which collapses the chain structure into more densely packed clusters (Ramachandran & Reist, 1995). This process occurs over a few hours (Moffet & Prather, 2009), although some observational campaigns have shown it to occur much quicker (Cappa et al., 2012; Jacobson et al., 2013; Peng et al., 2016). The ratio of CA to other species, the ratio of BC to OC, and the optical properties of the CA are dependent upon the source and the type of burning (Saleh et al., 2014). Open air biomass burning produces CA in turbulent plumes due to the heat involved, which have the ability to reach a few km in height (Liousse et al., 1996). The mixing of CA with other species to form internally mixed aerosols is found at all altitudes (Aquila et al., 2011).
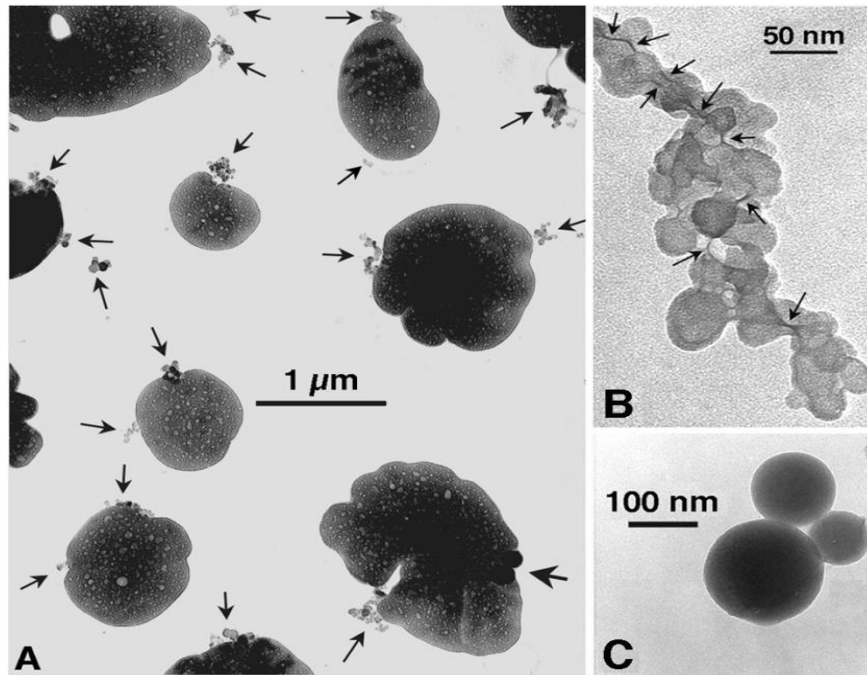
Figure 1-7 – Electron Microscope images of A) Ammonium Sulphate particles with small chains of black carbon (arrows) attached, B) A closer view of a chain-like black carbon structure with carbon filament which connects individual spheroids (arrows) and C) particles of ash from burning – Taken from Pósfai et al. (1999)

The total lifetime of BC and OC is impossible to measure, and can only be inferred through models based upon observations of aerosol characteristics in aerosol plumes, which change throughout the aerosols lifetime (Capes et al., 2008), or from the use of chemistry transport models (Riemer et al., 2010). The lifetime differs depending upon a variety of factors, including meteorology, initial plume buoyancy, availability of co-emitted species and the physical properties of the aerosol, but current understanding suggests that the global average lifetime is a few days (Kristiansen et al., 2016). A seasonal difference in aerosol lifetime has also been found in specific regions, but only when precipitation varied greatly on a yearly basis (Cape et al., 2012; Verma et al., 2011)

Optical Properties

BC and OC have different optical properties. The different types of burning and different sources of carbonaceous aerosol lead to different optical properties within BC and OC (Saleh et al., 2014, Chen & Bond, 2009). Other aerosol species also influence BC interaction with radiation. For example, when other species coagulate with BC, the mass-absorption coefficient (MAC), which is a measure of how effective the particle is at absorbing radiation,

is increased, enhancing the absorption and scattering, which leads to differences between the optical properties of fresh and aged BC (Scarnato & Kirchstetter, 2013; Zhang et al., 2008). In Cui et al. (2016), a coating of organic and inorganic matter was found to increase the MAC from 4.4 m^2 g^{-1} to 9.6 m^2 g^{-1}.

Refractive indices (RI) are mathematical descriptions of the scattering and absorption of an electromagnetic wave through a medium. They are made up of a real part, which characterises refraction, and an imaginary part, which characterises attenuation. Carbonaceous aerosols have a wide range of RI, which are dependent on several factors, such as the fuel type, temperature of burning and completeness of the burning. Part of the issue with determining values for individual carbonaceous aerosol types is the uncertainty in definitions of the various types, but also the variability from source to source. Figure 1-8 shows the range of retrieved and calculated refractive indices given for both BC and OC. BC values of real part of the RI range from 1.35 to 1.9 at 550 nm, whilst the imaginary part ranges from 0.08 to 0.79. A large majority of values from literature fall upon a line which shows a linear increase in both real and imaginary parts of the refractive index, which Bond & Bergstrom (2006) suggest shows a single value for the refractive index of pure BC exists, but measurement samples contain varying levels of void fractions (air pockets). OC has a range of refractive indices, and cannot be defined by a singular value. Within OC, there are aerosol which are slightly absorbing, whose refractive index varies not only with void fraction, but also within the source material and BC content of the emissions (Saleh et al., 2013; Saleh et al., 2014). The real part of the RI can also differ depending on the source of the aerosol. However, no singular value can reflect the range and diversity of the individual aerosol refractive index for OC.

Effect of Carbonaceous Aerosol on Clouds

Like all other aerosols, CA also affect clouds through both aerosol-cloud interaction and through aerosol radiation interactions. Unlike most other aerosols, most primary CA are insoluble, and so cannot independently act as CCN. As particles become encased in ever larger numbers of soluble aerosol and grow in size, they become soluble, potentially acting as a CCN (Pierce et al,. 2007; Spracklen et al., 2011). In this case, the number of CCN available is reduced because SOA and sulphates form through condensation onto the pre-existing CA,

rather than through nucleation (Crosbie et al., 2015; Riipinen et al., 2011). A reduction of CCN leads to duller clouds that reflect less radiation, assuming that the liquid water content remains constant. Secondary CA however are soluble, and the precursor gases are mostly emitted with primary CA. Increases in secondary CA leads to an increase in CCN, which is the opposite effect to the primary aerosol (Engelhart et al., 2011; Zhao et al., 2016) .

Absorbing CA can also affect cloud growth and development due to aerosol-radiation interactions, with effects largely dependent on the aerosols position compared to the cloud (Koch and Del Genio, 2010). Absorbing CA above low convective cumulus clouds can warm the atmospheric layers above the cloud, stabilizing the atmosphere below and inhibiting the growth of cumulus clouds. The same physics can also allow an increased amount of stratocumulus cloud to exist, as the more stable atmosphere reduces evaporation by dry-air entrainment, which is fed through mixing above the cloud. This increases the amount of cloud available to reflect radiation during the day, and retain longwave radiation during the night. The effects of warming from BC can also inhibit growth and reduce cloud when it is within the cloud itself, as the warming of the cloud leads to greater rates of evaporation of droplets (Hansen et al., 1997). When BC is below cloud, the warming effect can lead to a more unstable atmosphere, and so can enhance the growth of convective clouds, increasing the reflectance of shortwave radiation and thus cooling the atmosphere (Conant et al., 2002; Johnson et al., 2004). These effects, which are due to the change in heating rates caused by the aerosol, and the subsequent changes in the profile of temperature and moisture, are often termed as "Semi Direct effects" and are classified as rapid adjustments in the latest IPCC report.

Black Carbon Refractive Index values in literature

Legend:
- From Biomass Burning BC
- From Urban BC
- From General BC

1. Schkolnik et al. 2006
2. Schmid et al. 2009
3. Hungershoefer et al. 2008 - Savanah
4. Hungershoefer et al. 2008 - Musasa
5. Marley et al 2001 - Diesel
6. Batten 1985
7. Moteki 2010
8. Moffet & Prather 2009
9. Stagg & Charalampopoulos 1993
10. Wu et al. 1997
11. Bond & Bergstrom 2006 - Low
12. Bond & Bergstrom 2006 - Med
13. Bond & Bergstrom 2006 - High
14. Marley et al. 2001
15. Hess et al. 1998
16. Janzen 1979

Organic Carbon Refractive Index values in literature

Legend:
- From Biomass Burning OC
- From Urban OC
- From General OC

1. Schkolnik et al. 2006
2. Salah et al. 2013 - Low
3. Salah et al. 2013 - High
4. Lack et al. 2012
5. Dinar et al. 2007
6. Chakrabarty et al 2010 (Pine)
7. Chakrabarty et al 2010 (Duff)
8. Saleh et al 2014
9. Moffat & Prather 2009
10. Kirchsetter et al 2014
11. Chen & Bond 2010
12. Adler et al 2010 (OSC)
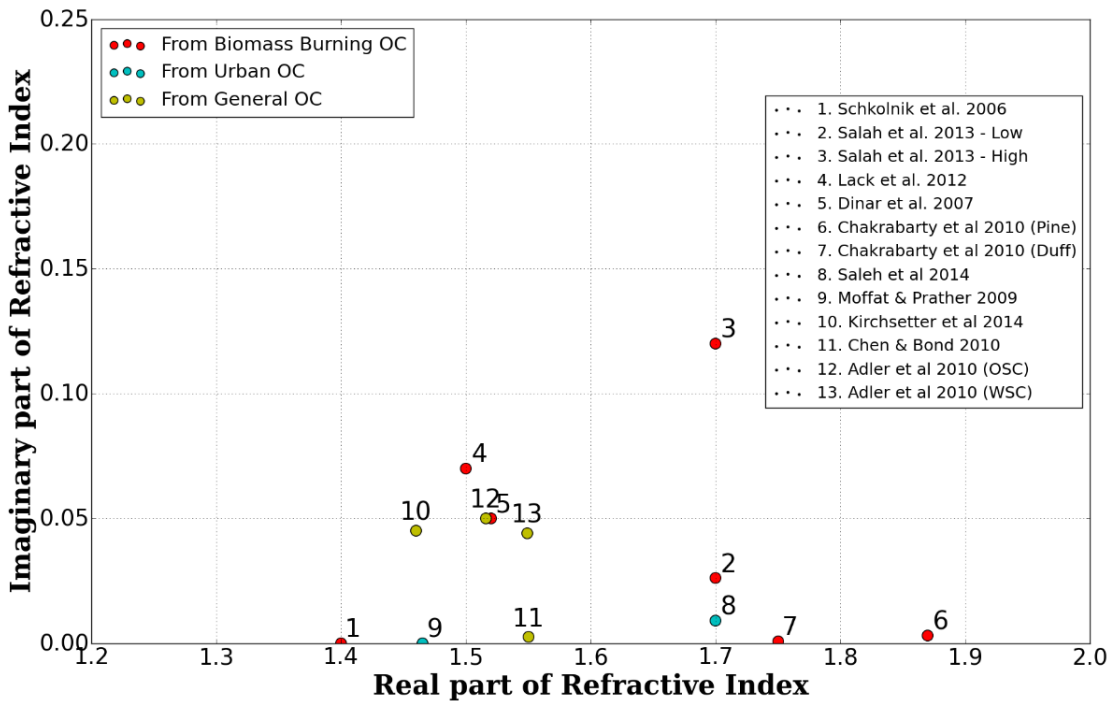13. Adler et al 2010 (WSC)

Figure 1-8 Refractive Indices of Black Carbon and Organic Carbon from the studies listed in the panel, either at or converted to be at 550 nm. Colours denote source of aerosols measured.

1.4 Measurements of Aerosols

The magnitude of the climate and health effects of CA are dependent upon the concentration of CA in the atmosphere. To determine CA properties effectively and accurately, there are two different types of measurement, in-situ and remote sensing, and both have their own advantages and disadvantages.

Ground site in-situ measurements have the advantage of recording the change in aerosols over long time periods. This is exceptionally useful for looking at changes or trends in aerosol composition for a range of time-scales, from daily variability, to seasonal trends and even longer (Gupta & Kumar, 2006; Putaud et al., 2014; Schauer et al., 2003). From these, it is possible to evaluate changes in aerosol, such as the effect of new environmental legislation, increased urban settlements or changes to local environment (Spracklen et al., 2016; Van Dingenen et al., 2009). However, surface in-situ measurements are limited to a singular point in space, and are unable to give information on the atmosphere above them, which limits their usefulness (Schutgens et al., 2016). Aircraft measurements have the advantage of sampling the atmosphere in 3-dimensions. This allows vertical profiles to be built, which can be used to calibrate remote sensing instruments that measure properties of an atmospheric columns (Emmons et al., 2004; Inoue et al., 2014). In addition, horizontal legs can be used to look at changes through different meteorological conditions, through different stages of the life cycle of an aerosol and changes through areas of different aerosol emissions (Capes et al., 2008; Hodgson et al., 2013; Jacob et al., 2010).

However, as CA is co-emitted with other aerosols, measuring CA alone requires specific devices to distinguish it from other aerosols (Formenti et al., 2003). BC in particular typically only makes up less than 10% of the aerosol burden at any time (Bond et al., 2013), even in biomass burning areas, making measurements difficult. Multiple other methods exist for retrieving BC mass, but these methods use proxy measurement and relationships based on assumptions of density, refractive indices and aerosol properties.

As well as measuring mass, there are various measurement techniques that measure or derive aerosol optical properties. There is a large range in the properties observed in an aerosol population. It is easier to sample a larger number of aerosols together, thus the properties of the bulk aerosol column are more commonly used to describe aerosol properties, rather than

individual component properties. Observations and understanding of bulk aerosol optical properties are needed by modellers so that the radiative effects of aerosol on climate and climate change can be simulated in a more precise manner.

A measurement of the optical properties of an aerosol column is the Aerosol Optical Thickness, or Aerosol Optical Depth (AOD). This is a unitless value that quantifies the extinction of incoming radiation at a given wavelength. The extinction is a combination of both absorption and scattering in a vertical column of atmosphere, and is related to both the properties of the aerosol itself and the amount of aerosol present. The optical depth is calculated from the total extinction of incoming solar radiation using the Beer-Lambert Law (Equation 1.1), where T is the transmittance, τ is the optical depth, and m is the path length through the atmosphere, taking into account the angle from the vertical the calculation is being made from. The optical depth can also be expressed as a function of mass (Equation 1.2), where k_{ext} is the mass extinction coefficient of the aerosol column, Q is the mass mixing ratio of the aerosol, ρ_{air} is the density of dry air and z is vertical height of the column.

$$T = e^{-m\tau} \qquad \text{Eq (1.1)}$$

Where:

$$\tau = \int k_{ext} * Q * \rho_{air} \, dz \qquad \text{Eq (1.2)}$$

An AOD of less than 0.1 at 550 nm would be considered a clean sky, whilst visible haze from pollution would lead to a value of AOD that was greater than 1 (Kim et al., 2015). AOD can also be used as a proxy for aerosol mass if composition and size distribution are known or constant, as it is sensitive to aerosol burden. However, it is also highly sensitive to the water content of the particles (Li et al., 2014), meaning that calculations using AOD in place of aerosol mass are not possible.

The Angstrom Exponent (AE or α) relates the change in AOD between two different wavelengths (λ_1) and (λ_2). The wavelength dependence of AOD is determined by the aerosols physical properties, and is inversely related to the aerosol size (Equation 1.3). This is true except in the case of large aerosols, where optical depth does not change much with

wavelength. Large aerosol, such as dust, have an AE of near 0, whilst small aerosol, such as newly formed sulphates, have an AE of around 2 (Dubovik et al., 2002).

$$\alpha = \frac{log\frac{\tau_{\lambda 1}}{\tau_{\lambda 2}}}{log\frac{\lambda_1}{\lambda_2}} \quad \text{Eq (1.3)}$$

The Absorbing Aerosol Optical Depth (AAOD) quantifies the absorbing part of the extinction only. The AAOD cannot be directly measured, as it is impossible to determine whether radiation that is lost in the direction of observation is lost through being absorbed or through being scattered in a different direction. However, it can be retrieved using assumptions of aerosol properties and size (Dubovik & King, 2000).

Subtracting the AAOD from the AOD gives the amount of extinction due to scattering from atmospheric aerosols. However, it is more common to express this as a ratio of the scattering to the total extinction, in the form of the Single Scattering Albedo (SSA). The SSA is a value between 0 and 1, where 0 is a fully absorbing aerosol column, and 1 an entirely scattering aerosol column (Equation 1.4). Pure biomass burning emissions have an SSA of between 0.85 − 0.95 at 550nm (Dubovik et al., 2002)

$$SSA = 1 - \frac{\tau_{abs}}{\tau_{ext}} \quad \text{Eq (1.4)}$$

Observations of both mass, optical depths and properties of CA aerosol are exceedingly useful for climate modellers to analyse the ability of aerosol schemes within models. Observations can be used to constrain aerosol mass and properties within climate models, and can be used as a benchmark for assessing both current models and developments to models.

1.5 Aerosol in Climate Models

The modelling of aerosols is not a simple task, with aerosol characteristics and mass being a function of emissions, transport, deposition and chemistry. The properties of aerosols are diverse and differ locally. Scientific understanding and computational resources represents limits to any numerical modelling, including aerosol modelling. However, modellers have created different methods of modelling aerosols, which can lead to large differences between

models when comparing aerosol concentrations, optical depths and aerosol effects (Mann et al., 2014; Tsigaridis et al., 2014; Wilcox et al., 2015).

Differing definitions of aerosols are used within different model. There is a wide range of complexity in how aerosols are modelled, depending upon the purpose of the model. In climate models, simplistic ideals of aerosols were initially used and only differentiated between one or two species of aerosol, mainly sulphate, which were considered important to determining radiative forcing. As understanding of aerosol radiation interactions and aerosol cloud interactions has evolved, the complexity of aerosol schemes in models has developed to contain several species of aerosol. Specific aerosol and chemistry models have exceptional levels of complexity, such as the AIM (Aerosol Inorganic Model), and represent large amounts of physical and chemical processes (Wexler & Clegg, 2002). In general, as computing power has allowed an increase in complexity, newer versions of climate models treat more components separately, and this has led to an improvement in modelling aerosol transport, lifetime and effects (Dufresne et al., 2013). However, models such as the AIM model are too complex and computationally expensive to run alongside a climate model. Therefore, aerosol schemes in climate models are forced to parameterise or ignore certain interactions. Table 1-1 shows the different processes and interactions that different types of models include.

Emissions, Transport, and Deposition

Emissions in aerosols are defined in one of two ways. Some aerosols, most often anthropogenic, are emitted according to emission inventories that are created using a mixture of observations, data assimilation and models. Present and near-past emission datasets are often combined from a variety of sources, including satellite estimates (Kaiser et al., 2012; Randerson et al., 2012), AOD measurements (Venkataraman et al., 2006) and mass-based measurements (Dentener et al., 2006). Others, such as sea salt and dust, are commonly emitted based upon atmospheric conditions within the model. More complex models, such as Earth System Models (ESM) can model vegetation and fires in order to provide dynamical emissions of biomass burning aerosol and volatile organic compounds (Hantson et al., 2016).

Model Type	Emissions, Transport, Deposition	Radiative Effects (ARI, ACI)	Feedback on Meteorology	Feedback on Chemistry, Ocean, Vegetation
Trajectory Model	Transport Only	✘	✘	✘
Dispersion Model	✓	✘	✘	✘
Chemistry Transport Model	✓	Yes, but without feedback	✘	✘
General Circulation Model	✓	✓	✓	✘
Earth System Model	✓	✓	✓	✓

Table 1-1 – List of aerosol processes included in various types of models which include aerosols.

Historical emission datasets are difficult to determine due to a lack of observations with which to constrain estimates. Proxies, such as concentrations of gases and aerosols in ice cores (Petit et al., 1999), estimates of fuel usage (Junker & Liousse, 2006) and even changes in sky colour in historical paintings (Zerefos et al., 2014) have been used in lieu of missing observations to attempt to determine historical aerosol mass, optical depths, and therefore derive emissions.

The interaction of aerosols with other aerosol species during transport also needs to be considered. In the simple trajectory or dispersion models, such as the Numerical Atmospheric-dispersion Modelling Environment (NAME) (Jones et al., 2007), aerosols are passive tracers and each separate species is moved around with the air mass in the model,

with simplified calculations of deposition rates. These are known as bulk-mass schemes, and are particularly useful for back and forward trajectories when analysing specific aerosol events (Stohl et al., 2005). In more complex models, aerosol interactions can be modelled as "active aerosols", in which aerosols interact with each other. Aerosols species can be mixed together. A common method for doing this is through a modal scheme, which allows aerosols with similar characteristics such as size, or solubility, be modelled as though they were mixed together, regardless of species. The aging of aerosols can also be modelled in different ways. As aerosols age, they coagulate with other species. Insoluble aerosols tend to become coated with more soluble species and the internal mixture become soluble. The increase in size and solubility leads to particles which are good CCN, and eventually leads to the removal of the aerosol through wet deposition. Simple schemes do not model aging in any meaningful way. Chemistry transport models may include separate species into which aerosol can classified as fresh or aged. Further complexity can be introduced using schemes which highlight the changing characteristics of aging aerosols. This includes modal schemes, which can move aerosol through different size and solubility states, which can be used to determine whether aerosol contributes towards CCN.

Deposition rates can also be calculated with different levels of complexity. Some models use simple equations based on reanalysis data to determine aerosol deposition. In more complex models, aerosol schemes are linked to dynamical cores, which give meteorological conditions. These can be used in conjunction with the more complex active aerosol schemes to determine deposition rates.

For models that include a radiation scheme, aerosol interactions with these schemes allow for aerosol radiation interactions to be calculated. In models with dynamical cores, the feedback from the radiative heating and cooling from aerosol can affect the atmosphere. For those that also have cloud schemes which interact with aerosols, the radiative effects from cloud-aerosol interactions can also be computed. Modelling the effect of aerosols with radiation can be done with differing levels of complexity. Bulk-mass schemes treat aerosols as an external mixture, where the effect of each aerosol species is calculated separately. More complex models treat aerosols as an internal mixture, where the aerosol species are mixed together in calculations. These schemes have a significant advantage over externally mixed aerosols when compared to radiative calculations, as they more closely resemble a realistic

aerosol particle, and tend to show an improvement in comparisons to observations of aerosol mass and optical depth (Lesins et al., 2002; McMeeking et al., 2011). Aerosol schemes which treat aerosols as an internal mixture creates single particles of multiple components in a unspecified arrangement, or in specific configurations, like a core and shell (Péré et al., 2009). These represent a core particles, usually dust or BC, coated with soluble aerosols, such as sulphate, nitrates or secondary organic aerosol. Core and shell schemes can lead to difference in extinction, scattering and absorption compared to a singular particle, as the outer coating acts like a lens, scattering more radiation towards the core, enhancing the absorption (Bauer et al., 2007; Lack & Cappa, 2010). Modal schemes, which increase the complexity of internal mixture schemes further, can represent both aerosol mass and number, which is important for determining the radiative effect of aerosols in the atmosphere (Bellouin et al., 2013).

The interaction between aerosols and radiation are important when studying both past and future climate. All climate models contain a radiation scheme, which uses the modelled values of aerosol distribution to calculate values of extinction, scattering and absorption in each model column. This can then be diagnosed as AOD and AAOD. The effect of aerosols on radiation is dependent upon the size of the particle and the RI. The amount of scattering and absorption of incoming shortwave and outgoing longwave radiation by aerosols is calculated by a set of equations called Mie calculations, as aerosols have a similar diameter to the wavelengths of radiation in those spectra. Mie calculations were defined by Gustav Mie in 1908 (Mie, 1908). Mie theory calculations provides extinction and absorption coefficients for aerosols. It assumes a homogeneous spherical particle that has singular properties of refractive index and density, although further assumptions can be made in order to provide coefficients for non-spherical particles (Mishchenko et al., 2010). In most models, to save on computing costs, pre-calculated values for extinction and absorption coefficients are stored in tables. These values are calculated from refined equations produced by Wiscombe (1980).

Models also differ in how aerosols interact with the atmosphere and clouds. Wilcox et al. (2015) shows how different methods and complexity of calculating soluble aerosol, and the following calculations of cloud condensation nuclei, cloud droplet number and effective radius, leads to large diversity in sulphate loading and distribution in different models. Models with a dynamical core are required in order to calculate aerosol-cloud feedbacks (Meehl et al., 2013). General circulation models that do model aerosol-cloud feedbacks parameterise

the interactions between soluble aerosols and clouds through schemes which compute the effect the physical changes from aerosol on clouds (Ghan et al., 2016; Bentsen et al., 2012; Syktus et al., 2011).

Future increases in complexity are focused upon interactions with elements outside the atmosphere, such as land surfaces, vegetation and the biosphere (Collins et al., 2011). These feedbacks include interactions through surface radiation, which can lead to snow/ice melting and increased vegetation growth (Cohan et al., 2002; Matsui et al., 2008), and interactions with surface and ocean chemistry, where aerosols may bring nutrients to oceans (Jickells, 2005). An example of a feedback loop is the impact of aerosol on the growth of forests. Vegetation is then used by dedicated models to calculate dynamic emissions of biomass burning carbonaceous aerosol and biogenic emissions of secondary organic precursor gases, which then influence the growth of more vegetation. This could lead to future models where the properties of aerosols can be linked dynamically in the model to their emissions.

1.6 Aims and questions for the Thesis

The effect of carbonaceous aerosols upon the climate system is still uncertain, with debate in literature ongoing. As shown in Figure 1-5, the IPCC denotes the radiative forcing to be +0.7 W m^{-2} for BC, with an uncertainty range of +0.25 W m^{-2} to +1.1 W m^{-2}, an uncertainty range which is only smaller than the effect of aerosol cloud interactions. However, the assessment by Bond et al. (2013) suggests that emissions of BC should be increased from 7.5 Tg to 17 Tg, with increases in both open biomass and energy-related emissions, particularly in Southern Asia where they suggest BC emissions are underestimated by a factor of 2 - 4 in emission inventories, and that the radiative forcing of BC should be nearer +1.1 W m^{-2}, with a 90% uncertainty range of +0.17 to +2.1 W m^{-2}. This would make BC the 2nd strongest positive forcing in the atmosphere after CO_2. The possibility of such a strong radiative forcing being attributed to BC has been questioned (Samset et al., 2014). Specifically, the methodology used to reach such a strong forcing is based primarily on scaling model fields to match AAOD observations. This is a method also used in other papers to determine emission factors for local sources, such as biomass burning (Petrenko et al., 2012). Such a scaling assumes that all absorption can be attributed to BC, that BC optical properties are correctly represented, and that a column integrated quantity like AAOD can usefully constrain emissions. Importantly,

the negative radiative forcing exerted by co-emitted OC partially offsets the positive forcing from BC, as noted by Bond et al. (2013), so the challenge is to quantify CA radiative forcing rather than BC radiative forcing alone.

To quantify the strength of CA radiative forcing, several key questions need answering. First, how much absorption can be attributed to CA? How is that absorption split between the different species of CA, especially BC and BrC, which may have different spatial distribution? And what is the anthropogenic contribution to this absorption?

In this thesis, we contribute to the work aimed at answering those questions by using CA simulated in the Hadley Centre General Environment Model with the UK Chemistry and Aerosol model (HadGEM3-UKCA). Is a multi-variable constraint a better method to evaluate a simulation of CA than just AAOD? Is increasing CA the only method available to increase CA absorption? And if other methods are required, is the model complex enough to represent the regional differences in CA physical and optical properties?

The work from this thesis goes towards the larger goal of ensuring that the HadGEM3-UKCA, and its future iterations, represent aerosol in a realistic and accurate manner. The model has previously been used in several scientific projects, which include simulating past climate events such as large volcanic eruptions, and future climate, based upon estimations of future emissions of greenhouse gases and aerosols. Improvement in the aerosol scheme is one of many ways in which the uncertainty of these simulations, and thus projects, can be reduced. More robust predictions of future events from climate change can be used to back up calls for action on atmospheric emissions and advise political leaders of the potential consequences otherwise.

The thesis is structured as follows: In Chapter 2, the current version of the model is evaluated regionally against various observations. Then we use sensitivity studies to explore the influence on the evaluation of three uncertain aspects of the model: The optical properties of CA (Chapter 3), the emissions of CA (Chapter 4), and the lifetime of CA (Chapter 5). The sensitivity studies are then used to create a model configuration which better compares to observations (Chapter 6). This improved model is used to quantify the ERF of CA.

Chapter 1: Introduction

2. Chapter 2: Evaluation of Current Model Performance

This chapter introduces the HadGEM3-UKCA model and analyses how the model currently performs when compared to observations of BC and OC mass, optical depths and retrieved aerosol properties.

2.1 Introduction to HadGEM3-UKCA

2.1.1 Model Description

The model used in this project is Hadley Centre Global Environment Model with the full United Kingdom Chemistry and Aerosol model included (HadGEM3-UKCA), which is maintained and developed by the UK Met Office and its academic partners. The version of HadGEM3-UKCA used in this work has 85 vertical levels, and a spatial resolution of 1.25° latitude by 1.875° longitude. It is configured in accordance with the Global Atmosphere 3 (GA3) setup described by Walters et al., (2011) and contains the GLOMAP-mode aerosol and chemistry scheme described in (Mann et al., 2010). HadGEM3-UKCA is the latest generation of climate model from the Hadley Centre, evolved from HadGEM2 (Collins et al., 2008). Differences between the two include a new prognostic cloud scheme (Wilson et al., 2008), which improves cloud representation in the model, and the new GLOMAP-mode aerosol and Strat-Trop chemistry scheme (Morgenstern et al., 2009; O'Connor et al., 2014). It includes several model levels in the stratosphere and the capability to include dynamic oceans, sea ice and vegetation modules (Hewitt et al., 2011). The full model runs with a time-step of 20 minutes, with the UKCA model being run every 3rd time-step due to the computational expense.

2.1.2 Current Carbonaceous Aerosol Processes in HadGEM3-UKCA

HadGEM3-UKCA uses the GLOMAP-mode aerosol modal scheme, and in this work we use a version of GLOMAP which models BC, OC, Sulphate and Sea Salt in 5 different bins. GLOMAP-mode models the aerosol number as well as the aerosol mass in an internal mixture within each mode, allowing a dynamical representation of aerosol size to be obtained. This has the advantage of being able to improve the representation of aerosol radiation effects, and aerosol cloud interactions. Figure 2-1 shows the schematic of the GLOMAP-mode scheme. The full GLOMAP-mode scheme consists of 7 modes, split depending upon size (Nucleation,

Aitken, Accumulation and Coarse) and solubility (Insoluble and Soluble), through which aerosol mass and number is moved through in its lifetime. In this version, only 5 modes are used, as the insoluble accumulation and insoluble coarse mode are used for dust only. Modal aerosol size distributions are lognormal. The modal radius is interactive in the model, whilst the standard deviation of the size distribution is prescribed and varies depending on the mode. GLOMAP-mode not only simulates the dry weight of the aerosol mass, but also simulates the mass of water attached to aerosols. It also includes the nucleation and condensation of H_2SO_4 (sulphuric acid) and condensation of secondary organic aerosol from the gas phase, which can interact with the aerosols in the scheme. The aging of Aitken insoluble aerosols, the mode into which all initial BC and primary OC are emitted into is crucial in the aging of CA, and allowing CA to be removed through wet deposition. Coagulation with other aerosols and condensation of SOA are responsible for changing CA solubility.
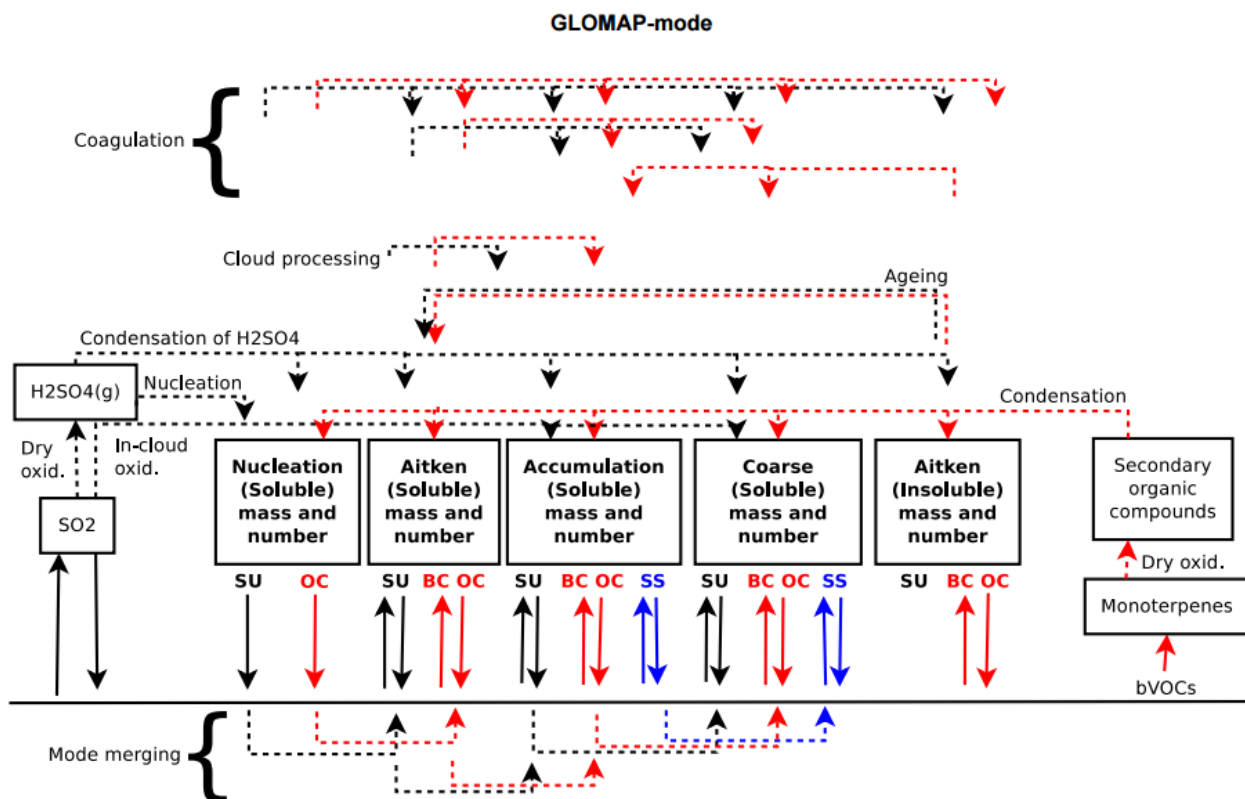

Figure 2-1 – Summary of the GLOMAP-MODE aerosol scheme, where sulphate (SU, black), black and organic carbon (BC and OC, red), and sea-salt (SS, blue) aerosols are internally mixed. Solid arrows represent the emission and deposition mass fluxes. Dashed arrows represent mass fluxes within the scheme. Figure taken from Bellouin et al., (2013)

Both BC and primary OC are emitted into the Insoluble Aitken mode. Once the aerosol mixture contains 4 times as much soluble aerosol as insoluble, the entire particle is considered soluble and is moved to a soluble mode. Through aging (increasing solubility through condensation of H_2SO_4 and SOA) and coagulation (collisions of particles in other modes), the particles become larger and move into the Accumulation and Coarse mode through a mode-merging scheme. This is done by moving a fraction of the mass and number to a mode of larger size based upon the mean particle diameter and spread of aerosol sizes within the mode. Secondary OC is mostly produced in the nucleation soluble mode after the dry oxidation of monoterpene and isoprene, but is also modelled as condensing onto other soluble aerosol in other modes to increase size through reactions with OH, O_3 and NO_3 (Spracklen et al., 2007). Gas to liquid phase equilibrium is described by Henry's law, which is dictates a linear relationship between the liquid water available and the concentration of the gas . Once condensed, all secondary OC is treated through the model in the same way as OC.

Aerosols in the GLOMAP-mode modal scheme are removed through two main processes. The first is through dry deposition, which is calculated from the gravitational velocity of the particles and the particle diffusion coefficient of the aerosol within the gridbox. Dry deposition can only happen within the boundary layer, with the rate dependent on particle size and the roughness of the land/ocean surface in the model. Within GLOMAP, dry deposition velocity is calculated from the equations derived in Slinn, 1982:

$$V_d = V_{grav} + \frac{1}{R_a + R_s} \qquad \qquad Eq\ 2.1$$

Where V_d is the dry deposition velocity, V_{grav} is the gravitational settling velocity, and R_a and R_s are the aerodynamic and surface resistance. Gravitational settling velocity is defined as:

$$V_{grav} = \frac{\rho_p D_p^2 g}{18\mu} C_f \qquad \qquad Eq\ 2.2$$

where ρ_p is the particle density, D_p is the geometric mean wet diameter, g is the gravitational acceleration, μ is the viscosity of air and C_f is the slip correction factor, which calculates drag effects on small particles (Mann et al., 2010) The second removal process is wet deposition, which includes nucleation scavenging through cloud droplets. GLOMAP not only scavenges from the cloud, but also simulates impact scavenging of aerosols from below the cloud based upon the raindrop-aerosol collection efficiencies from Sekhon & Srivastava (1971).

GLOMAP does not represent the re-entrainment of aerosols from precipitation that evaporates. Re-evaporation of water from cloud droplets is most likely to occur in convective clouds, and therefore is more likely in the Tropics. The effect of re-evaporation on aerosol amount is not included, although previous versions of HadGEM showed that as much as a quarter of precipitation in the model may evaporate before reaching the surface (Bellouin et al., 2007). Similarly, GLOMAP-MODE does not represent the re-suspension of dry-deposited aerosol on the surface (Bellouin et al., 2013), which may also be a source of error in the model.

The previous scheme used in the HadGEM climate model series, CLASSIC, is still used in HadGEM3-UKCA for simulating dust, as simulating dust in the modal scheme introduces further uncertainties and is currently less robust than the CLASSIC scheme. It is a bulk-mass scheme, as it treats each aerosol species as a separate tracer which are externally mixed in both the atmosphere and radiation code. It does model chemical production and deposition, but in a simpler manner. The CLASSIC scheme contains 6 different size modes for dust, each with a separate set of properties, and has a dynamic system so that the type of dust emitted depends upon the wind speed and location (Woodward, 2001).

The radiation scheme used in HadGEM3-UKCA is the Edwards-Slingo radiation scheme (Edwards & Slingo, 1996). The radiation code separates longwave and shortwave wavelengths, and then further divides them into 15 wavebands. The optical properties of aerosols and gases in the atmosphere are integrated across the wavebands to calculate radiative fluxes and heating rates. The aerosol-radiation interactions are calculated in HadGEM3 by UKCA-RADAER, which accounts for the variable internal mixture of particles and water uptake as simulated by GLOMAP-mode (Bellouin et al., 2013). GLOMAP-mode aerosol in the nucleation mode are ignored, due to the very small effect that aerosol of that size has on Mie scattering. In all other modes, a mass-weighted set of optical properties are derived

using the components refractive indices (Maxwell-Garnett, 1906), along with a number concentration of the aerosol (in particles per m^3). The weighted refractive indices and size distribution is used to determine the optical properties of the aerosol stored in look-up tables within UKCA-RADAER, which are used instead of a computationally expensive Mie-calculation. This determines the absorption coefficient, the scattering coefficient and asymmetry parameters required to calculate the radiative fluxes in each gridbox, and thus allowing a calculation of optical depth to be made.

Aerosols are also coupled to clouds through the ACTIVATE scheme (West et al., 2014). Aerosol can only act as cloud condensation nuclei (CCN) if they are both soluble, and are of a certain size. The activation dry radius of a particle, which is the minimum size of particle required to activate cloud droplets, is determined by a Kohler-based activation parameterisation based on Abdul-Razzak & Ghan (2000). Cloud Droplet Number Concentration (CDNC), particle size distribution and aerosol composition are used to calculate both cloud droplet effective radius and the percentage of aerosol lost to "rainout". These values are passed into the Edwards-Slingo radiation code used in HadGEM3 (Walters et al., 2011), where CDNC is used to calculate the cloud albedo. ACTIVATE is also coupled to the precipitation scheme, as the autoconversion rate of cloud water content to precipitation is dependent on CDNC.

2.1.3 Setup of HadGEM3-UKCA control run

For the control simulation, we use HadGEM3-UKCA with GLOMAP aerosol and CLASSIC dust (O'Connor et al., 2014). We simulate the model for the years 2006 and 2008, using biomass burning (BB) and volcanic emissions from those years, other aerosol emissions, including BC and OC from fossil and biofuel combustion (FFBF), from 2000, and ERA-Interim reanalysis from 2006-2008 to nudge low level winds. These years were chosen as there is a large amount of observation data for these years, and between them, they represent a year with globally high biomass burning emissions (2006) and low biomass burning emissions (2008). Results from the simulation are taken after a 4-month spin-up, which allows the development of an ambient background aerosol field and a balanced aerosol budget. Horizontal boundary-layer winds are nudged to ERA-Interim to minimise changes to aerosol transport. Table 2-1 shows the aerosol species used, and shows the modes used to model each one, along with emission inventories and refractive index. Emissions of fossil and biofuel combustion carbonaceous

aerosols are emitted at the surface at every time step, with changes on a monthly timescale. Biomass burning aerosols are emitted evenly throughout the boundary layer every time step, and change monthly. The biomass burning emissions are matched with the years modelled to limit the inaccuracy from time-dependent carbonaceous aerosol sources. Figure 2-2 shows the distribution of OC and BC emissions from biomass burning and fossil/biofuel combustion. The figure shows the difference in source material, with most BC and OC in South America and Africa coming from biomass burning sources, and most BC and OC in Northern Europe, North America and China coming from fossil/biofuel combustion. Volcanic and high level SO_2 is also emitted at multiple heights, based upon emissions from which represents the actual time series of degassing and erupting volcanoes.

Component	Modes used	Emission dataset	Refractive Index at 550 nm
BC	Aitken Insoluble Aitken Soluble Accumulation Soluble Coarse Soluble	FFBF: ECLIPSE (Stohl et al., 2013) BB: GFED 3.1 (Randerson et al., 2013)	$1.85 - 0.71i$
OC	Nucleation Soluble Aitken Insoluble Aitken Soluble Accumulation Soluble Coarse Soluble	FFBF: ECLIPSE (Stohl et al., 2013), BB: GFED 3.1 (Randerson et al., 2013) SOA: from isoprene and monoterpene CMIP5 ((Pacifico et al., 2011),(Lamarque et al., 2010))	$1.5 - 0i$
Sulphate	Nucleation Soluble Aitken Soluble Accumulation Soluble Coarse Soluble	Anthropogenic: ECLIPSE (Stohl et al., 2013) Volcanic: Diehl et al., (2012)	$1.53 - 0i$
Sea Salt	Accumulation Soluble Coarse Soluble	Dynamic	$1.548 - 0i$
Dust	CLASSIC only	Dynamic	$1.52 - 0.0015i$

Table 2-1 – List of modes used, emission references and optical properties of each aerosol species used in the control simulation. Sea salt and sulphate have imaginary refractive index parts on the magnitude of 10^{-7}.
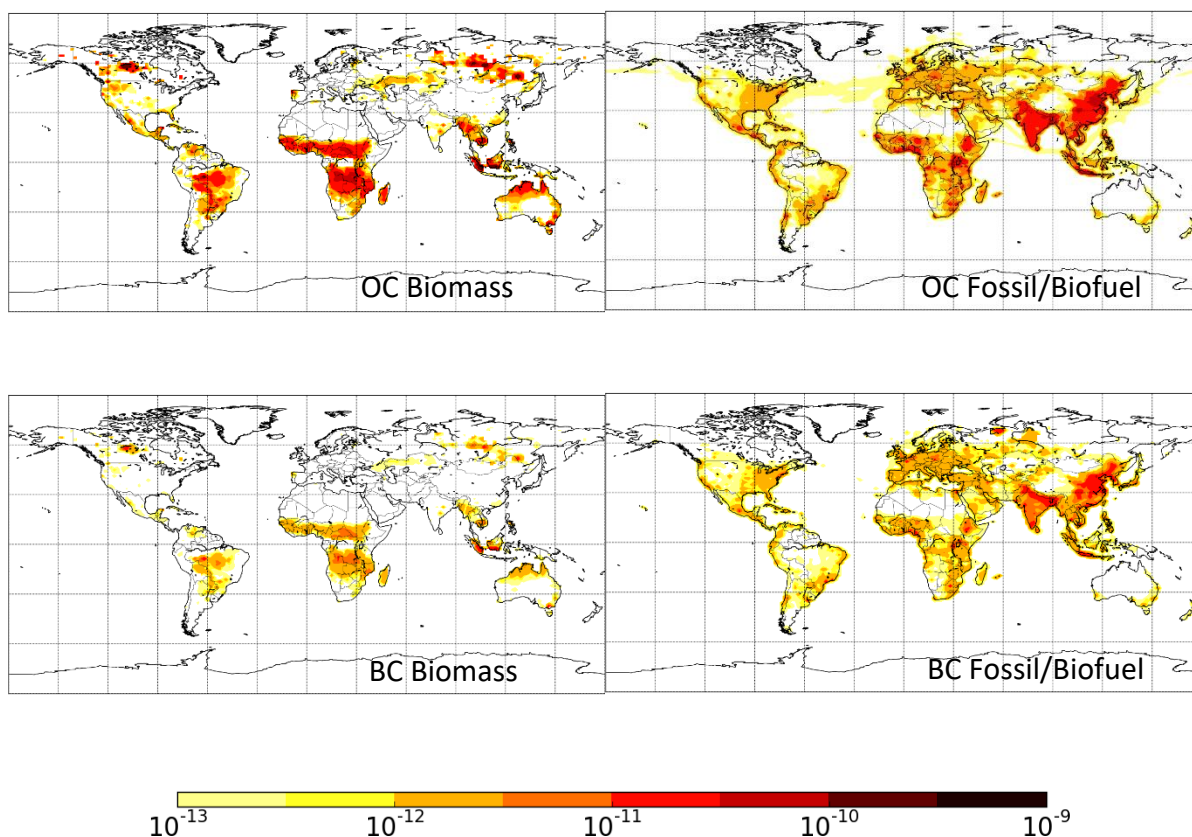
Figure 2-2 - Emissions in Tg yr^{-1} gridbox^{-1} of BC and OC from biomass and fossil/biofuel combustion for the year 2006, taken from the GFED3.1 (biomass burning) and ECLIPSE (fossil/biofuel) emission datasets.

All efforts have been made to ensure the model is up to date. Table 2-2 lists a number of bug-fixes that were applied to the original HadGEM3 setup to create the control and perturbed simulations.

UKCA Bugfix number	Description of Bugfix	Reason for bugfix
41	Increase OC emission factor to 1.4	Ancillary emissions which were previously in POM(kg) are now in OC(kg), and require scaling upwards.
42	Additional line required in RadAER files for long wavelengths	Long wavelength calculations of absorption were being extrapolated incorrectly in look-up tables
77	Increase of rates of scavenging of small aerosol: Increase rates of removal due to snow.	Previous error of magnitude 10 in implementation of equation
79	Alteration to impact scavenging: rates of scavenging now treat convective scavenging also.	Erroneous double call of dynamical scavenging and lack of convective scavenging.
81	Increased resolution of Look-up tables for RadAER	Lack of resolution led to small values of absorption being rounded down to 0.

Table 2-2 - List of bugfixes applied to the control simulation with corresponding description and explanation

2.2 Measurement Description

This section describes the observations and methods used to evaluate the model performance.

2.2.1 Surface Concentrations

Surface concentration measurements used for comparisons to the model in this configuration are from a variety of networks and campaigns. Table *2-3* lists the campaigns and networks used in this study to compare with the model, and details the instruments and number of sites available.

The variety of methods used to calculate BC is an issue, as different instruments measure BC according to different definitions, with different assumptions. Therefore, different instruments can give different values of BC concentration when measuring the same air mass.

Campaign/Network	Region	Years used	No. of sites	Type of instruments	Aerosol sampled	Reference
European Monitoring and Evaluation Programme (EMEP)	Europe	2006-2008	18	Mostly filter based aethalometers	BC & OC	(Simpson et al., 2007)
Interagency Monitoring of Protected Visual Environments (IMPROVE)	North America	2006-2008	43	Thermal/Optical Reflectance	BC & OC	(Chow et al., 1993)
Aerosol Radiative Forcing over India (ARFI)	India	2006	12	Aethalometers	BC	(Beegum et al., 2009)
South American Biomass Burning Analysis (SAMBBA)	South America	2006-2008	4	Laser-induced incandescence (SP2)	BC	(Morgan et al., 2013)
China Atmosphere Watch Network (CAWNET)	China	2000	10	Aethalometers	BC	(Zhang et al., 2008)

Table 2-3 - List of all surface concentration observations used for comparison to both modelled BC and OC in this work. Observations used are monthly values.

Aetholometers give an estimate of BC based upon attenuation of light on a filter. Figure 2-3 shows the inner schematic of an aethalometer. The instrument measures the attenuation of a single wavelength of light through a quartz-based filter (which is often on a tape), that becomes loaded with aerosols as air is pumped through at a controlled rate (Hansen et al., 1984). Some more modern versions of aethalometers do this for several wavelengths using multiple LEDs instead of a single solenoid. These instruments have the advantage of being able to give values in real time and with a high temporal frequency. Results can be displayed every minute on newer version of aethalometers, but the lower the time-step, the noisier the returned observations (Bond et al., 1999). However, deriving BC from absorption assumes all absorption comes from BC, and so do not take into account increases in absorption from the effects of internal mixing, nor any other absorbing aerosols, such as dust (Bond et al., 2013). The resulting derived mass is often quoted as "Equivalent Black Carbon", or BC_e, and is defined as strongly light-absorbing carbon with optical properties similar to those of BC (Lack et al., 2008).
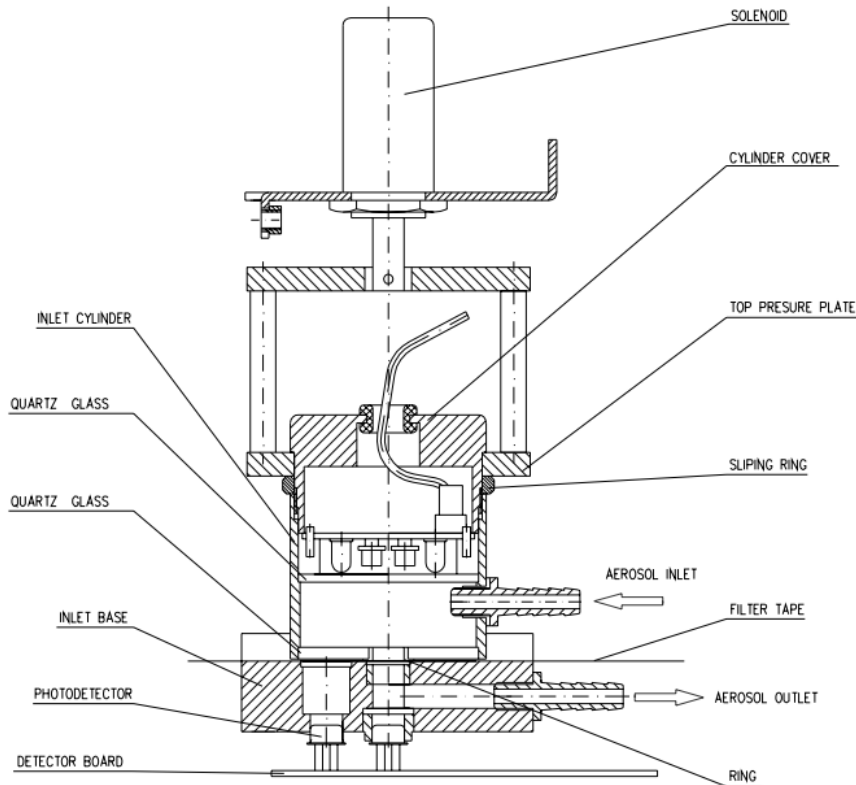
Figure 2-3- Schematic of the internal view of an aethalometer, showing how aerosol is input at a controlled rate to pass through a filter on tape, with changes in incoming light measured on photodetectors under the filter. Figure taken from Magee Scientific USA, 2006 manual for portable aethalometer (Figure 13).

Figure 2-4 shows a schematic of a Thermal Optical Reflectance and Thermal Optical Transmittance (TOR and TOT) instruments. To measure BC and OC, aerosol is collected on a filter, and then heated to approximately 700°C in an inert gas. The volatile OC is vaporized, and this effect can be measured, either through measurement of the gaseous remains (CO_2 or CH_4), or analysed optically as the difference between pre-and-post vaporization measurements of reflectance and transmittance of the sample when a laser is directed at the sample. The sample is then heated again to around 350°C, but this time, with available oxygen. The BC is then able to fully combust, and again, this optical difference is measured through one of the above techniques. The retrieved Black Carbon mass is given the name Apparent Elemental Carbon (EC_a) to distinguish the difference between black carbon and the limitation of only measuring the BC that is able to combust at a set temperature. Inaccuracies in this method come from the potential to "char" (convert OC to BC) the OC at high

temperatures, which decreases the volatility of the OC and increases the level of EC_a measured. Although methods have been introduced to attempt to quantify the errors, differences of up to 80% can occur in high EC load conditions, depending on which method is used, although the methods show low variability (±10%) at EC concentrations of less than 55 ugm^{-3} (Chow et al., 1993, 2004). Similarly, the difference in protocols for calibrating the temperatures can add to this uncertainty, and lead to values of EC that are different by an order of magnitude (Schmid et al., 2001).
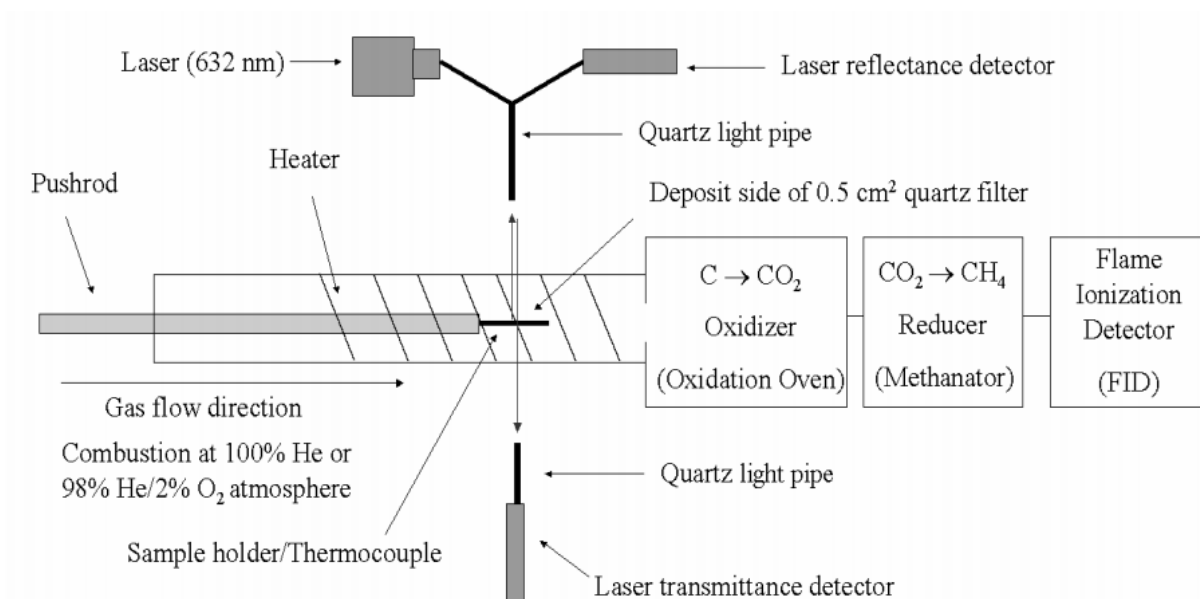
Figure 2-4 Schematic diagram of the DRI Model 2001 Thermal/Optical Carbon Analyzer (Atmoslytic,Inc., Calabasas, CA). The sample holder is open on top and bottom to minimize interference with the transmittance measurement. The carrier gas flows above and below (not through) the sample. The thermocouple is installed near the sample holder to characterize the filter temperature. Figure taken from Chen et al., (2004).

Finally, laser-induced incandescence instruments, such as the Single Particle Soot Photometer (SP2) instrument, which use short pulses of high energy lasers fired into a chamber. Figure 2-5 shows the setup of an SP2 instrument. The laser pulse is absorbed by absorbing aerosols, which heats them to around 4000 K. The hot aerosol re-emits this radiation as a near black-body, which is wavelength shifted due to the increase in temperature compared to other aerosols within the chamber. Measuring the increase in radiation at these wavelengths where radiation is re-emitted is proportional to BC volume fraction (Schwarz et al., 2006). This value

of BC mass measured is more often known as Refractory Black Carbon (rBC), which distinguishes that it only measures black carbon that has a vaporisation temperature high enough to reach incandescence in the instrument. The calibration of the instrument to convert the rate of radiation from rBC from ambient temperature to a BC mass, leads to the biggest variability in the value of measurements from this kind of instrument (Moteki & Kondo, 2010). There is also a limitation on the size range of aerosol measured in SP2 instruments, from around 80 – 700 nm. This is sufficient to retrieve most of the rBC mass in biomass burning areas, but not necessarily from urban environments (Chan et al., 2011; Schwarz et al., 2008).
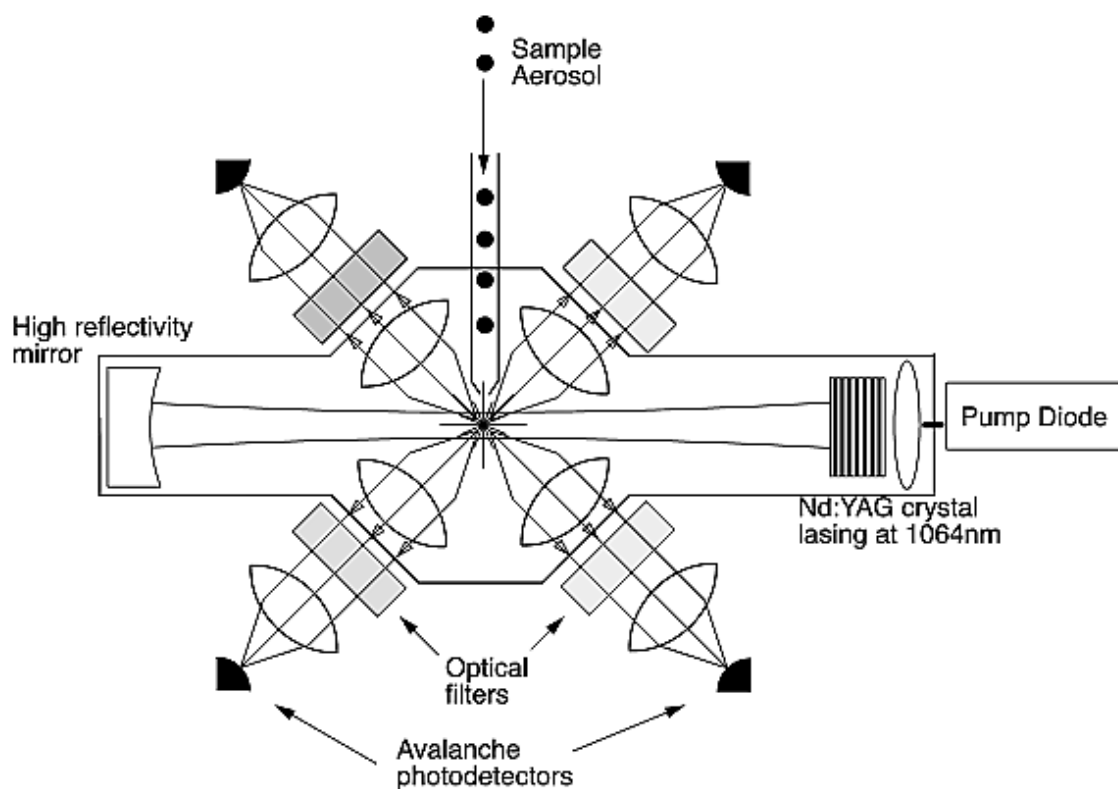
Figure 2-5- Schematic of the SP2 optical head showing the sample aerosol inlet, laser components, detection optics, and detectors. The light reaching the photodetectors is filtered to allow detection of specific wavelength bands of light. Taken from Schwarz et al., (2006)

All these methods use a mixture of proxy measurement and relationships based on assumptions of density, refractive indices and properties. Slowik et al., (2007) looked at a SP2 and Multi-Angled Absorption Photometer (MAAP), which is a multi-angle aethalometer, to

compare measurements taken between them in controlled conditions. The study found that for uncoated soot particles, the MAAP instrument gave a mass which was 50% higher than the SP2. When significant coating of an organic substance was added to the soot, the MAAP instrument estimate increased by a further 20%, despite the same amount of soot being present in both cases. A similar study by Cross et al., (2010) also found that the SP2 instrument was unaffected by any type or thickness of organic coating, and also unaffected by particle shape.

These studies show that observations of BC and OC mass from in-situ sites and still have significant uncertainties related to them. Changes in the assumptions of carbonaceous aerosol properties, changes in instrument and changes in calibration can all lead to different values being obtained from the same situations. For our work, this means that we are likely to see differences in comparisons between observations and model output which are due to the methods used to obtain the measurements. It also means that we must accept that a perfect comparison is not feasible, and our uncertainty on our measurements is dependent on the instrument used. This will add to other uncertainties which come from the methods of comparison and from the model itself. In section 2.3.1, we evaluate the effect of instrumental error on our comparison methods.

2.2.2 Aircraft Measurements

As the effects of BC on radiative forcing is highly dependent on its height compared with clouds, ensuring the vertical profile of BC is correct in the model is important. However, such campaigns are often limited in both time and space.

Table 2-4 shows the aircraft campaigns are used for comparison. Aircraft campaigns are often used to derive specific information about aerosols, and so are often deliberately flown into aerosol plumes or flown at times when specific conditions exist. We use the vertical profiles to constrain ambient background aerosol, as this is what the model should be able to represent. The campaigns listed all use Single-Particle Soot Photometer (SP2) to determine the amount and size of absorbing materials in aerosol mixtures. The EUCAARI campaign aimed to evaluate the climate effect of aerosols, with particular interest in the effect of long range transport. A high pressure system during the flights meant that locally emitted aerosols were recirculated around Europe and changes in aerosols could be sampled (Ryder et al., 2013).

The HIPPO campaign aimed to measure greenhouse gases and atmospheric constituents which relate to the carbon cycle. It was combined of 5 campaigns, spread across the seasons over 2 years. Figure 2-6 shows the flight paths taken by the HIPPO campaigns. All flights transect from the North Pole to the South Pole down the Pacific Ocean and back again over the course of around 28 days per campaign (Schwarz et al., 2010). The ARCTAS campaign uses two aircraft, and ran two sets of flights, one in the spring and one in the summer over North America. The campaigns main aim was to learn more about the state of aerosol distribution in the Arctic, and report on changes that have occurred due to pollution (Jacob et al., 2010).

Project name	Area Covered	Time covered	No of flights	Reference
European Integrated Project on Aerosol Cloud Climate and Air Quality Interactions (EUCAARI)	Southern UK, Germany, Holland, Belgium, Poland, Austria, Republic of Ireland	May 2008	12	Kulmala et al., 2011
Hiaper Pole-to-Pole Observations (HIPPO)	Length of Pacific, North and South Poles, Western America, Australasia	January 2009 – August 2011	52 flights over 5 campaigns	Schwarz et al., 2010
Arctic Research of the Composition of the Troposphere from Aircraft and Satellites (ARCTAS)	Alaska, Canada, Northern USA and Greenland	Spring/Summer 2008	49 flights over 2 campaigns with 2 aircraft	Jacob et al., 2010

Table 2-4 - Details of Aircraft campaigns used to record either Elemental or Black Carbon, which are used for comparisons to the model in this work.

2.2.3 Remote Sensing Products

Models can be compared to remote sensing products either from satellites or ground based networks. AOD is derived from measurements of irradiance through a sun photometer on the ground, or via a satellite instrument. These devices measure the extinction due to the atmosphere and isolate the aerosol contribution either directly in the case of ground-based photometers, or by inverting the radiative transfer equation in the case of space-borne instruments. The measurement of transmission needs to be corrected for the gaseous absorption, which uses assumptions about the atmospheric composition (Holben et al., 1998; Kaufman et al., 2002). Modern instruments take measurements at several wavelengths to derive the Angstrom Exponent.
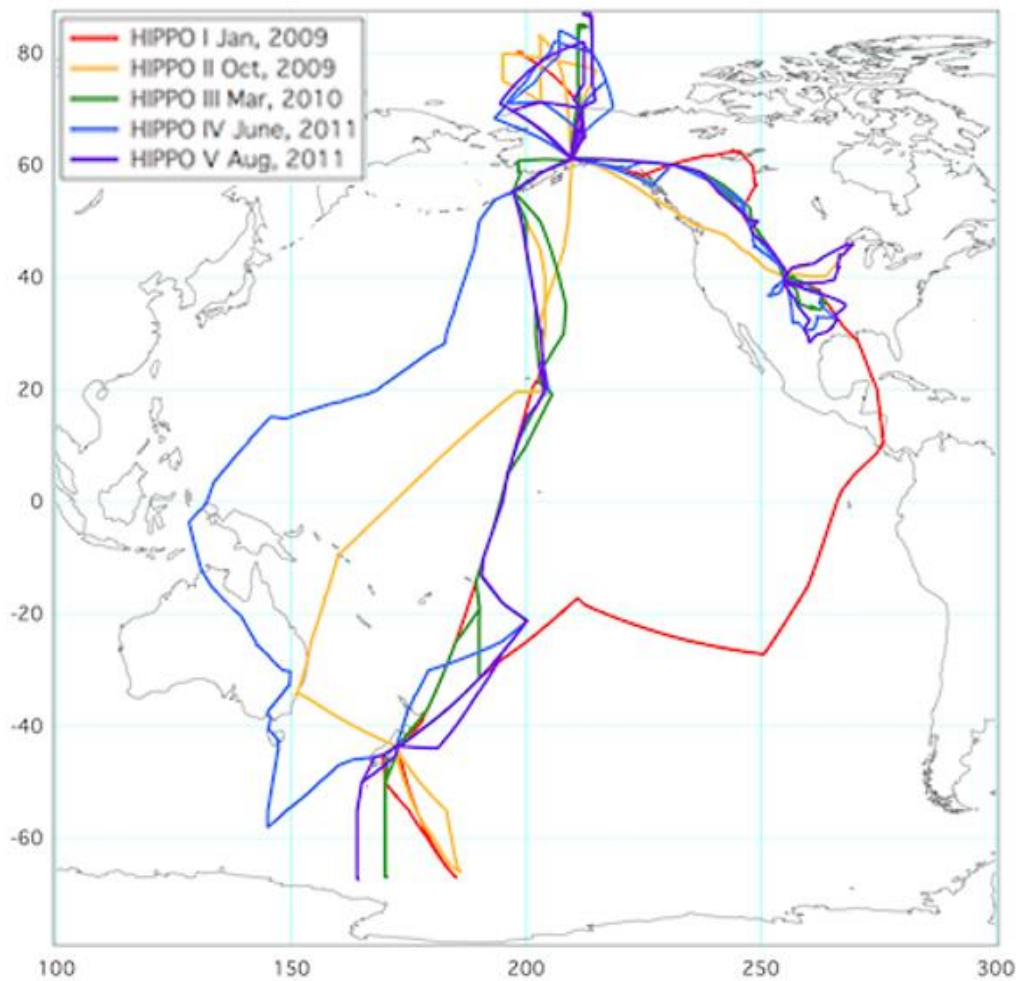
Figure 2-6 - Map of flight paths taken by HIPPO flights during all 5 phases. Figure taken from (NOAA & CCMI working group, 2017)

The Aerosol Robotic Network (AERONET) retrieves the AOD and AAOD at several wavelengths at over 280 sites throughout the world (Holben et al., 1998). The advantages of AERONET include the high frequency of retrievals, the spatial spread of sites and the ability to create long time series at a single site. This can be used for both model development, and validating new satellites. Like other in-situ surface measurements, the consistent observations from AERONET can be used to determine trends in aerosol levels through time (Kaskaoutis et al., 2012; Li et al., 2014), but importantly, also give an indication of the total loading of aerosol in the entire atmospheric column. AAOD and SSA are obtained from sun photometers through inversion techniques. These take measurents of the radiance in an almucantar plane at several wavelengths, looking away from the sun (Dubovik et al., 2002). Determining the

absorption requires measurements of irradiance from a minimum of four different angles and at four different wavelengths to give enough information for the inversion problem to be over determined. These measured transmissions contain scattering from several sources, including reflections from land and water. By subtracting approximations of the reflectance from land and water surfaces, and Rayleigh scattering additions from these measurements, aerosol optical properties can be derived (Dubovik et al., 2006; Dubovik & King, 2000). The full equations for the inversion are based upon a series of a priori constraints, which are a set of values that ensure that the output from the equations is both scientifically possible, and the most likely to be a true reflection of the aerosol properties. These equations are used to determine the particle size distribution and particle refractive indices, from which absorption can be derived (Dubovik & King, 2000; Holben et al., 1998). Therefore, for accurate results, retrievals are screened for days where aerosol is homogenously spread around the instrument, the sky is clear and AOD is high enough to give a clear signal that is outside instrumental noise (Holben, 2006).

Measurements of AAOD and SSA from satellites are also available. These are derived from the aerosol absorption index (AAI) which uses the spectral sensitivity of absorbing aerosol at ultra-violet wavelengths to separate their effects on radiation from surface reflectance, Rayleigh scattering and cloud scattering (Torres et al., 1998). This technique of measuring aerosol absorption is significantly better than using retrievals in the visible or infra-red spectrum, which are highly sensitive to surface albedo and water vapour (Torres et al., 2007). Some satellites with modern algorithms can use the same data to determine the height of absorbing aerosol, and where it is in relation to cloud (De Graaf et al., 2012; Peers et al., 2016). Satellites also have the advantage of being able to sample larger areas than ground based measurements. Satellite sampling better represents what climate models do. However, sampling from satellites is non-continuous and contains errors and uncertainties that exceed those from ground-based sites (Levy et al., 2007). Whilst satellite retrievals are exceptionally useful for case studies of aerosol plumes and spatial trends in aerosol, we do not use them here due to the large uncertainties associated with them.

Throughout this work, we use level 2 inversion products from AERONET for AAOD and SSA values. This is the quality controlled product released from AERONET, with errors in SSA of ±0.01 (Holben et al., 2006). However, to achieve this level of accuracy, the restrictions on

retrievals are much tighter. Two of the main restriction are that the AOD must be greater than 0.4 at 440 nm, and that the solar zenith angle must be greater than 45°, as these conditions provide a thicker layer of aerosols so that the accuracy of the retrievals and absorption algorithms is more accurate (Holben et al., 2006). This both limits the time in which measurements can be taken to just morning and evening, and only allows observation of large AOD events. It is therefore difficult to use AERONET absorption products to constrain background aerosol optical properties. Figure 2-7 shows the change in radiation that occurs in modelled clear sky conditions due to the effect of AOD. This was computed by calculating a linear equation for the relationship between AOD and outgoing radiation in clear sky conditions in the model, which is significant at a 99.9% confidence interval when calculated using a two-tailed p-value. To ensure that the effects of day length and longitude are not included, this was done over a 10-degree latitude band at the equator for one month at a time only. The equation was then used to determine the total radiation change from each grid-square each day due to AOD. These were then cumulatively added with increasing AOD. Comparisons shows that around 85% of aerosol radiative forcing occurs from when the AOD is less than 0.4. This result is backed up by other studies which find similar percentages of the aerosol and BC forcing which occur when the AOD is less than 0.4 (Andrews et al., 2017; Ogren & Andrews, 2014). This means that AERONET level 2 absorption products retrievals are unable to give us information on the majority of the radiative effect of aerosols, and so good comparisons with these products does not guarantee that predictions of aerosol forcing are accurate.

Each AERONET site conveys information on a single column measurement directly above the site, and local characteristics and emissions can differ from the large-scale aerosol characteristics. Satellites are able to cover much larger areas at regular time intervals but lack the same temporal resolution of AERONET, and are considered to lack the accuracy of AERONET AOD direct measurements. Figure 2-8 shows the location of AERONET sites which provide at least two AAOD retrieval over the period 2006-2008, the period simulated by HadGEM3-UKCA in this work. The location of sites is biased towards more economically developed countries, with many more sites in Europe and North American than in Africa, South America or Central Asia. It is therefore not meaningful to compare global averages from these sources and evaluation needs to be done on a regional basis.
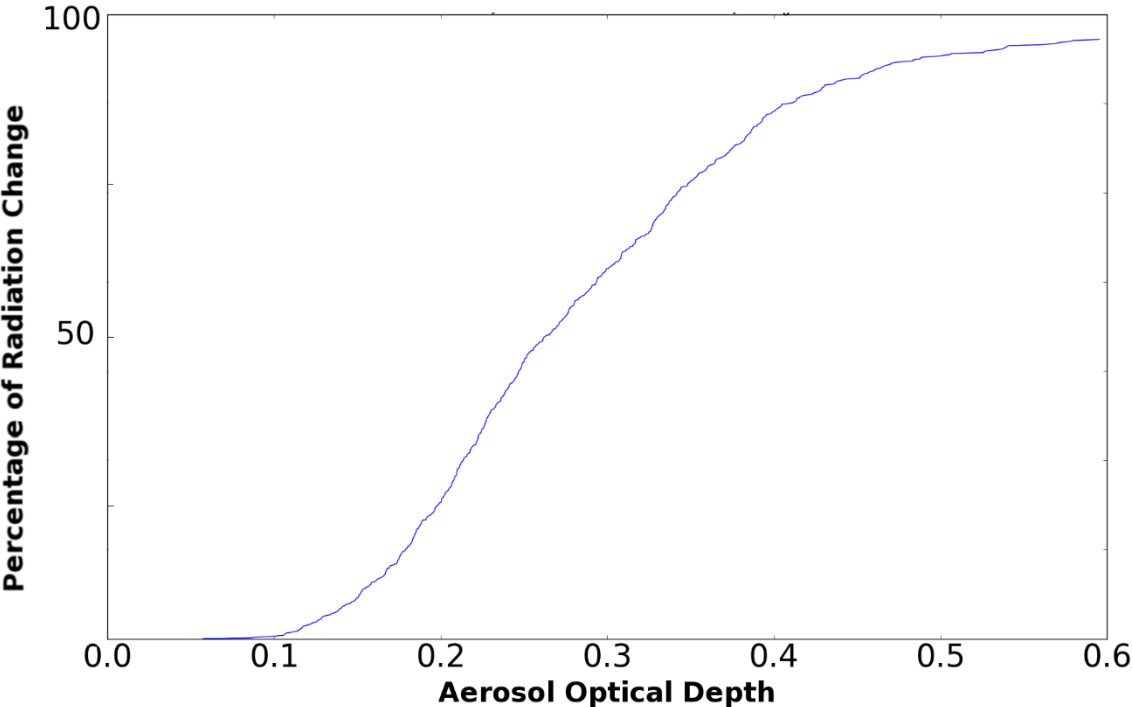
Figure 2-7 – Cumulative percentage changes in the total clear-sky outgoing radiation around the equator due to aerosol optical depth at 550 nm, calculated in HadGEM3-UKCA over a 3-year period.
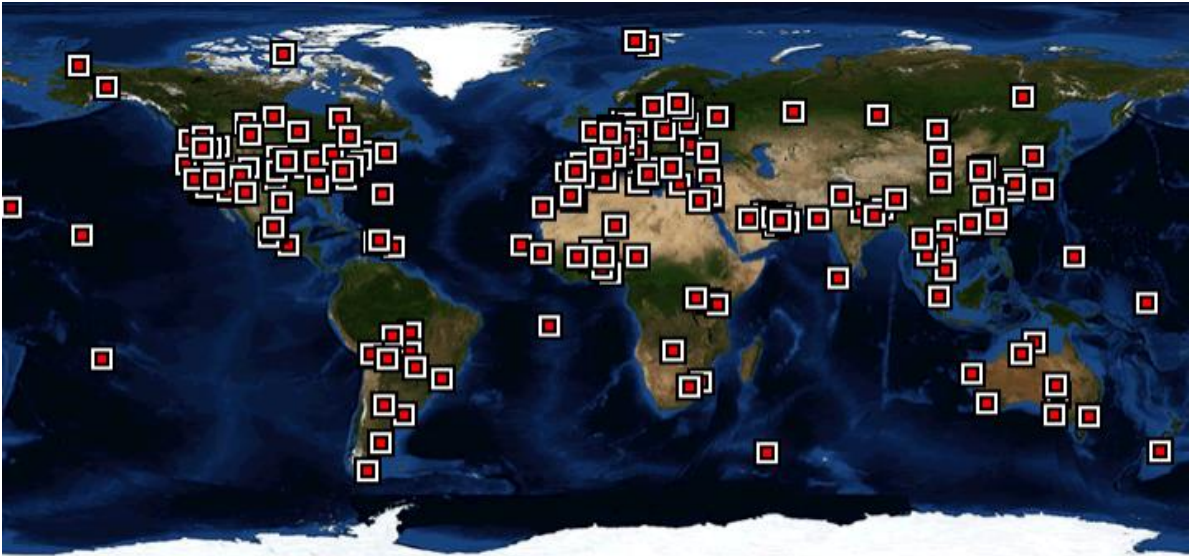

Figure 2-8 - Location of AERONET sites which provided retrievals and measurements of Aerosol Optical Depth and Absorbing Aerosol Optical Depth between 2006-2008.

2.3 Methods of measurement/model analysis

2.3.1 Surface Concentrations and Aircraft Measurements

Comparing the models to observations naively can result in the introduction of bias or errors purely from the method of comparison. Comparisons at timescales which are equal between both model and observations are important, as comparing a daily mean model value to a monthly observation would create a bias based on the comparison. Correctly comparing values on the same temporal scale can reduce sampling errors by a factor of 3 (Schutgens et al., 2015)The in-situ surface concentration measurements occur consistently enough throughout the month to allow a calculation of a monthly average which is similarly calculated to that which is created by the model. Each monthly calculated value at a site is compared to a co-located model gridbox value. This method reduces the effect of temporal biases, but cannot reduce the effect of spatial sampling. Where possible, the same month and year in model is used for comparison. Where it is not, a monthly 3-year average is used for that gridbox and site for comparison. We then use Equation 2.3 to determine the regional mean factor (MF) of overestimation:

$$\text{MF} = e^{\overline{\left(\ln\left(\frac{Mod_n}{Obs_n}\right)\right)}} \qquad \text{Eq 2.3}$$

Where Obs_n is an observation, Mod_n is a co-located modelled value, and the mean is taken over all sites within a region over the 3-year period. This is similar to a normalised mean bias factor, which allows a mean to be taken whilst maintaining the symmetry of the factor (for example, the mean factor of a factor of 2 and factor of 0.5 is 1). However, our method treats over or underestimations of high and low observations equally, whereas the normalised mean bias factor, which sums all observations and modelled values together before taking the natural log, is weighted towards the ability of the model to compare large observational values. We apply this equation on a continental basis, due to the geographically scattered nature of the observing networks, BC observations are grouped by continent (Europe, North America, South America, Asia). We make exceptions for sites which are above 60° North (Arctic) and those located on islands in the Pacific and Atlantic Oceans (Oceanic region).

Because surface OC concentrations are measured only in Europe and North America, sites are further split into sub-regions, which are based upon the expect aerosol emission type. North American regions are shown in Figure 2-9, whilst European sites are split between Arctic (greater than 60º North), Northern Europe (greater than 45º North), and Southern Europe. This method should allow differentiating between the ability of the model to replicate OC from boreal burning sources, urban sources and agricultural burning separately. A mean factor of overestimation is calculated in the same way as is done for Surface BC concentration comparisons.
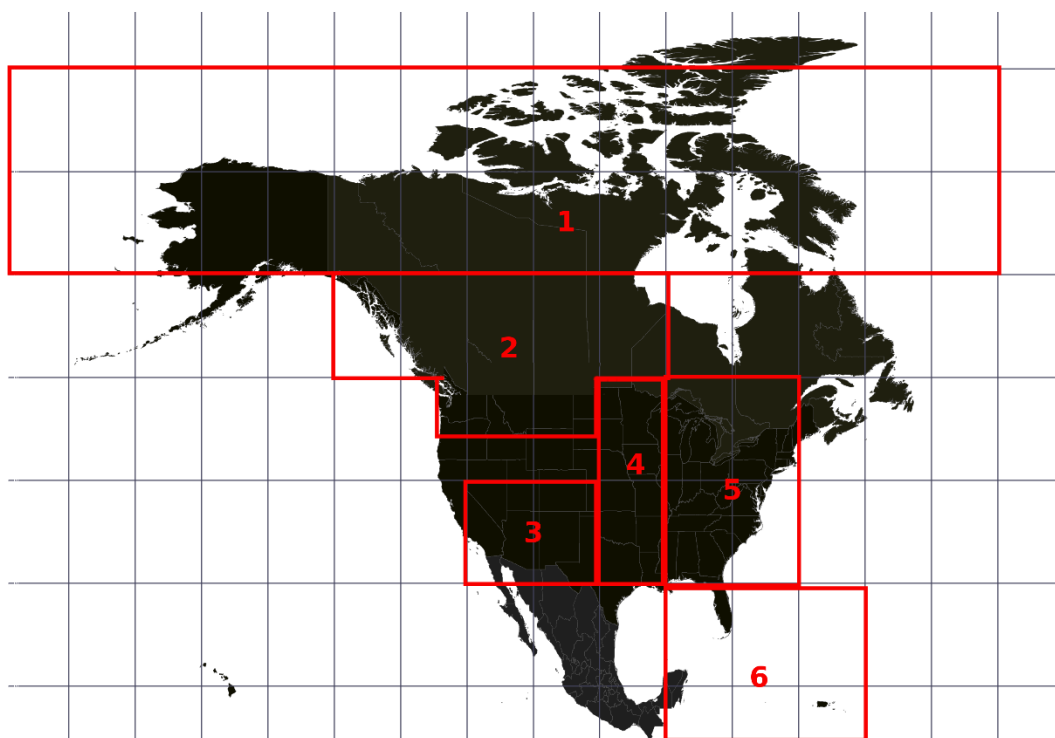
Figure 2-9 – Map of North American regions used for splitting Surface OC concentration comparisons, based upon local aerosol emissions. 1) Arctic, 2) Coniferous North America, 3) Desert North America, 4) Grassland North America, 5) North Eastern USA, 6) Caribbean

Aircraft measurements differ depending on the campaign. For HIPPO and EUCAARI, a direct comparison between each aircraft measurement on a flight and the corresponding monthly mean BC MMR in that grid-box is made. The bias between the two is calculated at each model level by:

$$bias = (\overline{Model} - \overline{Observations}) \qquad \text{Eq 2. 4}$$

This method allows a comparison of the ability of the model to simulate the vertical profile, by combining the observations by the model levels. It allows a comparison at each layer, regardless of the number of aircraft observations taken. For the ARCTAS, we use data products in which vertical profiles have been collated for individual areas on each campaign. These are compared to the monthly averages in the same way as HIPPO and EUCAARI are. In the case of campaigns spending several consecutive days in the same region, these are combined. In the case of campaigns returning to areas in different months, such as in the HIPPO campaign, the results are separated. In all other cases where a campaign straddles two months, the results are still combined. We use aircraft campaigns that analyse the background ambient aerosols, meaning that the error from sampling against monthly model mean rather than a daily model mean will be less. Ideally, hourly comparisons would be made with each flight point; however, not only would this would lead to a huge increase in the amount of model data needed and the time taken to run the model, the model also does not account for emission changes on a timescale less than monthly and so cannot represent the hourly or daily variability correctly. Therefore, hourly output from the model will not accurately represent the hour used for observations.

2.3.2 AERONET comparisons

Daily AERONET AOD and AAOD are compared with same-day, co-located model values, to avoid errors from the temporal sampling of the model. From this, we determine a mean factor of overestimation in the magnitude of AOD and AAOD in the model compared to observations on a continental scale, with a further region for oceanic comparisons (Arctic, Europe, Asia, Africa, North America, South America, Australia and Oceanic). We also compared continental values on a 30-day period. This will determine the model ability at replicating AOD and AAOD the correlation and variability on a monthly timescale in each region, as this best matches the monthly emission datasets in the model, which inhibits the ability of the model to match variability on a shorter timescale.

The methods of sampling used for AERONET described in the previous section makes comparing directly with a model value that is sampled identically difficult (Schutgens et al., 2015). Furthermore, the requirements devised for level 2 absorption retrievals in which daily averages can be created from a much shorter period of time in the day, and optically thin events cannot be retrieved are even more difficult to replicate in the model. This presents a

problem when trying to compare both AAOD and SSA daily averages for both model and AERONET, as the AERONET daily average is not the same as a 24-hour average from the model. This sampling difference leads to AAOD retrievals from AERONET overestimating the daily average by up to a factor of 2 (Andrews et al., 2017).

In an attempt to minimise these problems, both model and AERONET AOD and SSA retrievals were analysed by comparing the SSA at different AOD in a number of regions based upon the dominant aerosol type. This requires more specific regions than the continental scale regions used for AOD and AAOD comparisons, in order to ensure similar dominant aerosol types. Figure 2-10 highlights six of these regions which we use throughout this study. These regions were chosen for three reasons. Firstly, they all are regions where there are significant levels of CA in the atmosphere, but low levels of dust. This means that whilst are large amounts of observations from the Sahel and Saharan regions of Africa, the aerosol loading there contains a large amount of mineral dust, and errors in AAOD and SSA cannot be attributed solely to carbonaceous aerosols. Therefore, these areas are not used for comparisons. Secondly, the regions shown contain some AERONET sites, as the spatial distribution of AERONET means that some areas have little to no coverage. Thirdly, the selection of regions convey a wide range of different carbonaceous aerosol source emissions. Regions 1 and 2 (North East USA and Northern Europe) are regions of developed urban emissions, whilst region 3 (Industrial Asia) is a region where emission are predominately from developing cities and less-regulated industry. Region 4 (South East Asia) highlights mixed urban and biomass burning emissions. Regions 5 and 6 (Scrubland Africa and South America) highlight purer biomass burning emissions.
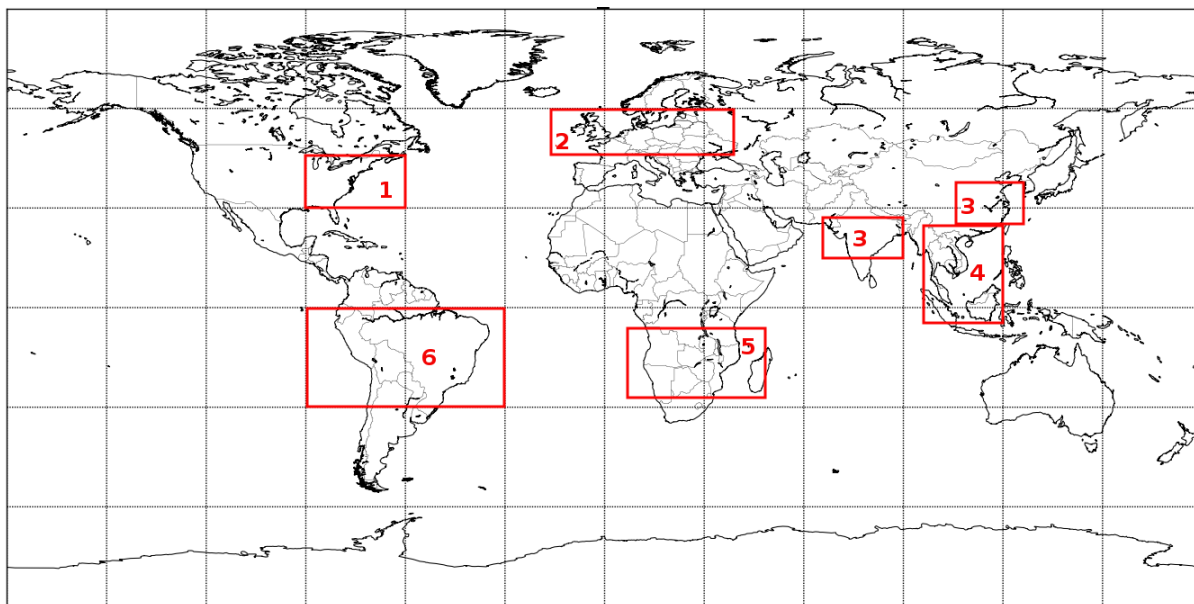
Figure 2-10 - Split of regional sectors used in this study for comparisons with single scattering albedo and Angstrom exponent, covering a variety of black and organic carbon sources. 1) North East USA, 2) Northern Europe, 3) Industrial Asia, 4) South East Asia, 5) Scrubland Africa, 6) South America.

Figure 2-11 shows the frequency distribution of SSA at a given AOD for both the model and observation in 6 of these regions. In the model, as AOD increases in a region, the range of SSA values decrease to a singular value. When AERONET is analysed in the same way with AOD greater than 0.4, the SSA has little variability. This suggests two things: Firstly, variability in SSA is negatively correlated to AOD, and secondly, AERONET level 2 retrievals constrains only high-level AOD events with limited variability in SSA compared to the model. This near-singular value of SSA could be linked to a singular aerosol composition, which is constant during high AOD events. As the choice of region is based upon the emissions of a similar aerosol source, it is likely that optically thick events are caused by these dominant aerosol types. A singular composition would guide a direct comparison between modelled and AERONET retrieved SSA, as the SSA of all optically thick events should be the same in both the model and AERONET. As AOD increases in the model, the variability of the SSA reduces. This further suggests that the singular value of SSA seen in AERONET is due to the restriction of a high AOD, and is not simply because of low variability in the region.

Figure 2-12 shows the frequency of Angstrom Exponent (AE) values at differing AOD for both the model and the level 2 AERONET product. The variability of AE in AERONET is lower than

in the model. The model shows a reduction in the AE variability at high AOD, suggesting that the near-singular value of AE is because of the requirement for high AOD. These two figures suggest that both AERONET and high value AOD in the model have near singular SSA and AE.

Figure 2-13 is taken from Russell et al., 2014, and shows that different combinations of SSA and Angstrom Exponent (AE) can be used to identify different combinations of aerosol which are synonymous with different emission sources. They use the absorbing angstrom exponent (AAE), which is a measure of the change in AAOD over wavelength, and SSA from AERONET retrievals compared with other observations of aerosol species recorded at or above the sites to determine the seven classifications of aerosol type and their characteristics in both AAE and SSA. These types shown are based upon commonly emitted aerosols. The work further shows that, these types can be specified through just the SSA and AE alone as well as through SSA and AAE.

The problem however is that by retrieving AAOD only when AOD is high, any temporal average of AERONET level 2 inversion products would be overestimated because the background is not observed. Because our model only changes emissions on a monthly timescale, comparing on shorter timescales is not appropriate. For example, where aerosol emissions are highly time dependent, such as in biomass burning areas, AERONET would only retrieve AAOD on days where there are large AOD from the fires. However, the model spreads emissions out, giving a more constant, but lower AOD and AAOD. However, because both the model and AERONET show near singular SSA and AE values in regions, as shown in Figure 2-11 and Figure 2-12, we can fit the composition to a particular emission source. The model has nudged winds and the comparison is done on a daily basis, so large scale transport of air masses is similar to actual synoptic conditions (Telford et al., 2007). Therefore, the same aerosol type should be present in both model and AERONET observations, and we assume that that aerosol type is dominant, even if amounts are underestimated in the model because of the spreading of the emissions over the whole month. This means that underestimation of AOD and AAOD due to the sampling bias in the observations are not an issue, as SSA and AE are nearly constant regardless of AOD because the composition of aerosol is the same. Any difference between SSA and AE in the model and observations is due to model errors, rather than sampling errors.
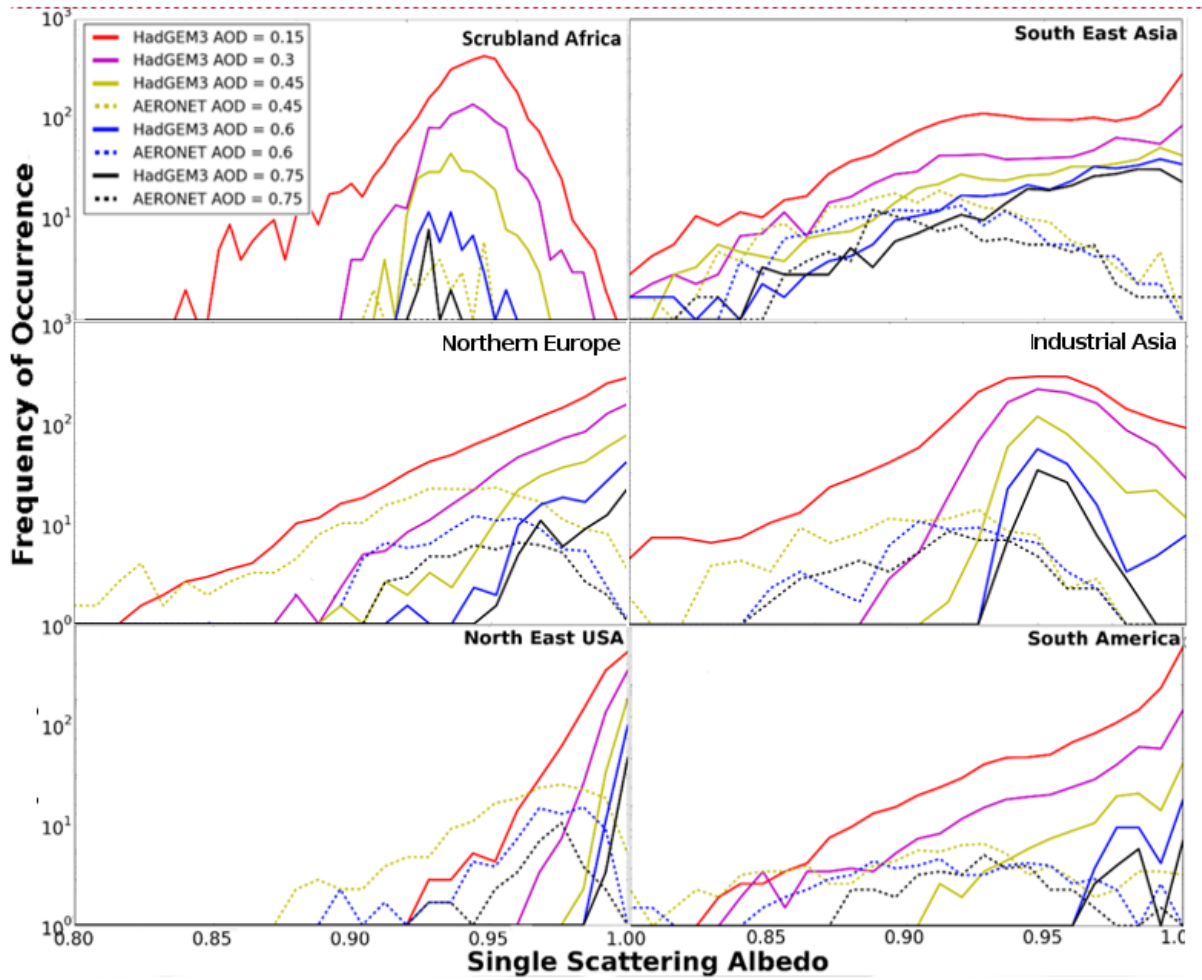
Figure 2-11 - Frequency of single scattering albedo found at differing aerosol optical depth for both the model (solid lines) and AERONET retrievals (dashed lines) between 2006-2008 in 6 regions with different aerosol burden characteristics.
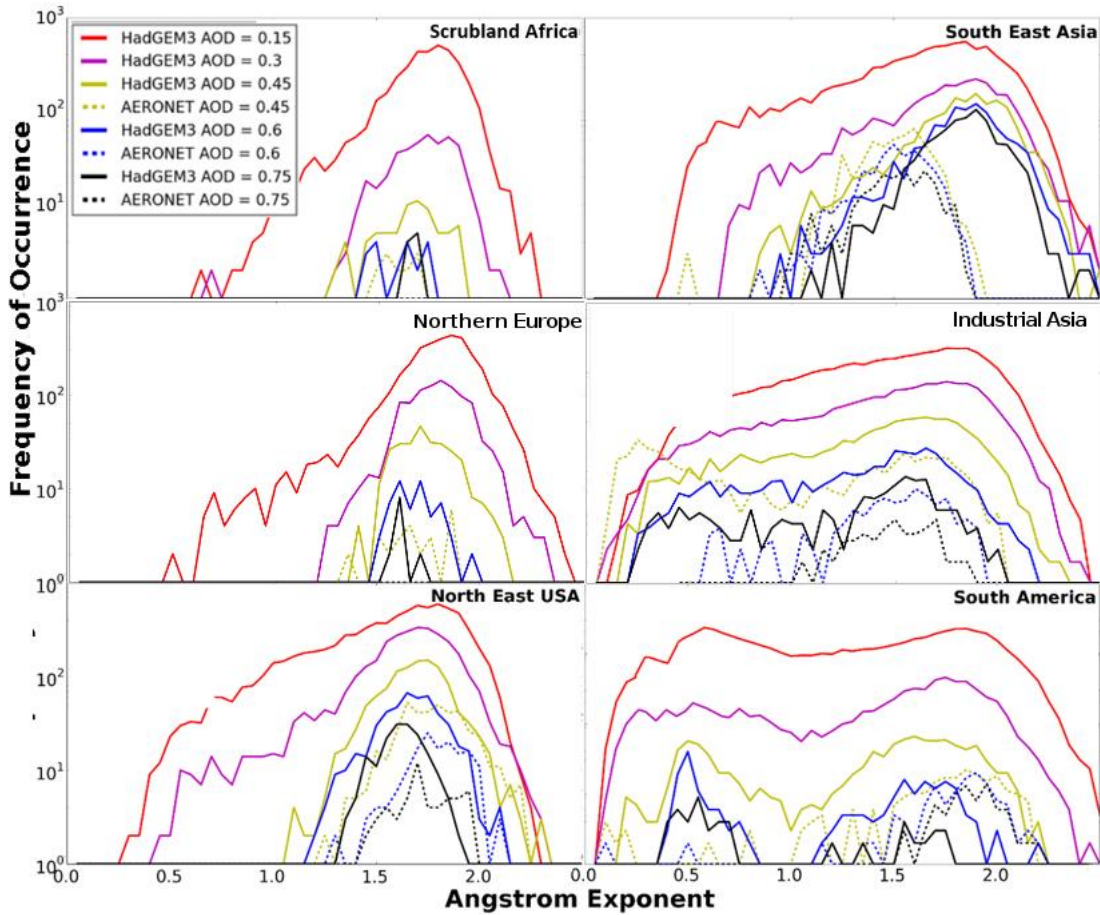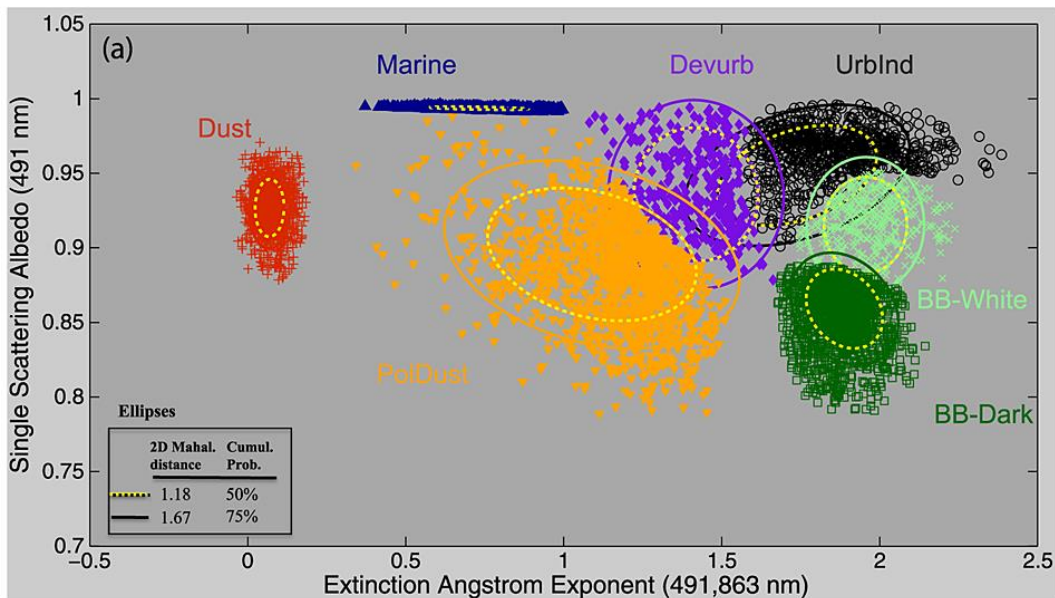
Figure 2-12 - Frequency of Angstrom Exponent found at differing aerosol optical depth for both the model (solid lines) and AERONET retrievals (dashed lines) between 2006-2008 in 6 regions with different aerosol burden characteristics.

Figure 2-13 – Identification of aerosol type as a function of angstrom exponent and single scattering albedo. PolDust = Polluted Dust, Devurb = Developed Urban emissions, BB = Biomass Burning emissions, UrbInd = Industrial Urban emissions. Taken from Russell et al., *(2014)*

We use this benefit of the sampling to compare AERONET with same day, co-located model values within the regions of where AE and SSA are near-singular and the aerosol burden sampled is therefore of a similar aerosol composition. By plotting both on axes of SSA and AE, we can directly compare the two and interpret any differences.

2.3.3 Potential Errors and Uncertainties

Despite using observations as a true reflection of the state of the atmosphere in this study, it must be understood that there are errors and uncertainties associated with all observations. For concentrations or mass measurements, the differences in instrumentation, method and setup will give a biases and errors when compared with each other, or with the model (Kondo et al., 2011; Slowik et al., 2007). Even identical instruments have been found to give differences in readings of up to 10% if calibrated in different ways (Laborde et al., 2012). For this reason, we accept that a perfect comparison between model and observation is unlikely, and that our work aims to improve the model within realistic uncertainties, and not to refine the model towards a specific set of observations. However, as discussed earlier in this chapter, we find that comparisons between model and observations for AERONET and BC concentrations can carry uncertainties of up to 160% purely due to the effect of the spatial scale difference between the two (Schutgens et al., 2016). Further uncertainties suggest that for direct comparisons, total uncertainties on the comparison may be greater than 200%. This is not including any biases, such as those seen in aethalometers compared to SP2 instruments. Consequently, absolute comparisons on a site-by-site basis may not be useful, but contrasting regions and seasons should hold information about CA.

2.4 Quality of Carbonaceous Aerosol simulations by HadGEM3-UKCA

In this section, we use the control simulation to assess the current model performance against observations and retrievals. This analysis of the control simulation forms the basis on which we will perturb the physics and parameters in order to improve the model in later chapters.

Table 2-5 shows the key modelled variables relating to BC and OC and the values within the model, such as lifetime, deposition and burdens, and how they compare with AeroCom models. The burden of BC in HadGEM3-UKCA is 0.1 Tg, whilst the OC burden is 9.5 times greater. Both burdens are at the lower end of the AeroCom ranges. BC is more likely to be removed through wet deposition than dry deposition, although there is not much difference.

However, OC is 3 times more likely to be removed through wet deposition than dry deposition. The percentage of removal through dry deposition exceeds the percentage in other AeroCom models. The lifetime of BC is 4.14 days, whilst for OC it is 3.99 days. These are below the range of BC and OC lifetimes suggested in AeroCom. However, since the AeroCom I submissions, literature now suggests that BC lifetimes below 5 days give better comparisons with observations (Samset et al., 2014). Therefore, we believe the lifetime in the model is still scientifically justifiable even though it is outside the range of AeroCom I models.

	BC	OC	AeroCom I Range for BC	AeroCom I Range for OC
Primary Emissions (average 2006-2008)	8.91 Tg yr^{-1}	36.11 Tg yr^{-1}	4.3–22 Tg yr^{-1}	17–77 Tg yr^{-1}
Total burden	0.10 Tg	0.95 Tg	0.1-0.4 Tg	0.9 – 1.8 Tg
Dry deposition	4.30 Tg yr^{-1} (47%)	19.12 Tg yr^{-1} (26%)	3% - 38%	3% - 23%
Wet deposition	4.81 Tg yr^{-1} (53%)	54.99 Tg yr^{-1} (74%)	62% - 97%	77% to 97%
Lifetime	4.14 days	3.99 days	5.5 to 15 days	4.2 to 11 days

Table 2-5 – List of key BC and OC numbers for the area-weighted average burden, deposition and lifetime in the control simulations, over the 3 years of the simulation. AeroCom ranges are taken from (Textor et al., 2006)

2.4.1 AOD

The AOD is affected by all aerosol concentrations, including CA. The effect of CA on the AOD varies depending on the location and time of year. In biomass burning areas, CA may make up the majority of the aerosol available, whilst in urban regions, CA may be responsible for only a small proportion of the aerosol. Figure 2-14 shows the comparison of AERONET AOD with daily co-located modelled AOD from HadGEM3, with a 3-year average mean factor for

each region. The model and observations show a good positive correlation, although analysing all sites together shows slight underestimation when high AODs are observed, and overestimations in the model at low AOD observations. However, the spread of individual modelled AOD can be as much as an order of magnitude higher or lower than the observed AOD. In South America, AODs greater than 0.1 are underestimated by an average of 90%, whilst AODs below 0.1 are overestimated in the model by an average factor of 4. The largest AODs in both the model and observations come from Africa and Asia. The AOD in most regions in the model is underestimated compared to AERONET, with AOD in Europe, North America, Asia, Africa and the Arctic underestimated by between 33-50%. Model values of AOD in Australia and South America underestimate observed values by less than 20%. In Oceanic regions, the modelled AOD is higher by 60% compared to AERONET AOD.
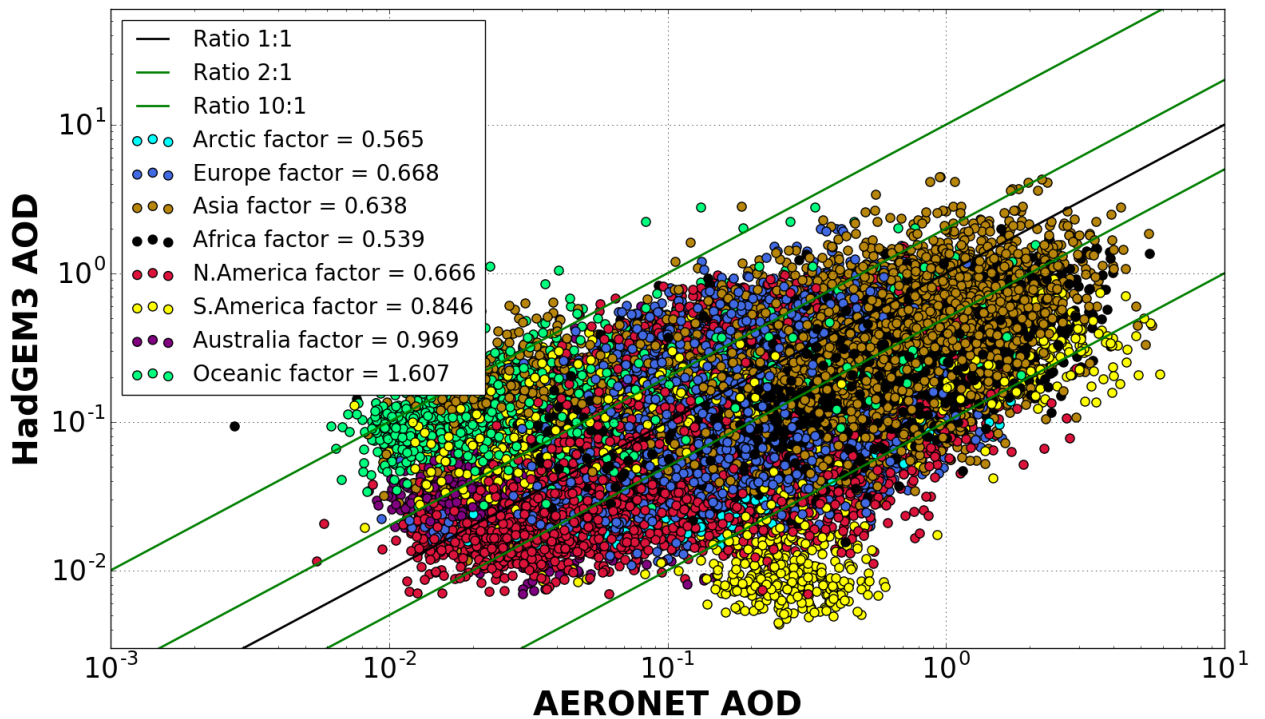
Figure 2-14- Comparison of daily aerosol optical depth from AERONET sites against time-and-location matched aerosol optical depth from HadGEM3-UKCA for the period 2006-2008, coloured by differing regions. Values given are the mean factor of model:observation ratio as discussed in the methodology.

The global pattern shows a lower level of variability of AOD in the model compared to observed values, shown in Figure 2-13. The effect of the biomass burning season can be seen in the spread of values in Africa, Oceanic and South America, with groups of high AODs separate from other comparisons in the region, often underestimated in the model.

Figure 2-15 shows the correlation and normalised standard deviation of the control simulation compared to AERONET AOD on a monthly timescale. The correlation between the model and observations is significant at the 99.9% confidence interval using a two-tailed p value in most regions, and especially good in North and South America, where correlation is above 0.9. The correlation is weakest in Asia, at 0.23, but this is which is only significant at the 90% confidence interval. The model underestimates the variability of AOD compared to observations, even on a monthly timescale, with regional differences. The standard deviation of AOD in the model in Oceanic and Asian regions is similar to that seen in the observations. However, in South America and Australia, the standard deviation of the model is under 20% of the standard deviation of the observations.

The decreased spread of model values can potentially be attributed to the spatial and temporal sampling of the model compared to AERONET. Whilst AERONET samples a singular point on a daily average, the model samples a whole gridbox, which is averaged over a large area. This will inevitably dampen the small-scale increases and decreases in AOD seen by AERONET, and reduce the temporal variability in the model compared to the observations. The model also uses the monthly BC and OC emissions values, so does not pick up the exact daily variability in emissions throughout a month. This is particularly an issue in biomass burning regions, where fires may only burn and emit aerosol for a few days at a time. In this case, the model will emit aerosol evenly throughout the month, underestimating the emissions on the days the fire was burning, but also overestimating the emissions on days when the fire was not burning. This acts to reduce the variability in the model compared to daily AERONET averages.
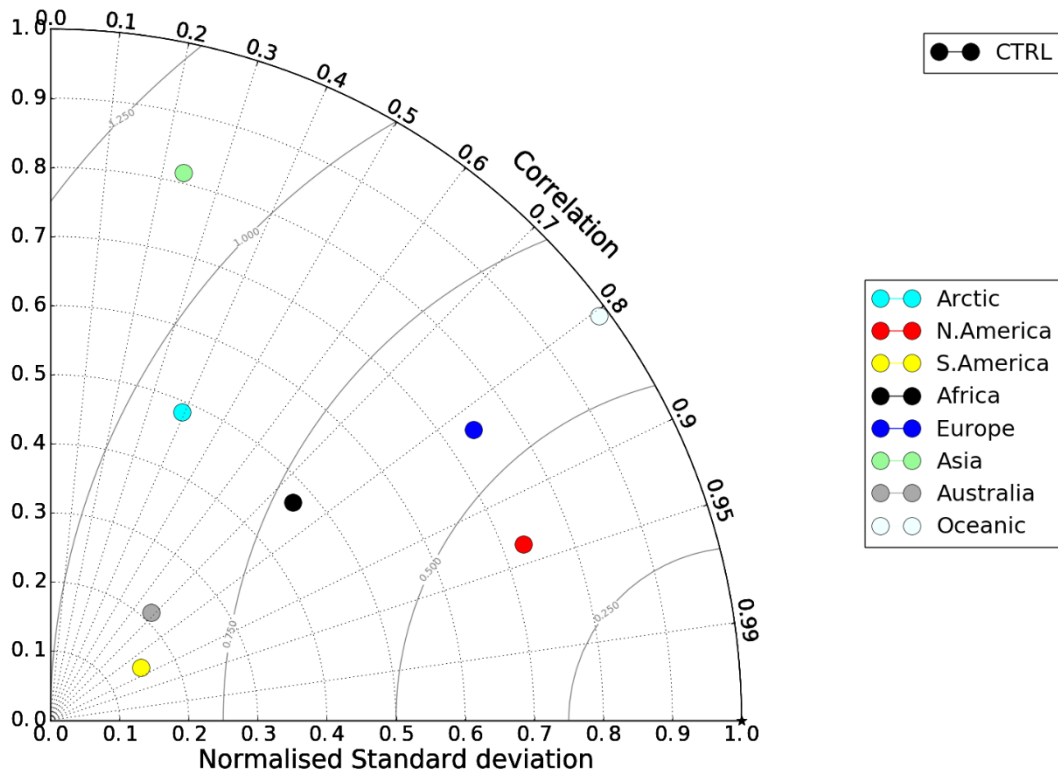
Figure 2-15 – Taylor diagram showing the temporal correlation and normalised standard deviation (the standard deviation of simulation over the standard deviation of the observations) of the CTRL simulation and AERONET AOD at 550 nm over a 30-day time scale, for the period 2006-2008. Colours denote different regions. A perfect model would be plotted at (1,1).

Exceptionally low normalised standard deviation in South America and Australia suggests that variability is still an issue, as even if we assume a 200% increase in temporal variability from the uncertainty in sampling techniques, these areas would still underestimate variability. The good correlation of the model is a sign that on a monthly timescale and a regional spatial scale, the model is successful in reproducing the AOD. However, Taylor plots do not show model bias or mean factors compared to observations, which is also shown to be underestimated from Figure 2-14. The results show that any future changes to the model should focus on increasing AOD and the variability of AOD in the model.

2.4.2 AAOD

The AAOD measures only absorbing aerosol, which in the model, are BC and dust. Therefore, for areas where there is no dust, the AAOD is almost entirely dependent upon BC. Figure 2-16 shows the comparison of daily AERONET AAOD compared with co-located AAOD from

HadGEM3-UKCA. Correlation between the two is not as obvious as the correlation for AOD. 45% of model comparisons underestimate the AERONET AAOD by more than a factor of 2, compared with only 8% in which the model overestimates AERONET retrievals by more than a factor of 2. Grouping sites by regions show low/no visual correlation in most cases, with a lack of variability in the AAOD in Europe, Africa and North America in the model. The model underestimates the AAOD in most regions compared to AERONET. AAOD in Australia is underestimated by 80% in the model, and by between 30 – 60% in Africa, Europe, North and South America. The average AAOD in Oceanic and Asian regions of the model is similar to that of AERONET. However, in Asia, the model overestimates high AAOD, but underestimates low AAOD. In Oceanic regions, low AAOD are overestimated, but high AAOD are underestimated.
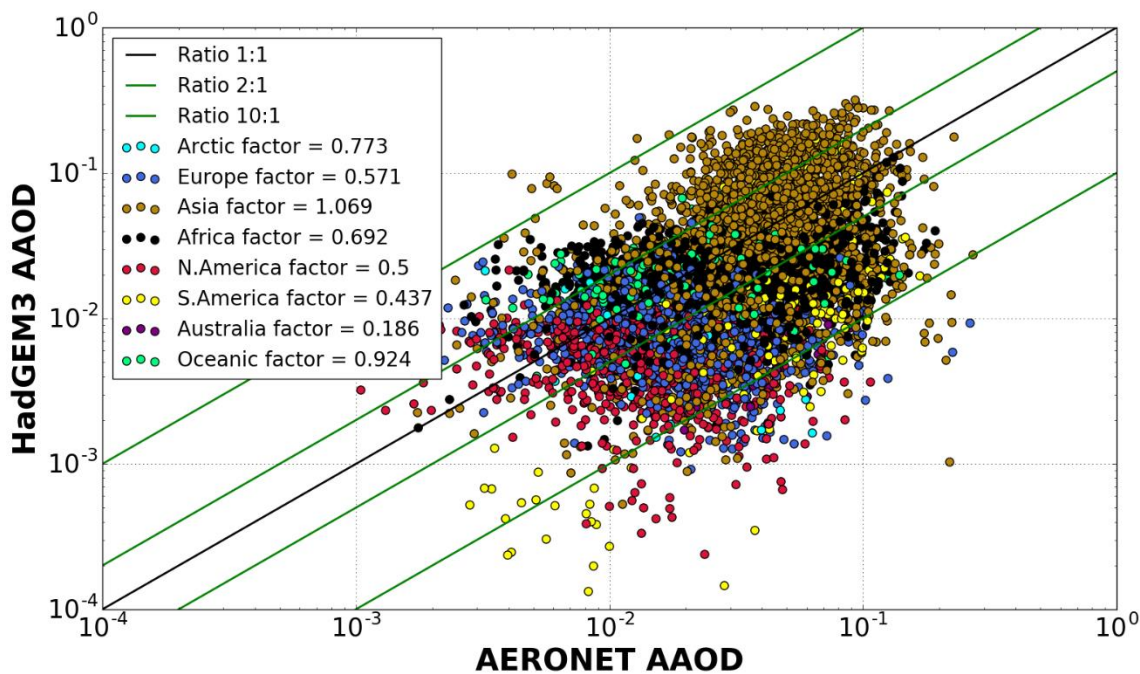
Figure 2-16 - Comparison of daily absorbing aerosol optical depth from AERONET sites against time-and-location matched absorbing aerosol optical depth from HadGEM3-UKCA for the period 2006-2008, coloured by differing regions.

The lack of variability in model AAOD could be partially due to the sampling technique, which is discussed in the previous section. Most regions follow this pattern, but still have underestimations of AAOD overall. However, in Asia, the opposite is true, where high AAOD appear to be overestimated and low AAOD underestimated in the model. Underestimations of AOD and AAOD elsewhere suggest that the reason for the model underestimating AAOD

may be due to underestimating the aerosol burden and that increasing emissions of absorbing aerosols could improve the comparisons.

Figure 2-17 shows the correlation and normalised standard deviation between AERONET AAOD and co-located AAOD from HadGEM3-UKCA on a monthly timescale. The correlation between AERONET and modelled AAOD is poor, with only sites in Africa and South America having a correlation greater than 0.4. Comparisons of AAOD in Europe and the Arctic show weak negative correlation. The correlation of AAOD in North America, Australia and Oceanic regions are also not significant with 99.9% confidence. The normalised standard deviation is below 1 in most regions, except for Asia, where the normalised standard deviation is 2.32. In North America and Australia, the normalised standard deviation is less than 0.3.
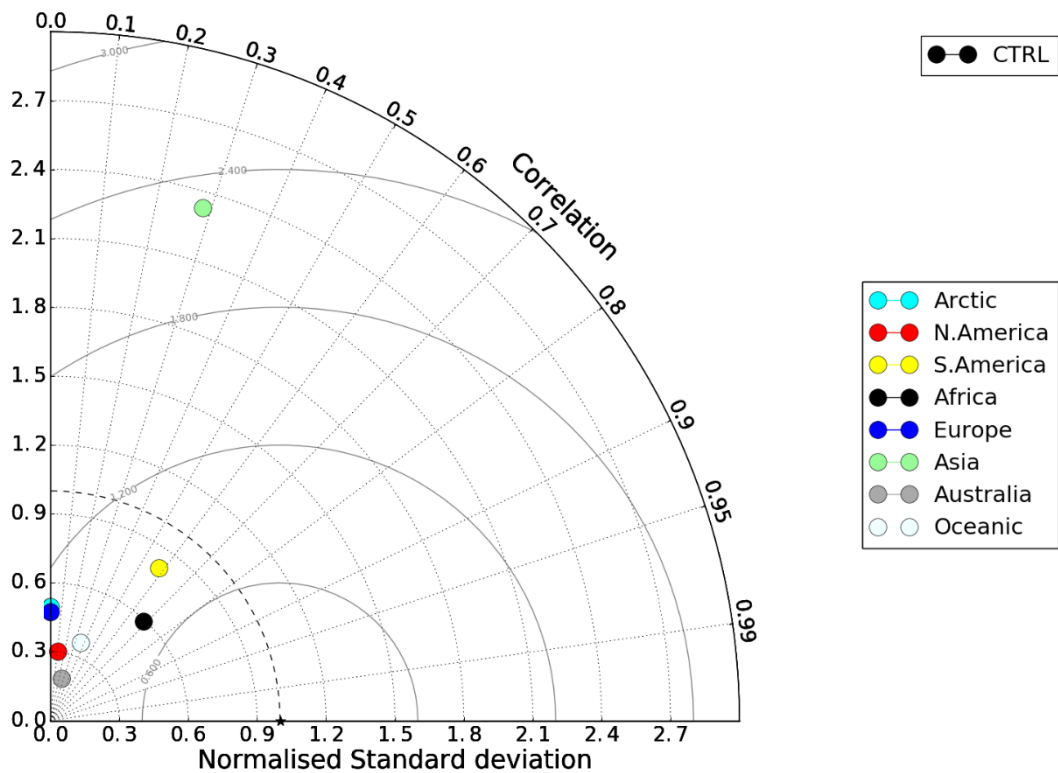
Figure 2-17 - Taylor diagram showing the correlation and normalised standard deviation of the control simulation and AERONET AAOD at 550nm over a 30-day time scale, for the period 2006-2008. Colours denote different regions.

The correlation when comparing AERONET and modelled AAOD is much lower than the correlation when comparing AOD, so AOD is much better represented in the model than AAOD. The negative correlation of AERONET and model in Europe and Arctic on a monthly

timescale suggests that there is potentially a significant problem with the current methods of modelling absorption and absorbing aerosol. In the model, both dust and BC contribute to the AAOD, but in most regions, BC is the main contributor. This shows that the model reproduction of BC is also poor, even on a monthly and regional timescale. The lack of variability seen visually from Figure 2-16 is confirmed in Figure 2-17, with the model unable to reproduce the variability of the AAOD in retrievals.

2.4.3 Surface BC and OC concentrations

Figure 2-18 compares monthly observed surface concentrations of BC aerosol to co-located model output. The comparison of model and observation shows good correlation, with a correlation of 0.36, which is significant at 99.9% certainty. Both model and observations show the highest concentrations of surface BC in Asia, with the lowest concentration levels in the Arctic and Oceanic sites. 73% of comparisons show the model underestimating the observations, with 59% of all comparisons showing the model underestimating the observed value by more than a factor of 2. Overall, the model underestimates observations in all regions by at least a factor of 2. The model underestimates surface BC concentrations in Asia and South America by a factor of 4, and in the Arctic and Oceanic regions by a factor of 7.

The correlation between the model and observations shows that the model is sufficiently replicating the spatial and temporal patterns of surface BC concentrations on a monthly timescale. The mean factor shows that the model is underestimating surface BC concentration in nearly all regions, suggesting that there could either be an issue with global emissions of BC, its lifetime, or its vertical distribution in the model. The comparisons show some resemblance to the comparisons of AOD and AAOD between model and observations, with sites that record higher levels of surface BC concentration within a region being underestimated by a larger factor in the model, which could be due to the larger scale of spatial sampling in the model compared to single point observation sites.
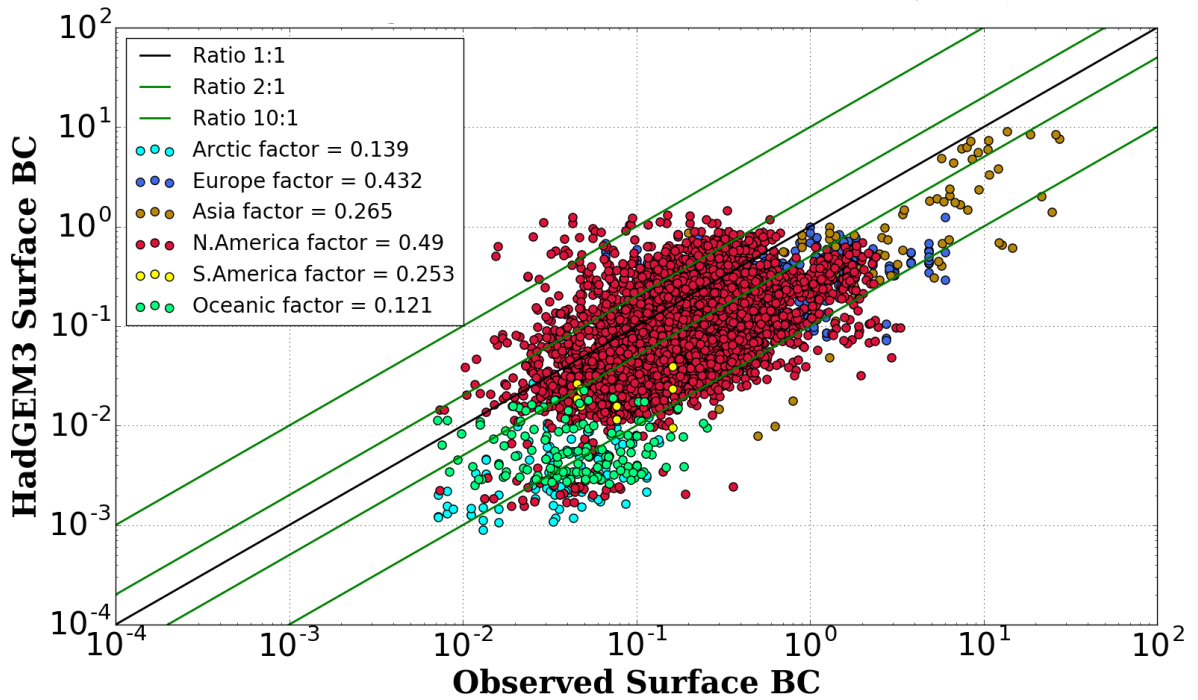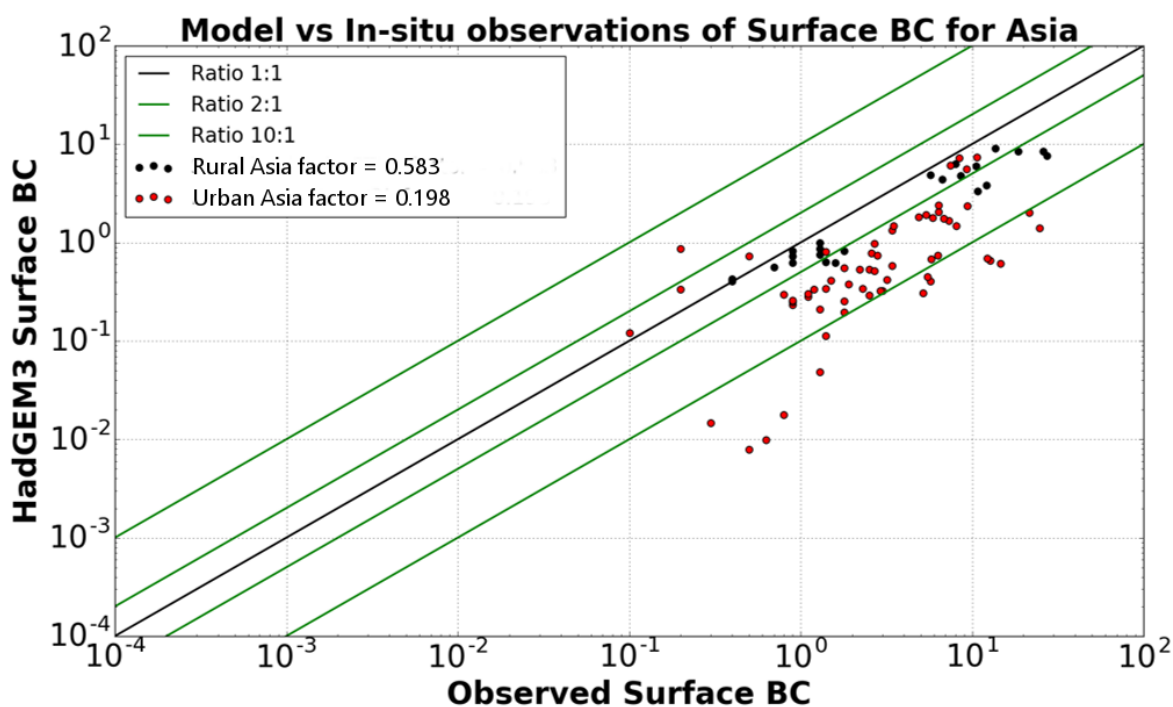
Figure 2-18- Comparison between surface concentration of BC measured at in-situ ground sites and BC surface concentration in the control simulation in μgm^{-3} between 2006-2008, with regional mean factors.

Figure 2-19 shows the comparison of surface BC concentrations between model and observations in Asia. The sites are split into two groups, Urban Asia, which are sites in areas of high urban density, and Rural Asia, which are sites in rural regions. There is a distinct difference in both the correlation and the bias of the two groups. Model comparisons to sites in Rural Asia show a much better correlation than those from urban areas. The underestimation of surface BC concentration in the model is twice as large in urban areas as it is in rural areas.

The greater underestimation of surface BC concentration in the model at urban sites compared to rural sites could be due to several reasons. Firstly, as previously discussed, the model's spatial scale is ill-chosen for resolving small scale changes in variables. Most towns and cities would sit within a model gridbox, but as the model does not resolve sub-grid scale variability, the average value across the gridbox is lower due to lower concentrations found outside of the city. At rural sites, where the concentrations are more likely to be homogeneous, the precise location of the observation site within the gridbox is less important. This would mean that surface BC concentration is still underestimated by approximately a factor of 2 in the model. A second issue could be that not enough BC is

emitted in urban areas, but that the lifetime is too long in the model, leading to a compensation of errors away from sources. We rule this out, as surface concentrations in the Arctic and Oceanic sites, which are further away from sources, show larger underestimations of surface BC concentration in the model. A final reason could be that the emissions are incorrectly located, either vertically or horizontally. We can compare the vertical profile in the model with observations, but this theory is also discounted as emissions from cities are mostly fossil or biofuel burning, which are emitted into the surface level only in the model. Therefore, if the vertical distribution of emissions were wrong, any change would only worsen the underestimation at the surface, meaning it is highly unlikely that missing BC in urban regions is at model levels above the surface.

Figure 2-19 - Comparison between surface concentration of BC measured at in-situ ground sites in Asia and BC surface concentration in the control simulation in µgm^{-3} between 2006-2008, split between urban sites and rural sites, with regional mean factors.

Figure 2-20 shows the comparison between monthly surface OC concentration observations and co-located monthly model surface OC concentration. There is a good correlation between the model and observations, with an r-value of 0.27 which is significant at 99.9%. 64% of comparisons with observations show the model to be underestimating surface OC

concentration, with 33% of all comparisons underestimated by a factor of more than 2, and 5% of all comparisons underestimated by a factor of 10. Surface OC concentrations from the model in Southern Europe underestimate observations by a factor of 3.5, whilst in Northern Europe the model underestimates observations by a factor of 8. In North America, comparisons between the model and observations are only slightly underestimated, with regional mean factors ranging from underestimations of 45% to overestimations of 8%.
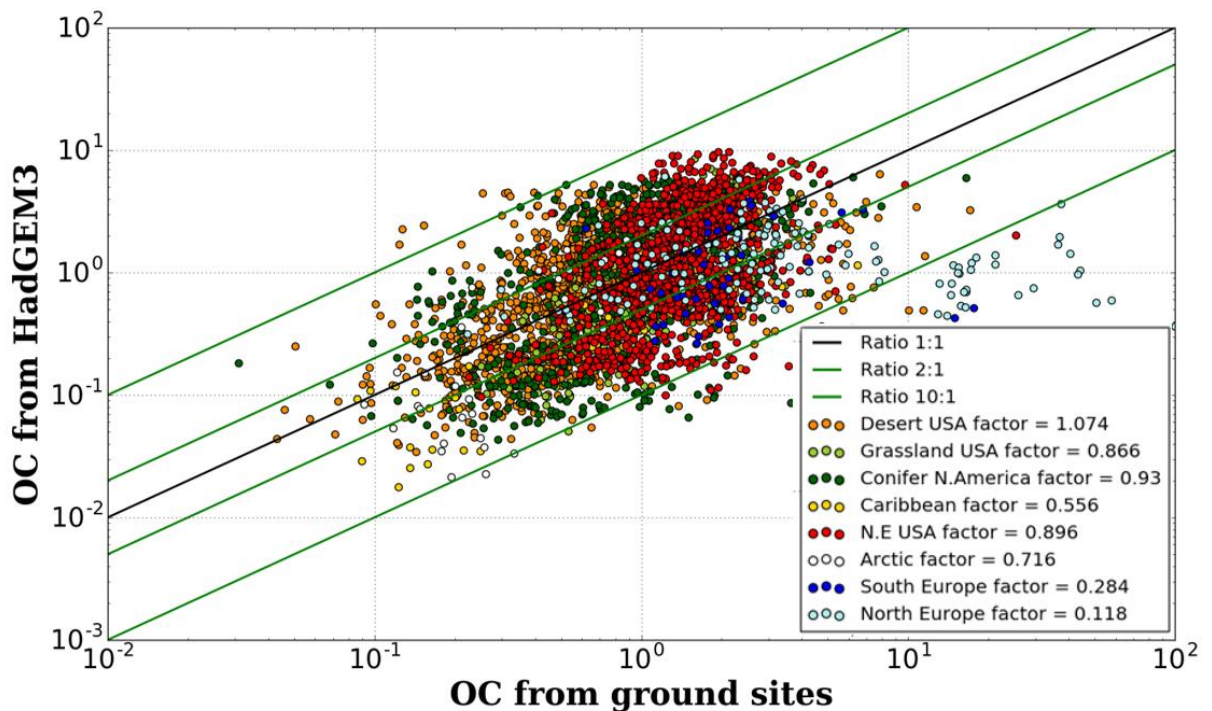
Figure 2-20 - Comparison between surface concentrations of OC measured at ground sites from the IMPROVE and EMEP, and OC simulated in the model in μgm⁻³ between 2006-2008, with regional mean factors.

The regional difference between model performance in comparison to European sites and North American sites is jarring. However, the sites have very different characteristics. North American sites from the IMPROVE network are based in national parks, mostly away from large cities and OC point sources. In Europe, the EMEP sites are in mixed locations. This includes a site in Amsterdam city centre in Northern Europe, seen on the far left of Figure 2-20, where comparisons are underestimated by over a factor of 20. Removing these sites

from the comparison brings the average mean factor for Northern Europe up to a similar level as seen in Southern Europe. As most other sites are in location where the concentration of OC is likely to be relatively homogenous across a gridbox, the conclusion from this plot is that surface OC concentration is underestimated in the model over Europe, but that there is relatively good agreement with observations over North America.

2.4.4 BC Mass Vertical Profile

In this section, we study how the model compares to BC burden observations, creating vertical profiles from flight data and simulating the observations that would be taken if the plane was to fly through a monthly average atmosphere of the model.

Figure 2-21 shows the comparison between monthly modelled BC mass mixing ratio (MMR) against observed BC MMR, arranged vertical profiles of difference by area. The MMR can be defined as the ratio of the weight of a chosen constituent to the total weight of air. This is a more stable comparison when comparing results where the density of air changes. In several regions, the comparison of modelled values to observations is good, with only minor differences in the vertical profile, with most differences in the boundary layer being less than 20% of the MMR in those regions. However, in the South Pacific Tropics, there is a constant overestimation of aerosol between 900 and 500 hPa. At lower latitudes, the phenomenon is only noticeable from one flight in November. In the flight in April, the model underestimates the BC aloft in all Northern Hemispheric zones, although this is not significant at all levels, compared with better comparisons at other times of the year.

Figure 2-22 shows the comparison of model values of BC mass mixing ratio with comparisons taken in from the ARCTAS and EUCAARI campaign. For ARCTAS, the model overestimates BC at higher levels in Northern Canada and Greenland, with a difference greater than 2 standard deviations from the average. The difference peaks at 600 hPa. For EUCAARI in Europe, the model vastly underestimates the BC near the surface, with the underestimation reducing as height increases. However, this is never outside the range of 2 standard deviations of the observations, showing that there is large variability in the observations of BC mass mixing ratio in this region.
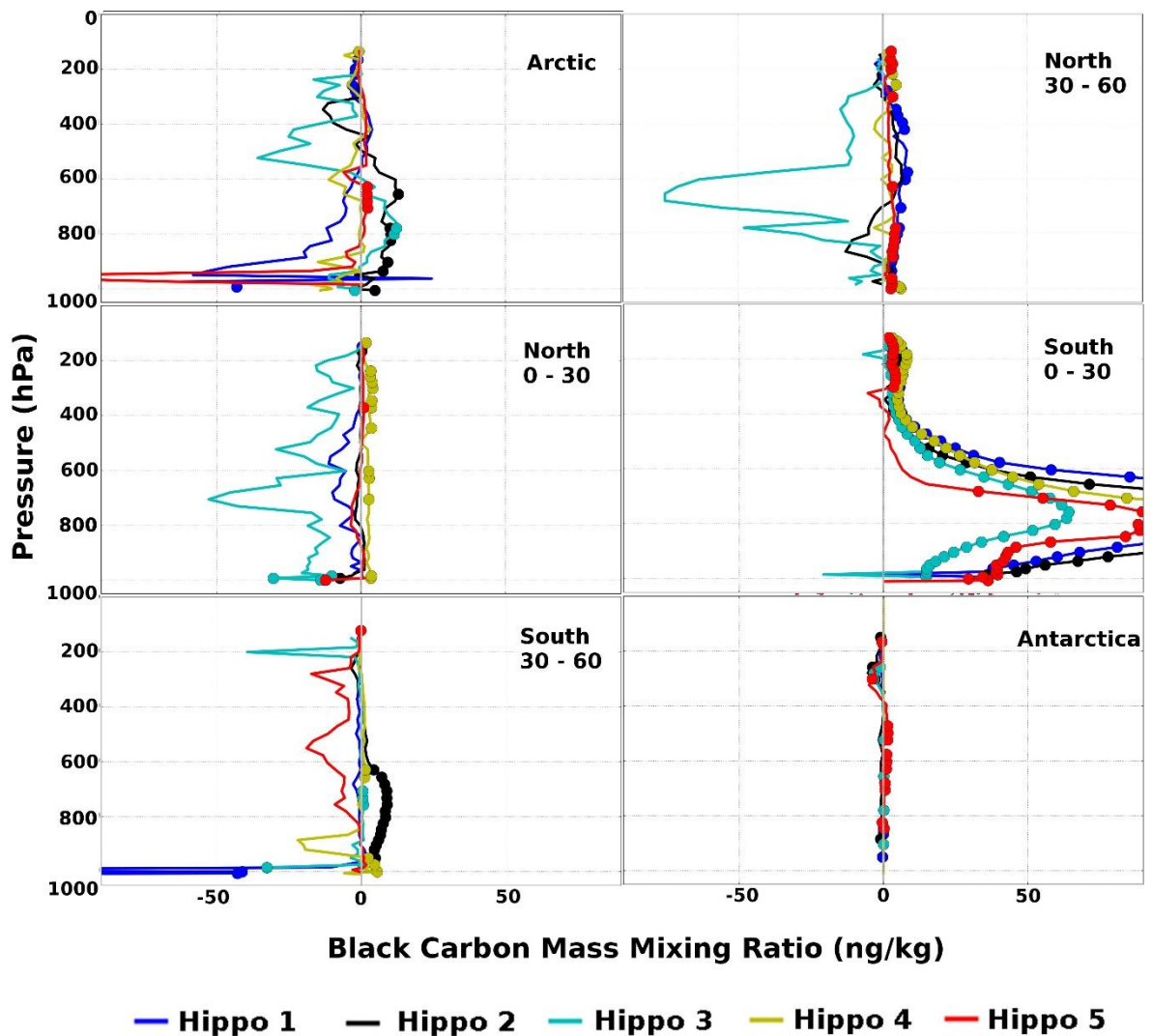
Figure 2-21 – Vertical profiles of differences in black carbon mass mixing ratio between model and the 5 HIPPO flights split by latitude bands and landmasses. Dotted points show difference greater than 2 temporal standard deviations of the observations.

The increase in BC mass mixing ratio aloft in the Southern Tropics of the Pacific (Figure 2-21) and over Northern Canada (Figure 2-22) are likely caused by different phenomena. The main source of BC in the tropics of the Pacific is transported from Asia and Indonesia, emitted from both biomass and fossil/biofuel burning. Overestimation in this region suggests that either the lifetime of aerosol is too long, or that too much aerosol is emitted at height in the model. The current lifetime of BC in the model is 4.14 days, which is shorter than most climate models

(Textor et al., 2006). Literature shows that most climate models that have BC lifetimes of less than 5 days compare better to aircraft observations of BC mass mixing ratio (Samset et al., 2014). In that respect, the lifetime of BC in HadGEM3-UKCA helps to ensure reasonable comparisons well with observations of ambient background BC.
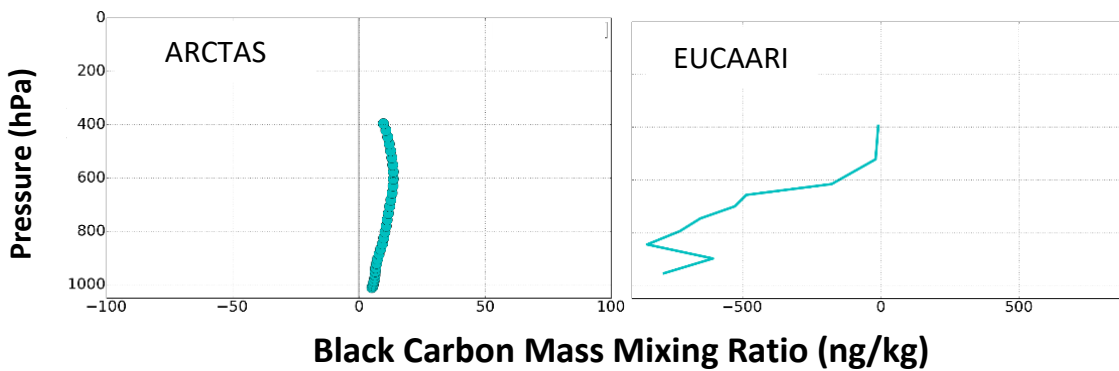
Figure 2-22 - Vertical profiles of differences in BC mass mixing ratio between a) ARCTAS aircraft measurements and Control simulation and b) EUCAARI aircraft measurements and Control simulation at varying heights. Differences greater than 2 standard deviations are represented by circles.

2.4.5 SSA and AE

Figure 2-23 shows the comparison between daily AERONET-retrieved SSA and co-located modelled SSA. In most regions, the majority of model and observed SSA are near 1, suggesting low absorption. Australia and South America are the only regions where this is not the case. In Africa, Asia and South America, the model is underestimating the SSA. In Africa, the underestimation of SSA in the model occurs more frequently at high SSA, whilst in Asia and South America, the model underestimates the SSA more at lower SSA. In North America and Europe, the model underestimates very high SSA, above 0.97, from AERONET retrievals, but overestimates retrievals below 0.97. The size of the overestimations increases with decreased SSA in these regions. Comparisons in Australia show a similar pattern, but with a less severe overestimation at low SSA. However, we would expect to find large amounts of mineral dust in these comparisons, which means the pattern may not be due to CA.

Figure 2-24 shows a Taylor plot of the correlation and normalised standard deviation of SSA between AERONET retrievals and model output over a 30-day timescale. The best correlation is found in Oceanic and African regions. Comparisons in the Arctic show a negative correlation, whilst comparisons in North America, South America, Australia and Europe are not significant at 99.9% certainty. In Asia, the normalised standard deviation is 2.73, showing a large overestimation in the modelled variability of SSA compared to retrieved values. In South America, North America and Africa, the normalised standard deviation is slightly underestimated in the model, whilst in Europe and Australia, the model underestimates the standard deviation by over a factor of 2.
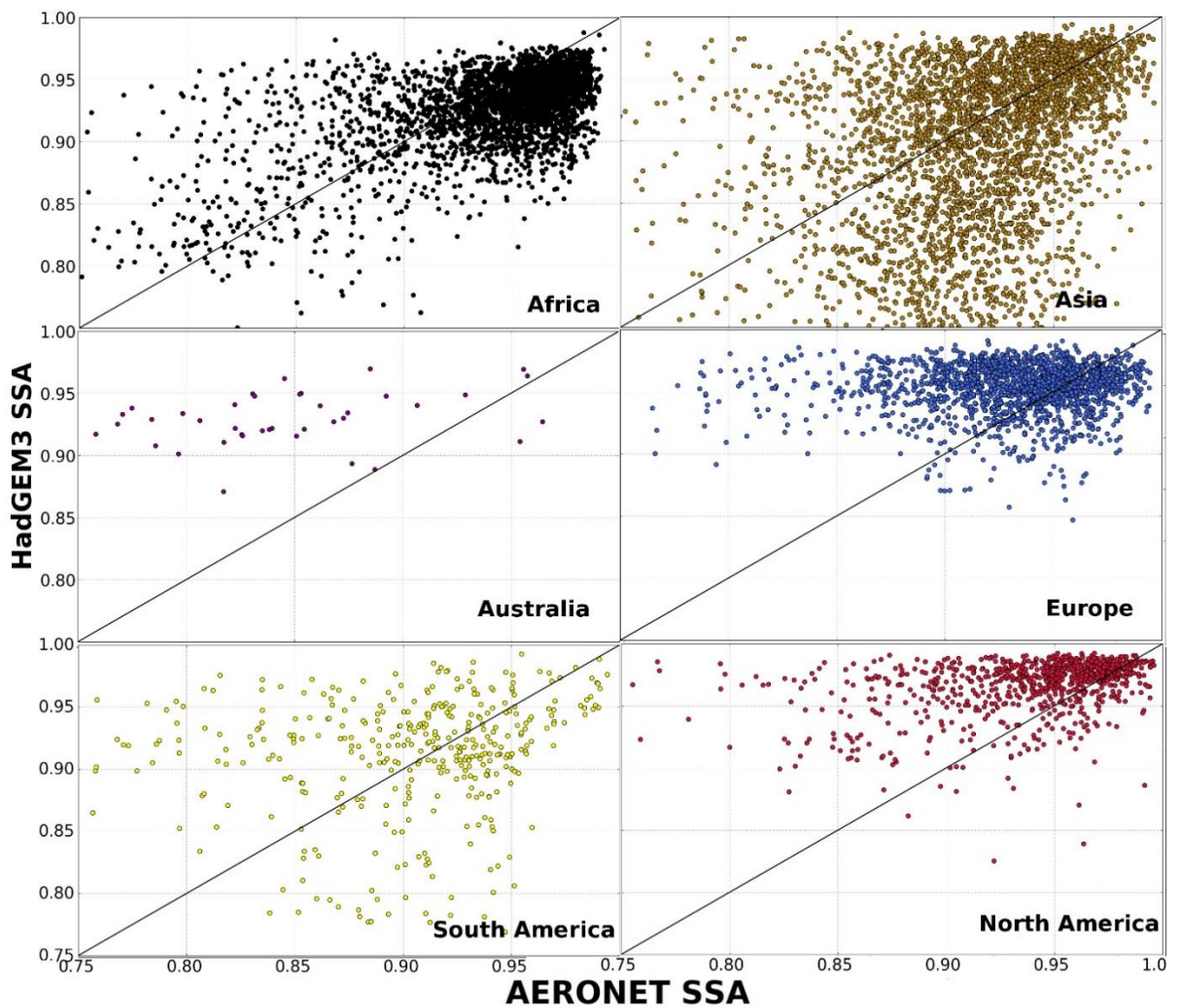
Figure 2-23- Regional comparisons of daily, site-specific, single scattering albedo from AERONET and time-and-location matched single scattering albedo from the control simulation. Solid line shows a 1:1 factor.

Several reasons can be given for the different regional behaviour of the model compared to observations of SSA. In Asia, the combination of the model underestimating SSA, overestimating the variability of SSA, but having a reasonable correlation with observations suggests that the model is able to replicate absorbing aerosol in the right place at the right time, but there is too much absorbing aerosol in the model, too little scattering aerosol in the model, or that absorbing aerosol are too effective at absorbing incoming radiation.
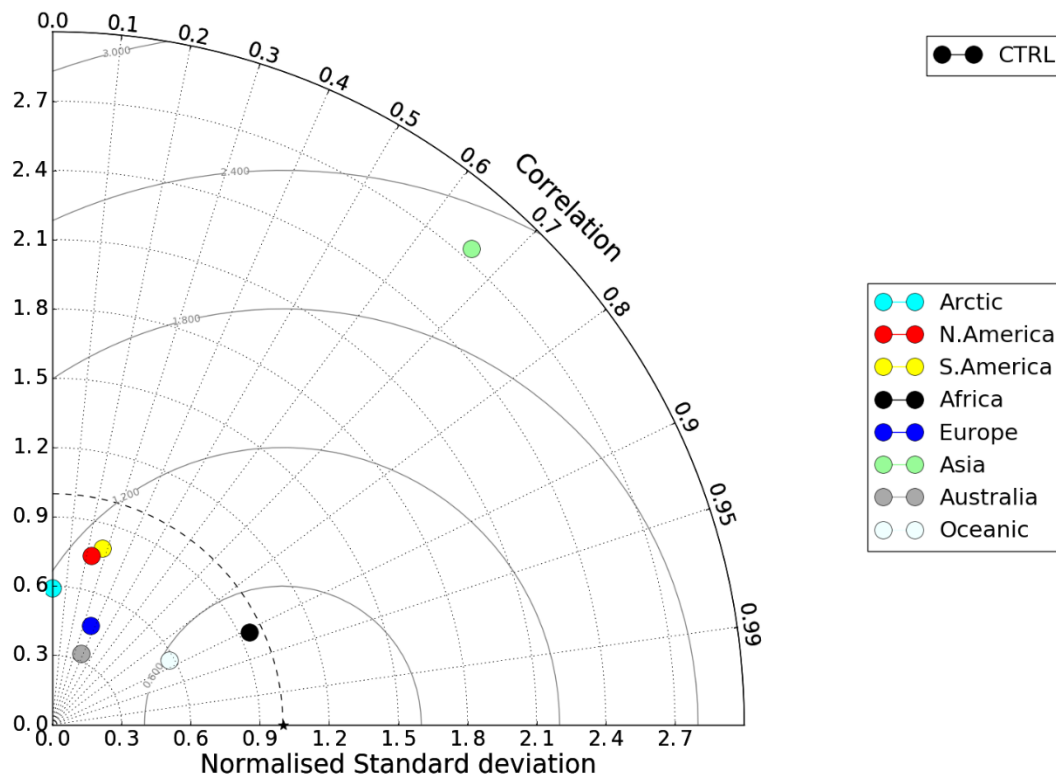
Figure 2-24 – Taylor plot showing the correlation and normalised standard deviation between the model and AERONET retrievals of SSA. Different colours denote regions.

In Europe and North America, the model overestimates the SSA compared to AERONET, especially at low SSA. Comparisons also suggest an underestimation of the variability of SSA values, and poor correlation between model and observations. These results are symptomatic of a lack of absorption in the model when retrievals show absorbing aerosols present. This could be due to either an underestimation of absorbing aerosols, an underestimation to the efficiency of the absorption of the aerosols, or a large overestimation in the mass of scattering

aerosols. Daily comparison in Australia show similar results, although the overestimation of SSA is not as severe.

In Africa and South America, the model shows reasonable ability in simulating the variability in SSA compared to AERONET retrievals. However, the correlation is much better in Africa than in South America on both a daily and monthly timescale. As discussed previously in this section, absorption in the model comes from dust and BC aerosol. In South America, nearly all the absorption is from BC, which are emitted on a monthly timescale, meaning that daily variance is unlikely to be well constrained in the model. In Africa, absorption in large parts of the region is dominated by dust, which is interactive in the model and based upon wind speeds, moisture and surface roughness. It is possible that mineral dust could therefore influence how the model performs and explain the differences between the two regions.

To fully understand and attempt to diagnose why the model SSA differs from observations in each region, consideration of the ability of the model to simulated both the AOD and AAOD must be considered. Furthermore, to distinguish between the need for increasing the mass of absorbing aerosol or increasing the absorptivity of the aerosols, the ability of the model to replicate mass burdens of BC and OC is also required. Underestimations of both BC mass and AAOD in Europe and North America, as seen in previous figures, can explain why the SSA is also overestimated compared to AERONET retrievals. Similarly, the increase in variability in AAOD in Asia explains why an overestimation in variability is seen in SSA in Asia. However, surface BC concentration is underestimated in South America, but SSA is not. We do not have a vertical profile to compare, and similarly, have no mass comparisons for Africa, which makes attributing reasons for differences in SSA and AAOD in those regions difficult.

Figure 2-25 shows the most frequent values of SSA and AE in AERONET and sampled model in the 6 regions shown in Figure 2-10. From Figure 2-23, we saw that SSA is well replicated in some regions. We see similar results in Figure 2-25, which more clearly shows that the SSA is well replicated in the model compared to AERONET in South America and South East Asia. However, in Scrubland Africa and Industrial Asia, the model underestimates SSA. In Europe and North East USA, the model does not fully replicate the range of SSA seen in AERONET, particularly lower SSA values. In all other regions, the range of the model is similar to the range of AERONET retrievals. The AE in the model compares well with the AE from AERONET

in both value and range in North East USA, Northern Europe and South America. However, the AE is overestimated in the model by about 0.5 in both Asian regions and in Scrubland Africa, although the variability compares well.
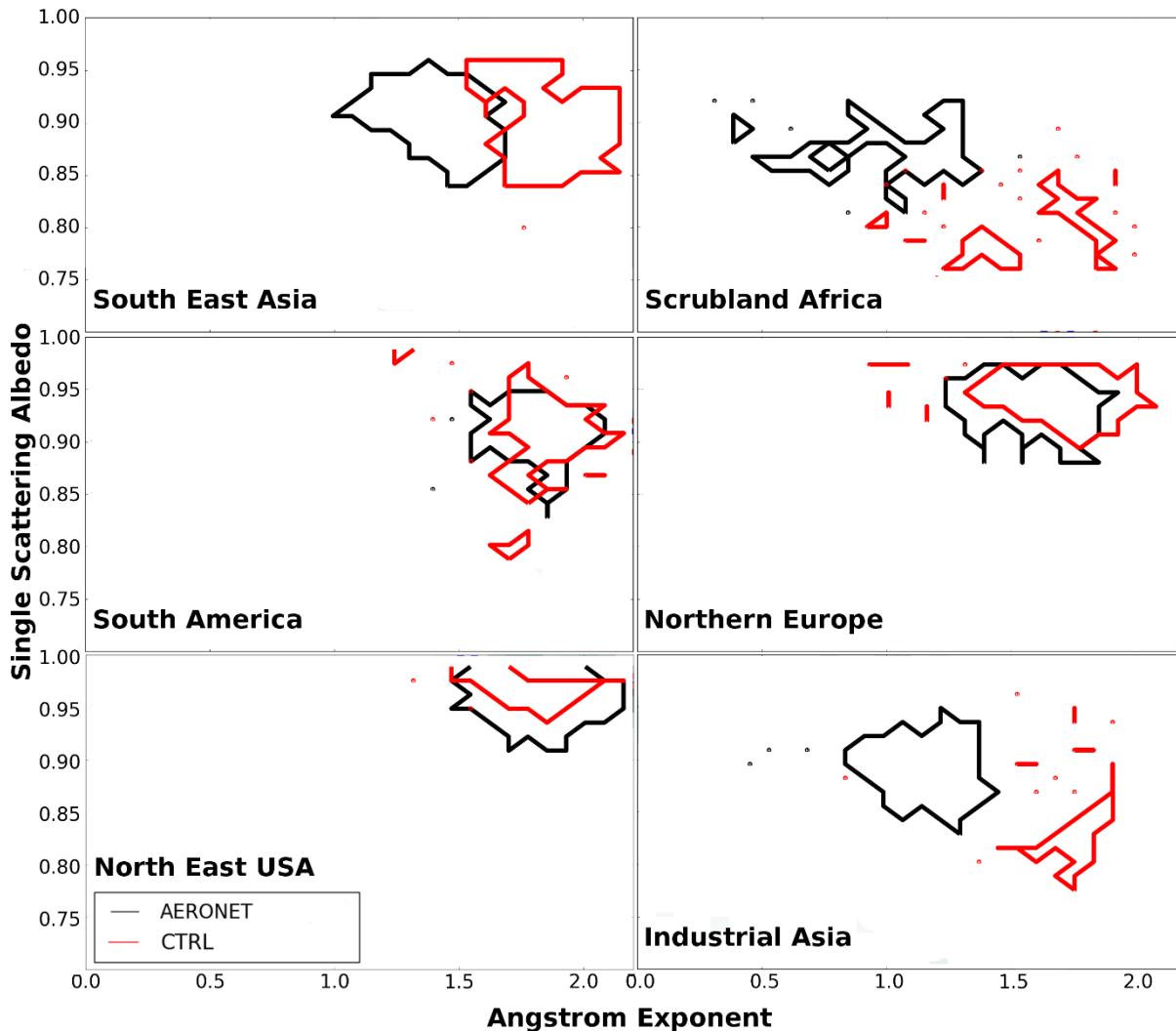

Figure 2-25 – Single scattering abledo as a function of Angstrom exponent for AERONET retrievals (black contour) and Control simulation (red contour). Contours encircle areas where the frequency of values are 10 times the amount of an even distribution.

The AE difference in Asia and Africa shows that the size of particle in these regions in the model are too small compared with observations. There could be several reasons for this. Firstly, the emitted particles may be too small in both Asia and Africa. Secondly, the proportion of smaller particles, such as sulphates, may be too large compared to larger particles, such as carbonaceous aerosols, thus giving a higher average AE. This is possible for

Asia, but there is not much sulphate in Southern Africa. Thirdly, these are regions where dust may be transported too. Work by Wang et al. (2015) and Xin et al. (2015), shows that observations of CA size within South East Asia are larger than what is seen in most models. In their work, they hypothesise that the most likely cause is coated dust, which is seen as carbonaceous by instrumentation. As dust does not internally mix with carbonaceous aerosol within the model, missing this interaction might account for the increased AE in these regions.

2.5 Conclusions and future hypotheses

This section shows that the model and observations differ both globally and regionally across several variables. Several key differences between the model and observations can be explained by similar reasons. These reasons give a good set of paths to follow in this work, and show the advantage of using a multi-variable approach.

Comparing the mass of both BC and OC in the model show underestimations that depend on region, height and time of year. Surface BC concentration is underestimated in nearly all regions. However, this could be due to a lack of mass in the total column, or a lack of mass only at the surface. By analysing the vertical profile, in Europe, we find an underestimation of BC in the entire column. This means that the model lifetime or emissions rates are incorrect, rather than the initial injection height of the emissions, although the three are linked. Similarly, we can compare the results of comparisons of AOD and AAOD with those of surface BC concentration in several regions to show that regions where the model underestimates surface BC concentration, it also underestimates AOD and AAOD. This underestimation could be due to a lack of BC mass. However, we note that in Asia, surface BC concentration is underestimated in the model, yet AAOD is well replicated. Therefore, if the mass is wrong but the absorption right, the model may be incorrectly simulating the absorptivity of BC. Comparisons of SSA in biomass burning areas, such as South America, also show deficiencies in BC mass. This also could be explained by incorrect absorptivity of CA.

The complexities of the model are also clear from this chapter. We show that surface OC concentration in Europe is severely underestimated, but in North America is well represented in the model. However, both regions show similar underestimations of surface BC concentration in the model. We note that using the SSA/AE identification method of Russell et al. (2014), both regions shows that most aerosol in these regions is developed urban

aerosols, and that the SSA and AAOD show similar levels of misrepresentation in the model. This highlights the difficulty of improving only a small part of a full aerosol model, as there are several other factors, many of which relate to other aerosols, which could explain why the ability of the model to replicate surface OC concentrations differs in the two regions despite showing similar abilities in SSA and surface BC concentration. This is also the reason why this work is about making the model scientifically accurate rather than fine-tuning the model to observations, as further work on another aerosol species or physical or dynamical processes in the future could lead to CA becoming poorer than its current state. Not only are SSA and AE dependent upon other aerosol within the scheme, they are also dependent on many other parts of the model, such as transport, clouds and precipitation. These parts of the model are liable to change as they are further developed, which would change the ability of the model to replicate aerosol mass or optical depths. Using a physical-driven development approach makes the model improvements more resilient to future changes and better supported by observations.

Our investigations into the current ability of the model and of potential reasons for differences with observations have consistently led to three areas of the model which could be responsible for model deficiencies. Changes to the mass, optical properties and lifetime are likely capable of improving the comparison of the concentrations of both OC and BC, as well as AOD, AAOD, SSA and AE. The next three chapters of this thesis uses sensitivity studies to investigate these three potential solutions in turn using the same variables as used in this chapter to assess the model.

3. Chapter 3: Solution One – Mass Absorption Coefficient

In this chapter, we examine the uncertainty in the refractive index of CA, especially focusing on how absorbing organic carbon, or brown carbon, is defined and modelled. We analyse how a different refractive index of BC affects how the model compares to observations, and discuss whether high BC values of refractive index currently used in the model are accurate and scientifically justifiable. We also analyse how crudely attributing the absorption from BrC to OC in the model affects comparisons with observations, and discuss whether, if modelled in a more accurate and effective way, the addition of BrC could further improve the model.

3.1 Carbonaceous Aerosol Refractive Index

In HadGEM3-UKCA, and in many other climate models, CA is split into two types: BC and OC (Myhre et al., 2013). Based on the literature available in the early 2000s, the refractive indices of the BC and OC reflected the view that BC absorbed incoming shortwave radiation, and OC was purely scattering (Hess et al., 1998). BrC was not modelled, meaning that all absorption was being attributed to BC. In reality, the optical properties of CA, such as refractive index, are highly variable, depending on several factors. Source of emissions, and for CA linked to combustion, the method of burning, material burnt and temperature of burning all affect the optical properties of the aerosol produced (Andreae & Gelencsér, 2006; Bond et al., 2013; Bond & Bergstrom, 2006). Variability in the ratios of BC and OC produced also differ for similar reasons. Aerosols produced have a range of refractive indices that are linked to the individual aerosol composition, from the most strongly absorbing to purely scattering. BrC also has a range of refractive indices, and means that measurements of absorption or scattering from any burning event correspond to aerosols with a wide spectrum of optical properties (Andreae & Gelencsér, 2006; Feng et al., 2013). These properties change rapidly over time as aerosols age, making identifying a singular, or even several, refractive indices to CA a difficult task.

Old observations of CA also split into just BC and OC. BC is determined mostly through proxies which measure absorption. These assume that all absorption is due to BC alone. However, absorption from BrC will also contribute to any optical measurements, but may not contribute to refractory mass measurement techniques. This would lead to an overestimation of the

amount of absorption per unit mass, or mass absorption coefficient (MAC) of BC, when in reality the extra absorption is coming from BrC. As understanding of BrC has developed, and new techniques have been created to observe BrC (Chakrabarty et al., 2010), the effects of BrC are slowly being implemented into climate models, either through making OC absorbing or through adding a new tracer (Wang et al., 2014a).

An ideal method of improving HadGEM3-UKCA would be to simulate the wide range of refractive indices seen in each plume, but although realistic, this is also impractical given both the variability of the range of refractive indices in different burning types, and the computational expense of modelling such a scheme. Instead, using just the two tracers available, we can only determine whether making OC slightly absorbing, to account for the BrC content, improves the comparison of the model to observations. Similarly, if an overestimation of BC absorption has occurred due to previous observational errors in absorption attribution, then it is possible that BC is less absorbing than previously thought.

3.2 Sensitivity to Carbonaceous Aerosol Optical Properties

Previous studies have examined the effects of CA optical properties. Figure 1-8 in Chapter 1 shows the difference in refractive index of OC that can be found through different classifications and measurement techniques. It also shows the effect of different burning condition on BC refractive index, which is a significant problem when having to use a unique global BC refractive index. Dubovik et al. (2000) shows the difference in the optical properties in similar situations by analysing SSA of biomass burning plumes. They find that there is a relationship between the average SSA at various wavelengths and the ratio of ambient BC:OC, foreseeing more recent results in (Saleh et al., 2013).

Several observational studies attempt to determine a value for BC RI through comparisons with both BC mass and AAOD (Barnard et al., 2007; Schuster et al., 2005). Applying similar methods, Bond et al. (2013) and Kirchstetter et al. (2004) suggest that models with correct mass underestimate absorption in regions where CA is the dominant absorptive aerosol. However, these studies do not consider the impact of a BrC component. More recent observational studies, such as Saleh et al. (2013) and Lu et al. (2015) attempt to distinguish the absorption between BrC and BC using mass observations, and determine an "observed" RI for both BC and BrC. Yuan et al. (2016), finds that absorption from BrC is sizeable during

summer in Asia, whilst Alexander et al. (2008), found highly absorbing BrC being emitted from Asia into the Pacific, with a RI of 1.67 – 0.27i at 440 nm. That imaginary part is not as high as that of BC (0.4i to 0.9i), but is also much higher than any other brown carbon RI quoted in previous literature.

In response to those new observations, BrC has been recently added to some climate models for sensitivity studies. Feng et al. (2013) and Jo et al. (2016) use chemistry transport and climate models to determine that BrC can be used to explain missing absorption in their models, although the refractive index of BrC needed to correlate AERONET retrievals of absorption optical depth with their models varied regionally. Neither study tested whether the absorption of BC should be reduced to compensate for increase BrC absorption. Wang et al. (2014a) additionally adds a BrC tracer from both primary and secondary OC, and shows that there is a reduction in the underestimation of AAOD in the GEOS-Chem climate model, particularly in biomass burning regions. However, regional underestimations of AAOD still existed in the model.

Using the suggestions set out through previous literature work, and from analysing the needs of the HadGEM3, we wish to test two hypotheses. Firstly, that making OC absorbing to represent a BrC component can improve the lack of absorption in the model, as it has done in the studies cited above. Secondly, that reducing BC absorption is required to account for possible overestimations of absorption attributed to BC from observations.

3.3 List of Sensitivity Studies

To calculate a potential set of RI for an absorbing OC tracer, we use from Saleh et al. (2013), which gives a series of values for all primary OC (both BrC and OC combined) from a set of lab flame tests of biomass burning. We use Figure 3-1 from Saleh et al. (2013) to determine a suitable increase in the imaginary part of the OC refractive index. This figure shows how the imaginary part of the RI of POA and SOA, which are both BrC and OC together, varies for several different burning materials and the corresponding mathematical fit. They consider two limiting cases, one which considers an external mixture, and the other a core and shell mixture, as low and high extremes of absorption. We choose to increase the imaginary part of OC and SOA in HadGEM3-UKCA from 0i to 0.03i at 550 nm, and recreate the wavelength dependence seen from both Saleh et al. (2013) and Kirchstetter et al. (2004) (green triangles

in Figure 3-1b), which show good agreement with each other. There is no literature that shows whether the real part of the refractive index changes between BrC and OC, so the original values currently used in HadGEM3-UKCA will be kept (1.5 at 550 nm with wavelength dependence).

The BC refractive index currently used in HadGEM3-UKCA is 1.85 − 0.71i, and is at the high end of those quoted in literature. Using Figure 1-8 in Chapter 1, which shows the graphite vaporization line proposed by Bond & Bergstrom (2006), we reduce the refractive index of BC to 1.4 − 0.4i, one of the lowest values represented in literature for BC, reducing the value at all wavelengths by the same proportion.

Table 3-1 summarises the two simulations that were devised to determine the model sensitivity to BC and OC RI.

Name	Description	Change	Supporting Literature
OCAbs	Increase in imaginary part of the OC RI	Increase in OC RI imaginary part from 0 to 0.03i at 550 nm, following wavelength dependence of Saleh et al (2013), decreasing to 0 at 1000 nm.	(Saleh et al., 2013)
BClow	Decrease of both imaginary and real part of BC RI	BC RI reduced from 1.85 − 0.71i to 1.45 − 0.4i at 550 nm, and proportionally reduced at other wavelengths to retain the wavelength dependance.	(Batten, 1985; Hungershöfer et al., 2007)

Table 3-1 – List of simulations used in this chapter, with descriptions of changes compared to Control simulation.
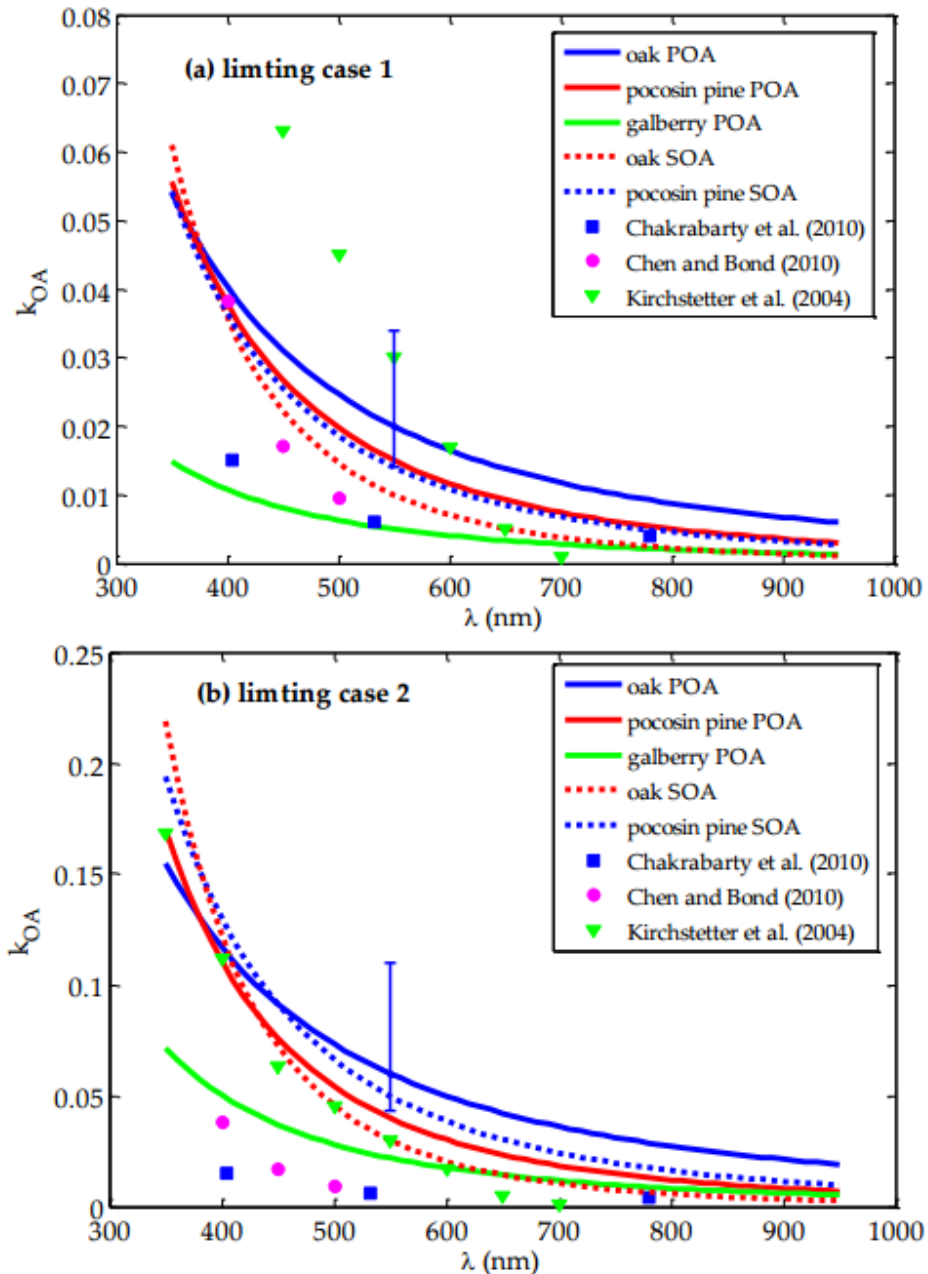
Figure 3-1 – The value of the imaginary part of the refractive index for organic aerosols at differing wavelengths. Different studies are shown by different symbols, and coloured lines show values found from different burning material. Limiting case 1 shows the values of the imaginary part in external mixtures, with limiting case 2 showing a core shell representation. Figure is taken from Saleh et al., (2013)*, who describe the limiting cases as low and high extremes.*

3.4 Results

In this section, we discuss the effect of altering the refractive indices of BC and OC on both mass and optical variables in the model, and analyse how changes affect comparisons between the model and observations.

3.4.1 AAOD

Figure 3-2 shows the distribution of percentage changes to AAOD when OC and BC refractive indices are altered. When OC is made absorbing, the global AAOD is increased by 52% in the model. Local increases of over 200% in AAOD are seen in South America and Indonesia, with increases of up to 100% over North America and the Pacific Ocean. Increasing absorption in OC increases AAOD in Saharan Africa, the Middle East and Central Asia by only 20%. When BC absorption is reduced, the global average AAOD is reduced by 42%. Reductions in AAOD occur in all regions, with decreases of up to 60% occurring in South America, Southern Africa, Indonesia and the Central Pacific. Decreasing BC absorption reduces AAOD by only 10% in Saharan Africa, the Middle East and Central Asia.

Increasing absorption from OC, which is non-absorbing in the CTRL simulation, increases the AAOD. Similarly, reducing the absorption from BC reduces the AAOD. The largest local increases in AAOD when OC absorption is increased are found where OC emissions are both greatest in magnitude and proportion of the total aerosol mass. These regions are predominately biomass burning regions, as biomass burning emissions have an OC:BC ratio of around 10, which are generally much higher than those from fossil or biofuel burning emissions, which have an OC:BC ratio of around 1.5 (Novakov et al., 2005). One exception is Central Africa, where biomass burning is a major source of aerosol, but AAOD is only increased by 60% locally. In this region, there are also sources of dust from the Makgadikgad and Kalahari dust pans (Bhattachan et al., 2015; Prospero et al., 2002). As dust is the other absorbing species within the model, changes to the AAOD from changing absorption from carbonaceous aerosols are dampened by the absorption from constant dust. In areas where dust is responsible for the majority of absorption, such as desert areas, altering the absorption from either BC or OC has little effect on the overall AAOD. There is also more BC from biofuel burning in this area, meaning that the OC:BC ratio is lower in this region (around 6) than most

other biomass burning regions. Therefore, the effect of increasing OC absorption is lower, but removing BC absorption still has a large effect in Central Africa.
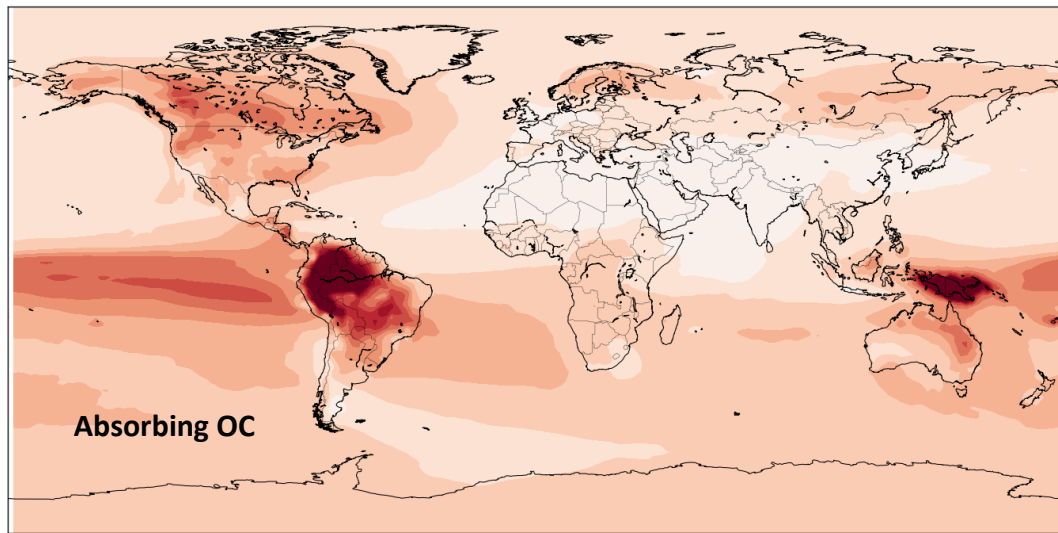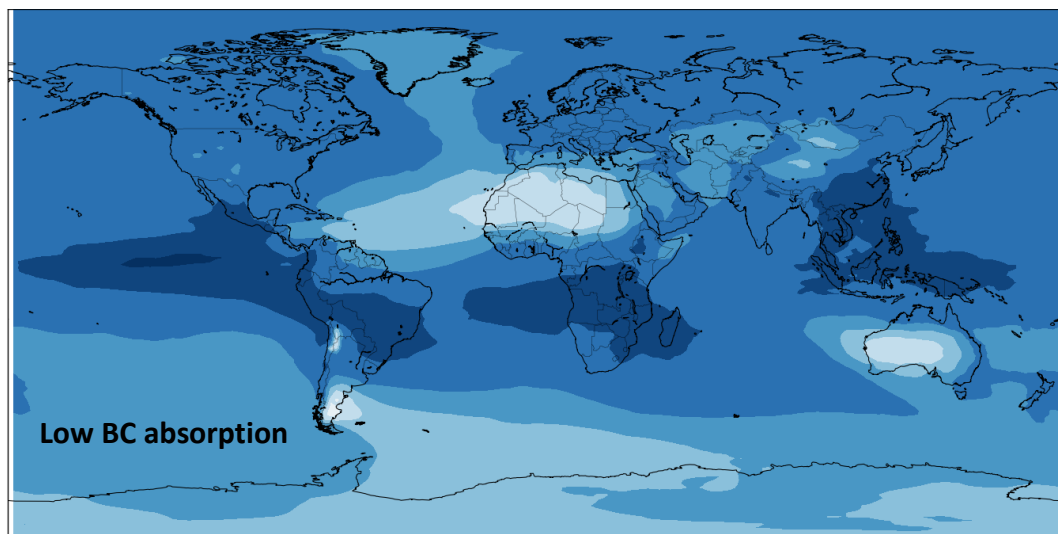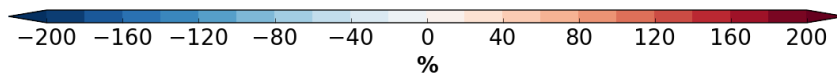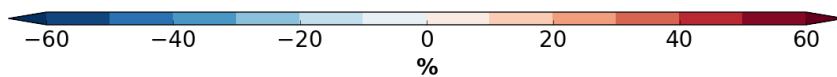

Figure 3-2 - Global distribution of percentage changes in absorbing aerosol optical depth between control simulation and absorbing OC and low BC absorption simulations for the period 2006-2008

Figure 3-3 shows the mean factor of modelled AAOD against retrieved values from AERONET sites. We explain in Chapter 2 why retrievals from AERONET are likely to overestimate AAOD, meaning that a comparison mean factor of less than 1 is preferential to a comparison mean factor of greater than 1, although quantifying a specific value which is "most correct" is not possible. Increasing OC absorption increases the mean factor in all regions, with the largest increase seen in the Arctic. Increasing the absorption improves the comparison between model and observations in most regions, except Asia and the Arctic, where AAOD is overestimated in the model by 24% and 42% respectively. In contrast, reductions in BC absorption lead to a reduction in the mean factor in all regions, with the largest decrease occurring in Asia. Decreasing BC absorption is detrimental to the comparison between model and observations in all regions.
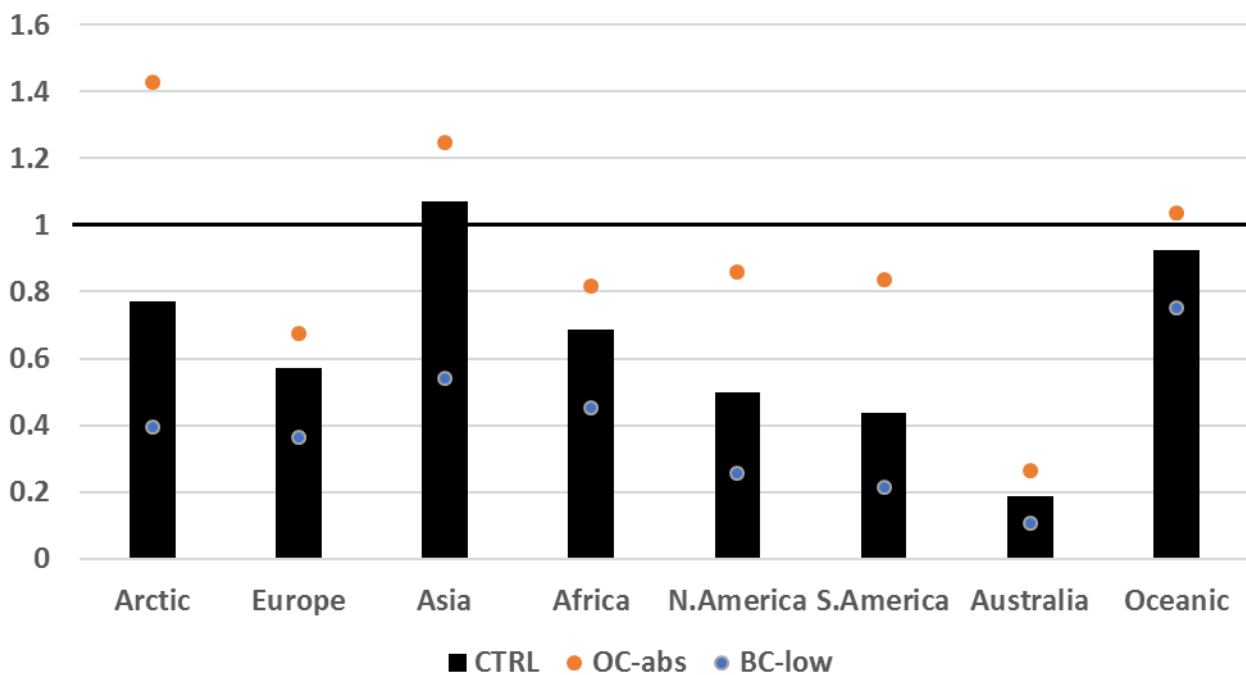
Figure 3-3 – Mean factors between modelled AAOD and AERONET retrieved AAOD at 550 nm in the control and two altered absorption simulations. A value under 1 shows the model underestimating compared to observations, above 1 shows a model overestimation.

Different regions also show different magnitudes of changes between the two altered absorption simulations. Including OC absorption induces a larger magnitude of change in the Arctic, South America and North America, whereas reducing BC absorption gives a larger magnitude of change in Asia, Europe and Africa. Areas which show lower OC : BC ratios are

more responsive to reduced BC absorption, whilst areas with higher OC : BC ratios are more responsive to increased OC absorption.

Figure 3-4 shows the correlation and normalised standard deviation of the model compared to observations. Increasing OC absorption increases the normalised standard deviation in all regions, suggesting that modelled AAOD has become more variable in time. This increase improves the representation of standard deviation in most regions, but is detrimental to Asia and South America. In most regions, increasing the OC absorption does not change the correlation of the comparison between model and observations. However, at Oceanic sites, the correlation is increased by 0.2, whilst in North America, the correlation is decreased by 0.1. Decreasing the BC absorption decreases the normalised standard deviation in all regions. This is detrimental to the comparison between modelled and observed AAOD in all regions except Asia. The decrease in BC absorption does not alter correlation in most regions, except in North America and Oceanic regions, where correlation is decreased by approximately 0.15. In both altered simulations, the largest changes are seen in Asia (not shown), South America, Africa and the Arctic. Even with the increase in OC absorption, the standard deviation of AAOD in the model is still underestimated in most regions.
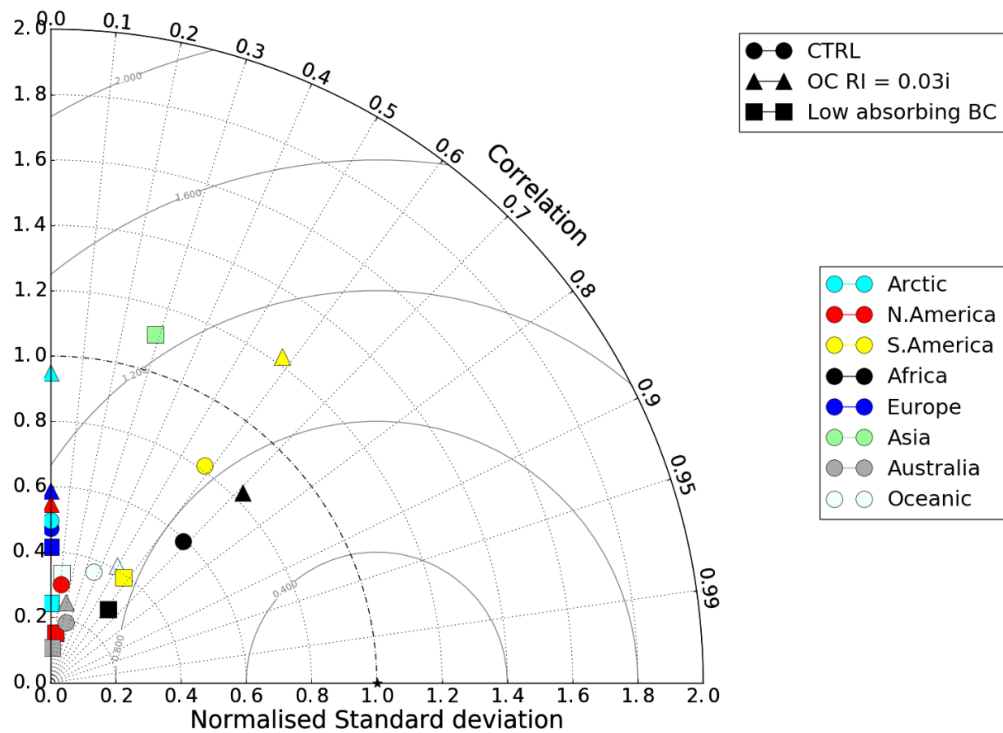
Figure 3-4- Change in correlation and normalised standard deviation ratio between control and altered simulations and AERONET absorbing aerosol optical depth on a 30-day timescale.

Comparisons of modelled AAOD to observations show that increasing OC absorption is beneficial to the comparisons in most regions. Both mean factors and standard deviations in the model are increased, which is an improvement in most regions. However, in Asia, where both AAOD and the standard deviation of AAOD are overestimated, this worsens the model significantly. Taking the comparison at face value suggests that, particularly in biomass burning regions, an increase in OC absorption can improve the comparison of observations with the model. However, we would have to be able to quantify the error from our method of comparing AERONET level 2 products to the model, which requires the use of our new SSA/AE metric.

3.4.2 SSA and AE

Figure 3-5 shows the distribution of changes to SSA between the altered refractive indices simulations and CTRL simulation. When OC is made absorbing, global SSA is reduced, as expected. All regions show reduction, with the largest changes are seen near biomass burning emission sources, with decreases of up to 0.07 in areas of Central Africa and South America where emissions are located. The reduction of SSA decreases as distance from the source sites increases. Further reductions of up to 0.03 can be seen in Northern Australia and urbanised regions of North America and Asia. When BC refractive indices are reduced, SSA increases globally. In Africa and India, SSA is increased by up to 0.08, whilst in urban areas of Asia and North America, decreasing BC refractive indices reduces SSA by up to 0.05. As with increased OC absorption, changes in SSA are reduced as distance from CA source regions increases.

Changes in SSA due to changed refractive indices are broadly the opposite sign of the changes to AAOD, as the effect on AOD are much smaller. Increased OC absorption leads to decreased SSA and increased AAOD in similar areas, Similarly, reducing BC refractive indices decreases the AAOD and so increases SSA.

Figure 3-6 shows the correlation and normalised standard deviation of SSA between AERONET retrievals and modelled SSA. In all regions, when OC is made absorbing, the normalised standard deviation is increased, showing that the SSA in the model is more variable in time. The largest increases occur in Africa, South America and in the Arctic. The correlation between observations and modelled SSA is also reduced in South America, Europe and North America.

When the BC refractive index is reduced, the normalised standard deviation is reduced in all regions. The largest decreases occur in Africa, Asia, and South and North America. In Oceanic regions, South America and North America, the correlation between observations and model is also reduced.
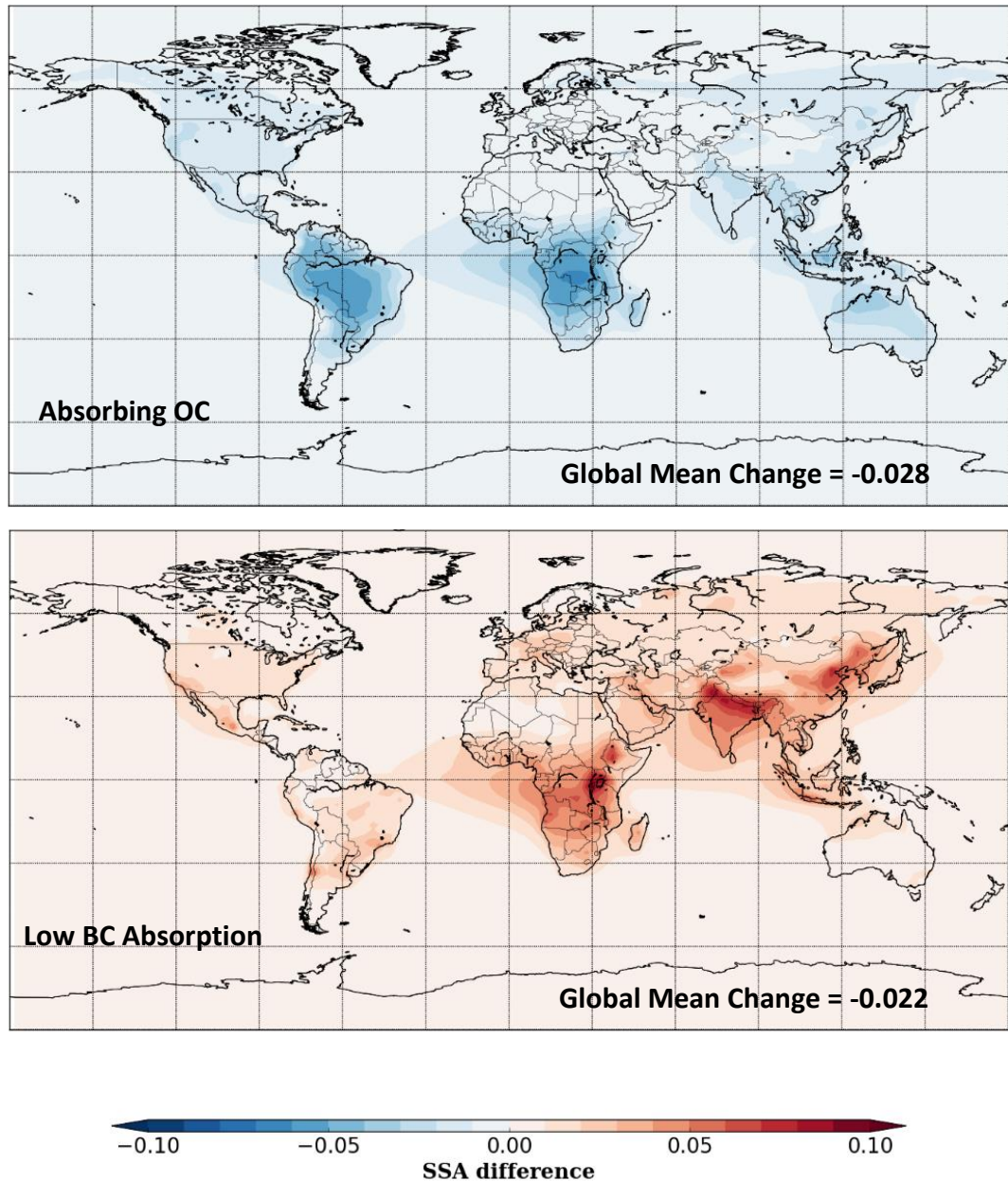

Figure 3-5- Global distribution of percentage changes in single scattering albedo between control simulation and absorbing OC (top) and low BC absorption (bottom) simulations for the period 2006-2008.
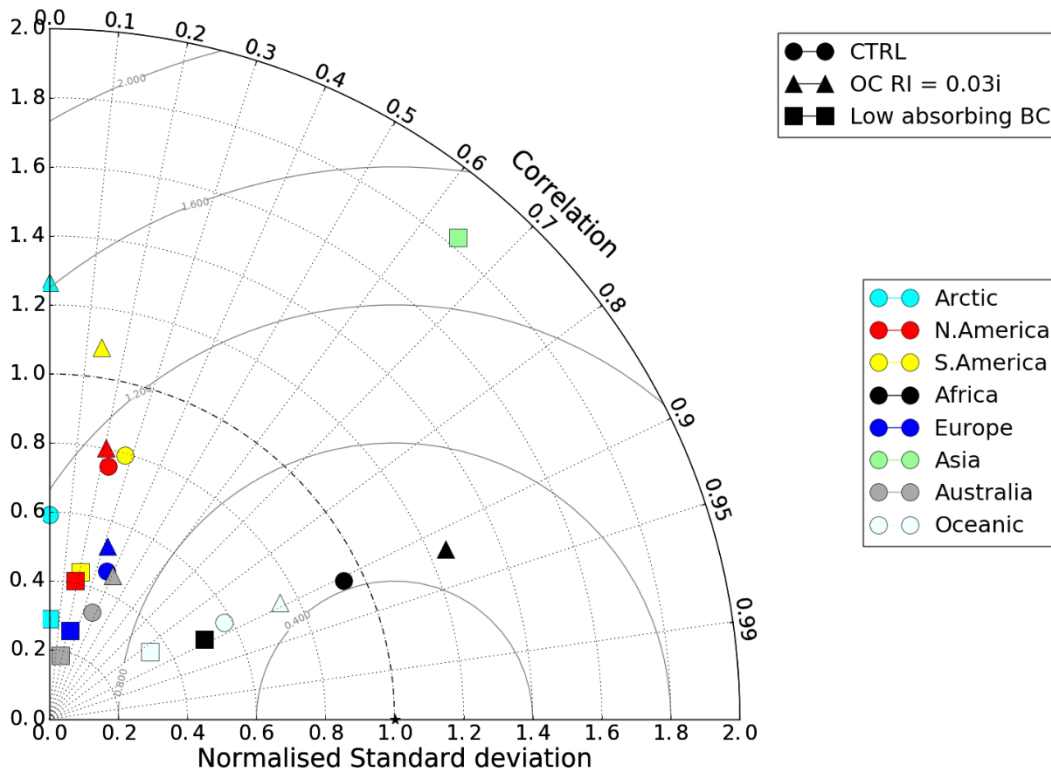
Figure 3-6 - Taylor diagram showing the correlation and normalised standard deviation of the control and altered simulations with AERONET SSA at 550 nm over a 30-day time scale, for the period 2006-2008. Colours denote different regions.

The effect of increasing OC absorption improves the comparison with model in Arctic, Australia and Oceanic regions due to increased normalised standard deviations and little effect on the correlation. The increase in absorption leads to lower values of SSA being present, and so a wider range of values in the model. In Asia, the increased normalised standard deviation further overestimates the range of retrieved SSA, worsening the model. In Africa, increased OC absorption also leads to overestimations of the SSA range, whilst decreased correlation in South America is also detrimental to the comparison. Decreasing BC refractive index weakens the model to observation comparison in all regions except Asia, as decreased absorption reduces the frequency of low SSA. However, the reduced value of the normalised standard deviation (1.83) still shows that the model range of SSA is doubled that found in retrievals. All other regions show that reductions in the standard deviation from a low BC refractive index lead to model standard deviations which are over 2 times smaller than retrieved values.

These results show that improvements in correlation and variability of AAOD do not necessarily coincide with improvements in correlation and variability of SSA when compared to observations. In Africa, increasing OC absorption leads to an overestimation of SSA variability, but the variability of AAOD is still underestimated. Similarly, the correlation of SSA is decreased in South America with increased OC absorption, but the correlation of AAOD remains constant. This important result shows that regions which show similar changes in a variable in the model can differ in how the changes affect comparisons to observations.

Figure 3-7 shows the frequency of SSA and AE from both AERONET retrievals and the model when OC is made absorbing. As previously shown, making OC absorbing reduces SSA in all regions, with the largest changes seen in Africa, South East Asia and South America. In Scrubland Africa and South America, which are dominated by biomass burning aerosols, there is an increase in both low and high SSA in the model, which is detrimental to the comparison to AERONET. In South East Asia, only low SSA are increased, expanding the range beyond observations and decreasing the model-to- observation comparison. In Europe, North East USA and Industrial Asia, making OC absorbing increases the frequency of lower SSA, whilst the frequency of high SSA are effected less, because these represent SSA of near 1, which suggests very little CA aerosol in the column. In Northern Europe and North East USA, this increase in low SSA improves the model comparison in SSA/AE space, whilst in Industrial Asia, it worsens the comparison.

Figure 3-8 shows the frequency of SSA and AE from both AERONET retrievals and the model when the BC refractive index is reduced. SSA is reduced in all regions. In Scrubland Africa and South America, the frequency of the lowest SSA seen in the model is decreased, but the frequency of higher SSA is increased. In Scrubland Africa, this improves the comparison of the model to AERONET retrievals, whilst in South America, decreasing the BC refractive index makes the model SSA too high compared to AERONET retrievals. In North East USA, Northern Europe and the two Asian regions, the reduction in the frequency of the lower SSAs in the model is more prominent than any increase in frequency of higher SSAs. In Northern Europe, South East Asia and North East USA, this worsens the model by reducing the frequency of low SSAs seen in AERONET. In Industrial Asia, the increase in high SSA frequency improves the model comparison, but the reduction in low SSAs worsens the comparison to AERONET.
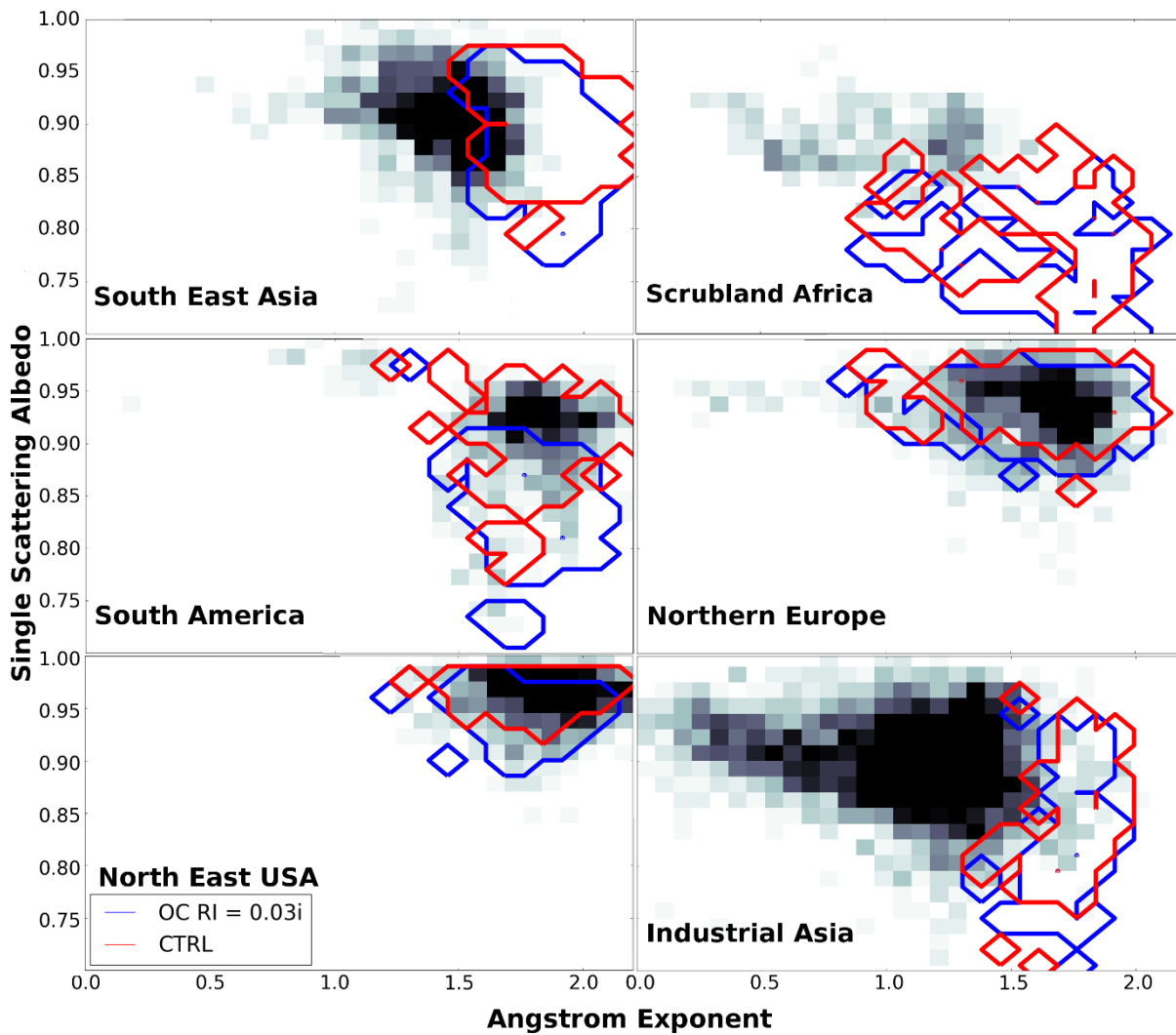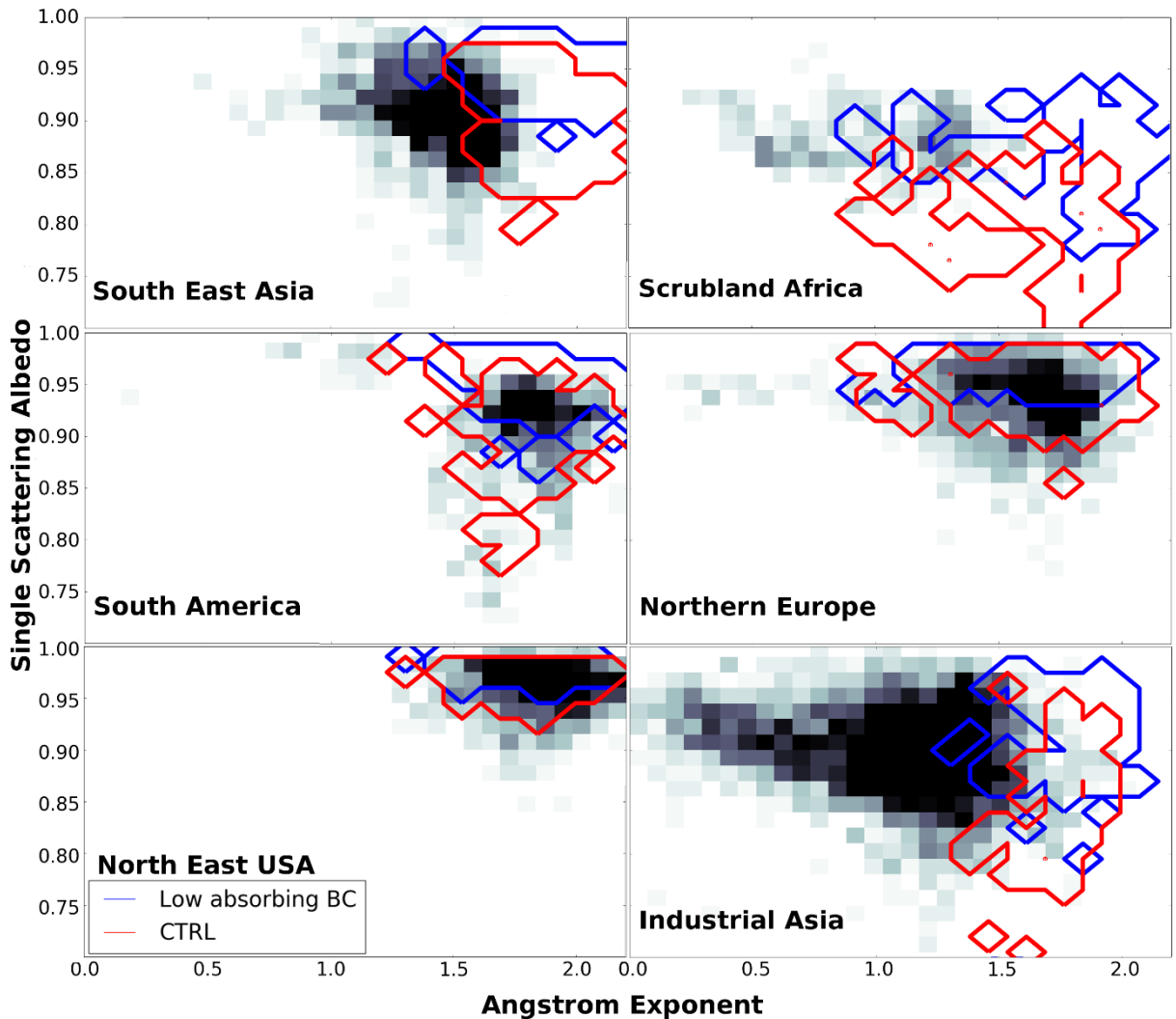
Figure 3-7 – Single scattering albedo at 550 nm as a function of Angstrom exponent between 670 nm and 440 nm for AERONET retrievals (black density boxes) compared and co-located modelled values from control (red) and OC absorption (blue) simulations in six regions.

SSA is altered differently in biomass burning regions compared to fossil fuel burning regions when refractive indices are changed. When OC is made absorbing, SSA in biomass burning regions shows an increase in frequency of lower SSA and decrease in higher SSAs, whilst in fossil fuel burning regions the frequency of the highest SSA is unchanged, but lower SSAs increase in frequency. The opposite is true for reduced BC refractive indices. This is because biomass burning is mostly carbonaceous aerosol, and so in biomass burning regions, all SSAs deviate when CA absorption is altered. However, in fossil fuel burning regions, high SSA are symptomatic of low CA, and so changing CA absorption has little effect on SSA. Lower SSA in

these regions correspond to when the CA proportion of the aerosol burden is higher, and so the effects when CA refractive indices are changed are stronger. South East Asia, as a region which contains high levels of both fossil fuel and biomass burning emissions, exhibits both responses.

Figure 3-8 - Single scattering albedo at 550 nm as a function of Angstrom exponent between 670 nm and 440 nm for AERONET retrievals (black density boxes) compared and co-located modelled values from control (red) and BC low absorption (blue) simulations in six regions.

Comparisons of the SSA to observations suggests that in biomass burning regions, increasing OC absorption is ill-advised. This is contrary to the analyse of the AAOD, which suggested otherwise. Modelled SSA is improved in fossil fuel burning regions when OC is made absorbing, despite evidence that BrC is rare from these emissions. The comparison in fossil fuel regions is also severely worsened when the BC refractive index is reduced in the model,

suggesting that BC should have a highly absorbing refractive index in order to ensure good comparisons between models and observations. However, both AAOD and SSA comparisons require correct amount of CA mass, and therefore any deviation between model and observation in mass may influence how SSA and AAOD compare.

3.4.3 Surface BC & OC Concentration

Figure 3-9 shows the distribution of average percentage changes to surface BC concentration when the refractive indices of carbonaceous aerosols are changed. When OC is made absorbing, the global average surface BC concentration is not changed by more than the annual variability of global surface BC concentration changes (2%). However, most regions show a decrease in surface BC concentrations, with the largest decreases occurring in the Indian Ocean (12%), Atlantic Ocean off the coast of Southern Africa (10%) and in Central Asia (8%). When BC refractive indices are reduced, surface BC concentrations are increased globally by 2%, which is of a similar proportion to the annual variability. Increases in surface BC concentration of up to 20% occur in the Indian Ocean and up to 12% in the Atlantic Coast off the south of Africa. However, a decrease in surface BC concentration of up to 8% occurs in Central Asia.

Figure 3-10 shows the distribution of percentage changes in surface OC concentrations when OC and BC refractive indices are altered. When OC is made absorbing, surface OC concentration is reduced by 0.7%, which is less than the annual variability. The largest localised reductions occur in the Indian Ocean and off the coast of Africa, where surface OC concentrations are reduced by up to 8%. When BC refractive indices are reduced, surface OC concentrations are increased by 1.17% globally. Increases in surface OC concentration of up to 12% occur in the Indian Ocean and of up to 10% off the coast of Central Africa. Most regions show an increase in surface OC concentrations when BC refractive indices are reduced, except Central Asia, where decreases in concentrations of up to 8% occur.
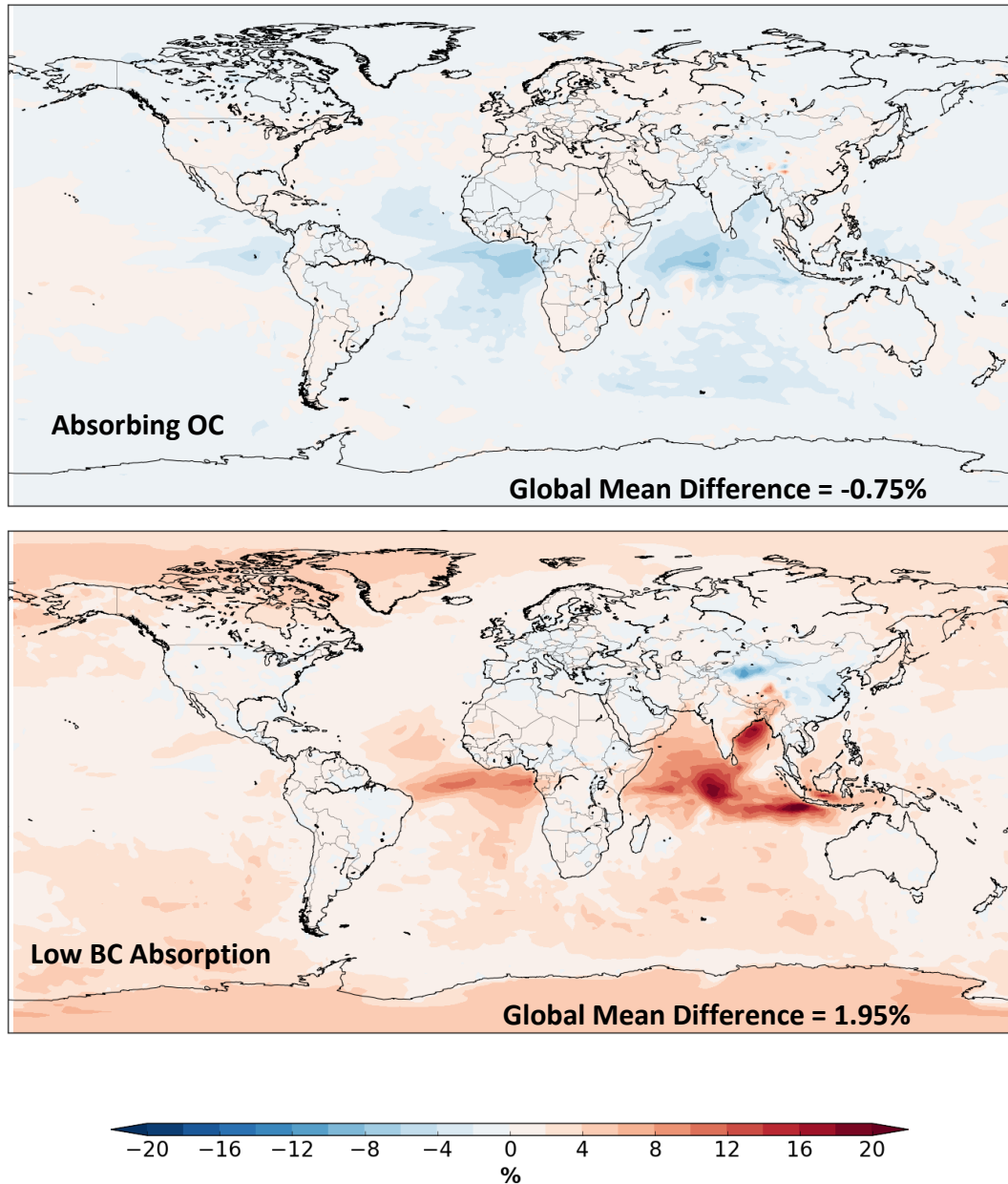
Figure 3-9- Global distribution of percentage changes in surface BC concentrations between control simulation and OC absorbing and BC low absorption simulations for the period 2006-2008.

As shown in the above figures, there is very little change in the surface BC and OC concentrations, particularly over land. We find no discernible change to the comparison between modelled and observed surface BC or surface OC concentrations, and so do not show or discuss it within this section.

The spatial distribution of changes in surface OC concentrations when carbonaceous aerosol refractive indices are changed mirrors that of changes to surface BC concentrations. Global

increases show correlation with absorption; increased absorption through making OC absorbing decreases the surface concentrations of BC and OC, whilst decreasing absorption through a reduced BC refractive index increases surface BC and OC concentrations. We propose that this is the effect of changes in radiative heating from the altered absorption, which alters buoyancy of the air parcels. Increases in absorption near the surface increase the radiative heating, which leads to aerosol being advected away from the surface to higher model levels.

If this is the case, we would see a change to the vertical profile of CA in the model. We would expect that increasing OC absorption would lead to a decrease in the surface levels but an increase of OC aloft. Reduced absorption would reduce the buoyancy, and so more aerosol would remain in the surface level of the model, with reductions of CA aloft.

3.4.4 BC and OC Vertical Profiles

Figure 3-11 shows the differences in globally averaged BC and OC vertical profiles in the altered absorption simulations compared to the control. When OC absorption is included in the model, both the BC and OC mass mixing ratio is decreased in the lowest 2000 m of the model. The peak of these changes occurs slightly above the surface, and both are three times greater than the annual variability in changes to the vertical profile. Between the 2000 m and 10000 m, increasing OC absorption leads to an increase of both the OC and BC mass mixing ratio, with two distinct peaks at around 3000 metres and 15000 metres. When the BC refractive index used in the model is reduced, the opposite is seen, with BC and OC mass mixing ratio increased below the 2000 metres. Similarly, peaks in decreased BC and OC mass mixing ratio occur near the 3000 metres and 15000 metres.

2000 metres is around the height at which low cloud forms. This suggests that the changes that occur below that occur because of purely dynamical reasons. The results from analysing the vertical profile suggest that our theory of increased absorption equating to an increase of aerosol buoyancy is correct. We also note that dry deposition of both BC and OC are reduced by up to 10%, although changes in the lifetime are on the order of 20 minutes (0.02 days), and within the annual variability. This suggests that more aerosol is removed through wet deposition. This would correlate with increased buoyancy and increased aerosol in cloud-producing levels of the model. We note that there is reduction in the size of changes around

6000 metres. We suggest that this is due to interactions of extra aerosol with clouds, which will have different effects depending on region, aerosol position and time of year. The highest peak of changes, 15000 meters, is roughly equivalent to where we would expect to find the tropopause, and represents a physical barrier for aerosol uplift.
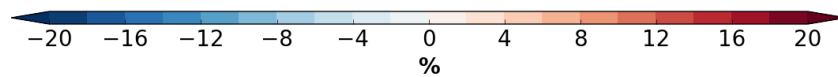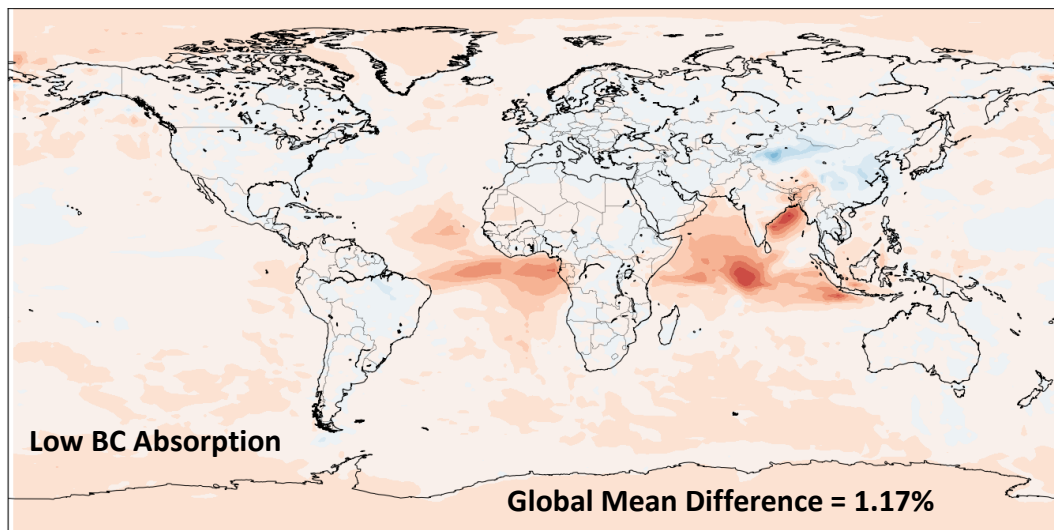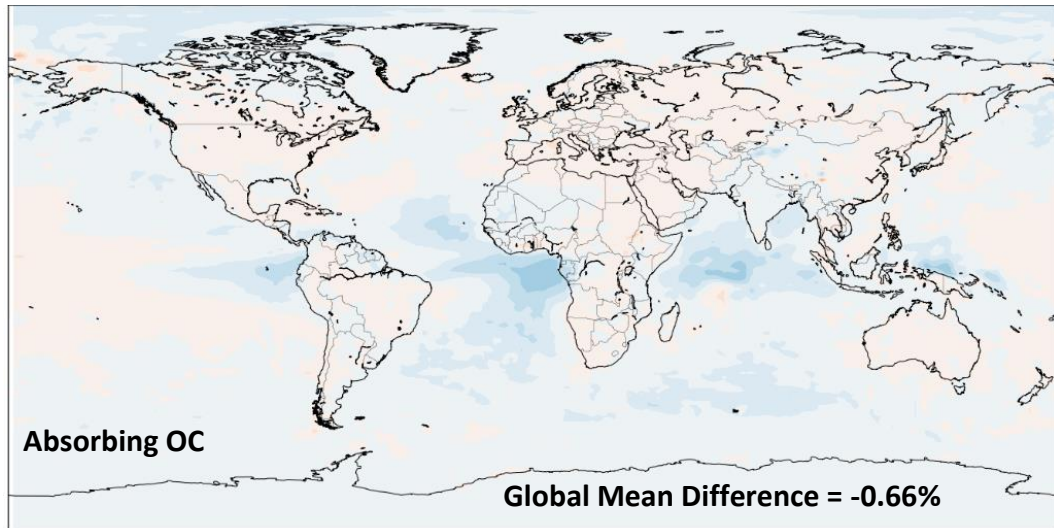
Figure 3-10 - Global distribution of percentage changes in surface OC concentrations between control simulation and OC absorbing and BC low absorption simulations for the period 2006-2008.
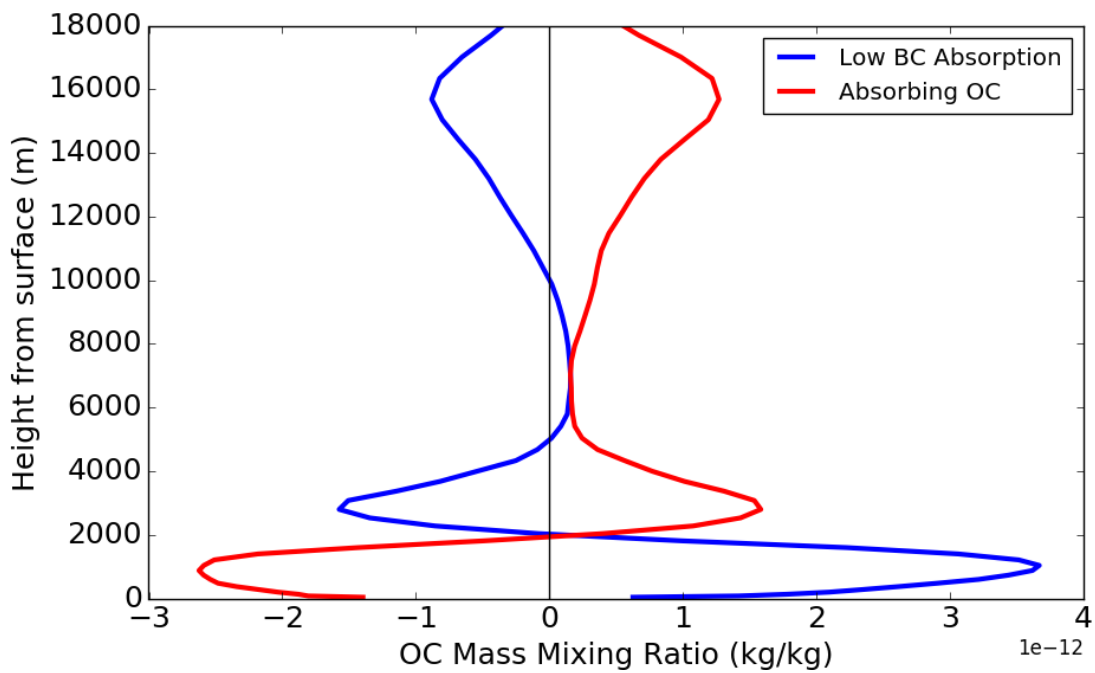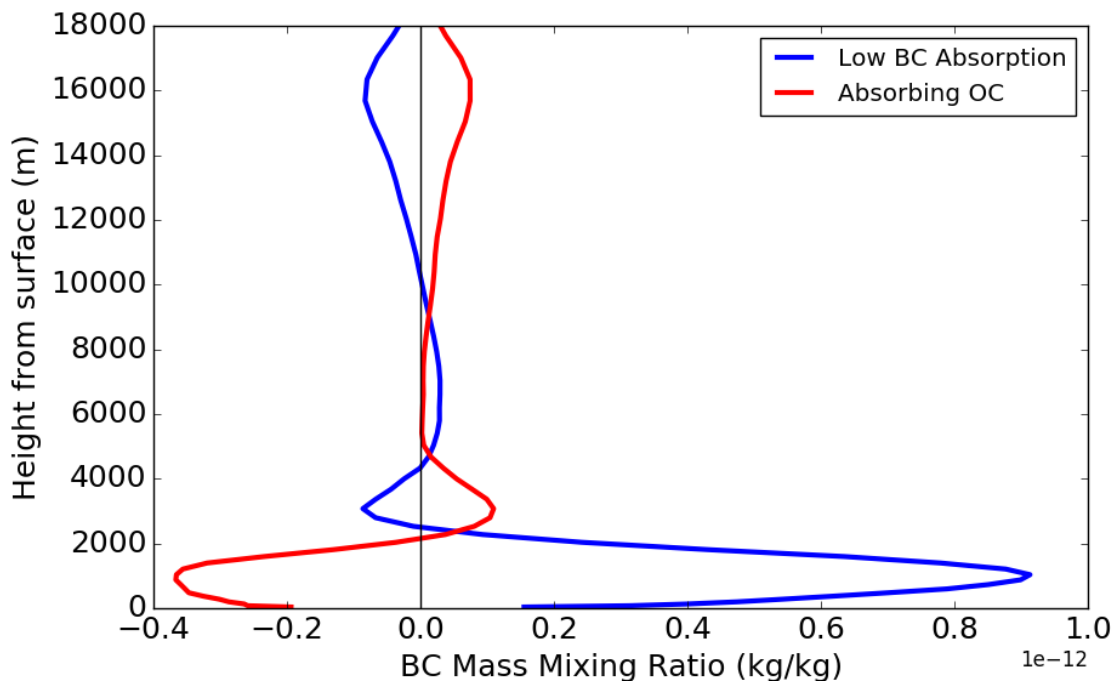
Figure 3-11 – Differences between the global average vertical profile of BC (top) and OC (bottom) mass mixing ratio in altered absorption simulations compared to control simulations

Figure 3-12 shows the distribution of the average percentage change in BC burden when CA refractive indices are altered. When OC is made absorbing, global BC burden is reduced by

0.2%, indicating no significant change, as the annual variability of the burden is 2.5%. However, changes to BC burden locally can be both positive and negative. In Central Asia and the Indian Ocean, BC burden is reduced by up to 6% when OC is made absorbing. In the Central Pacific and off the West Coast of Africa, BC burden is increased by up to 6%. When BC absorption is reduced in the model, BC burden is increased by 0.9% globally, still below the annual variability. In the Indian Ocean, increases in BC burden reach 16% locally, whilst increases of up to 6% also occur across much of the Arctic and Antarctica. However, reducing BC absorption leads to decreases in BC burden of up to 6% over the Central Pacific Ocean, Central Asia and off the West Coast of Africa. Figure 3-13 shows the distribution of average percentage change to the OC column burden when CA refractive indices are changed. When OC is made absorbing, OC column burden is increased by 0.1%. OC column burden is increased by up to 6% in the Pacific Ocean and off the coast of Western Africa, but decreased by up to 4% in the Indian Ocean. When BC refractive indices are reduced, OC burden is increased by 0.2%. Both these global changes are well below the annual variability of the OC burden. In the Indian Ocean, OC burden is increased by 10%. However, over the Pacific Ocean, Central Asia and African Coast, OC burden is reduced by up to 6%.

The spatial pattern of changes in both BC and OC burden show differences between those seen in the surface at many sites. Several regions show a decrease in both OC and BC surface concentrations when OC is made absorbing. However, these same regions show increases in the total column burden of BC and OC. This suggests that the reduction of aerosol seen at the surface has been transported vertically, which reduces dry deposition and so has increased lifetime. However, this is not the case for all regions. In the Indian Ocean, both surface concentrations and total column burden of BC and OC are reduced when OC is made absorbing. Figure 3-14 shows the difference in mass mixing ratio between the vertical profiles of BC and OC between the perturbed simulations and control for an average vertical profile of the Indian Ocean, which shows changes of the same sign in both surface CA concentration and CA burden, and a vertical profile of the Atlantic Ocean near Eastern Africa, where changes to CA surface concentrations and CA burden are of opposite signs. For the both East African and Indian Ocean profiles, increasing absorbing OC decreases the surface levels of BC and OC below 2000 metres, matching those seen in the global average.
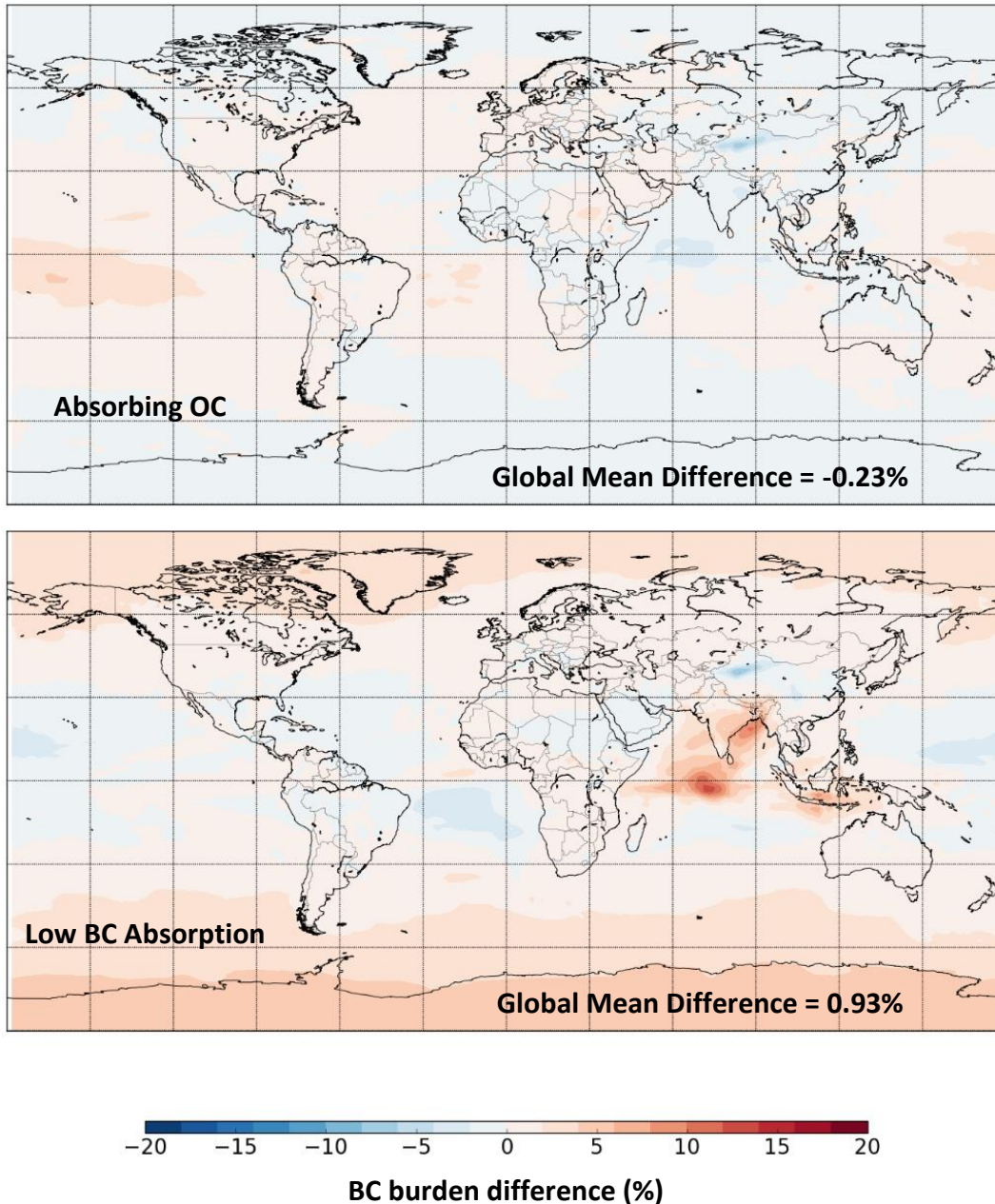
Figure 3-12- Global distribution of percentage changes in BC burden between control simulation and absorbing OC (top) and low BC absorption (bottom) simulations for the period 2006-2008.

However, between 2000 and 5000 metres, the averaged profile over Eastern Africa shows that increasing absorption increases BC and OC mass, as seen in the global average, whilst in the Indian Ocean, there is still a decrease in BC and OC mass at these levels. This explains why a decrease in both surface concentrations and total column burdens of BC and OC exists in that regions, but does not other regions. Therefore, there must be a process which is removing the aerosol from this altitude in the Indian Ocean which causes a reduction in both surface concentrations and CA burden that is inhibited in other regions. As it occurs in model

layers where cloud is created, we propose that these changes occur because of interactions between aerosol and cloud, having indicated in Chapter 1 that the position of absorbing aerosol is critical to the growth of clouds (Wang, 2013).
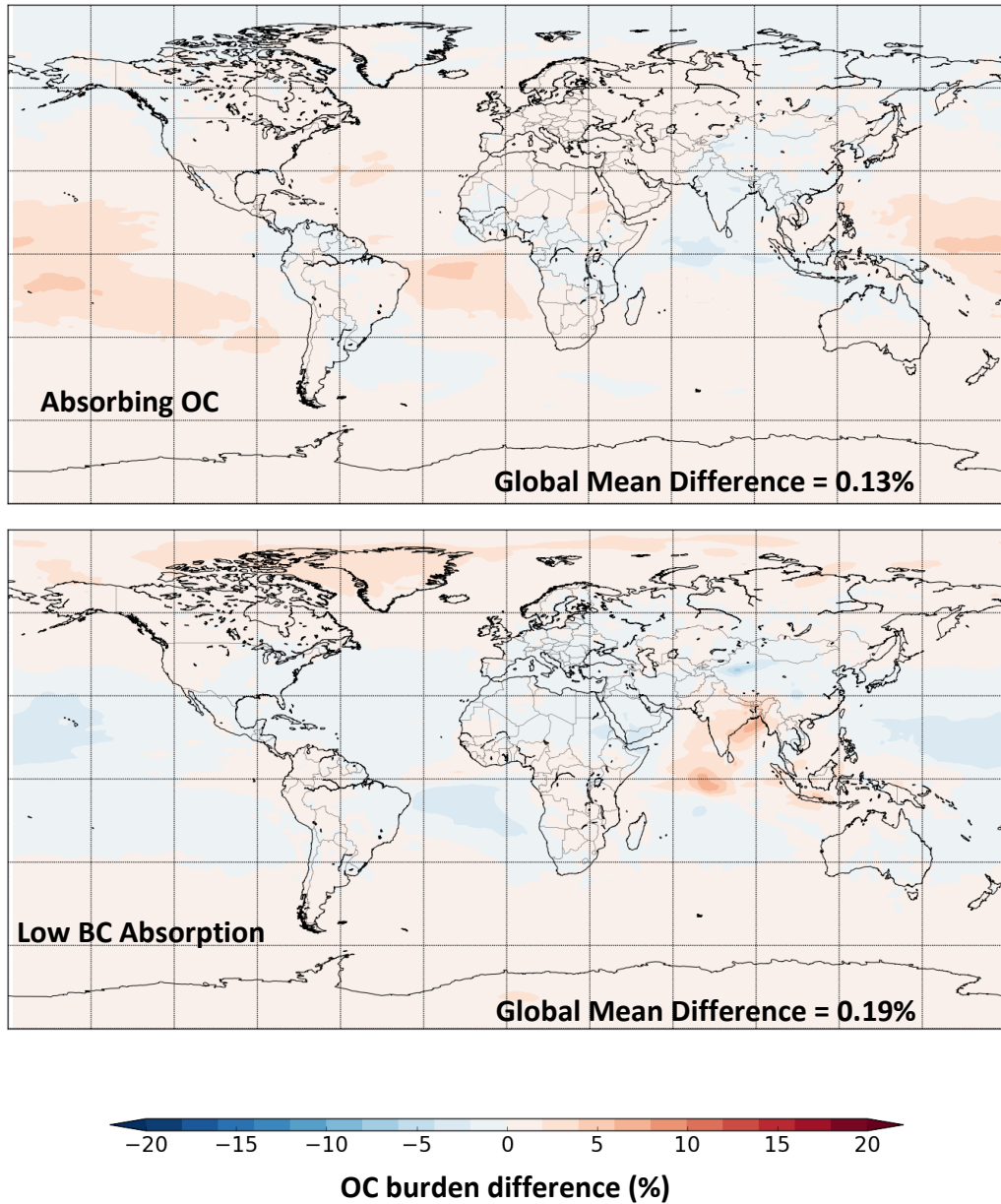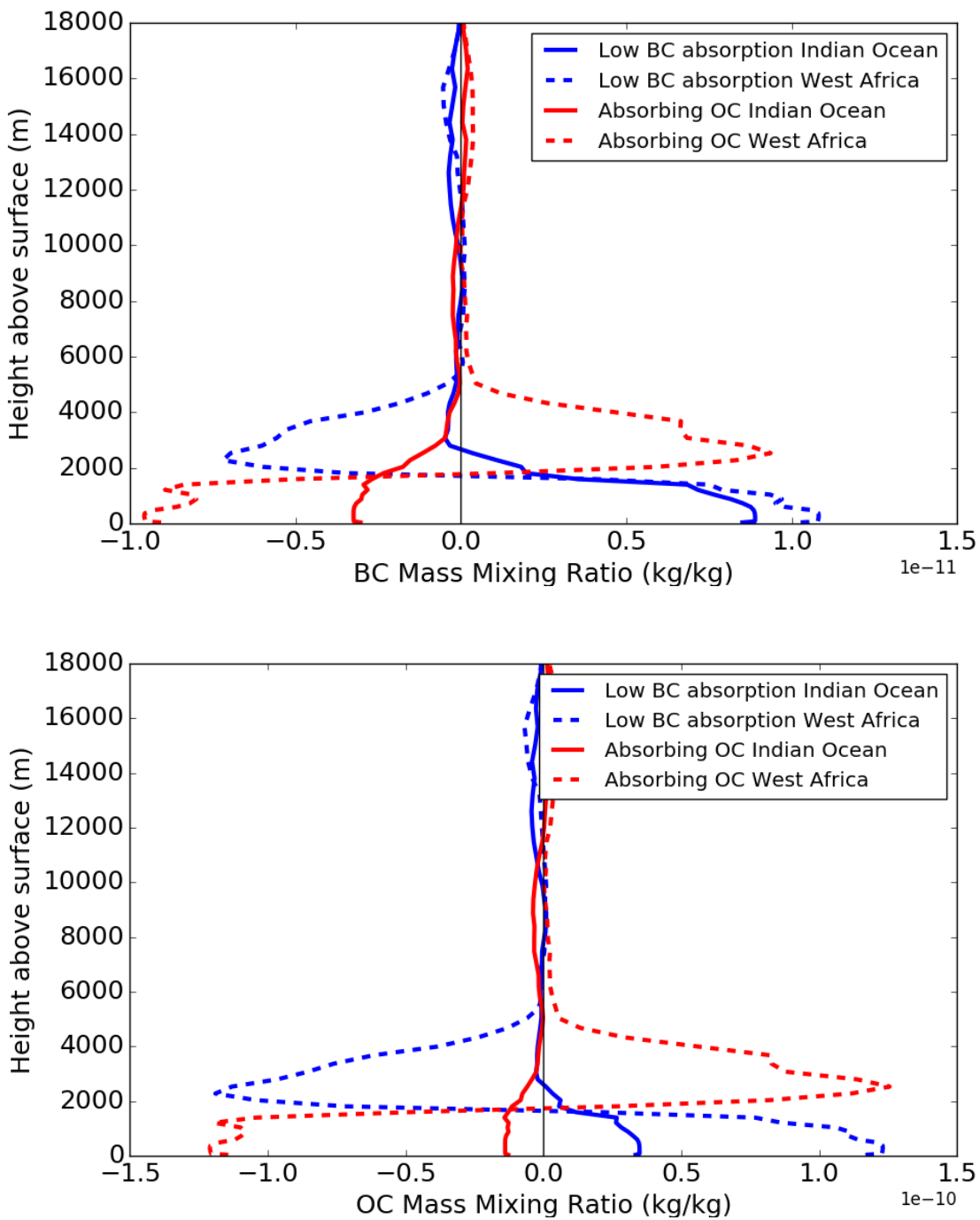

Figure 3-13 - Global distribution of percentage changes in OC burden between control simulation and absorbing OC (top) and low BC absorption (bottom) simulations for the period 2006-2008.

Figure 3-14 - *Differences in the vertical profile of BC and OC mass mixing ratio between the perturbed simulations and control, averaged globally and over the Indian Ocean*

There are several reasons why the Indian Ocean may be more sensitive to changes in radiative heating. Vertical transport in this region is strongly related to the daily convective nature, which are likely to be more sensitive to changes in heating. Similarly, the area has been

intensely studied as the Indian Monsoon is an important feature of the local seasonal dynamics which has proven difficult to reproduce in climate models, and shown high sensitivity to local conditions (Bush et al., 2015). It is possible that parameterisations which are specific to conditions found in this region are responsible for higher local sensitivity to changes in radiative heating.

3.5 Summary and Conclusions

Altering the mass-absorption coefficient of CA by changing the refractive indices has large implication on modelled aerosol optical properties, as changes in AAOD of up to 150% in biomass burning regions can be achieved. In these regions however, the lower SSA that accompanies the higher AAOD worsens the comparison between the model and retrievals of SSA from AERONET. This suggests that where SSA in the model and observations are well matched, AOD and AAOD need to be increased in similar proportions, whereas increasing OC absorption increases AAOD by a greater proportion than AOD. Saleh et al., (2014) suggests that OC from biomass and biofuel burning sources is more absorbing than OC from fossil fuel combustion. The refractive index of OC which we use in this study reflects a refractive index of combined OC and BrC for biomass burning. Thus, as we increase all OC absorption in the model, we would have expected to find that absorption was overestimated in fossil fuel burning regions, and improved in biomass burning regions. However, improvements in AAOD occur regardless of the main emission sources. Increasing OC absorption also leads to underestimation of the SSA in biomass burning regions. This means one of two things. Either AOD must be increased in biomass burning areas if we intend to implement any form of absorbing organic carbon scheme, or the absorption from BC needs to be reduced. This former could be implemented through either increases in non-absorbing aerosols, whilst the latter could be improved through reducing either BC mass or BC refractive index.

In addition to showing an improvement when OC is made absorbing, the comparison of AAOD and SSA in fossil fuel combustion regions are worsened when the BC refractive index is reduced. Thus, we use this to determine that BC refractive index should remain at the higher end of the spectrum of values in literature. There also appears to be scope for further increases to absorption in both Europe and North America through other methods. However, these changes must ensure that absorption is assigned correctly to ensure that changes

balance the need for addition absorption from fossil fuel, but do not increase absorption from biomass burning areas.

Despite there being no change in emissions, secondary effects on the lifetime can be seen, with some regional changes effecting surface concentrations and burden by up to 20%. This is due to a change in the vertical profile, with increased absorption from absorbing OC moving aerosol to higher model levels, reducing the surface concentrations and dry deposition rate of CA. The change in column integrated burden is dependent on the region chosen, showing that the effect of CA on the local atmospheric system differs in different locations. These results are also good for any further attempts to improve the model on a regional basis, as a global perturbation in the refractive index of BC and OC has local effects of differing signs and magnitudes. The increase of absorption in the model from OC absorption increases improves the comparison between the model and observations in most regions.

The above conclusions highlight that there are methods of increasing CA mass and optical depths that are not associated with increased emissions. Whilst there are now improved comparisons with AAOD, there are still large underestimations of mass in most regions. A perfect comparison of AAOD in all regions show that absorption is not correctly attributed if mass is still underestimated. In the next chapter, we evaluate the sensitivity of the model to emission inventories of CA, and investigate how changing emissions of CA can affect both the model, and its comparison with observations.

4. Chapter 4: Solution Two – Emissions and Mass

Chapter 4 has two main aims. Firstly, to determine a range of uncertainty in emissions of BC and OC. Secondly, to assess spatial and numerical changes to the model that occur when emissions are scaled within the range of uncertainty determined. Analysis of how emission changes affect model variables both globally and regionally is of importance in assessing whether emission scaling can improve the comparison of the model with observations, and decrease the differences in regional biases that exist presently.

4.1 Sensitivity to Carbonaceous Aerosol emissions

There is a large amount of literature highlighting the uncertainty in emission of carbonaceous aerosol. Bond et al. (2013) reviews the need for CA emission scaling. They determine that there are wide ranges in BC and OC emission values based on a variety of factors, including the methods used to estimate emissions. Ranges of global all-source BC emissions for the year 2000 ranged from 2 to 29 Tg yr^{-1}, with the majority ranging from 6 to 18 Tg yr^{-1}. The range of emitted primary organic aerosol ranged 18 to 180 Tg yr^{-1} worldwide. Bond et al. (2013) also highlights large differences between datasets in regional emissions, with no consistent bias, and large differences in sector by sector emission inventories. The authors compare modelled averages from the AEROCOM comparisons with both observed BC surface concentrations and retrieved AAOD. These comparisons highlight large underestimations of BC in Asia, but relatively good agreement elsewhere. AAOD is shown to be underestimated in models worldwide compared to AERONET observations, with the largest underestimation in Asia in Autumn and Winter. From these results, and results of inverse modelling of emissions, the paper concludes that increases of between 60 and 170% are required to correctly replicate BC burden, and higher to correctly replicate AAOD. However, this method has drawn criticism, and others studies have been able to account for biases in BC surface concentrations and absorption through changing the horizontal resolution (Wang et al., 2016) or changing the BC lifetime (Samset et al., 2014).

Gadhavi et al., (2015) uses a similar method to Bond et al., but on a regional scale. The authors use several emission inventories, including the ECLIPSE dataset, in a Lagrangian particle dispersion model and compare output with surface BC concentration observations in

Southern India. The paper reports that to get a good comparison, the ECLIPSE dataset required scaling by a factor of 1.7.

Several more papers focus on the emissions of biomass burning. Kaiser et al. (2012) compares GFED3.1 to the Global Fire Assimulation System emissions, which is a similar product, and then determines the increase needed to match with concentrations of PM10 and MODIS AOD retrievals. The author determines that GFED3.1 has missing emissions due to small fires, and recommends an increase in emission rates by a factor of 2 – 4. Liousse et al. (2010) uses the ORISAM-TM4 global chemistry transport model to compare to local observations of BC surface concentrations and scattering coefficient to determine the suitability of GFED2 emission inventories for Africa. They report that emissions need to be scaled by a factor of 2.5 for model values to be comparable with observations. Akagi et al. (2011) compares GFED3.1 with new emission factors, also report that underestimations occur in the GFED product for some emission sources, particularly in tropical regions, by about 75%. The paper does state that other sources, such as crop burning, agree with their evaluation of emissions. Johnson et al. (2016) compares AOD from the South American Biomass Burning Experiment (SAMBBA) campaign to a slightly different version of the HadGEM model than is used in this work. They also found that increasing GFED3 emissions by a factor of 2 was required to get good comparisons between model and observations.

The current Met Office standard jobs suggest that a factor of 2 is applied to the biomass burning using GFED emissions (Johnson, *personal communication*). Bond et al. (2013) describes the range of present day emissions of BC from biomass burning as being between 2-6 Tg yr^{-1}, with OC emissions ranging between 20 – 27 Tg yr^{-1}.

Recent literature also discusses the effect of the conversion factor of OC to particulate organic matter (POM). Most models use a factor in the range of 1.2 to 1.6, with 1.4 being the most frequently chosen ratio (Tsigaridis et al., 2014). Brito et al. (2014) use observations from the SAMBBA campaign to characterize biomass burning aerosols. They report that the POM:OC ratio in biomass burning emissions should be higher, possibly as high as 1.8. Tiitta et al. (2014) uses a similar method on African biomass burning emissions and reports a similar result from the biomass burning there. Johnson et al. (2016) highlights observations which suggest that the POM:OC ratio may be much higher for OC emissions, nearly double the original estimates.

This increases uncertainty in the current ratio of POM:OC used in the model, where near-source ageing is not represented because the model time-step is 1 hour, which may be longer than some aging processes.

4.2 List of Sensitivity Studies

This section outlines the different simulations used, based upon the literature described above. Table 4-1 lists the perturbed simulations used in this section, with a description of the changes made and supporting references. Increases in biomass burning and fossil/biofuel emissions are obtained by the most common scaled values used in literature (2 and 1.7). Separate simulations which scale only BC emissions are also done to capture the uncertainty in the BC:OC emission ratios in the emission inventories. We take a larger value of the POM:OC ratio (2.8) for biomass burning emissions only, to determine the upper limit of changes that can occur from using the previous constant value of 1.4.

Name	Description	Supporting Reference
FFx1.7	Increase in Fossil and Biofuel burning emissions of BC and OC by a factor of 1.7	Gadhavi et al. (2015), Bond et al. (2013)
BBx2	Increase in biomass burning emissions of BC and OC by a factor of 2	Mann et al. (2010), Liousse et al. (2010), Kaiser et al. (2012)
FFBCx1.7	Increase in Fossil and Biofuel burning emissions of BC only by a factor of 1.7	Gadhavi et al. (2015)
BBBCx2	Increase in biomass burning emissions of BC only by a factor of 2.	Bond et al. (2013), Pan et al., (2015); Reddington et al., (2015)
POM:OC	Doubling of Particulate Organic Matter: Organic Carbon ratio in Biomass burning emissions from 1.4 to 2.8.	Brito et al. (2014), Johnson et al. (2016)

Table 4-1 - Name and description of simulations used in this chapter, with references supporting the choice of sensitivities.

4.3 Results

4.3.1 Surface BC and OC Concentrations

Figure 4-1 shows the distribution of average percentage changes in surface BC concentration between BBx2, BBBCx2 and the control simulation. Doubling both BC and OC biomass burning emissions increases globally averaged surface BC concentration by 24%. This is much greater than the maximum inter-annual changes seen in global surface BC concentrations (2.5%) over the same period. Surface BC concentrations are more than doubled in areas of biomass burning aerosol source regions such as South America, Central Africa, Northern Australia and Boreal regions of North America. The BBBCx2 simulation also increases surface BC concentrations by up to 60% in areas where biomass burning aerosol is transported, such as the Southern Atlantic and Southern Pacific oceans. In the BBBCx2 simulation, the globally averaged surface BC concentration increases by 28%, which is 4% more than in the BBx2 simulation. Regionally, surface BC concentration is increased by up to 100% in Central Africa, Northern Australia and Boreal North America, with a similar spatial pattern to the increases seen in BBx2. BBBCx2 shows increases in surface BC concentrations in regions of biomass burning aerosol transport by up to 80%, greater than increases seen in the BBx2 simulation.

Figure 4-2 shows the distribution of average percentage changes in surface OC concentration when biomass burning emissions are increased. In the BBx2 simulation, the global average surface OC concentrations increases by 25%. Increases of up to 100% are seen in biomass burning source regions, such as Africa, South American and Boreal regions. Increases of up to 60% are seen in remote transport regions, such as Central Pacific, Arctic and Antarctica. Regions where OC emissions are predominately from fossil or biofuel burning, such as Europe, Central Asia and USA show increases in surface OC concentration of less than 20%. In the BBBCx2 simulation, surface OC concentration is not significantly reduced globally compared to the control, although surface OC concentrations drop by up to 15% off the coast of Western Africa with increases of up to 6% in the Indian Ocean and Pacific Ocean.
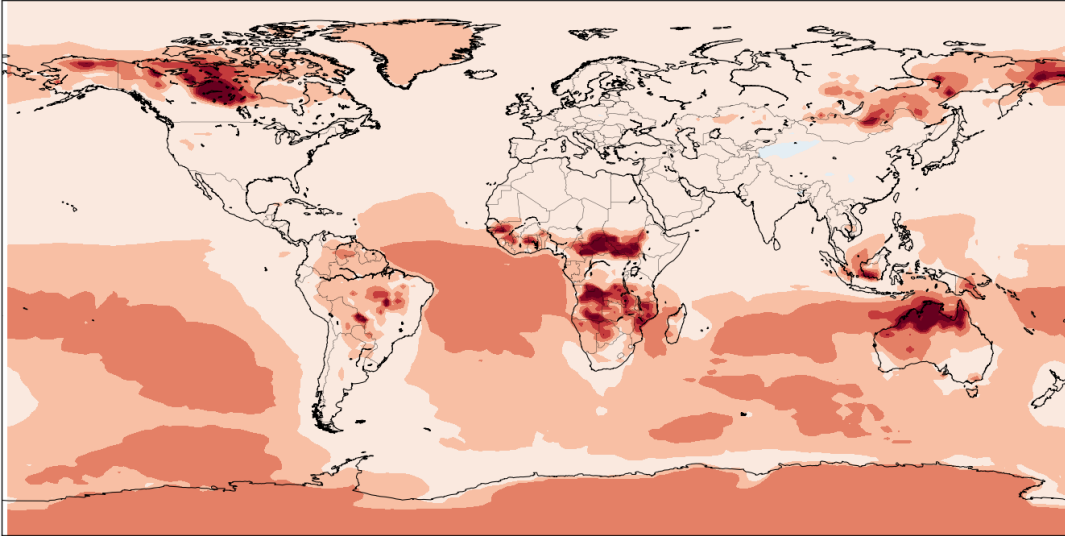
Figure 4-3 shows the distribution of percentage changes in surface BC concentrations between increased fossil/biofuel burning emission simulations and the control simulation, averaged over 3 years. In the FFx1.7 simulation, surface BC concentration is increased on

average globally by 52%. In Central Europe and Eastern Asia, local increases in surface BC concentration reach up to 70%, with increases of up to 50% in North America and in areas of fossil fuel burning transport. When FFBC is increased by 1.7, the area-weighted global average surface BC concentration is increased by 48%. The spatial distribution of increases is a mirror of the increases seen in the FFx1.7 simulation, except in the Pacific Ocean and other areas where fossil and biofuel aerosol are transported. In these regions, the increase in surface BC concentration is around 20% less than when both BC and OC are increased.

Figure 4-4 shows the distribution of surface OC concentration percentage changes when fossil and biofuel emissions are increased. When both FF is increased by 1.7, globally averaged surface OC concentration increases by 18%. Regionally, there are changes of over 60% in regions with high fossil/biofuel emissions, such as East Asia, Europe and East Africa. Increases to surface OC concentration reduce as distance from the sources increases. Increases in surface OC concentration of up to 60% also occur off the coast of Antarctica and South America in the model. When just FFBC emissions are increased by 1.7, the surface OC concentration not reduced globally by a significant amount. However, a decrease of up to 16% is observed in the Indian Ocean, with no other region showing any increase or decrease of over 6%.

Figure 4-5 shows the distribution of average percentage changes in surface BC and OC concentrations between the increased POM:OC ratio simulation and the control simulation. When the POM:OC ratio is doubled, global surface BC concentration is reduced by 2.2%. In most biomass burning emission regions, surface BC concentration is decreased by up to 20%. Regions of biomass burning aerosol transport show decreases of up to 15% in surface BC concentration when POM:OC ratio is doubled. However, in Boreal North America, and at some sites in Africa and Northern Australia, surface BC concentration is increased by up to 30%. Surface OC concentration is increased by 26% when the POM:OC ratio is increased, with increases of up to 80% in source regions such as Central Africa and Boreal regions of North America and Asia. Increasing the POM:OC ratio leads to smaller increases in surface OC concentration in regions known to be areas where biomass burning aerosol is transported than when all biomass burning aerosol emissions are increased.
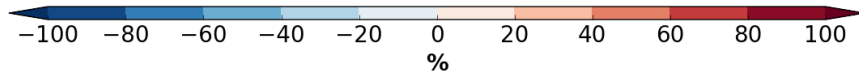
BB emissions x 2 and CTRL = 23.57%

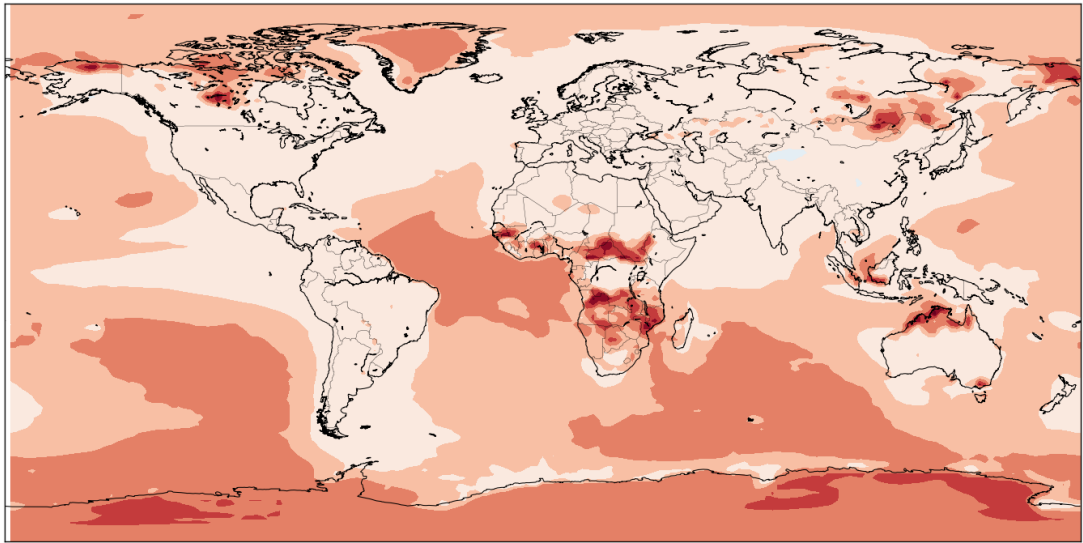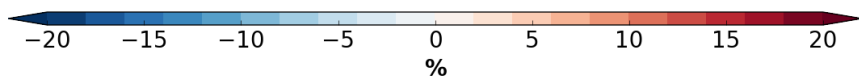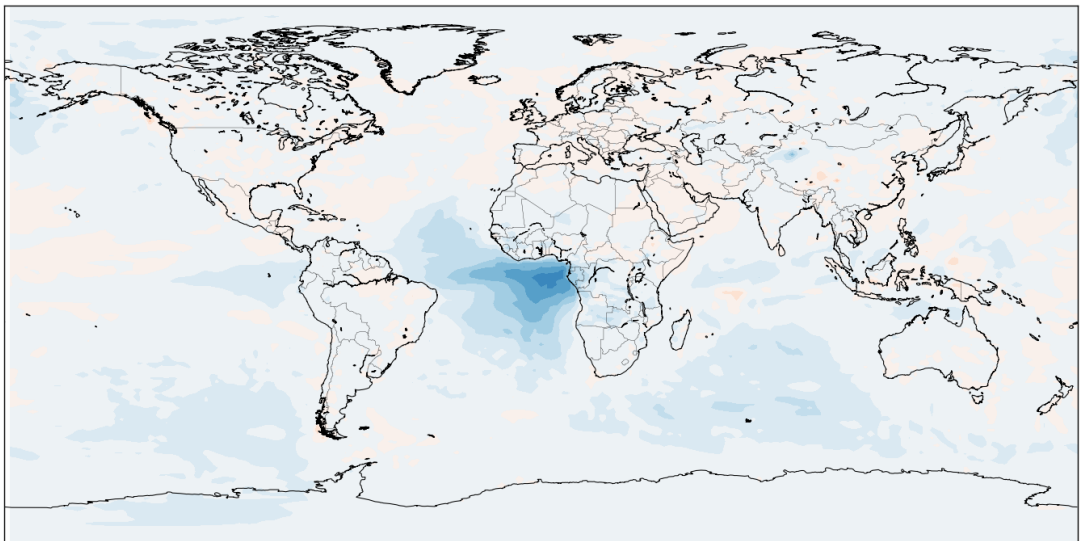### 2 x BBBC and CTRL = 27.81%
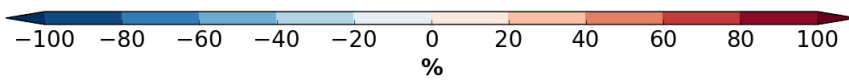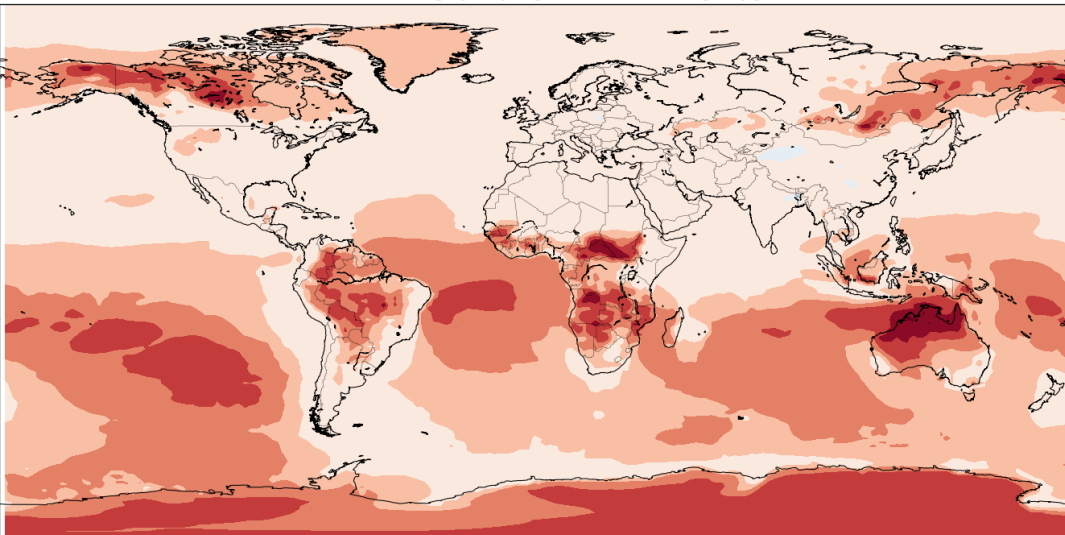
Figure 4-1 - Global distribution of percentage changes in surface BC concentration between simulations with increased biomass burning emission and the control simulation for the period 2006-2008
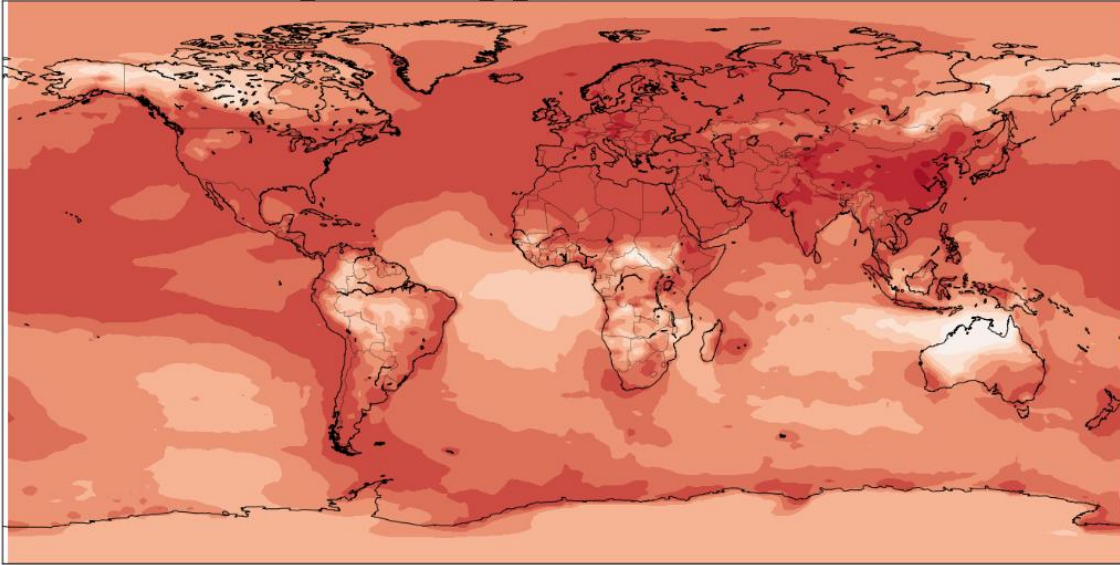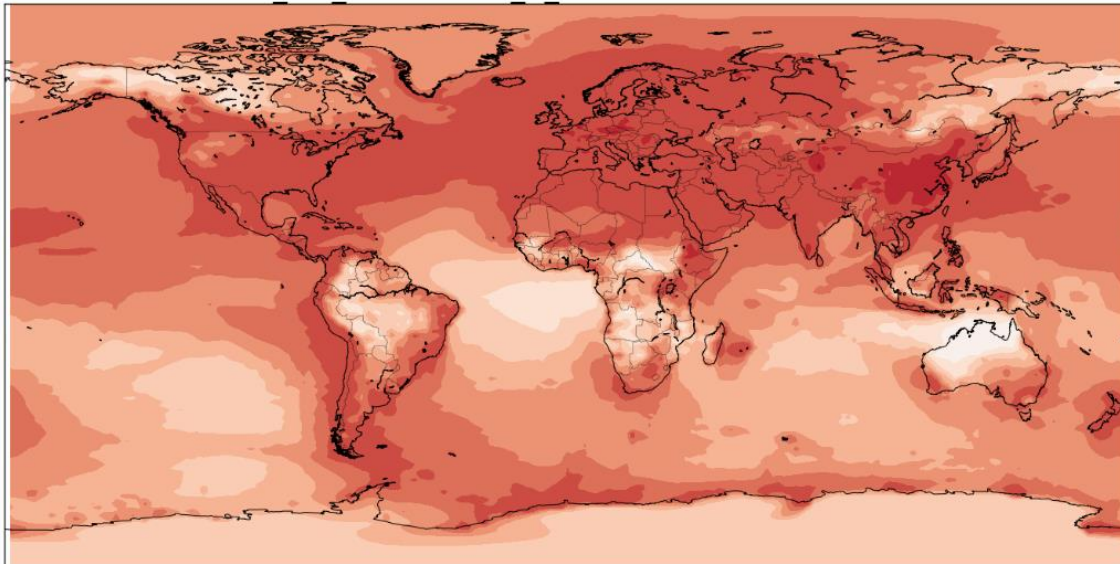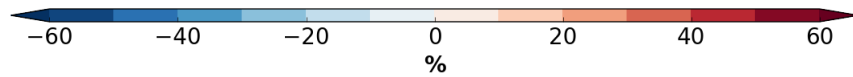
BB emissions x 2 and CTRL = 24.6%

2 x BBBC and CTRL = -1.11%

Figure 4-2 - Global distribution of percentage changes in surface OC concentrations between simulations with increased biomass burning emissions and the control simulation for the period 2006-2008
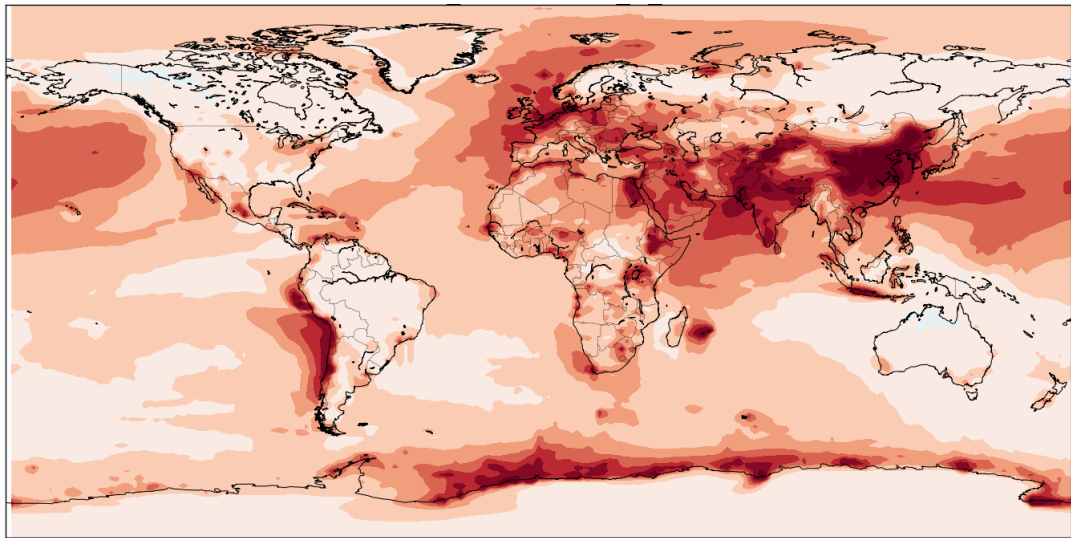
Figure 4-3 - Global distribution of percentage changes in surface BC concentrations between simulations with increased fossil/biofuel burning emissions and the control simulation for the period 2006-2008

FFBF emissions x 1.7 and CTRL = 18.29%

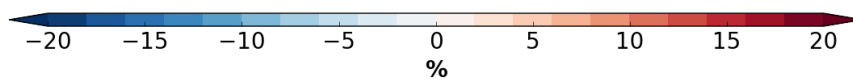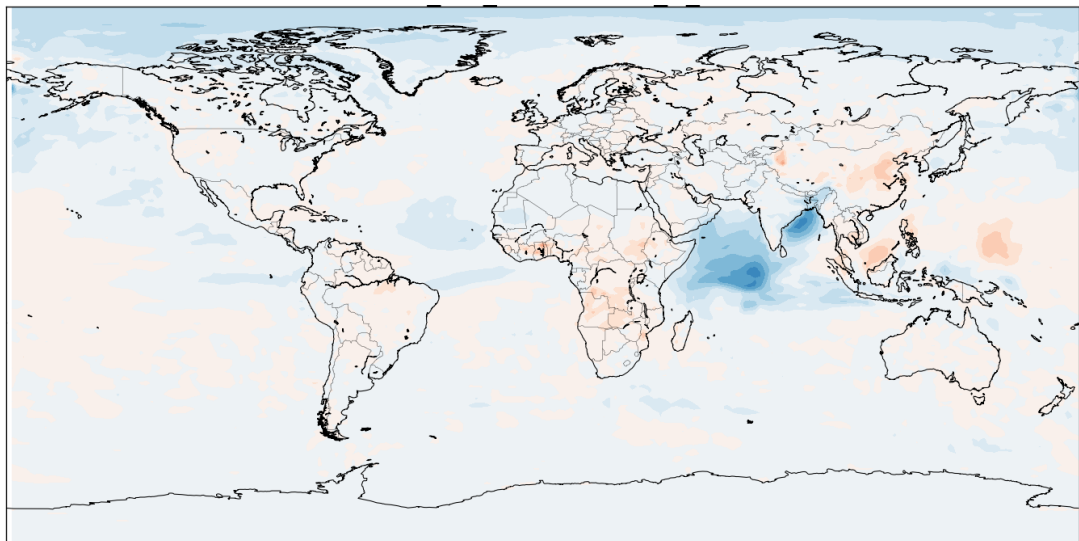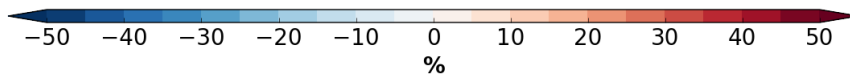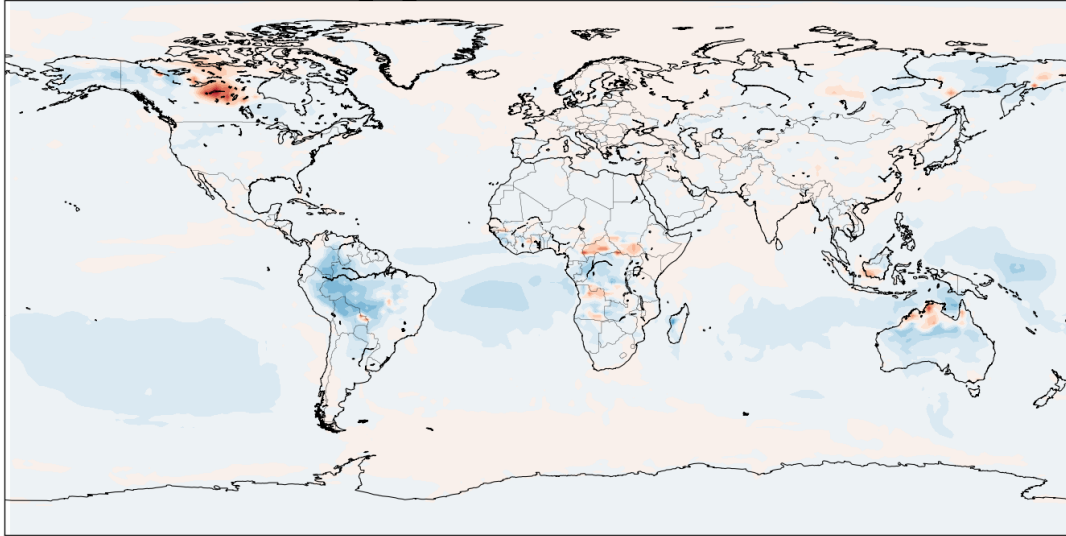**FFBF BC emissions x 1.7 and CTRL = -0.62%**

Figure 4-4 - Global distribution of percentage changes in surface OC concentrations between simulations where fossil/biofuel burning emissions are increased and the control simulation for the period 2006-2008

Increase_in_OC:POM and CTRL = -2.22%

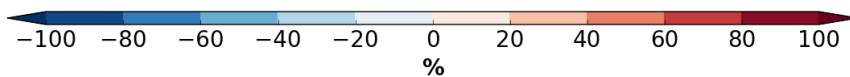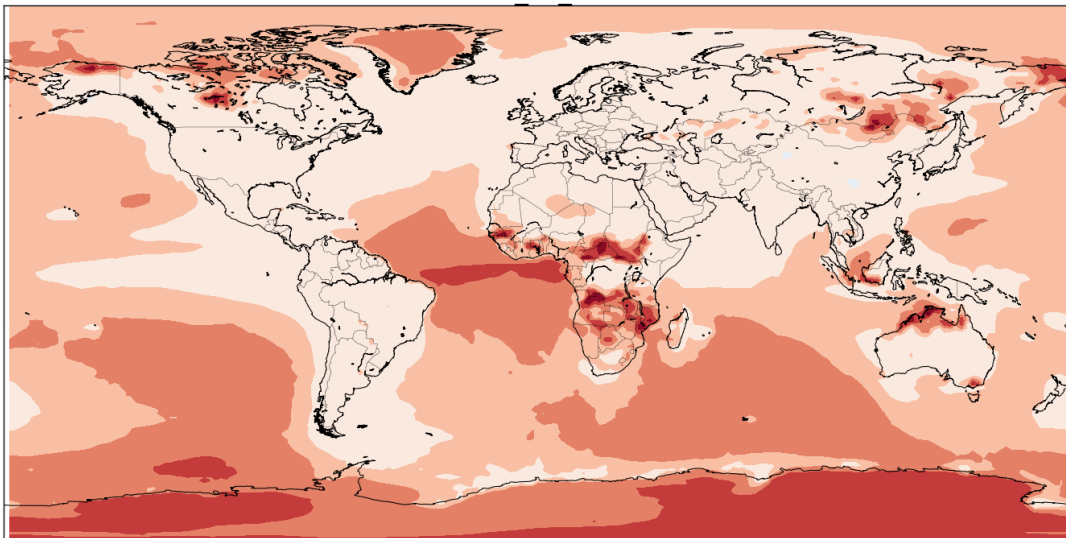## Increase in OC:POM and CTRL = 25.95%

Figure 4-5 - Global distribution of percentage changes in surface BC (top) and surface OC (bottom) concentrations between the increased POM:OC ratio simulation and control simulation for the period 2006-2008

The patterns seen in the figures above can be explained through the same mechanisms. Firstly, increasing emissions of BC, regardless of source, increases the global average of surface BC concentration. Increasing fossil/biofuel emissions of BC shows the largest change at the source, with reducing changes as distance from source areas increase. When biomass burning emissions are increased, surface BC concentration only contains a small part of the extra emissions, and is influenced by changes to the vertical transport of aerosol. Therefore, changes to surface BC concentration are larger over source regions, but also in remote regions where BC aerosol sediments from higher model levels. Increases in surface OC concentrations in the BBx2 simulation show a similar spatial pattern and magnitude to changes in surface BC concentration, because of the nature of the internal mixing of aerosol and similar life cycles BC and OC have in the model. The effect of the BBBCx2 simulation surface BC concentration is spatially similar to the effect from the POM:OC changes for surface OC concentration. Therefore, the spatial pattern of increases can be explained through similar reasoning.

Secondly, in the BBBCx2 simulation, a large decrease in surface OC concentration is reported off the coast of Africa, despite there being no change to OC emissions. We suggest that the increased BC levels in the atmosphere increases absorption of incoming radiation, which in turn increases the radiative heating. We show the vertical transport in response to increase absorption in Chapter 3, where the increased heating transports aerosols to higher model levels. This is a known effect, and is described by Koch & Del Genio, (2010) and if this was the case, we would expect no change to the lifetime. We find that whilst there is a slight increase in the globally averaged OC lifetime of less than an hour, this is not significant as it is within the inter-annual variability of the model.

Globally, increases in the surface BC concentration in the BBx2 simulation are lower than those in the BBBCx2 simulations, despite the same level of BC emission. Regionally, in BBx2, there are increases surface BC concentrations in biomass source regions but decreases surface BC concentrations in aerosol transport regions compared to the BBBCx2 simulation. In areas of predominately fossil fuel burning, source and transport regions both have larger increases in surface BC concentration in the FFx1.7 simulation compared to the FFBCx1.7 simulation. This increase in mass due to OC must be caused by an altered vertical distribution of the aerosol, as lifetime is virtually unaffected.

Figure 4-6 shows the mean factor of surface BC and OC concentrations between the increased emission simulations and ground site observations, grouped by regions. When any kind of emissions are increased, the mean factor of surface BC concentration is increased in all regions. Increasing fossil/biofuel gives the largest increase in the mean factor for all regions, improving the comparison between model and observations. In North America, increasing fossil and biofuel emissions decreases the underestimation of surface BC concentration from 52% to 17%. Increasing emissions of OC leads to increases in the mean factor of surface OC concentrations in all regions. Increasing only BC has little effect on the comparison between surface OC concentration in the model and observations in the areas considered. In several American regions, increasing both fossil /biofuel emissions of BC and OC increases the mean factor above 1, showing that the model overestimates surface OC concentration in those regions when these emissions are increased.

Comparing with surface OC concentration shows that increasing fossil/bio fuel emissions by 70% is potentially unjustified in America, although further increases in OC are needed to get better comparison between model and observations in Europe. Several European sites are within large cities. The model does not have the resolution to resolve OC concentration peaks within grid boxes from a city, which could explain why surface OC concentrations from European sites are underestimated in the model. In contrast, the sites in North America are in national parks and other rural areas. Therefore, the sites are more representative of a model grid square. Increasing emissions shows different characteristics when comparing surface OC and surface BC concentrations. With increases to emissions, surface BC concentrations are still underestimated in the model in all regions. This could hint that the OC:BC emission ratio is incorrect in the model, and that increasing BC by a factor greater than OC would improve the model in North America. However, this would not improve the model in Europe, where OC concentrations are underestimated by a larger amount than surface BC concentrations.

This section shows that increasing emissions leads to increases of surface OC concentration in both source and transport regions. It also shows that increasing BC emissions alone can influence the surface concentrations of other species, although this is smaller than the effect of increasing the emission of the species itself. This section also reports that increases to BC emissions still do not increase surface BC concentrations by enough to have a good

comparison with observations. However, this work also suggests that increasing OC in fossil fuel burning regions by 70% may be excessive when compared to rural North American sites, where we would expect background levels of OC to be consistent within a gridbox. This shows that simply scaling emissions globally is not necessarily good enough to resolve issues on a regional basis, and re-iterates that incorrect emissions cannot be solely responsible for the different between models and observations.
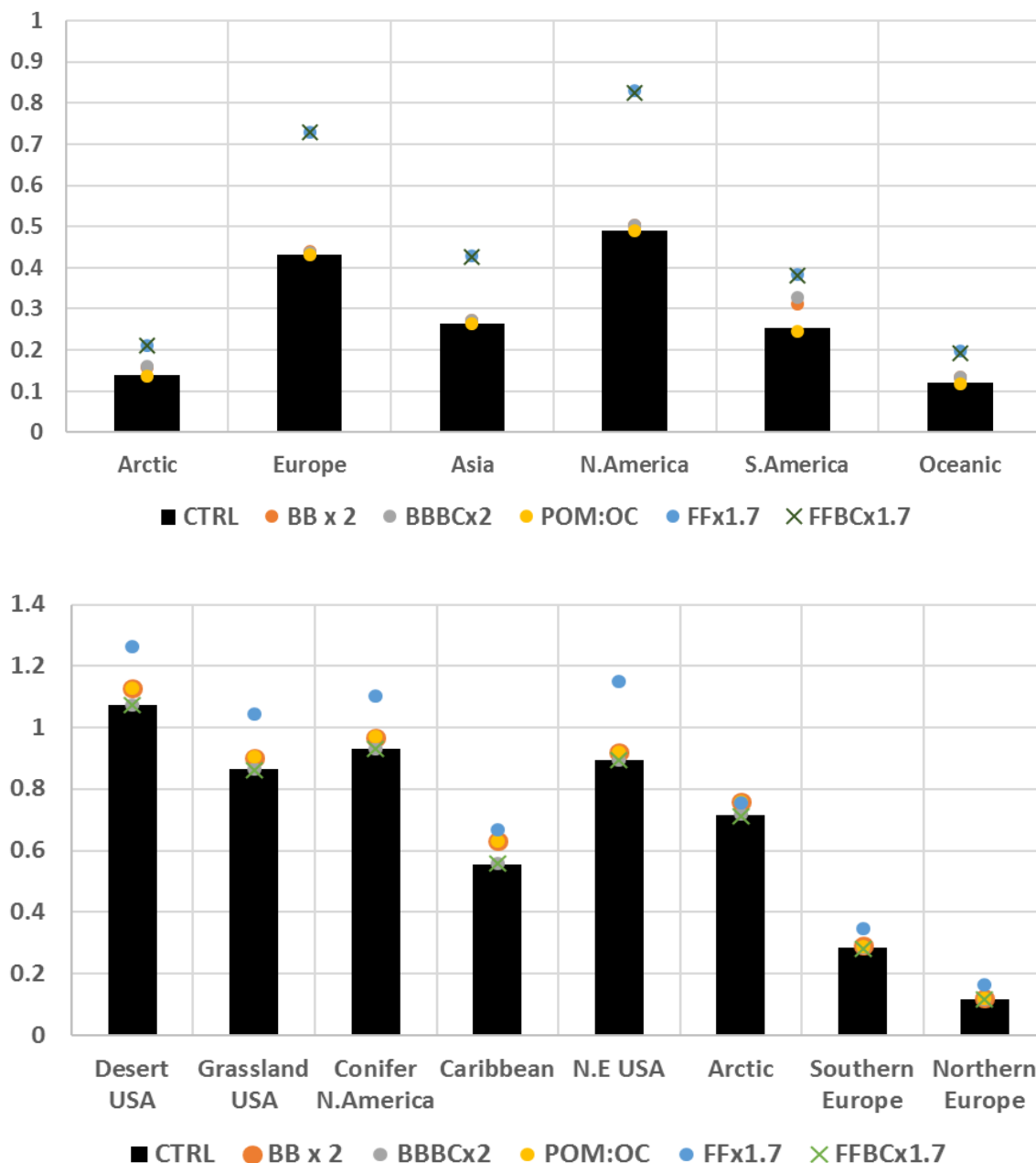

Figure 4-6 – Mean factor between modelled surface CA concentrations and observations of surface BC (top) and surface OC (bottom) concentrations from ground sites. A value under 1 shows the model underestimating compared to observations.

4.3.2 BC and OC Burden

Figure 4-7 shows the distribution of changes to BC burden between the increased biomass burning emission simulations and the control simulation. When both BC and OC biomass burning emissions are doubled, BC burden increases by 23% globally. Larger increases of up to 100% occur regionally in areas of biomass burning sources, such as Boreal regions, South America and Central Africa. Further increases of up to 80% occur in regions where biomass burning aerosol is transported, such as the Southern Ocean and South Atlantic. Areas of high fossil fuel emissions, such as Europe and North East USA show only small increases to BC burden when biomass burning emissions are doubled.
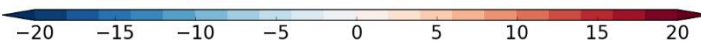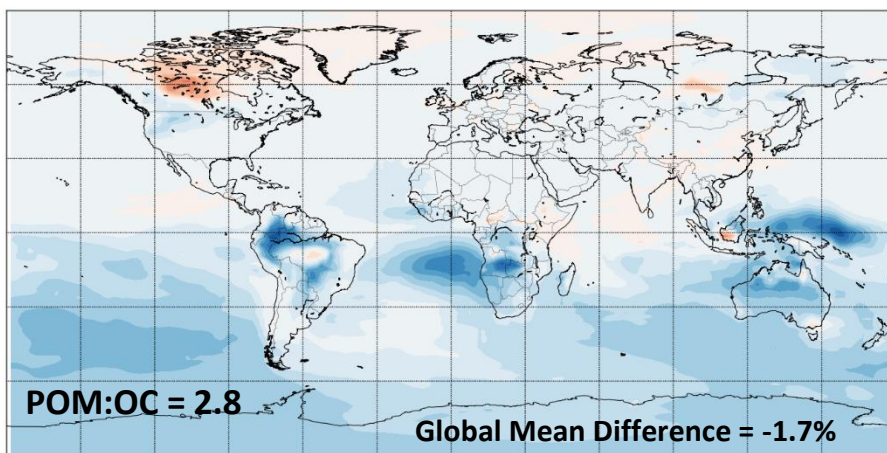
When only BC biomass burning emissions are doubled, the BC burden increases by 26% globally, which is not significantly different to when both BC and OC emissions are doubled. The spatial pattern of increases mirrors the changes seen when both BC and OC are increased. BC burden is increased by up to 100% in most biomass burning source regions, but also in the Southern Pacific, whilst increases of up to 80% occur in the South Atlantic and Boreal North America. Spatial spread of the increases in BC burden when only BC biomass burning emissions are increased are larger than the spread of increases when both BC and OC are increased. When the biomass burning POM:OC ratio is increased to 2.8, BC burden is not significantly decreased globally. Regional differences in how the BC burden changes when the POM:OC ratio is doubled mirror the regional differences in BC burden between doubled BC only and doubled BC and OC simulations.

Figure 4-8 shows the percentage change in BC burden between increased fossil and biofuel emissions and the control simulation. When both BC and OC fossil/biofuel combustion emissions are increased, the BC burden increases globally by 57%. Increase up to 80% are widely spread across the whole Northern hemisphere, both in source and remote regions. In the Southern hemisphere, up to 60% increases in BC burden occur, though these are limited to areas of large urban habitations.
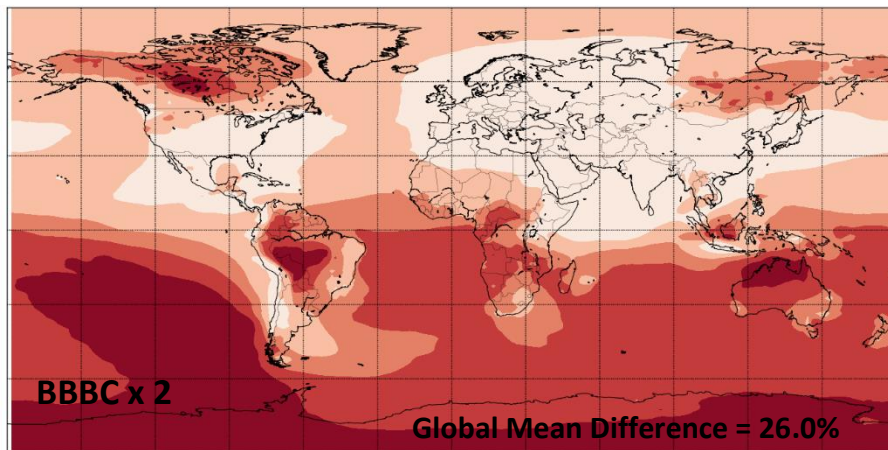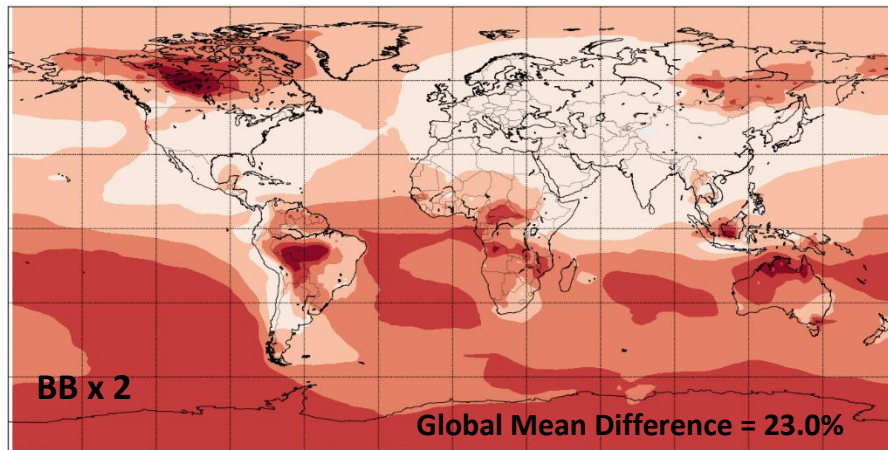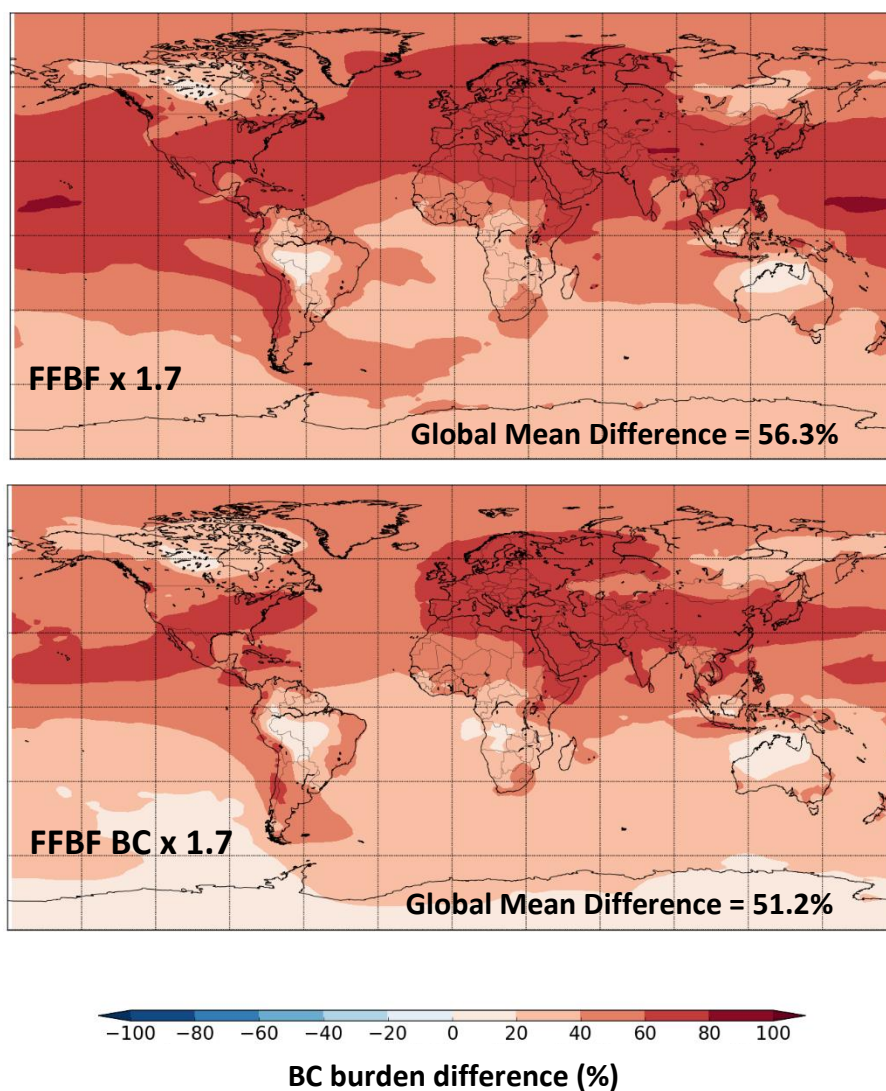
Figure 4-7 – Global distribution of percentage changes in BC burden between control simulation and simulations where biomass burning emission are perturbed for the period 2006-2008

When only BC fossil and biofuel emissions are increased, BC burden is increased by 52%, 5% less than when both BC and OC are increased. Increases in BC burden of up to 80% occur in the Northern Hemisphere, but the spatial spread of increases is reduced compared to when both BC and OC are increased. The largest increases occur only in areas with high fossil/biofuel emissions, such as Europe, Asia and Eastern North America. Increases in BC burden in the Southern Hemisphere when only BC emissions are increased are also smaller than when both BC and OC emissions are increased, particularly in remote regions such as Antarctica and the Southern Pacific.

Fossil and biofuel combustion, which accounts for the other 75-80% of BC emissions, also appears to increase global BC burden linearly when increased by 70%. Changes in BC lifetime are less than the variability in the annual mean lifetime of BC in the control simulation for all increased emission, varying by up to 0.03 days. This suggests that any effects on BC lifetime are local and not important globally. The hemispheric split found when fossil and biofuel emissions are increased is symptomatic of both the location of emissions and the dynamics of the atmosphere. The large majority of fossil and biofuel emissions come from the northern hemisphere, northwards of the inter-tropical convergence zone (ITCZ). Whilst air mixes horizontally through transport in the atmosphere, they rarely cross the ITCZ, mostly trapping the emissions within the hemisphere they are emitted into (Prather et al., 1987) . The effect of simultaneously increasing OC and BC on BC burden is similar to the change seen in surface BC concentration, with increased OC biomass burning decreasing BC burden, but increased OC fossil/biofuel burning increasing BC burden.

Figure 4-9 shows the average percentage change in OC burden when biomass burning emissions are scaled. When only BC biomass burning emissions are doubled, change in the OC burden are less than the annual mean variability seen in the control simulation. Only in parts of Central Africa does the burden decrease by more than 5% locally. When both BC and OC biomass burning emissions are doubled, the OC burden increases by 30%. Local increases in OC burden reach 100% in Boreal North America, and 80% in Boreal Asia and Central Africa. Increases in OC burden reduce as distance from source regions increases. When the POM:OC biomass burning ratio is doubled, the OC burden is increased by 31%. The spatial pattern of increases in OC burden is almost identical to those seen when both BC and OC are doubled. In source regions, the increase in OC burden from POM:OC ratio changes is less than that from

both BC and OC biomass burning emissions doubling, but in remote regions, the increases in OC burden are slightly higher.

Figure 4-8 – Global distribution of percentage changes in BC burden between control simulation and simulation in which fossil/biofuel burning emission are perturbed for the period 2006-2008

Figure 4-10 shows the change in OC burden when fossil fuel and biofuel burning emissions are scaled. Increasing both BC and OC fossil and biofuel burning emissions increases the OC burden by 20%. Local increases in burden of up to 70% occur in China, with increases of up to 50% across much of Asia and Europe. Increases in OC burden decrease as distance from source areas increases. When only fossil and biofuel BC is increased, there is no significant increase in OC burden.

Increases in OC burden when biomass burning emissions are increased follow similar patterns to increases in BC burden. The effect of increased BC on the OC burden is smaller than the effect of increased OC on BC burden. This is expected, as OC is more abundant in biomass burning emissions, and any changes from OC will likely be larger because of this. Changes to the OC burden when BC biomass alone is increased show an initial decrease in burden near source, but increases further from source regions. However, when fossil and biofuel is increased, the spatial pattern of the effect of BC on the OC burden is the opposite to increases BC biomass burning emissions, and is spatially similar to the change to surface OC concentrations.

Figure 4-11 shows the change in vertical profile of OC when BC fossil and biofuel burning, BC biomass burning and absorbing OC are simulated in the model. All simulations show similar patterns in vertical distribution change between 10 m and 2000 m, where OC is reduced overall in both cases. Above 2000 metres, both the absorbing OC simulation and increased fossil fuel BC simulations show increases in OC MMR. Above 10000 metres, all three simulations show increased in the OC MMR. The two simulations show two peaks in MMR increases, whereas the BBBCx2 simulation only shows one. These peaks occur at around 3500 m, which is just above the level low cloud is produced at, and at 16000 m, which is roughly the level of the tropopause. We propose that two processes are at work, which are the same as those proposed in Section 3.4.4. Firstly, that the increased BC increases absorption and moves aerosol into higher model levels. This reduces dry deposition, as we previously showed in Chapter 3, and increases lifetime locally. This leads to decreases in aerosol at the surface, and increases aloft. However, the increase in radiative heating and aerosol aloft increases cloud and precipitation, which increases wet deposition and decreases lifetime locally. Secondly, the increase in aerosol at height has an impact on cloud production and wet deposition. As biomass burning emissions are emitted at height initially, and fossil fuel emissions are emitted only at the surface in the model, increases in biomass burning BC lead to increased radiative heating at height, and so increases convection, cloud production and wet deposition. Analysis of these variables could provide further backing to these theories, but are not included in these simulations. This theory however explains why increasing BC from biomass burning emissions reduces the OC burden, but increases in fossil fuel burning BC emissions increase OC burden. It also explains why different regions have different signs

of change in OC burden, as the different processes are dominant in different regions. However, these changes lead to no overall global change to lifetime of BC or OC in the increased emissions simulations.

The influence of nudging in these scenarios is important. As only horizontal winds are constrained by the nudging scheme, the vertical motion of air can still react to changes in the increased radiative heating, altering the vertical transport of aerosol. However, this may lead to slight differences due to changes in the horizontal transport as aerosol at height may move differently to aerosol near the surface. However, the effect of altered radiative heating on the dynamics in the horizontal is not seen in these simulations. In a free-running model, the feedback of the changed radiative heating in different areas and at different heights can alter the horizontal movement of air through changes to cloud, weather systems and radiative heating. However, the downsides explained in Chapter 2, such as a lack of consistency of aerosol transport compared to real-world observations, meaning that in this study, the effects of dynamics processes to these changes in aerosols contains limited feedbacks.
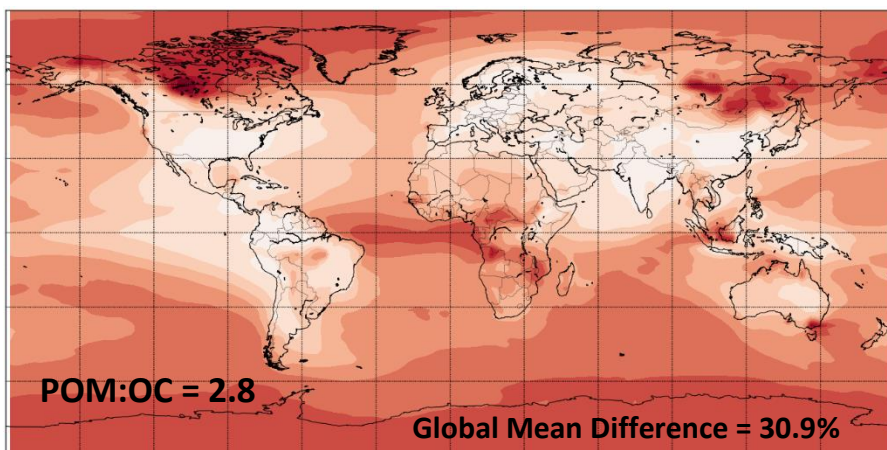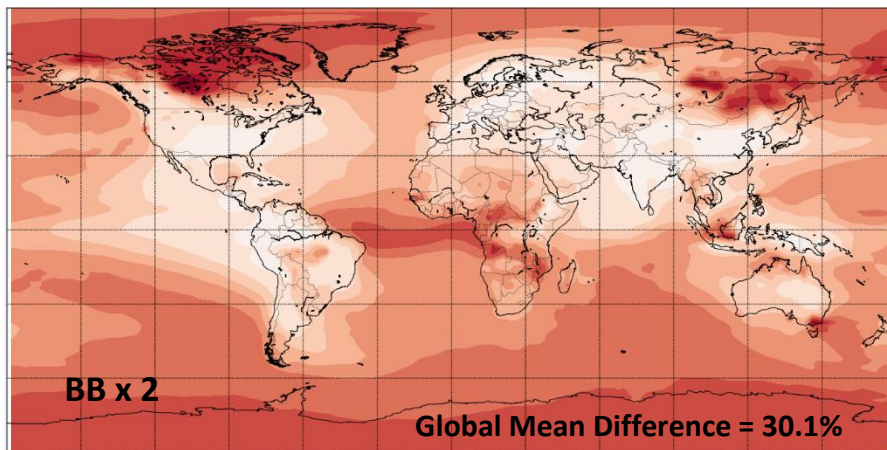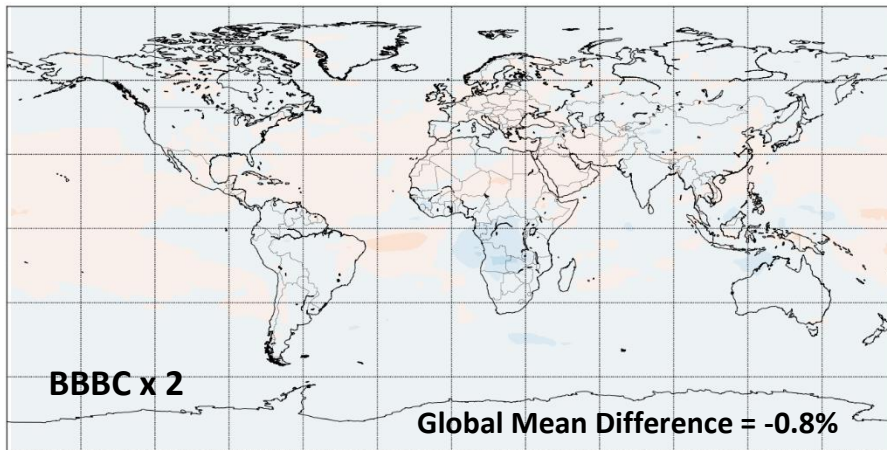
Figure 4-9 - Global distribution of percentage changes in OC burden between control simulation and simulations in which biomass burning emissions are perturbed for the period 2006-2008
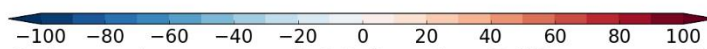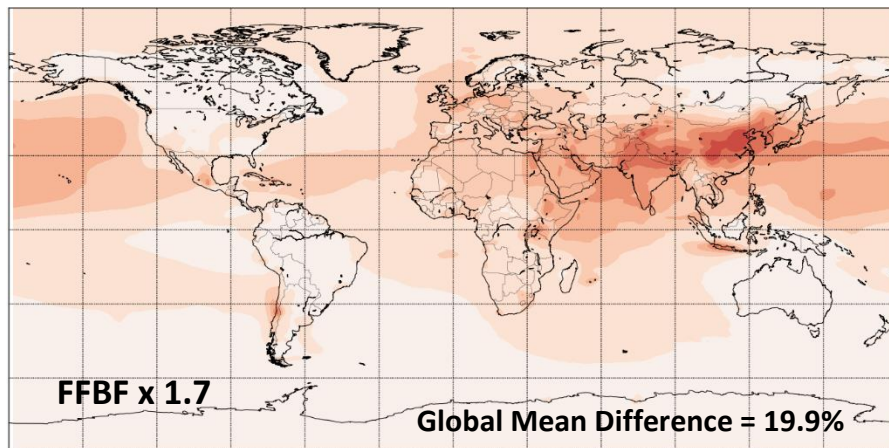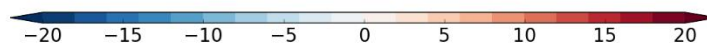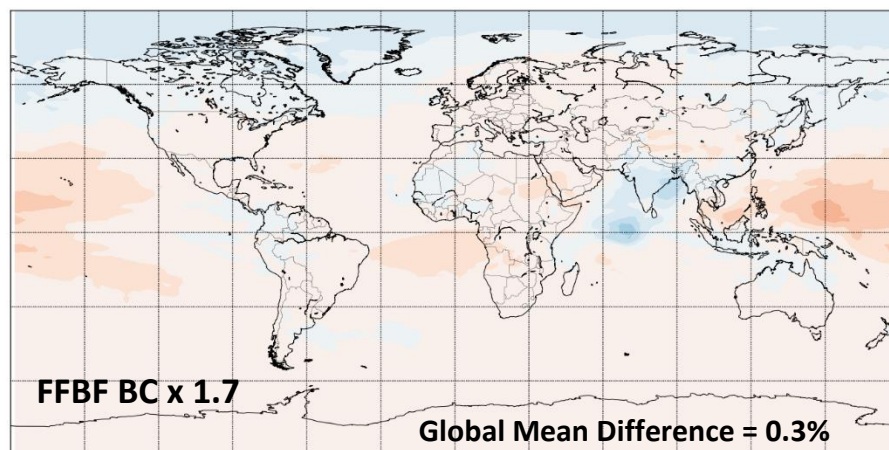
Figure 4-10 - Global distribution of percentage changes in OC burden between control simulation and simulations in which fossil/biofuel emission are perturbed for the period 2006-2008

Figure 4-11 - OC mass mixing ratio global average change between increased fossil fuel BC emissions, increased BC biomass burning emissions, Absorbing OC, and control simulations, averaged over a 3-year period

4.3.3 AOD

Figure 4-12 shows the distribution of AOD percentage changes when biomass burning emissions are increased, averaged over the years 2006-2008. When both BC and OC biomass burning emissions are doubled, globally averaged AOD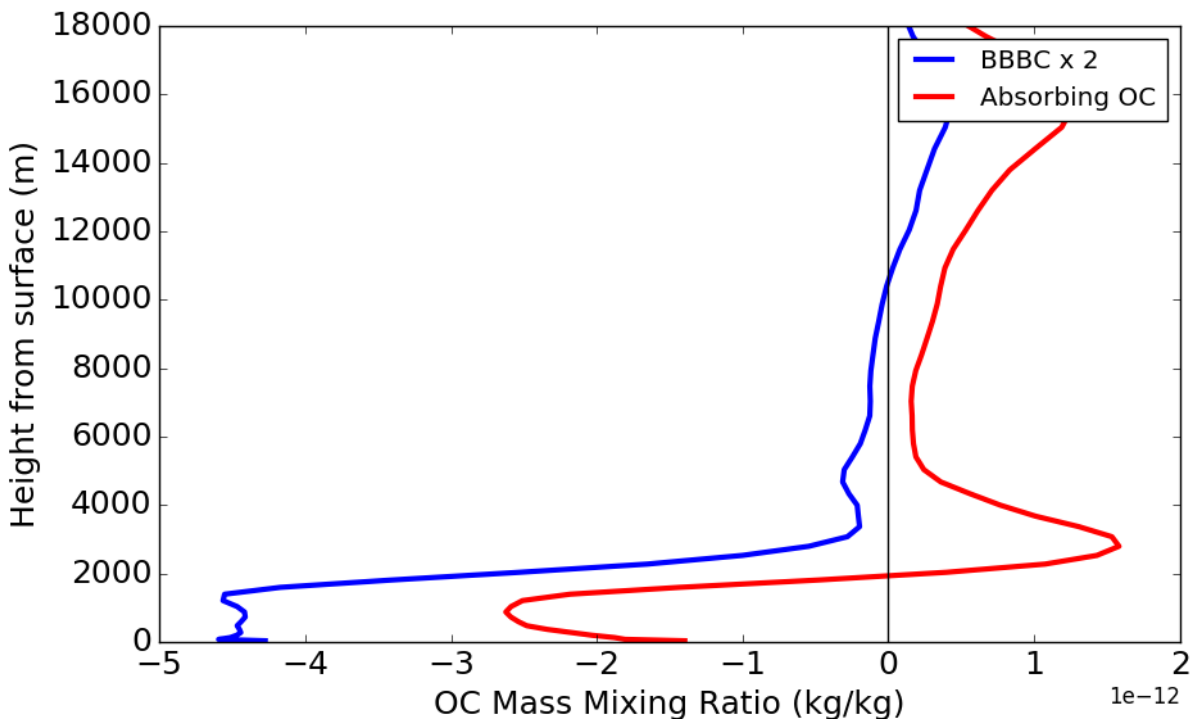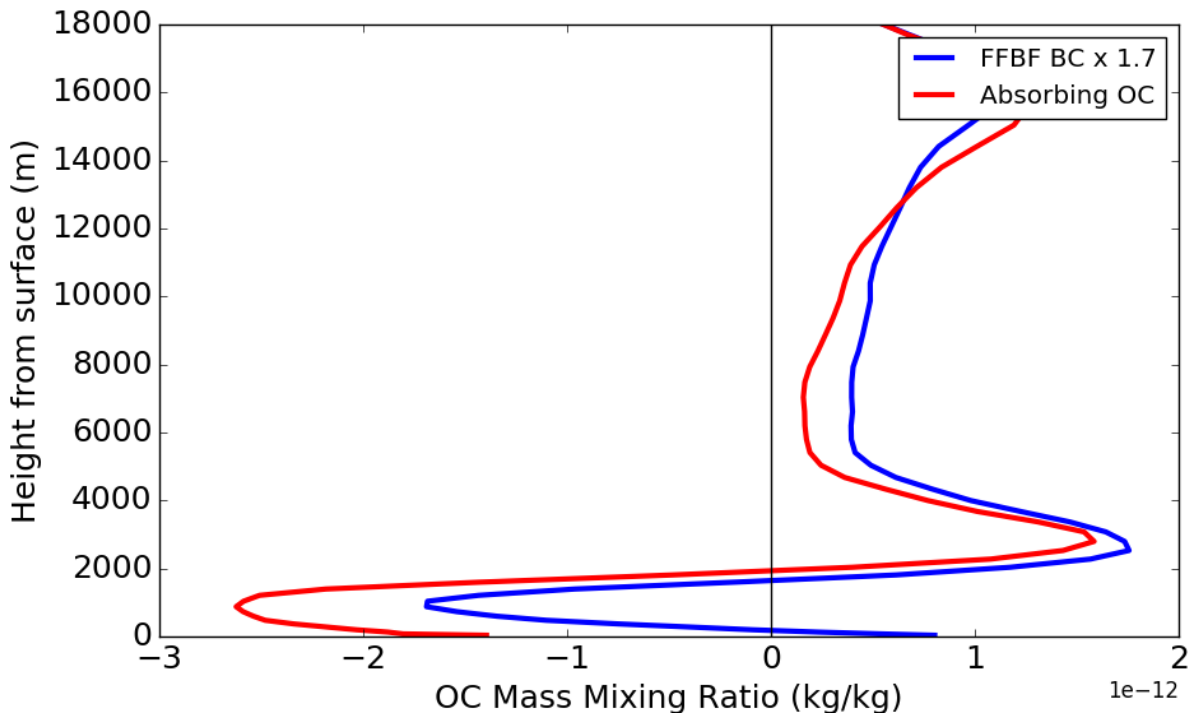 increases by 2.7%. All regions show increases in AOD, with increases of up to 50% in Central Africa. AOD in South America, South East Asia and Boreal regions of Asia and America increases by up to 25% with doubled biomass burning emissions in the model. The largest increases in AOD are found at biomass burning emissions sources, with the magnitude of changes decreasing as distance from sources increases. When only BC biomass burning emissions are doubled, the globally averaged AOD does not change significantly. AOD is however increased locally by up to 10% in Central Africa, and up to 6% in South East Asia and South America. Other regions show small increases or decreases in AOD by up to 2%.

The distribution of changes to modelled AOD when carbonaceous fossil fuel and biofuel burning emissions are increased is shown in Figure 4-13. When BC and OC are increased by a factor of 1.7, globally averaged AOD is not changed. However, in India, the increase in emissions increases AOD by up to 35% locally, whilst in Eastern China and Eastern Africa, AOD is increased by up to 20%. When only BC fossil and biofuel emissions are increased, worldwide average AOD does not increase by an amount greater than the annual variability seen in the control simulation either.

Figure 4-14 shows the distribution of AOD percentage changes when the POM:OC ratio is increased to 2.8 for biomass burning emissions in the model, averaged over 2006-2008. Increasing the POM:OC ratio increases globally averaged AOD, but not by a significant amount. The AOD is increased locally by 45% in Central Africa, and by up to 25% over other areas of biomass burning regions. Increases in AOD are reduced as distance from source regions increases.
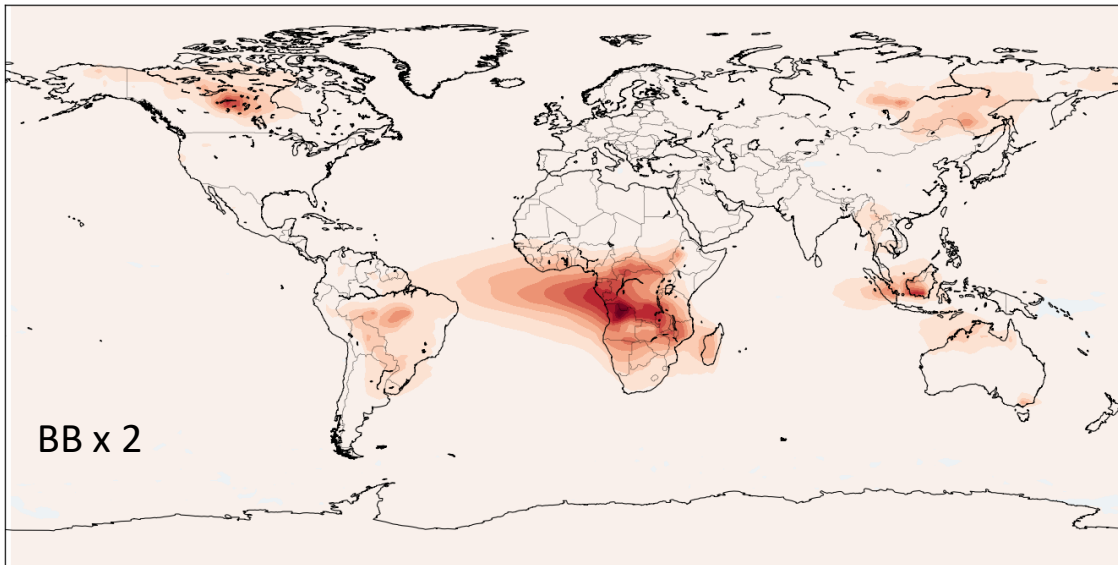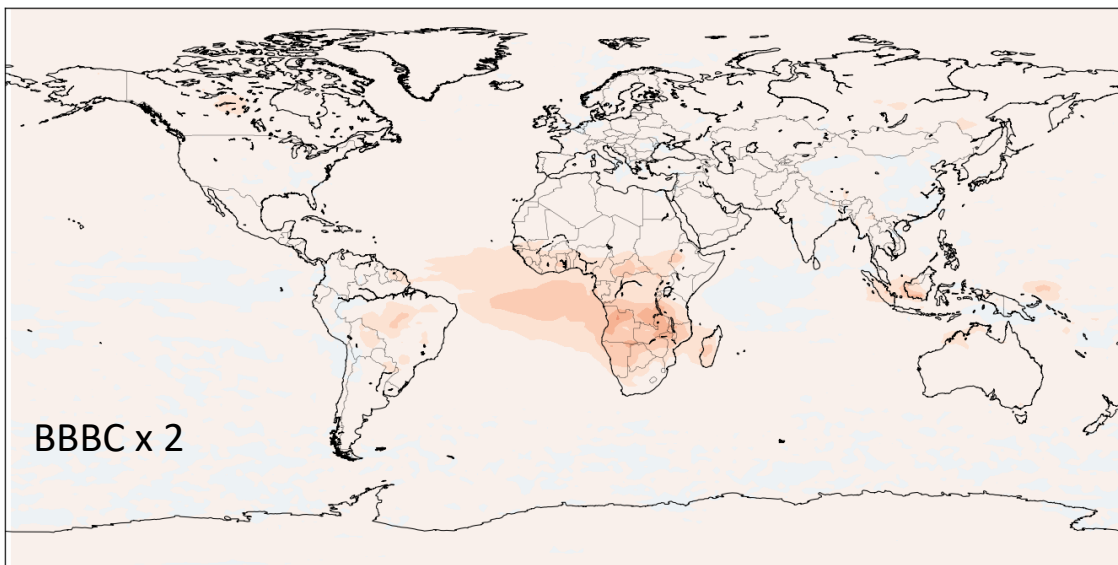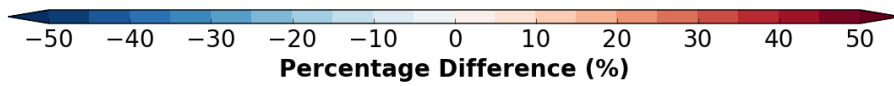
Figure 4-12 - Global distribution of percentage changes in aerosol optical depth between control simulation and simulations where biomass burning emission are increased for the period 2006-2008

Figure 4-13 - Global distribution of percentage changes in aerosol optical depth between control simulation and simulations where fossil/biofuel burning emission have been increased for the period 2006-2008

Area-weighted percentage difference = 2.21%

Figure 4-14- Global distribution of percentage changes in aerosol optical depth between control simulation and a simulation where biomass burning POM:OC ratio is doubled, for the period 2006-2008

Increasing emissions increases the number of aerosol particles in the atmosphere, as initial particle size and kept constant in the model. To a first approximation, AOD is proportional to the mass of particles, so increasing aerosol mass increases the AOD. The largest increases in AOD are located in areas where the increased emission type is highest. When biomass burning emissions are scaled, the largest increase occurs in Africa, where carbonaceous aerosol make up a larger proportion of the aerosol burden than in other biomass burning regions. This spatial pattern is repeated when POM:OC ratio is increased, as doubling the POM:OC ratio is equivalent to doubling OC biomass burning emissions. Increases in biomass burning emissions increase AOD locally by a greater magnitude than increases in fossil and biofuel emission. Partially, this is because they are scaled by a larger factor, but it is also due to the amount of other aerosol species, such as sulphate that are co-emitted with carbonaceous aerosols in fossil fuel burning regions. In all cases, source regions are where the mass fraction of carbonaceous aerosol is largest, and that fraction decreases with increasing transport distances. The increase in global AOD from doubling both OC and BC biomass burning

emissions is five times that of increasing BC biomass burning emissions alone. The ratio of BC:OC in biomass emissions is approximately 1:5, indicating that a linear relationship exists between increases in aerosol burden and increases in AOD. The linearity can also be seen when adding the AOD increases of BC only and POM:OC ratio doubled simulation. The combined change is of the same magnitude as when both BC and OC are doubled separately.

4.3.4 AAOD

Figure 4-15 shows the percentage differences of AAOD when biomass burning emissions are doubled in the model, averaged over 3 years. When BC and OC biomass burning emissions are doubled, AAOD increases by 28.6% globally. Increases in AAOD of up to 100% occur in South America and Boreal North America. Other areas of biomass burning sources and regions of aerosol transport in the Central Pacific and Central Atlantic increase by up to 60%. When only BC biomass burning emissions are doubled, AAOD is increased globally by 33%, 4% more than when both BC and OC biomass emissions are doubled. Regionally, AAOD increases by 70% in South America and in parts of the Central Pacific. Increases in AAOD in other biomass burning regions are lower than increases when both BC and OC are doubled. Areas where biomass burning emissions are transported to have a larger spatial spread of increases in the Central Pacific and Central Atlantic than when both BC and OC are doubled.

Figure 4-16 shows the average percentage differences of AAOD when fossil fuel and biofuel burning emissions are increased in the model. When both BC and OC emissions are increased, AAOD is increased globally by 39%. AAOD is increased in all regions, with local increases of up to 90% in the Central Pacific. AAOD is increased by up to 60% in source regions of fossil and biofuel burning, such as Europe, Eastern Asia, Eastern Africa and North America. Increasing only BC emissions of fossil and biofuel burning increases AAOD globally by 32%. AAOD is increased locally by up to 70% in Central Pacific, and up to 60% in other source regions. However, increases in AAOD are less spatially widespread downwind of source regions when only BC is increased.

Figure 4-17 shows the average percent differences of AAOD when the POM:OC ratio in the model is increased from 1.4 to 2.8. AAOD is reduced globally by 2.4%, which is only slightly

higher than the annual variability of AAOD. Not all regions show the same sign of change in AAOD in response to increased POM:OC ratio. In biomass burning aerosol transport regions, AAOD is reduced by up to 20%. However, AAOD is increased by up to 20% in Boreal North America, and by 10% in South America and Boreal Asia.
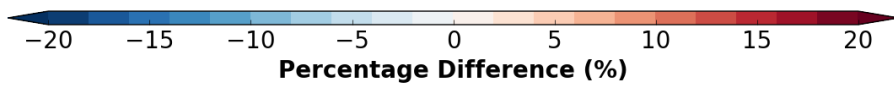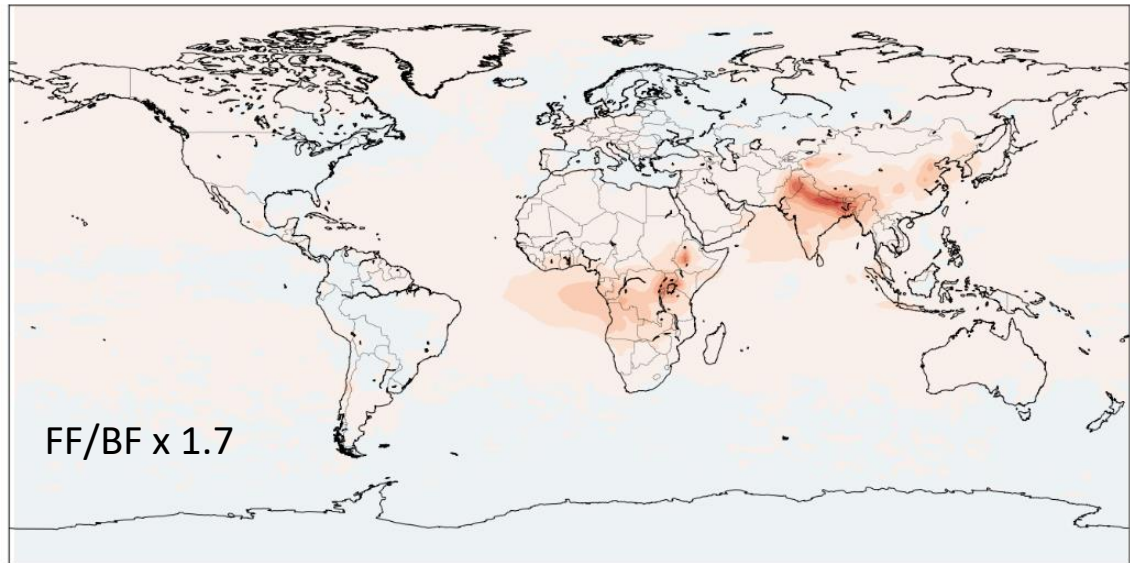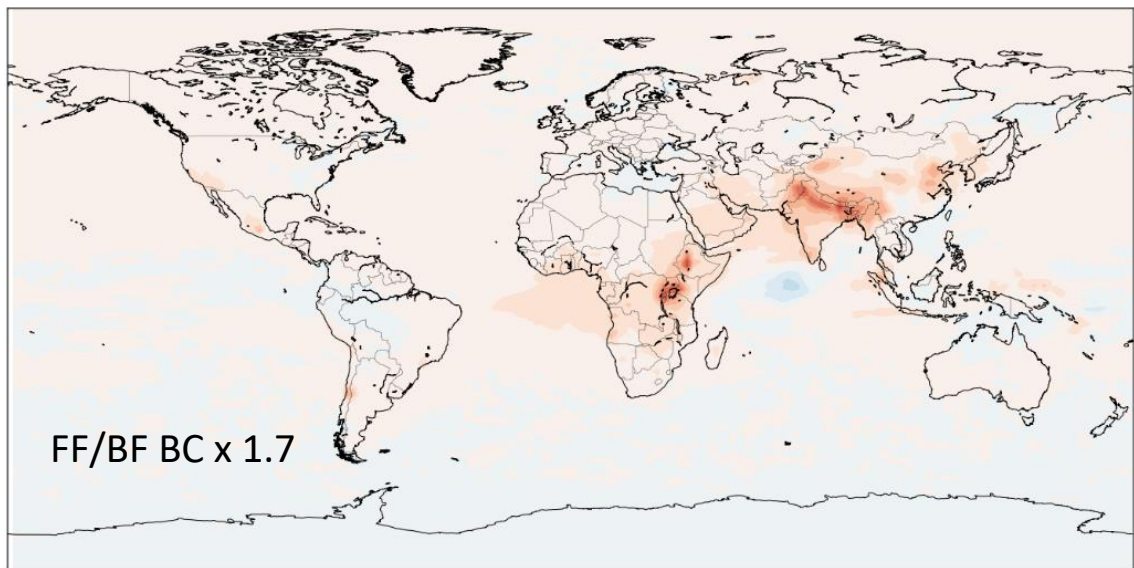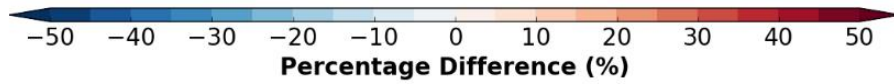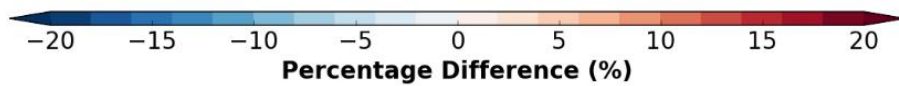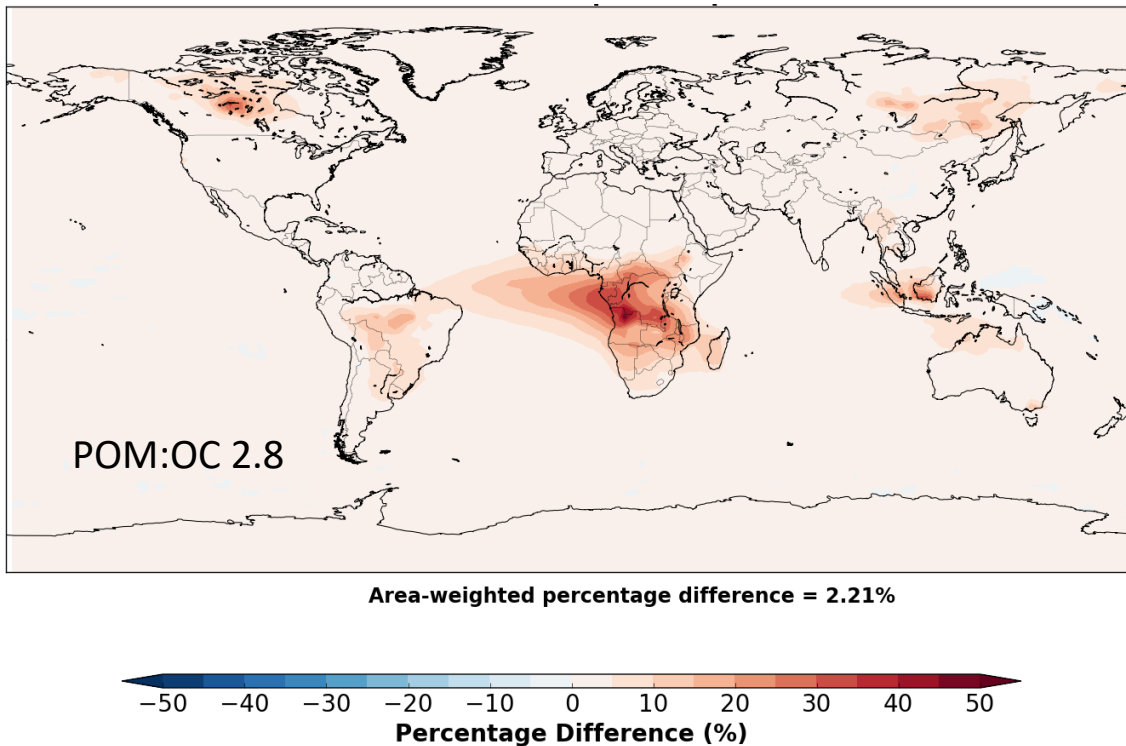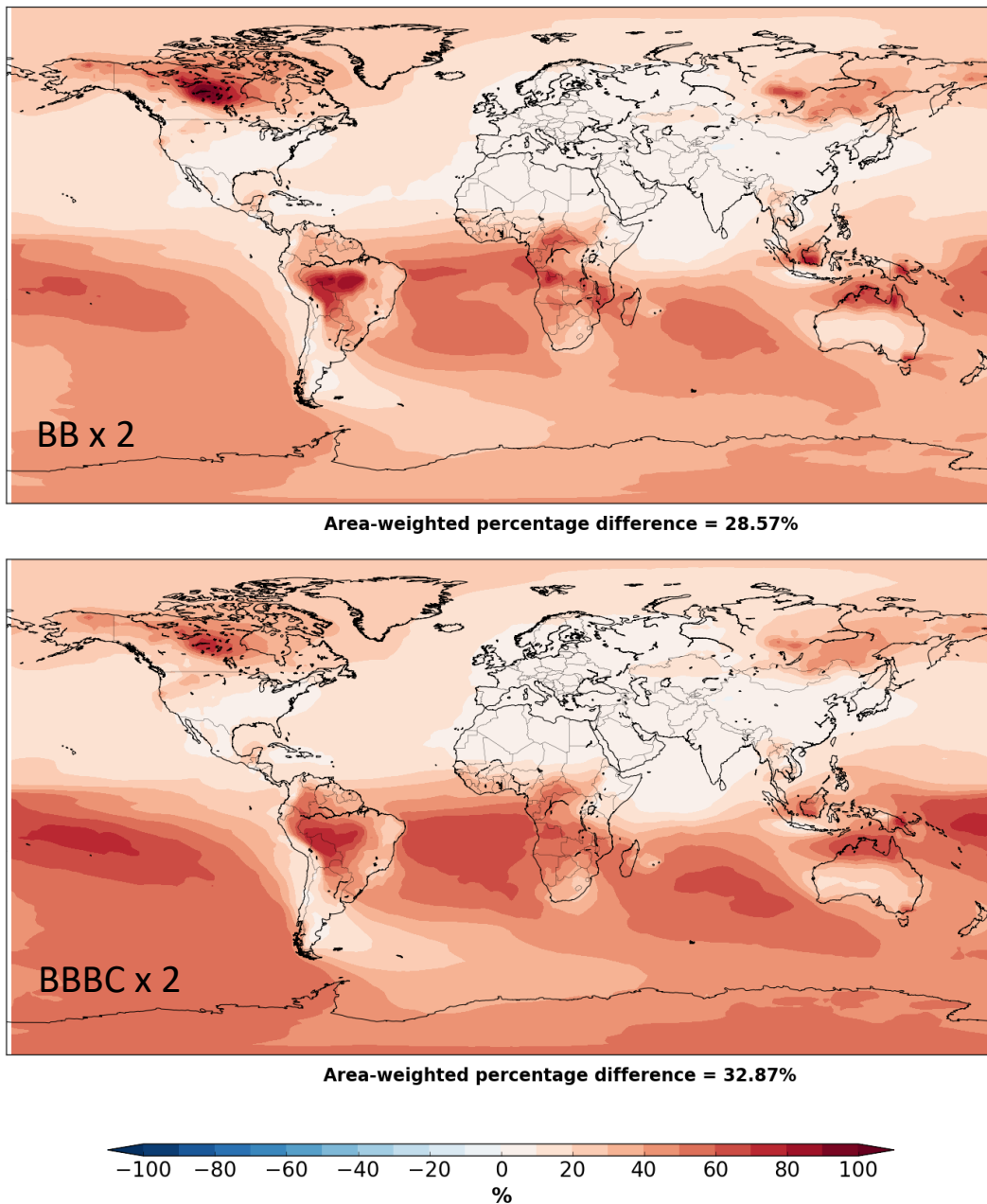

Figure 4-15 - Global distribution of percentage changes in absorbing aerosol optical depth between control simulation and simulations where biomass burning emission are increased for the period 2006-2008

Increasing emissions of BC generally increases the AAOD for the same reason the AOD increases with increased aerosol emissions. Because BC is removed mostly through wet deposition, which is not gradual, increases in BC are transported with the aerosol plume. This is why increasing biomass burning BC emissions increases the AAOD predominately in biomass burning source and transport regions. When increasing fossil and biofuel aerosol emissions, AAOD is increased further in fossil and biofuel source regions. Biomass burning makes up approximately 20% of the BC mass emitted, with the other 80% coming from fossil and biofuel emissions in the model. Despite this, increases in AAOD are similar in magnitude between increases in fossil/biofuel emissions and biomass burning emissions. The effect of both increasing biomass burning emissions by a larger factor, and the effect of emitted biomass burning emission at height rather than at the surface, explains this phenomenon.

The role of co-emitted organic carbon on AAOD differs between the two emission sources. When OC is increased with BC in biomass burning regions, source regions show larger increases in AAOD than when just BC emissions are increased. However, in transport regions, and on average overall, AAOD increases are reduced compared to just increasing BC. When increasing fossil/biofuel emissions, increasing both OC and BC magnifies the increase in AAOD in both source and transport regions compared with just increasing BC aerosol. Changes in AAOD that occur when the POM:OC ratio is doubled show the same effect on AAOD; increases in source regions and decreases in aerosol transport regions. The use of an internal mixture of aerosols in the model means that changes to OC can affect BC. The increase in OC at sources increases the particle number, but reduces the proportion of BC in each mixed particle. This increases the AAOD as a greater number of less absorbing particles is more absorbing than a fewer number of more absorbing particles.
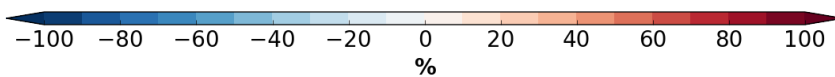
Figure 4-16 - Global distribution of percentage changes in absorbing aerosol optical depth between control simulation and simulations where fossil/biofuel burning emission are increased for the period 2006-2008

Area-weighted percentage difference = -2.35%

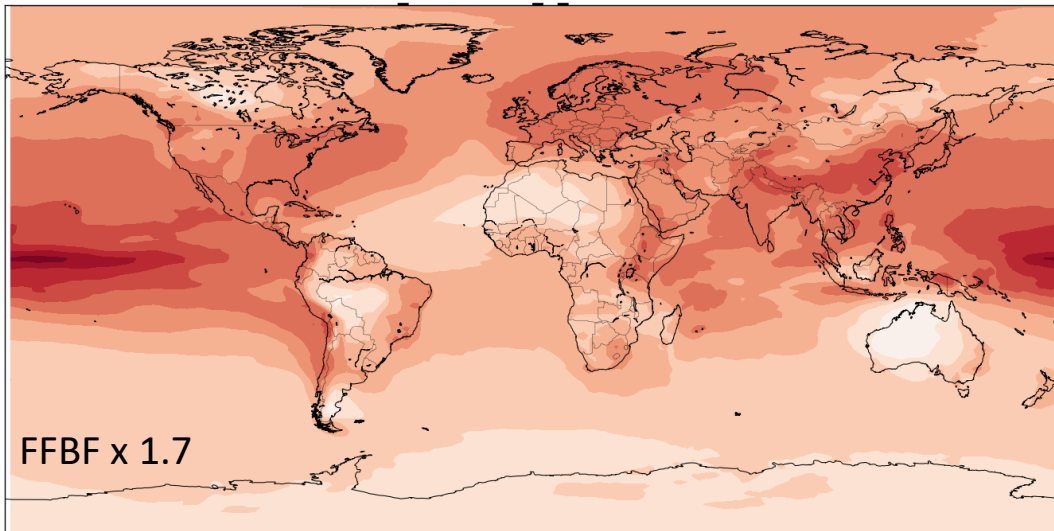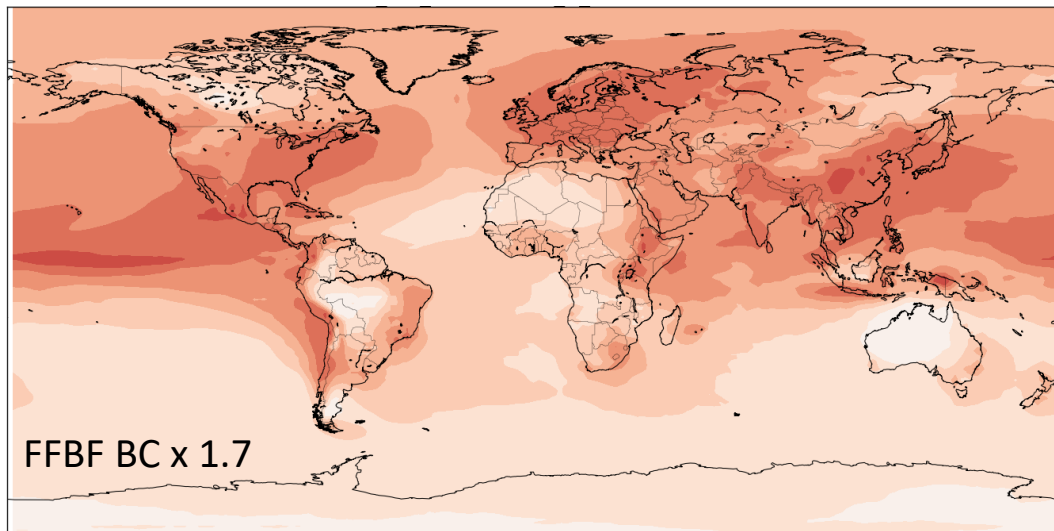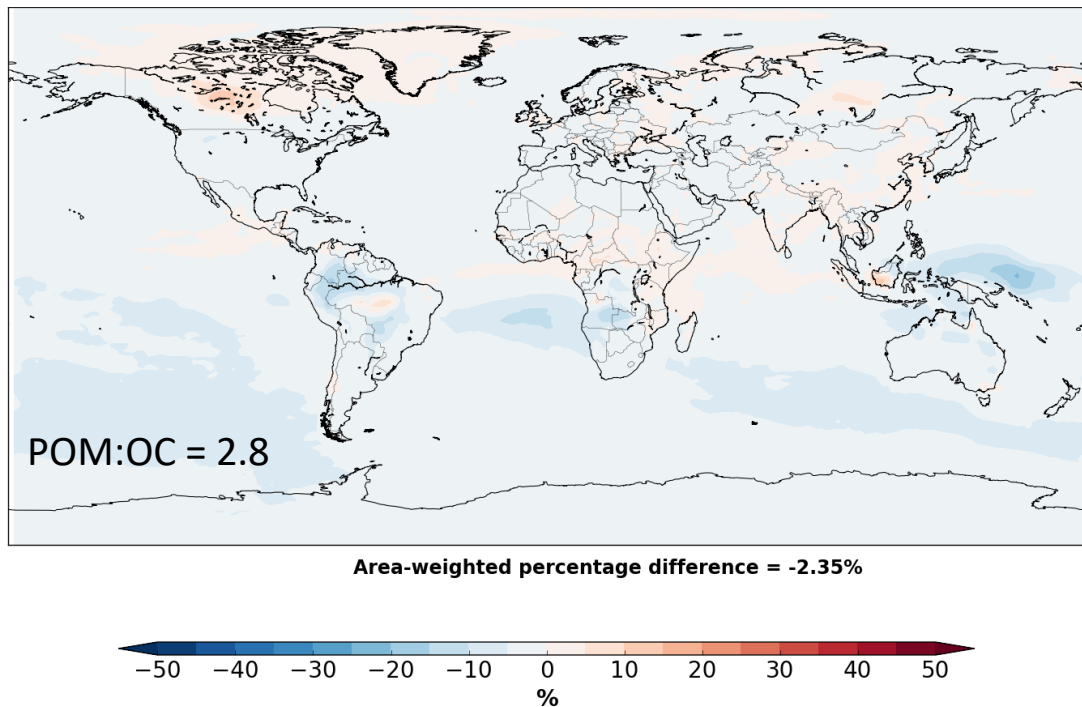*Figure 4-17 - Global distribution of percentage changes in absorbing aerosol optical depth between control simulation and a simulation where the POM:OC ratio is doubled for biomass burning, for the period 2006-2008*

Figure 4-18 shows the mean factor between the model and AERONET AAOD retrievals. Increasing emissions increases the mean factor in all regions, but the magnitude of the changes varies regionally. In South America, Australia and the Arctic, increasing biomass burning emissions produces a larger change in the mean factor. In all other regions, increasing fossil and biofuel burning produces the largest change in the mean factor. Increases in the bias in most regions improve the comparison between model and observations, bringing the mean factor nearer to 1. However, increases in the mean factor worsen the model in Asia, for increases in emissions, and in the Arctic for biomass burning emission increases. Increasing the POM:OC ratio has little effect on the comparison between the modelled and observed AAOD. If we assume a linear increase in AAOD with further increases, we can project that regional AAOD will compare better with observations in most regions if both biomass burning and fossil/biofuel emissions were increased. Notable exceptions to this projection are Asia, Oceanic regions and the Arctic, where implementing both increases would lead to greater overestimations of AAOD.
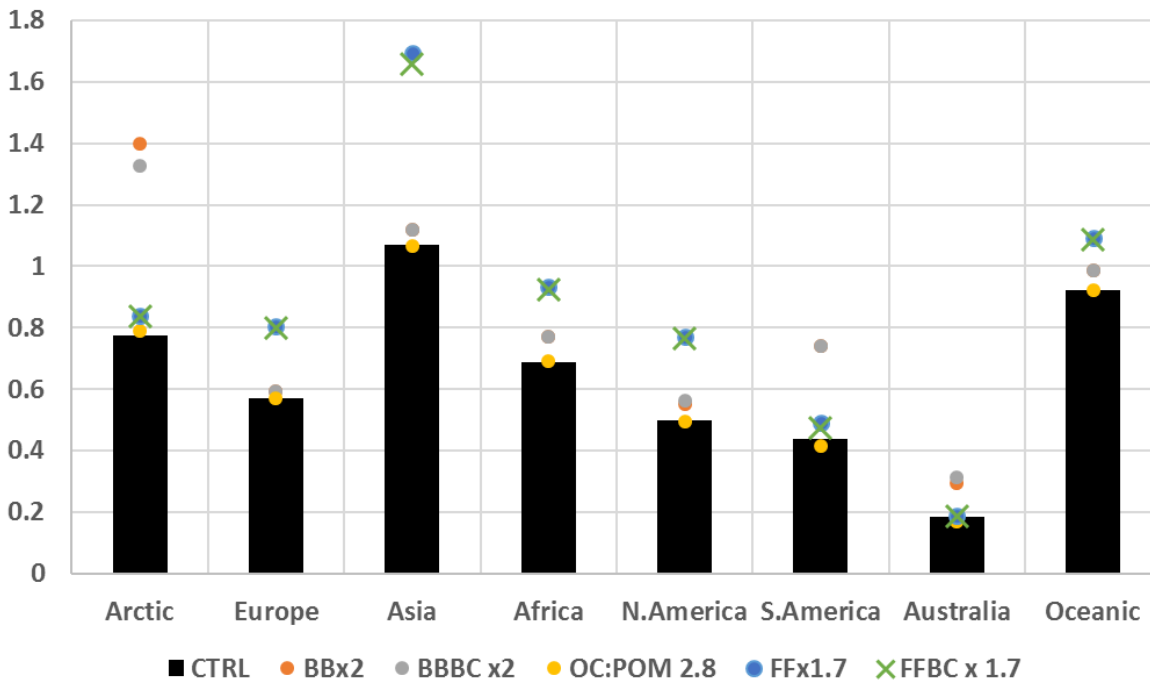
Figure 4-18 – Mean factor between modelled AAOD and AERONET retrieved AAOD at 550 nm. A value under 1 shows the model underestimating compared to observations, above 1 shows a model overestimation.

Figure 4-19 shows the correlation and normalised standard deviation of the various simulation and AERONET-retrieved AAOD. Increasing both BC and OC biomass burning emissions further increases the normalised standard deviation in most regions, except in Australia, where it is reduced, but correlation between the model and observations is reduced in South America. When just BC biomass burning emissions are increased, increases in normalised standard deviation occur in most regions, most notably in South America and Africa. In Asia, increasing just BC biomass burning emissions reduces the normalised standard deviation. In both Africa and Oceanic regions, the correlation between model and observation is also increased with BC biomass burning increases. When the POM:OC ratio is increased, small changes to both correlation and normalised standard deviation occur. The magnitude and direction of changes is dependent upon the region. Similarly, when fossil fuel emissions are altered (bottom panel), the effect on comparisons differs regionally. In Europe, North America and Asia, increasing fossil /biofuel emissions increases the normalised standard deviation ratio, but does not alter the correlation. In Africa, the normalised standard deviation ratio is increased, but the correlation is reduced in both altered simulations. However, in

South America, altering fossil/biofuel emissions increases the correlation, but not the normalised standard deviation ratio.
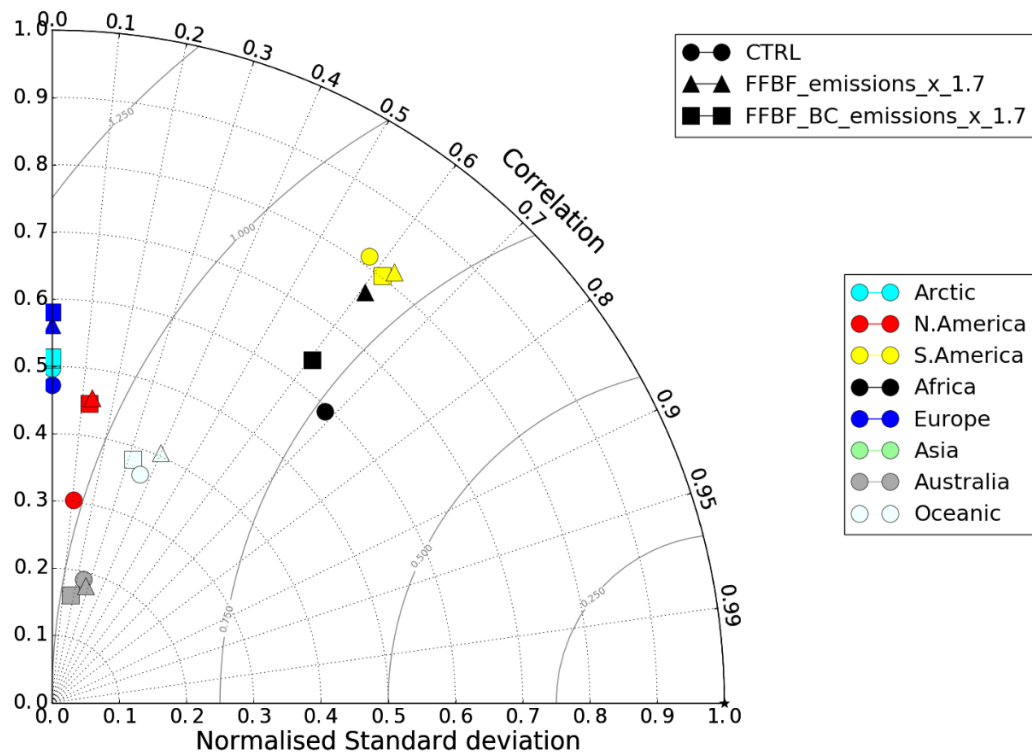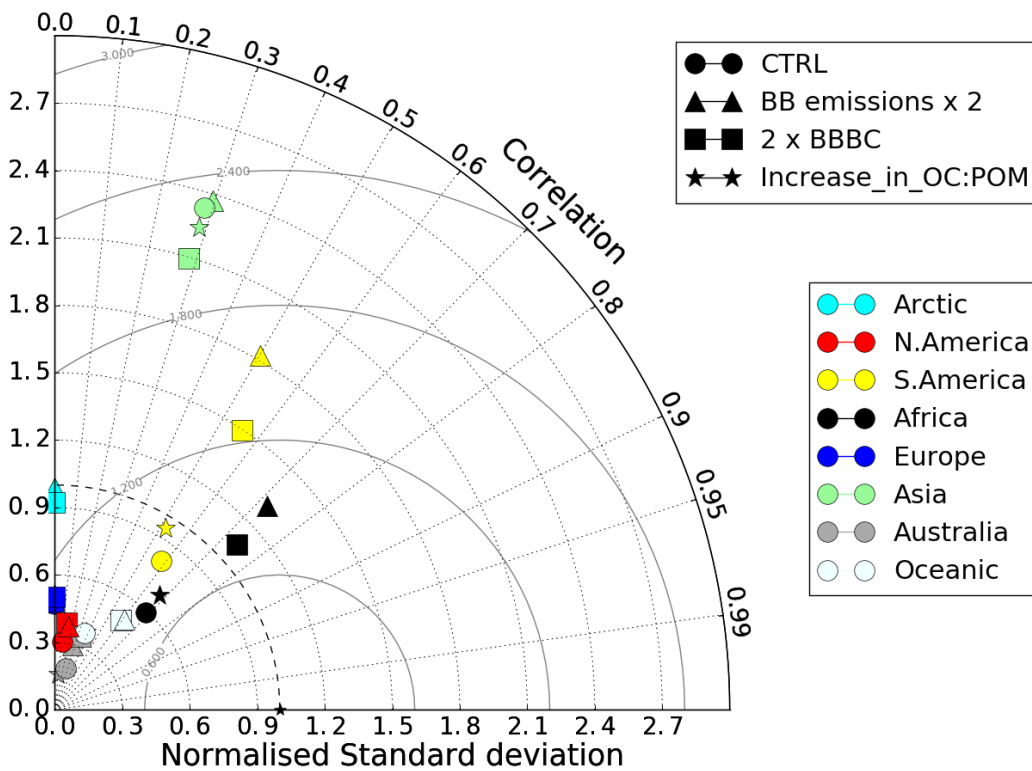
Figure 4-19 – Taylor plot showing the correlation and normalised standard deviation of increased emission simulation AAOD against AERONET retrieved values at 550nm, compared on a monthly basis.

Increases in biomass burning emissions improve the model in several regions. However, in South America and Africa, the increase in normalised standard deviation ratio means the increase in the spread of modelled AAOD now exceeds the observed spread. This suggests that increasing biomass burning emissions further increases the highest AAODs. Several regions still show significant underestimations of AAOD variability in the model despite increased biomass burning emissions. Increases in fossil and biofuel emissions improves the model ability in all regions except Asia, where the spread of modelled AAOD is further increased beyond observed ranges, and Africa, where correlation between the model and observation is decreased, despite a better comparison in standard deviation. The pattern in Africa suggests that increased emissions are required to improve the range of values in the model, but that increasing fossil/biofuel emissions in this way increases the model range in the correct time and places.

4.3.5 SSA and AE

Figure 4-20 shows the distribution of changes that occur in single scattering albedo when biomass burning emissions are altered. When both BC and OC biomass burning emissions are doubled, SSA is reduced in all regions. Locally, reductions in SSA of up to 0.02 occur in Central Africa and Australia, both biomass burning source regions. Small decreases occur in South America and Boreal regions of Asia and North America. SSA is less affected as distance from source areas increases. When only BC biomass burning emissions are doubled, SSA is decreased globally by three times the amount compared to when both BC and OC are doubled. Decreases in SSA of up to 0.06 occur in Central Africa, with decreases of 0.03 in South America and North Australia. Decreases in SSA reduce as aerosol is transported from source regions. When the biomass burning POM:OC ratio is increased to 2.8, SSA increases globally. In Central Africa, this increases SSA by up to 0.04. Increases seen in source biomass burning regions are larger than those seen elsewhere.

Figure 4-21 shows the distribution of changes that occur when fossil fuel and biofuel emissions are altered. When both OC and BC emissions are increased, SSA is decreased in the model. SSA decreases by up to 0.05 in India, East Africa and Eastern Asia when emissions increase. These are areas of high fossil/biofuel burning emissions. Decreases in SSA of up to

0.03 also occur in Europe and urbanised regions of North and South America. When only BC emissions are increased, SSA is decreased by twice as much as when both BC and OC are increased. Decreases in SSA of up to 0.07 occur in India and decreases of 0.06 occur in China and Eastern Africa, higher than when both BC and OC emissions are increased. SSA in Europe and North America is reduced by a similar amount when only BC is increased as when both BC and OC are increased.

In all the simulations, the strongest changes to SSA are at the source of the altered emissions. This is unsurprising, as these are the areas where the proportion of carbonaceous aerosol in the aerosol burden will be the highest. Decreases in SSA occur in all regions when only BC emissions are increased, regardless of increases in OC. In most regions, BC is the most dominant source of absorption, whilst OC is not always the most dominant extinctive aerosol in the burden. This means the increase in absorption is always likely to be proportionally higher than the increase in extinction. Areas with high sulphate co-emission levels, such as Europe and North America, have smaller changes in SSA with increased source emissions.

Figure 4-22 shows the regional distribution of SSA and AE for simulations of increased biomass burning emissions, the control simulation, and from AERONET retrievals. This figure focuses on South America and Scrubland Africa, two regions where biomass burning changes in the model shows significant increases/decreases in SSA.

Increasing both BC and OC biomass burning emissions gives a slight decrease in SSA in both regions. This decrease occurs both at high SSA and low SSA in both regions, meaning that the range of SSA is unaffected. The decrease in SSA worsens both simulations comparison to AERONET. The value and range of AE is not noticeably affected by the increased emissions. Increasing just BC emissions decreases SSA in both regions. In South America, SSA is reduced at both high and low SSA, meaning the model no longer replicates high SSA seen in AERONET. The effect in Africa is weaker, but noticeable. The decrease in SSA further worsens the model compared to AERONET. Increasing the POM:OC ratio in the model increases SSA. In both regions, this increase is seen more prominently in low SSA, reducing the range of SSA from the model. This improves the model comparison to AERONET in Africa, although the SSA is still underestimated in the model.
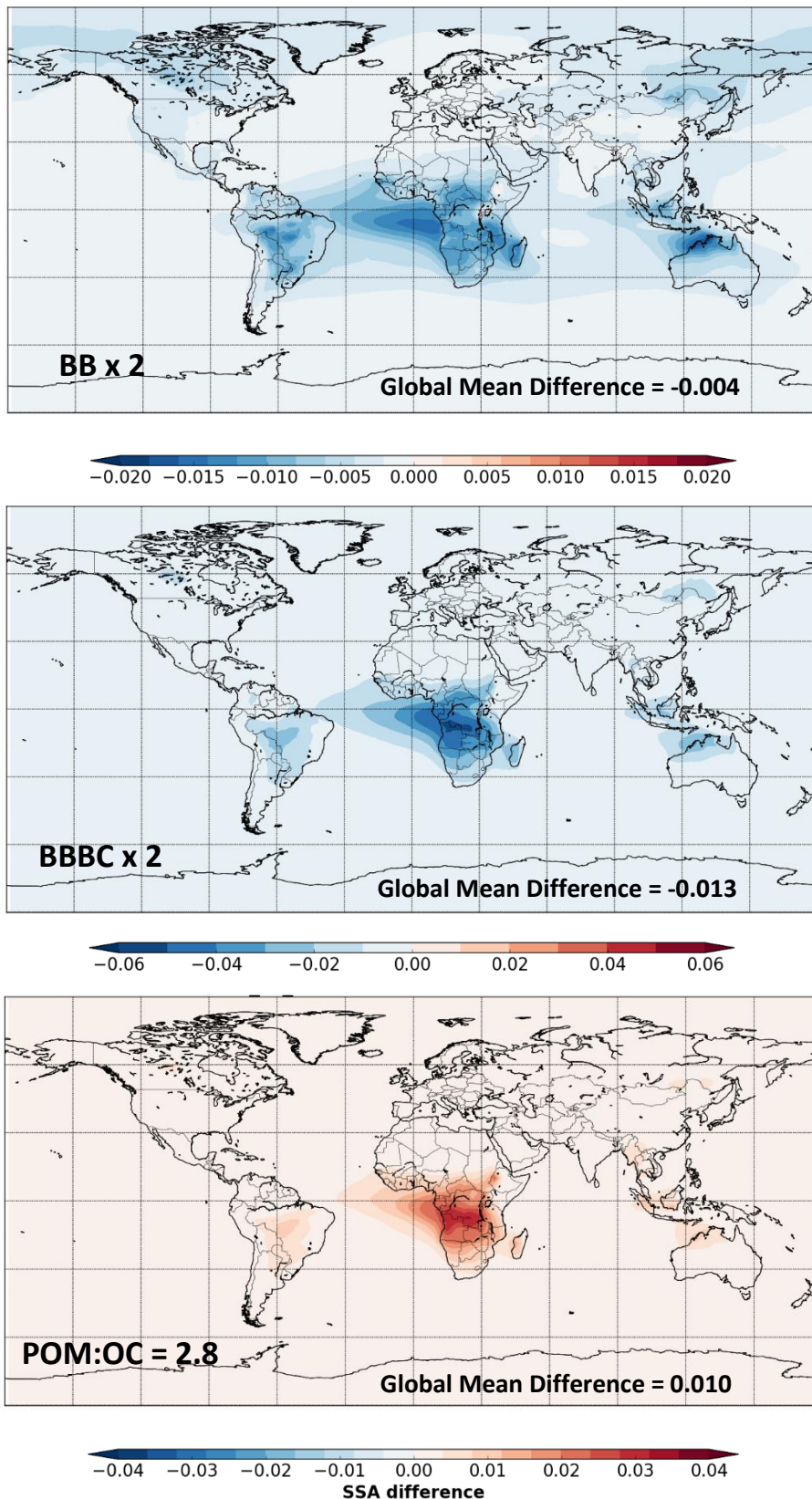
Figure 4-20 - Global distribution of percentage changes in single scattering albedo between control simulation and simulations where biomass burning emission are increased for the period 2006-2008
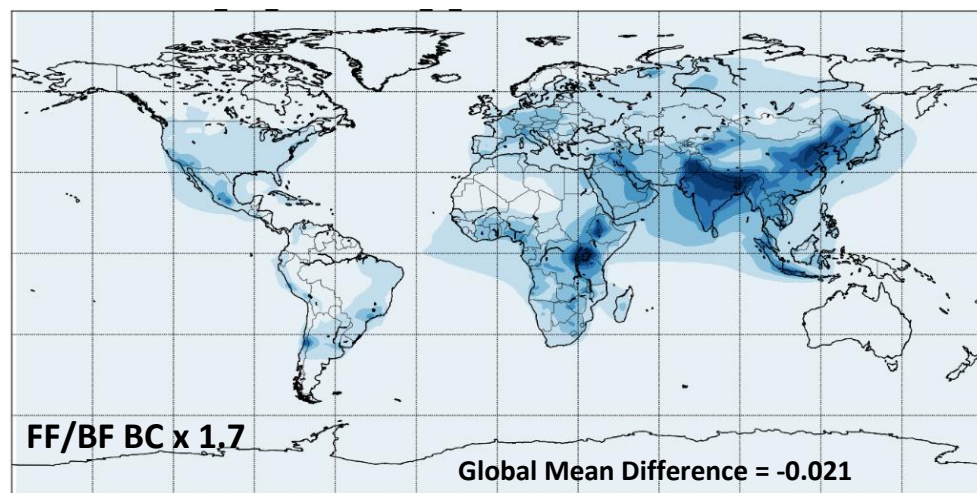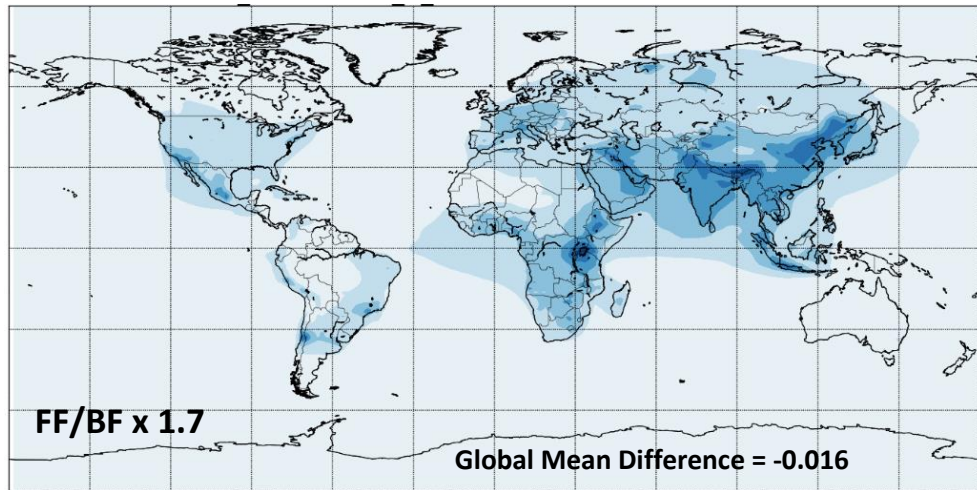
Figure 4-21 - Global distribution of percentage changes in single scattering albedo between simulations with increased fossil/biofuel emissions and the control simulation for the period 2006-2008
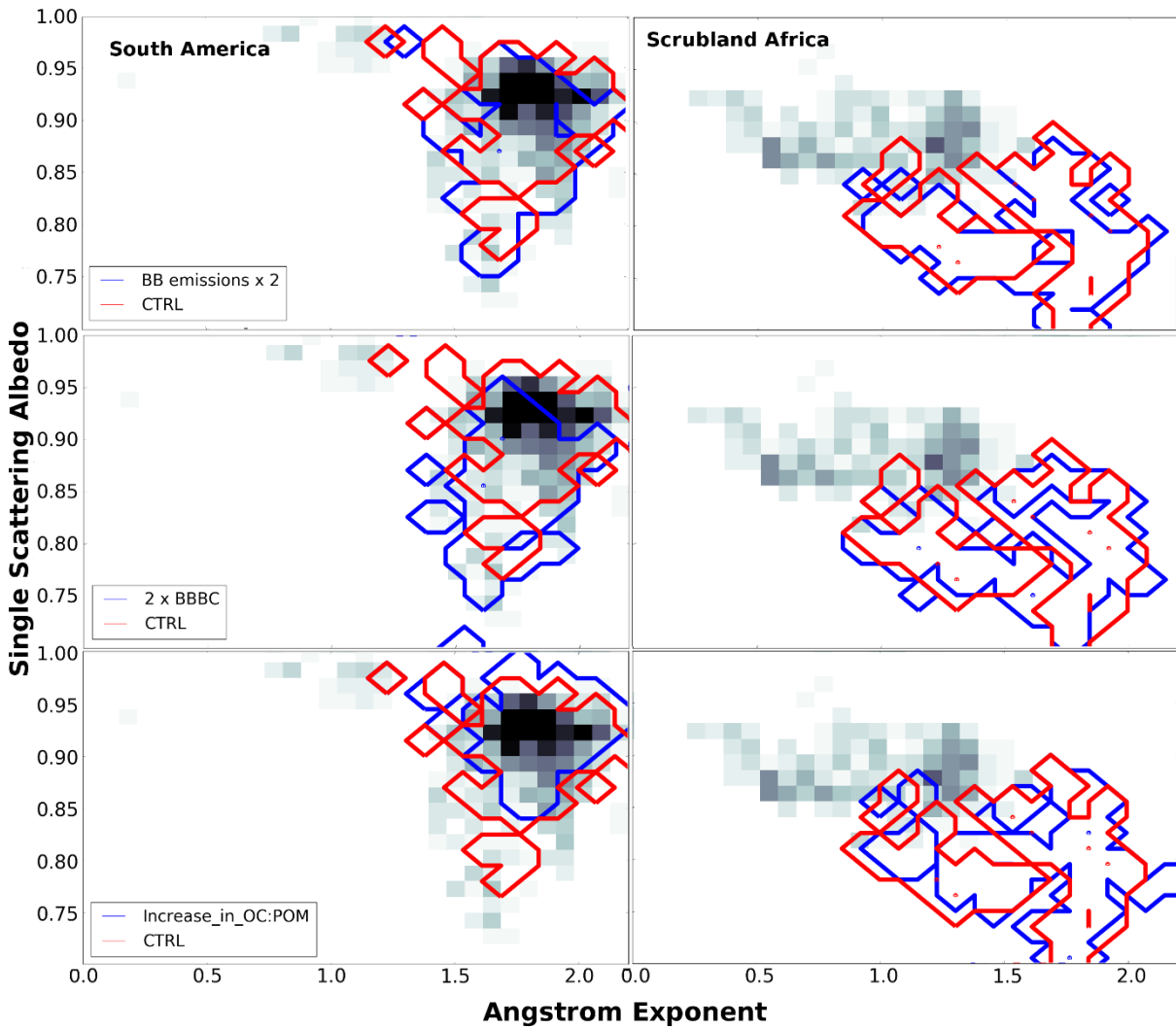
Figure 4-22 – Single scattering albedo as a function of Angstrom exponent for AERONET retrievals (black density boxes) compared and co-located modelled values from control (red) and biomass burning altered emission (blue) simulations in biomass burning regions.

Figure 4-23 shows the distribution of SSA and AE in Northern Europe, North East USA and Industrial Asia for increased fossil/biofuel emissions simulations, the control simulation, and from AERONET retrievals. Increasing both BC and OC decreases SSA in the three regions. The SSA range is also increased in all three regions, with low SSAs decreased further than high SSA in the model. In Northern Europe and North East USA, the decrease of the frequency of high SSA in the model decreases the comparison with AERONET retrievals, but the increase in frequency of low SSA in the model improves the comparison with AERONET. In Industrial Asia, decreases to the SSA mean and increases to the SSA range worsens the model comparison with AERONET. When only BC is increased, the pattern of change is almost identical in Europe

and North America. In Industrial Asia, the SSA is further decreased, magnifying the changes when both OC and BC emissions are increased.
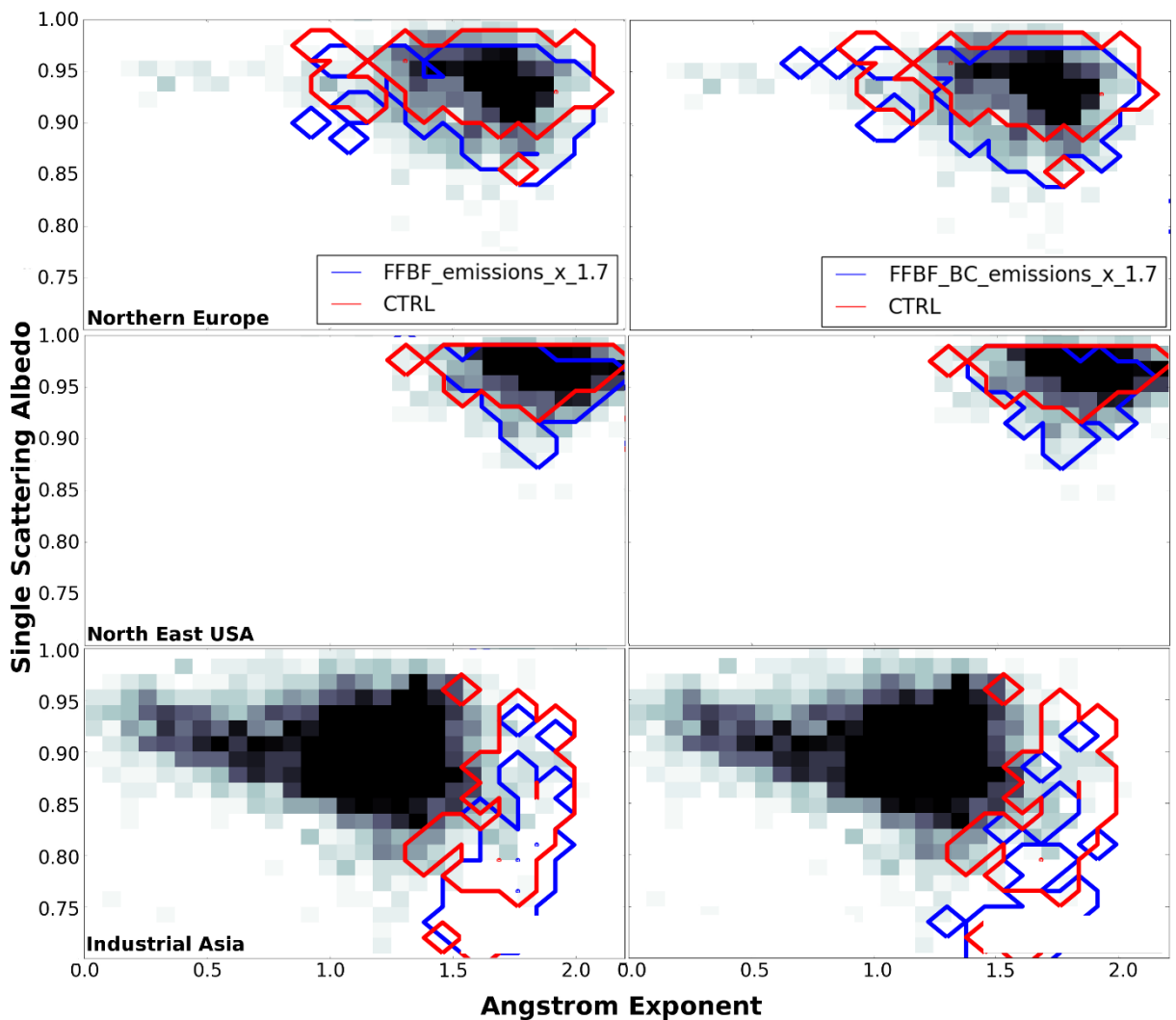
Figure 4-23 - Single scattering albedo as a function of Angstrom exponent for AERONET retrievals (black density boxes) compared and co-located modelled values from control (red) and fossil/biofuel emission (blue) simulations in fossil and biofuel burning regions.

The impact of increasing emissions on the comparison between model and observation is dependent upon the regions. Larger changes in SSA are seen in the model in Africa than are seen in South America, yet the changes in SSA/AE space show larger changes in South America. This can only be because of the location of AERONET stations, which are located mainly along the East and South coast of Africa, and so are not in the areas of highest change

in SSA. Increases in fossil/biofuel burning emissions also decrease the SSA, with mixed effects on the ability of the model, depending on region.

4.5 Summary and Conclusions

Chapter 2 highlighted the underestimation of mass concentrations globally in the model when compared to surface observations. This chapter determines that improvements can be made to the ability of HadGEM3-UKCA when emissions are increased in line with evidence from the recent literature discussed in section 4.1. Increasing emissions can not only alter the total BC and OC mass globally, but also regionally, depending on source. Increases in fossil/biofuel can be used to increase mass in Asia, North America and Europe, whilst biomass burning emission scaling increases the mass further in Africa and South America. This allows for a low level of customization when attempting to improve a model on a regional basis.

However, this section also determines that scaling emissions, even when separated by source, cannot solve all discrepancies between the model and observations alone. Differences in how the model compares to mass and optical retrievals within the same region after increasing emissions suggest that other changes are required to achieve similar improvements in all regions. For example, we show that increasing BC emissions improves the comparison between surface BC concentrations in Asia, but worsen the comparison in AAOD, meaning that a unique scaling value of emissions in this region cannot provide a good comparison with both sets of observations. Increases in BC can also lead to overestimations of AAOD mean and AAOD variability in regions where surface concentrations of BC are still underestimated. Furthermore, we highlight that increasing emissions can overestimate surface concentrations of OC whilst still underestimate the AOD in North America. This proves that simple increases of emissions, regardless of spatial scale, cannot resolve model errors. This is in contradiction with the studies of Bond et al. (2013) and Petrenko et al. (2012) highlighted in the introduction to this section, where increasing emissions is the only method used to improve model-to-observation comparisons.

Increasing emissions also altered the proportion of the aerosol burden that is made of carbonaceous aerosol. The proportion of BC strongly determines the SSA in the model. In regions where carbonaceous aerosols are the dominant aerosol species, SSA can only be altered significantly by increasing BC and not OC, rather than increasing both simultaneously,

as this alters both AOD and AAOD by similar proportions. The ability of changes to the BC:OC emission ratio to improve the comparison of the model to observations is dependent on the region, further demonstrating that separate emission-scaling global factors for BC and OC could not achieve good model to observation comparisons alone. This chapter also shows that increasing emissions of carbonaceous aerosol can be used as a means of improving the model on a regional basis. Biomass burning emissions are emitted only in small areas, over small timescales and at varying heights, whereas fossil fuel burning emissions are emitted almost constantly over wider areas. When focused on individual sites in biomass burning regions for changes in biomass burning seasons, the effect of biomass burning emissions on surface BC concentration is stronger than increases in fossil and biofuel fuel. Although increasing emissions shows improved comparisons between the model and observations, there remains discrepancies between remaining underestimations in different regions. This further shows that using incorrect emissions alone cannot be responsible for differences between models and observations.

In the next section, we look at how lifetime can be changed within the model, and how altering the lifetime can influence the comparison between the model and observations.

5. Chapter 5: Solution Three – Lifetime

Chapter 5 has two main aims. Firstly, to determine a range of uncertainty in parameters which directly affect the lifetime of BC and OC. We also will assess how these uncertainties will affect the model. Secondly, we aim to assess whether the model can be improved if these parameters are altered within the range derived from the literature.

5.1 Lifetime of Carbonaceous Aerosol

One of the key factors that may affect the lifetime of carbonaceous aerosol in a model is the deposition. One of the ways aerosol can be deposited is through dry deposition. The velocity at which aerosols fall is dependent on particle size, density and air viscosity, as shown in Equations 2.1 and 2.2 (Mann et al., 2010a). In the model, particle growth is dynamic, with initial emissions sizes based upon AEROCOM recommended settings, with modification from Stier et al., (2004). The density in the model is set to 1.5 g cm^{-3} for both OC and BC (Mann et al., 2010a). However, more recent literature suggests that these values need to be updated. BC density is quoted as being in the range of 1.8 – 2.0 g cm^{-3}, with 1.8 g cm^{-3} the standard density used in SP2 BC measurement algorithms and in several other climate models (Schkolnik et al., 2007; Schwarz et al., 2013; Wang et al., 2014b). OC density is quoted as being between 1.1 – 1.4 g cm^{-3} in literature, varying depending on material burned (Kuwata et al., 2012; Schkolnik et al., 2007). In this section, we will focus upon determining the impact that new BC and OC density values have upon the HadGEM3-UKCA model.

Deposition of CA also occurs through precipitation, either by particles being scavenged in clouds, or through impact with other rain or cloud droplets. A study on the effect of cloud scavenging was undertaken by Kipling et al. (2013) in the HadGEM3-UKCA model. They found that coupling the convective transport to convective scavenging in the model increased the scavenging rate in the tropics and other highly convective areas. These changes also improved the comparison of the model to HIPPO aircraft observations of aerosol concentration in the Pacific. Changes made to the model by that research are included in the control simulation, as described in section 3.4. We therefore believe there is little benefit in re-analysing the sensitivity when it has been recently done and we are using the same observations to determine skill.

139

Other factors include the height at which aerosol is injected into the model. In the boundary layer, aerosols have a much shorter lifetime than aerosol injected into the free troposphere. This is because the air in the free troposphere both contains very little water, reducing the rate of droplet formation, cloud formation and wet deposition. The free troposphere is also not well mixed with air in the boundary layer, reducing the rate of dry deposition (Donnell et al., 2001; Timonen et al., 2014). Currently, biomass burning emissions enter HadGEM3 throughout a pre-assigned boundary layer, with injection heights of emissions pre-determined by the type of biomass being burnt (Dentener et al., 2006). The use of a constant boundary layer means that there is the possibility of low levels of aerosol being injected into the free troposphere when a very shallow boundary layers exists. Biofuel and fossil fuel carbonaceous aerosol emissions are emitted only at the surface. Amiridis et al. (2010) and Labonne et al. (2007), which use different satellite retrievals to measure aerosol injection heights in different regions, agree with assumptions made in Dentener et al. (2006) which are used in the model. A study by Veira et al. (2015) using these height injection assumptions in the ECHAM6 global circulation model finds that the distribution of aerosol at height compares well with the Multiangle Imaging Spectroradiometer Plume Height Project (MPHP) data set, based on satellite retrievals. However, they also infer that the exact injection height is not as important as aerosol processes and emission inventories. Further work also debates whether improving the aerosol injection height is important in climate models. Raffuse et al. (2012) also finds that injection height profiles offer limited improvements in comparisons of aerosols concentrations, as long as aerosol is injected into the correct layer, such as the boundary layer, free troposphere or stratosphere. Given the evidence suggesting that aerosols are not hugely sensitive to injection heights, and the success of the current profile that is being used, we reason that better improvements can be made to the lifetime through other means.

5.2 Sensitivity to Carbonaceous Aerosol lifetime

There are limited publications on the role of BC and OC lifetime on model skill. Samset et al. (2014) uses several models from the AeroCom inter-comparison project and compared how well they replicate BC concentrations from a selection of flight campaigns. The group found a strong correlation between the bias seen in models compared to observations and the lifetime of BC. Models used in the study had lifetimes ranging between 3.5 and 17.1 days. The work states that "short BC lifetime appears necessary, but not sufficient" to compare well

with observations, with models that have BC lifetimes of under 5 days comparing best with observations.

Hodnebrog et al. (2014) also discusses the effect of BC lifetime on both AeroCom models and the Oslo CTM2 model's ability to replicate BC vertical profiles. Altering deposition efficiency in the model to shorten BC lifetime to 3.9 days improved the Oslo CTM2 model's correlation and bias with observed flight campaigns, and reduced overestimations of BC aloft in remote regions. Wang et al. (2014b) uses a mixture of AAOD retrievals and BC mass observations to determine a lifetime for BC. They state that older models are likely to overestimate the lifetime of BC, and that their model improves with a lifetime of 4.4 days, compared with the AeroCom mean of 7.3 days. The lifetime of BC in HadGEM3-UKCA is 4.1 days, which is comparable to the values given in the above literature, and is less than the 5-day lifetime that gives better comparisons with observations, according to Samset et al. (2014). OC lifetime is currently 4.0 days.

5.3 List of Sensitivity Studies

Name	Description	Supporting literature
BCdens	Increase in BC density from 1.5 g cm^{-3} to 1.8 g cm^{-3}	Schwarz et al. (2013), Schkolnike et al. (2006)
OCdens	Decrease in OC density from 1.5 g cm^{-3} to 1.2 g cm^{-3}	Schkolnike et al. (2006), Kuwata et al. (2012)
OC+BCDens	Increase in BC density from 1.5 g cm^{-3} to 1.8 g cm^{-3} and a decrease in OC density from 1.5 g cm^{-3} to 1.2 g cm^{-3}	As above

Table 5-1- Description and name of simulations used in this chapter

Based upon the potential options available to assess lifetime described above, we choose to evaluate the effect of CA density in the model, as changes are required. For BC, we use the density of 1.8 g cm^{-3}, which is commonly used by both measurement scientists and modellers.

This value is more representative of the range of densities that was discussed in section 5.1. It will also allow continuity with the value used in some of the surface BC concentration observations. For OC, a value of 1.2 g cm^{-3} has been chosen, based upon a median value from the range given in literature. The simulations used in this section are listed in Table 5-1.

5.4 Results

5.4.1 BC & OC burden

Figure 5-1 shows the distribution of percentage BC column burden changes between altered density simulations and the CTRL simulation, averaged over 3 years. When OC density is decreased, BC burden is increased by 4% globally, double the inter-annual variability for global BC burden. All regions show an increase in BC burden. The largest increases in BC burden are seen off the west coast of Central Africa, Antarctica and in the Central Pacific, where BC burden is increased by up to 25%. Regions of high biomass burning emissions, such as South America and Central Africa, show increases of up to 15%. When BC density is increased, the global BC burden does not significantly change. Most regions show small decreases of less than 5% in BC burden, however, in the Indian Ocean, increasing BC density increases the BC burden by up to 5%. In Central Asia, increasing the BC density decreases the BC burden by up to 10%. When both BC and OC density are altered, the BC burden is also increased by 4%. Regions where large increases are seen when OC density is decreased, such as Central Africa, South America and central Pacific, show similar spatial and quantitative increases in BC burden when both OC and BC density are altered. In Central Asia, the same spatial and quantitative decrease in BC burden seen when BC density is increased is also seen when both BC and OC density are altered.

Figure 5-2 shows the distribution of OC column burden percentage change when OC and BC densities are altered compared to the control simulation, averaged over 3 years. When OC density is decreased, there is a global increase in OC by 5%, double the inter-annual variability. The regional distribution of changes to the OC burden mirrors the spatial pattern seen in changes to Surface OC concentrations when OC density is decreased. In high latitudes, OC increases by up to 30%. In regions where the aerosol type is predominantly aged biomass burning, such as the Central Pacific and Southern Atlantic, decreasing OC density increases OC by up to 20%. Decreasing OC density increases OC by only 5% in regions with high fossil

fuel emissions. When BC density is increased, there is no change. Most regions show small decreases of less than 5%. In Central Asia, increasing BC density decreases the OC burden by up to 10%. When both BC and OC densities are altered, the OC burden is increased by 4%, showing good additivity of the individual density changes in the model. The OC burden is reduced by up to 30% in Greenland, with decreases of up to 20% in other high latitude areas and regions of aged biomass burning. Altering both densities decreases the OC burden in Central Asia by up to 10%, the only region where OC burden is decreased.

In GLOMAP-mode, the optical and physical properties of the aerosol internal mixture are weighted by the volume of each component, whilst the size of each aerosol particle, and the total mass of emission are pre-set. Decreasing OC density makes the internal mixture lighter, meaning each individual aerosol particle in the mixture is lighter. Changes to both BC and OC burden are almost identical, both spatially and numerically, when the density of CA is changed in the model, which confirms that the changes to either aerosol affect the internal mixture. Regions of large increases in both BC and OC burden when OC density is decreased are consistent with areas of high biomass burning emissions, or areas where the aerosol burden is mostly aged biomass burning aerosol. As CA burden has increased, so do the lifetimes, with both BC and OC lifetimes increased by around 4 hours (from 4.14 days to 4.33 days for BC and 3.99 days to 4.14 days for OC). The increases in CA burdens can therefore be attributed to the same changes to CA lifetime caused by lighter OC particles in the internal mixture. When BC density is increased, particle weight is increased in the internal mixture, leading to a small reduction in lifetime (4.08 days for BC, 3.93 days for OC). The effect of BC density on lifetime is smaller than the effect of OC density, mostly due to the smaller proportion of the aerosol burden that BC accounts for compared to OC.

OC Dens

Global Mean Difference = 4.0%

BC Dens

Global Mean Difference = -0.3%

BC+OC Dens

Global Mean Difference = 3.8%

BC Burden difference (%)
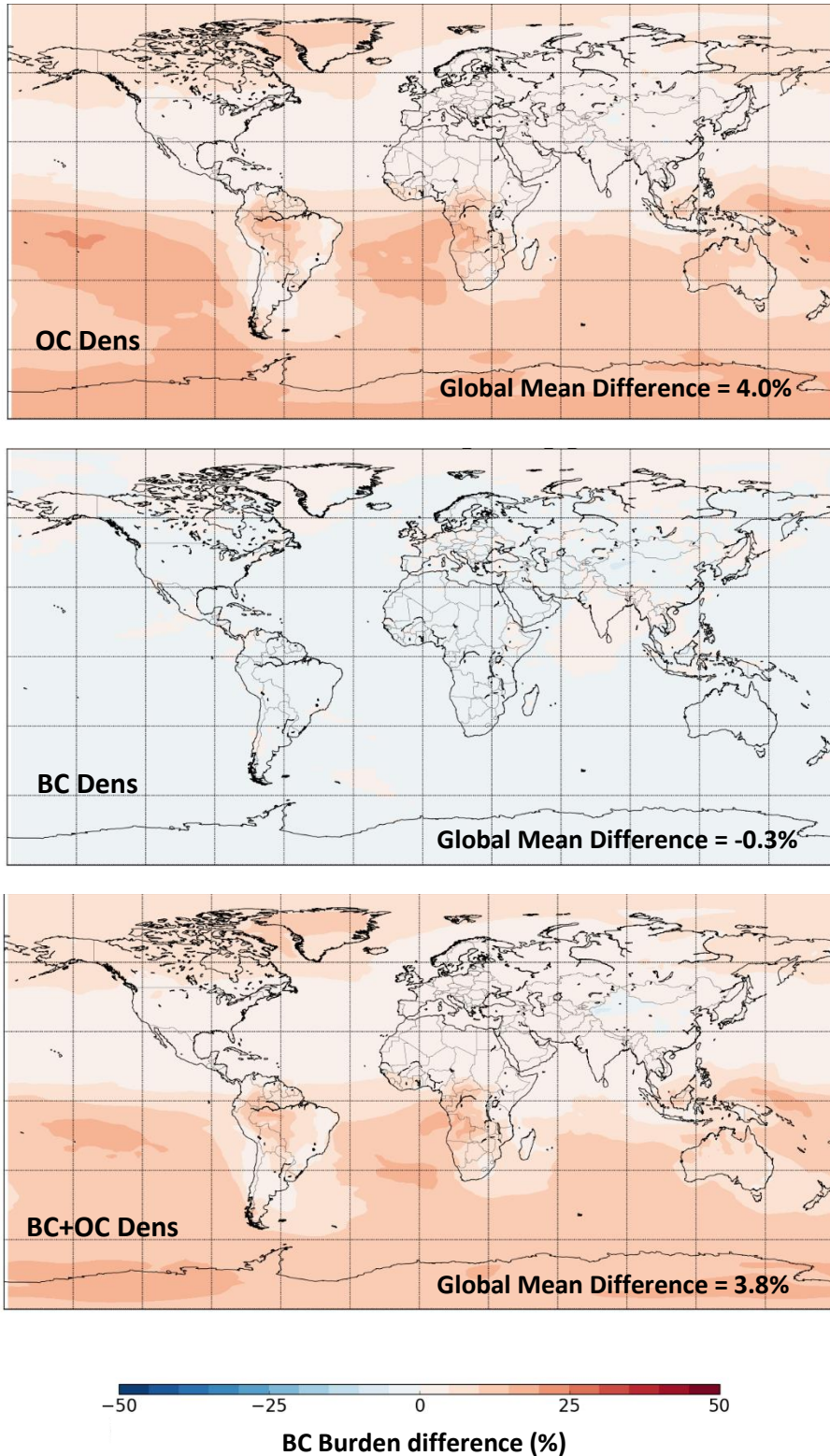
Figure 5-1- Global distribution of percentage changes in BC burden between changed density simulations and the control simulation for the period 2006-2008
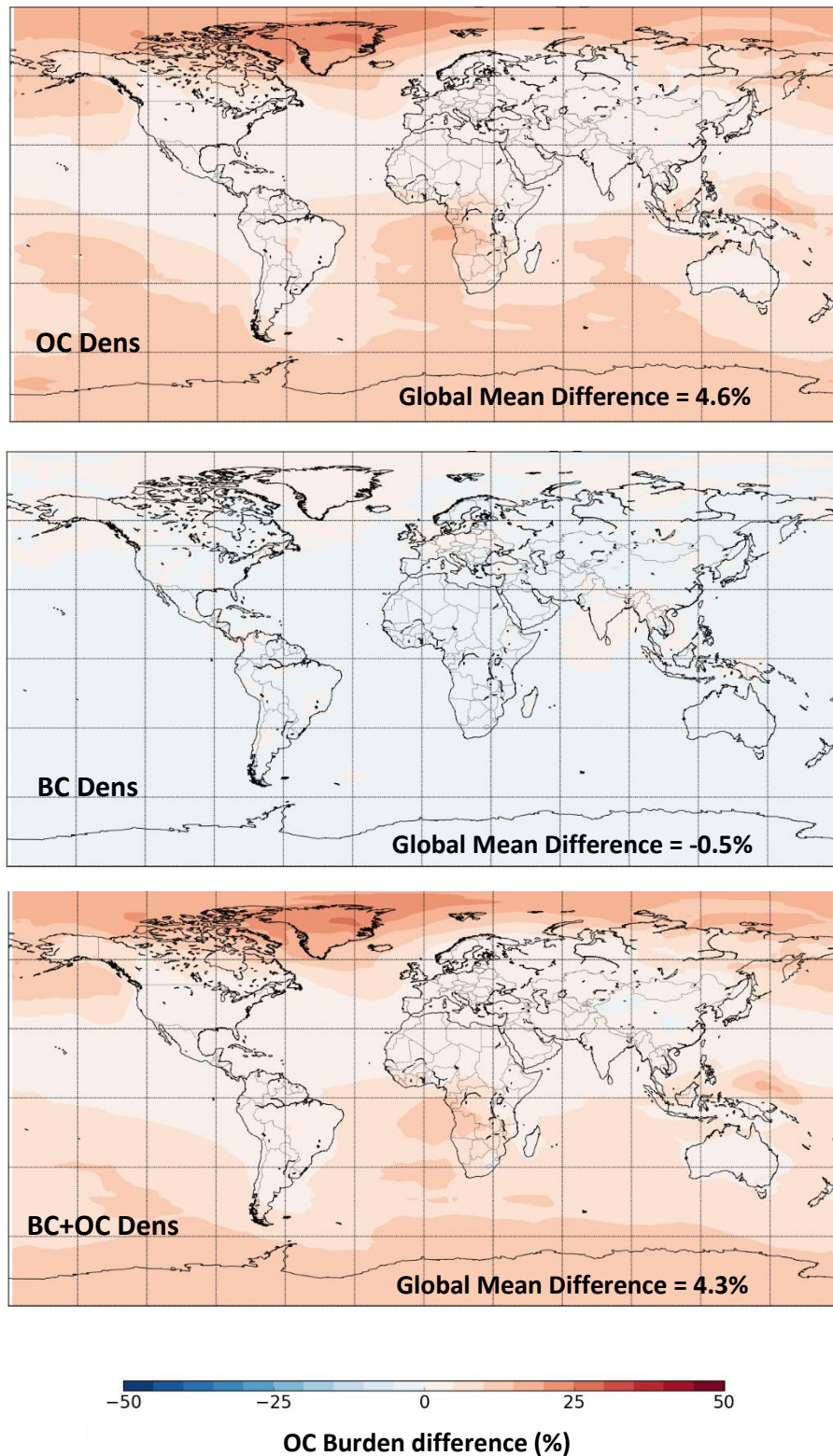
Figure 5-2 - Global distribution of percentage changes in OC burden between changed density simulations and the control simulation for the period 2006-2008

The good additivity in mass shown when altering BC and OC density separately and in unison shows that the changes are linear, and suggests that scaling density between the values simulated will scale the increases/decreases proportionally. A reduction in lifetime suggests that there is a reduction in one of the deposition methods in the model. Figure 5-3 shows the distribution of the average dry deposition rate difference between the increased OC density and control simulation. When OC density is decreased, the dry deposition is reduced globally by 4%, which is larger than the inter-annual variability in dry deposition. Decreases of up to 20% occur in areas where biomass burning plumes are transported. This proves that the increase in burden seen when OC density is reduced is due to a reduction in dry deposition. This decrease in deposition is due to the change in weight of the internally mixed particles, and shows that changes in the physical properties of one aerosol species can affect others in the scheme. A reduction in dry deposition rate would also lead to a cumulative proportional increase in BC, explaining why areas of predominately aged biomass burning aerosol show increases in CA burden which are as large or larger than increases in source regions.
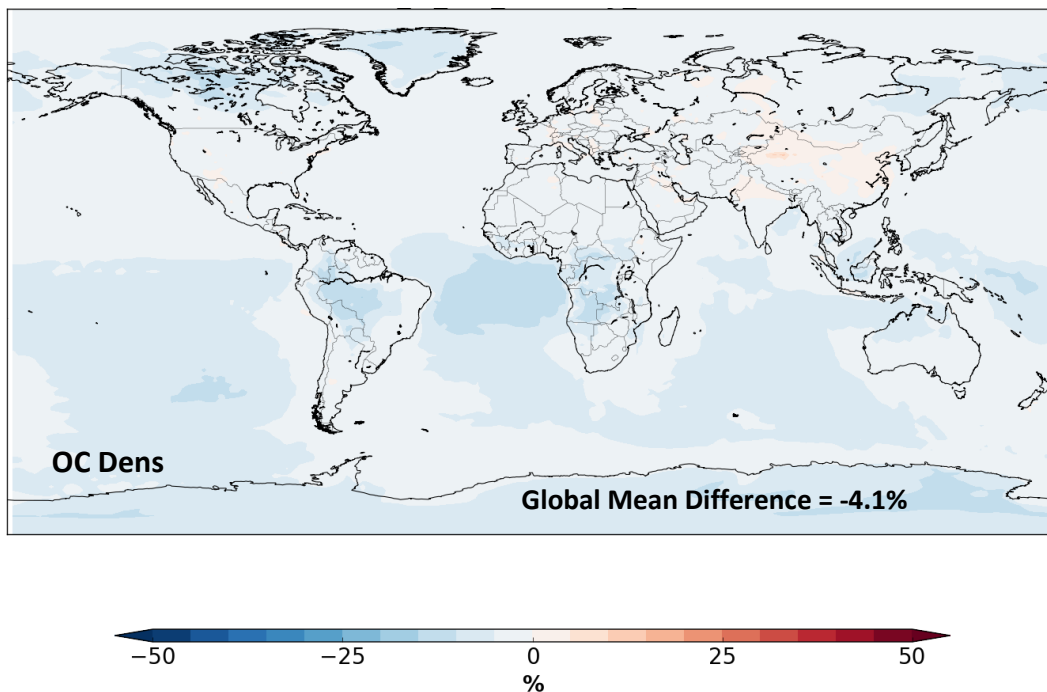
Figure 5-3- Global distribution of BC dry deposition percentage changes between decreased OC density simulation and control simulation, for the period 2006-2008

Figure 5-4- Global distribution of percentage changes to freshly emitted CA aerosol number when OC density is reduced, averaged over 3 years shows the percentage change in the column-integrated Aitken Insoluble aerosol number, which is the initial mode into which BC and OC are emitted, due to decreased OC density. Globally, the aerosol number is increased by around 40%, with low variability spatially. Larger increases of up to 60% occur over biomass burning regions and areas where biomass burning emissions are transported to, with increases of only 30% over fossil fuel burning areas such as Europe and India. These changes are significantly higher than the proportional change in lifetime discussed above. The increase in number occurs because of the restriction on size and emitted mass in GLOMAP-mode. As well as creating lighter individual particles, the need to emit the same amount of mass means that there must be an increase in number. Increases in aerosol number can have several effects, including affecting the optical depths, which will be discussed in the next section, and increases the potential amount of CCN when particles become soluble.
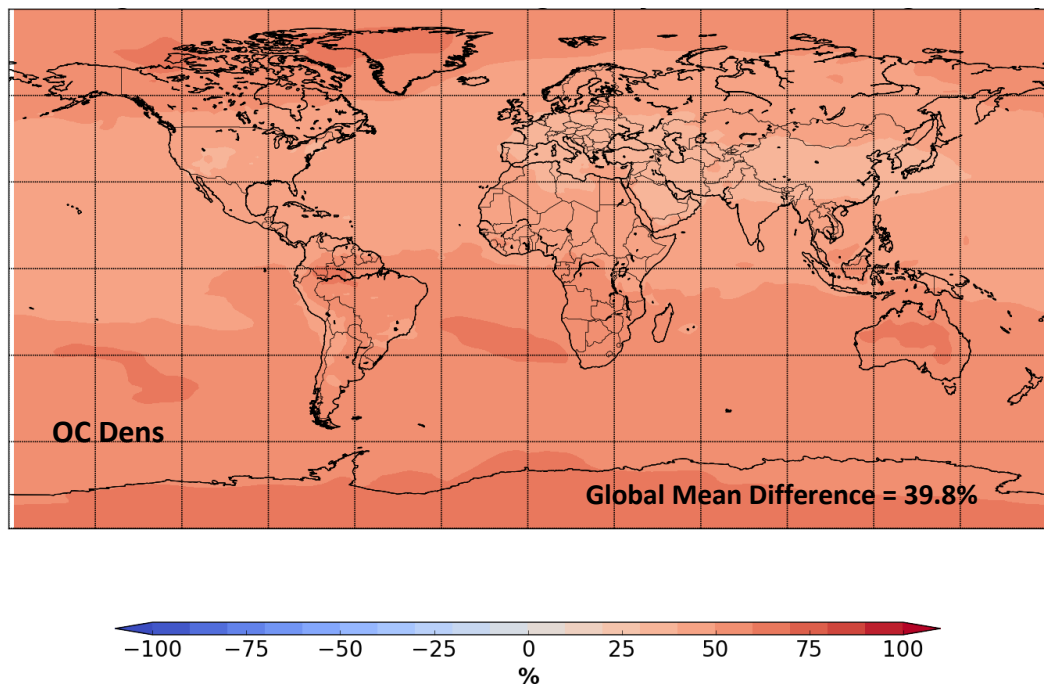
Figure 5-4- Global distribution of percentage changes to freshly emitted CA aerosol number when OC density is reduced, averaged over 3 years

5.4.2 AAOD

Figure 5-5 shows the distributions of the 3-year average percentage change in AAOD when OC density, BC density or both densities are altered. Reducing OC density increases the global average AAOD by just over 3%, which is equal to the variability seen in the model on a yearly basis. The sign of the AAOD change depends on the region. Central Africa, South America, Boreal regions and remote oceanic areas (regions of biomass or transported aerosol) show an increase in AAOD, whilst North America, Europe and Central Asia (regions of fossil fuel combustions) show decreases. The percentage change in AAOD increases with distance from biomass burning sources. Increasing BC density decreases the globally averaged AAOD by 13%. This is larger than the change in BC burden seen in Figure 5-1. All regions show a decrease in AAOD. Fossil fuel and biomass burning source and transported regions, see the largest percentage decrease in AAOD. Areas with large amounts of mineral dust, such as Saharan Africa and Western Australia, show the smallest percentage changes in AAOD. Altering both BC and OC densities decreases the globally averaged AAOD by 10%, suggesting a good level of additivity of the individual density changes. The AAOD decreases in all regions. Fossil fuel burning regions, such as Europe and North East America, show the largest relative decreases because changes to OC and BC density both decrease the AAOD in those areas. In remote regions, BC density decreases AAOD more strongly than OC density increases AAOD, so the net impact is a decrease.

A decrease in OC density increases the number of OC particles and the total volume of OC for a given mass. The dry deposition velocity is reduced, increasing the lifetime of all aerosols, including BC, which increases AAOD. However, the imaginary part of the refractive index of the internal mixture is smaller, which reduces AAOD. Results suggest that in biomass burning regions, where BC and OC are emitted at height, the effect of the reduced deposition of BC is stronger than the effect of reduced absorption from increased OC volume. However, in fossil fuel combustion areas, BC and OC are emitted at the surface only, and the effect of the reduced absorption is stronger than increased absorption due to the change in dry deposition. The effect of reduced OC density on lifetime accumulates as the aerosol ages, explaining why changes in AAOD are greater in aged biomass burning plumes than fresh plumes.
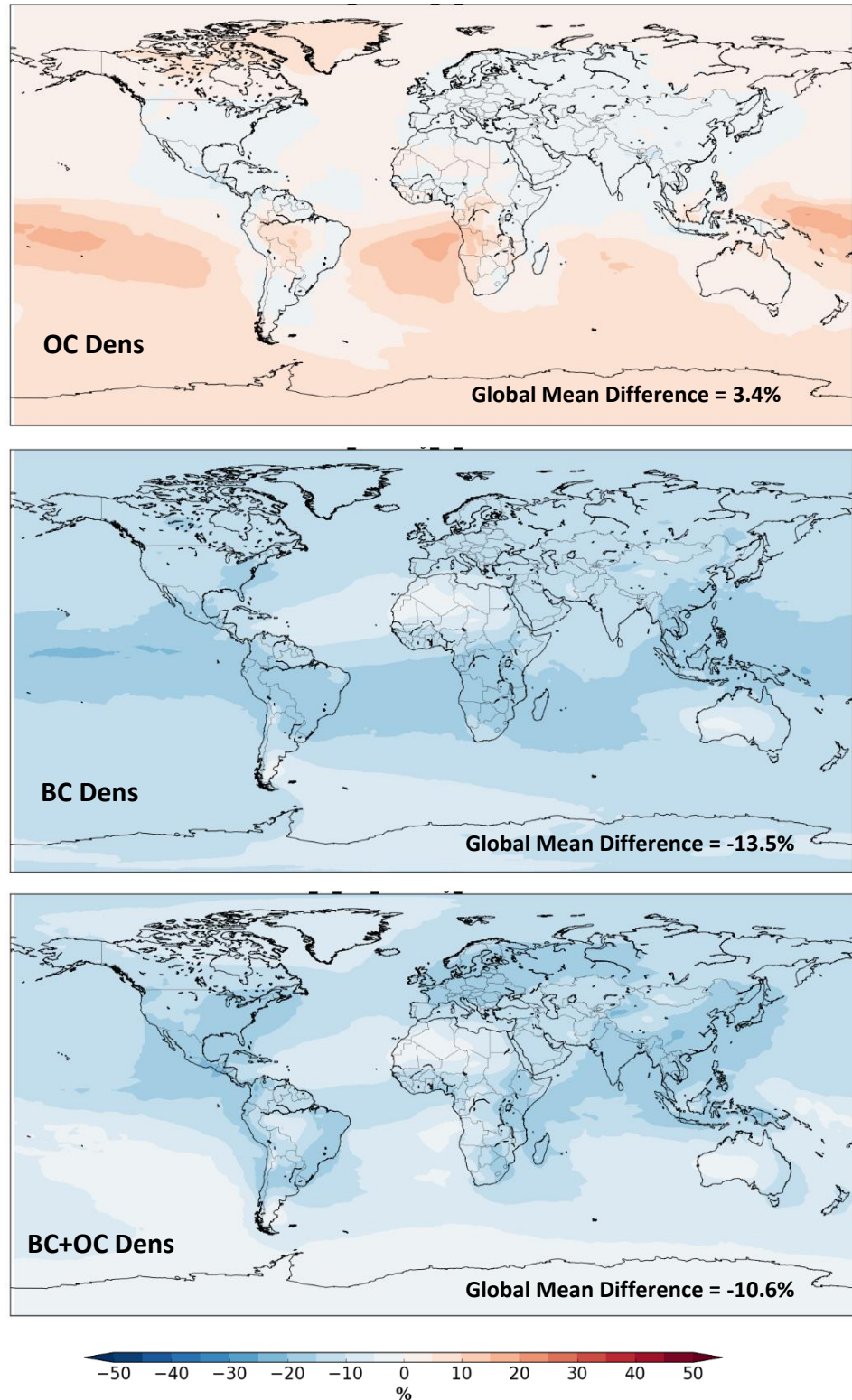
Figure 5-5 - Global distribution of percentage changes in absorbing aerosol optical depth between changed density simulations and the control simulation for the period 2006-2008

The weight of the internal mixture increases when BC density is increased, but the number of emitted BC particles decreases. As seen in section 5.4.1, increasing BC density leads to increased dry deposition rates and a shorter BC lifetime, which in turn decreases AAOD. In addition, the decrease in emitted BC particle number further decreases AAOD. As shown in the burden, the effect of increased density on the deposition rate is cumulative over time. Therefore, biomass burning plumes, where aged BC makes up a higher proportion of the aerosol burden, lose a higher percentage of BC, and so are associated with higher percentage reduction in AAOD. Areas with the smallest changes in AAOD are areas where mineral dust concentrations are high and dominate AAOD. Therefore, changes to BC have less of an impact on AAOD in these regions. The additivity of BC and OC density changes shows that the multiple feedbacks between changing both densities simultaneously are negligible.
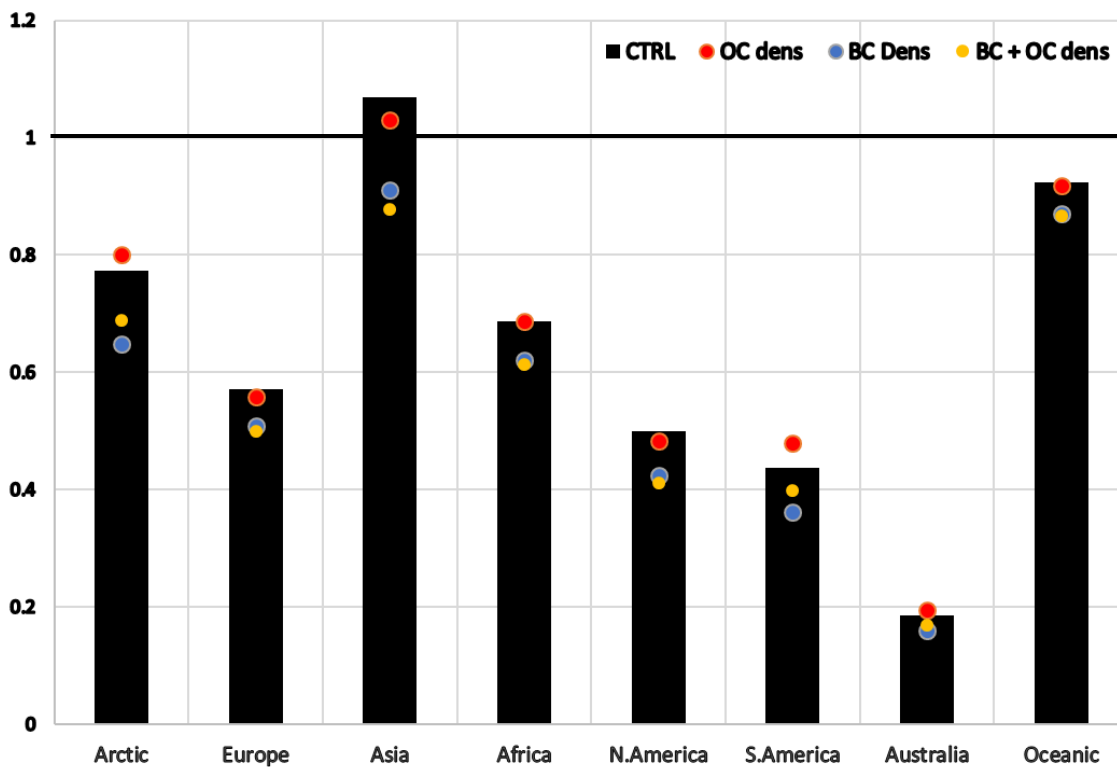
Figure 5-6 – Mean factor between modelled AAOD and AERONET retrieved AAOD at 550 nm. A value under 1 shows the model underestimating compared to observations, above 1 shows a model overestimation.

Figure 5-6 shows the regional ratios of the co-located modelled and AERONET retrieved AAOD over the period 2006-2008. The increases in AAOD in biomass burning and remote regions when OC density is decreased improve the comparison between the model and observations in most regions. In South America, the increase reduces the deficit of the model by 10%. The decrease in AAOD in North America and Europe further decreases the model ability to replicate AAOD. In Asia, where AAOD is overestimated in the control simulation, reducing the OC density decreases modelled AAOD to nearer AERONET retrieved values. When increasing BC density, in both Asia and the Arctic, the reduction worsens the ratio of modelled to observed AAOD by up to 0.15, whilst in other regions, the ratio is reduced by up to 0.1. In all regions except Asia, this decreases the ability of the model to determine AAOD regionally. When both BC and OC densities are altered, the modelled to observed ratio is similar to the addition of the individual density changes, so the combined changes in density reduces the modelled to observed AAOD ratio. In most regions, this decreases the ability of the model compared to the observations. However, in Asia, the combined density changed simulation underestimates observations by 10%, compared to a 5% overestimation in the control simulation. As explained in Chapter 3.1.2, we believe that AERONET level 2 absorption products contain a systematic bias towards higher AAOD, meaning that in Asia, the simulation where AAOD is underestimated by 10% is likely better than the control simulation, which overestimates by 5%. It is clear that altering BC and OC density has differing effects on the AAOD. The comparison of the model to observations of AAOD from AERONET suffers when BC density is changed in the majority of regions, but is improved when only OC density is decreased.

5.5 Summary and Conclusion

This set of results shows the difficulty of understanding and then responsibly developing the performance of climate models which have an internally mixed aerosol scheme. Here, we have demonstrated that the concentration of BC aerosol is more sensitive to the density of OC than to its own density, because of the internal mixing scheme and the higher concentrations of OC in the atmosphere. It suggests that there are other possibilities to alter aerosol species mass by changing other aerosol species properties or mass. Ideally, every

parameter within the aerosol scheme for every component should be looked at to determine the sensitivity of the model variables, something which can only be achieved through thousands of altered simulations or perturbed parameter emulators (Carslaw et al., 2013). However, in this project we choose to focus on the effects of OC and BC parameters, with the knowledge that there is further scope for changes to the variables when model development alters other aerosol species.

The results also show that a small change in BC lifetime can have a large regional influence on AAOD. The global BC lifetime is changed by only a few hours, but changes to the burden locally mean this can change AAOD by up to 30% in some regions. However, the sensitivity of BC global lifetime in the model to BC and OC density is unlikely to be as large as the sensitivity to cloud scavenging and wet deposition schemes, which have been shown to change global lifetime by up to 10% (Vignati et al., 2009). This shows that the range of BC lifetimes that provide the best fit to aircraft observations in remote regions, which is in the order of 5 days, could be achieved through several model changes, only some of which are related to the aerosol scheme.

Finally, this chapter highlights the need for finding a compromise when updating and improving a climate model. We have shown that altering the density of both BC and OC density in the model is detrimental to the ability of the model to replicate observations. However, scientifically, the changes to density reflect improvements in understanding and knowledge, and more accurately represent a mean value of the density of BC and OC. Therefore, the change to density need to be added to the model regardless of how they affect performance. Adjusting the density means that improvements in the model must be found through other parameters.

6. Chapter 6: Implementation of Combined Changes and Impact on Radiative Forcing

6.1 Synthesis of Sensitivity Studies

The past three chapters have looked at the sensitivity of the model to three key uncertainties in attempts to model carbonaceous aerosols accurately. Each solution has altered the model uniquely, both spatially and quantitively. We have shown that no single solution can be used to improve the model with a global equal effect. However, a combination of the alterations made in the three solutions could offer a method of improving the comparison of the model with observations in simultaneous regions. Figure 6-1 shows the distribution of changes to SSA that can be produced from perturbing different parameters in the model. It shows that there are a wide variety of options available to modellers which can change the absorption of aerosols, and thus influence the AAOD and SSA, beyond just scaling emissions. It also highlights the challenges of finding a correct balance between these changes so that all variables are improved in comparison to observations. Figure 6-2 shows the distribution of changes to surface BC concentration that can be produced from perturbing different parameters in the model. This also highlights the variety of options which are available to modellers. Importantly, comparing to Figure 6-1 also shows that the magnitude of changes in AAOD does not necessarily match the magnitude, or even the sign, of a change in surface BC concentration. Surface BC concentrations also show that for some changes, such as changes to OC, the sign of the change in surface BC concentration is regionally dependent. This complication can be exceptionally useful to allow for better model comparisons with observations, if utilised properly when making changes to the model.

In this chapter, we propose combinations of the three solutions and further analyse potential new schemes aimed at improving the model. We use the analysis of the sensitivity simulations described in Chapters 3, 4 and 5 to identify a set of parameters and changes to the model which will improve its comparison to observations, whilst still being scientifically justifiable. We also aim to test whether global changes in OC absorption can be split further within the

153

model by attributing different levels of absorption to different emissions. We hope this will achieve a better comparison of regional model to observation comparisons than simple global changes to all OC emissions. Finally, this chapter will also analyse the changes to radiation that occur from alterations to the model, and describe how these changes effect radiative forcing for carbonaceous aerosols compared to previous model versions.
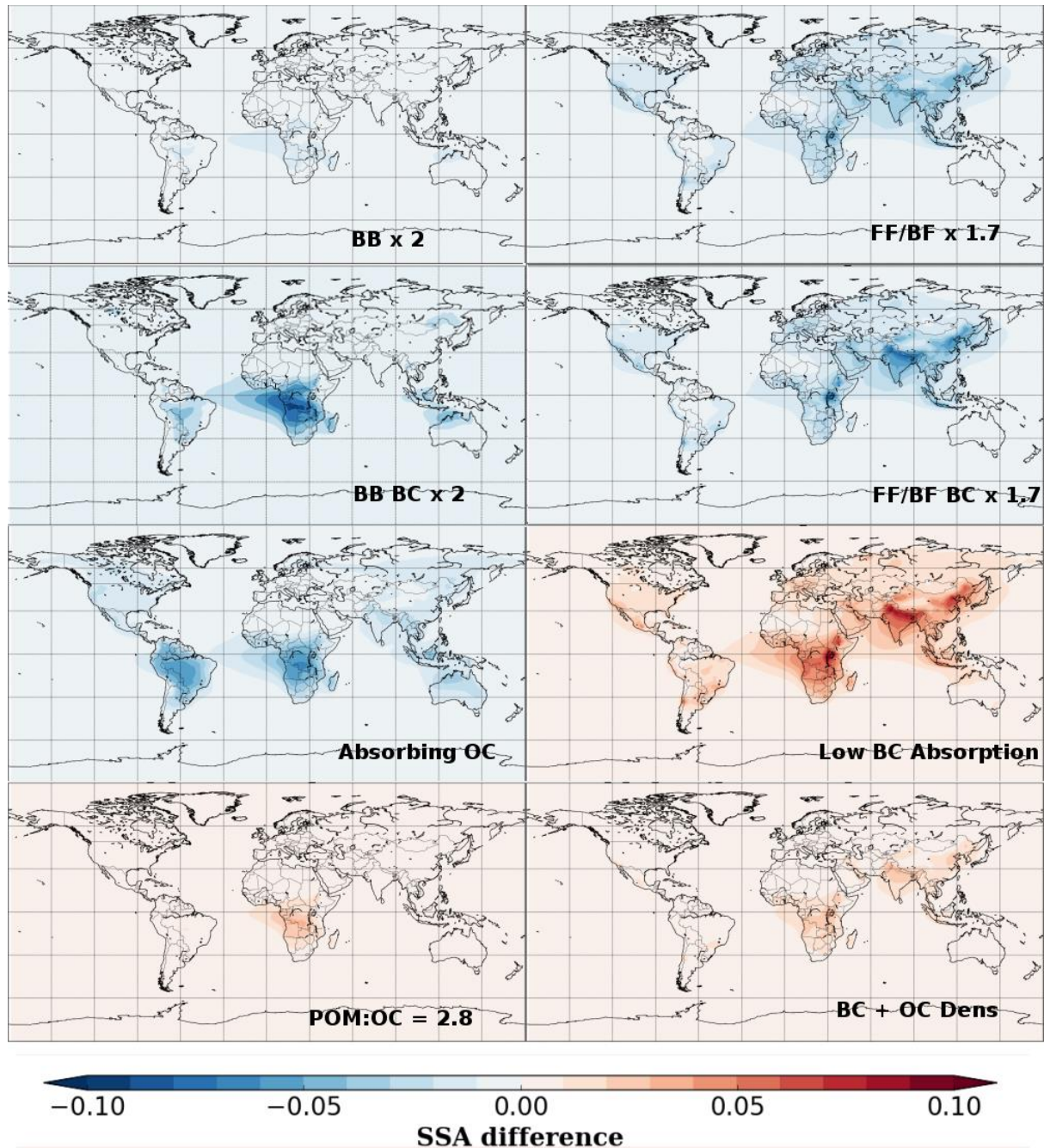
Figure 6-1 – Global distribution of changes to SSA in perturbed simulations compared to the control, averaged over 3 years.
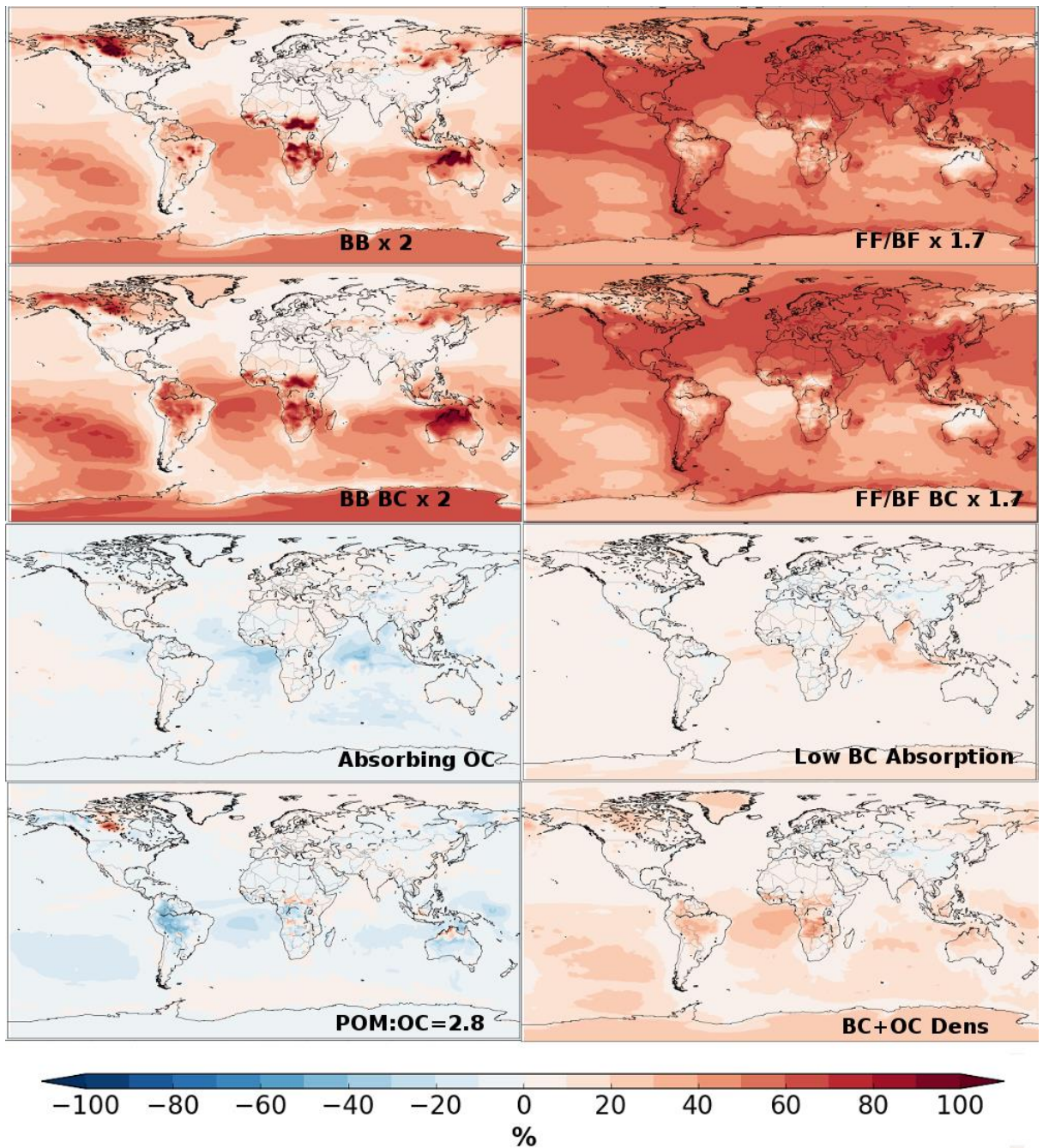
Figure 6-2 - Global distribution of percentage changes to surface BC concentrations in perturbed simulations compared to the control, averaged over 3 years.

6.2 Implementation of combined and non-global changes

6.2.1 Adoption of new parameters

The decision of which model improvements to use is based upon two main specifications. Firstly, does the current model use values for parameters that require updating according to

modern literature? In this case, the change is included, regardless of the impact on model performance. Secondly, if parameters are inside the currently accepted ranges, does the change improve the model? If that is the case, the combination of changes that leads to the best improvement is determined by adding the changes to the mean factors for each variable. Where sets of combined changes influence the mean factors of different observation sets or regions in opposite directions, we focus upon areas where perturbations have the largest impact, which are also areas where BC and OC are dominant species, and variables in which CA is a major factor. For example, correctly replicating surface BC concentrations in South America is considered more important than replicating AOD in Australia.

Changes to both BC and OC density satisfy the first condition, as the values of 1.5 g cm^{-3} are no longer considered suitable as a mean value for density, nor reflect the range of densities derived from modern observations. This is why these values are no longer used in calculations which derive mass from optical techniques. Therefore, despite the slight worsening of the model compared to observations, we include these changes.

There is also a strong case for increases in emissions to be included. Although the current emission inventories used are justifiable, studies using both other mass derivation techniques and model comparisons to mass observations suggest that increases are necessary to comply with real world (Bond et al., 2013; Gadhavi et al., 2015; Johnson et al., 2016). We note from the analysis in Chapter 4 that increases in both BC, OC and POM:OC ratio together in biomass burning regions improved nearly all aspects of the models comparison to observations. However, in fossil fuel burning areas, clear improvement was only seen when BC alone was increased, and not both BC and OC, as an increase of mass of OC over North America, where OC emissions are predominately from fossil and biofuel combustion, worsened the model's ability to replicate observations of surface OC concentrations.

We then analyse how the model is affected by the refractive index changes discussed in Chapter 3. Our work suggests that in fossil fuel regions, where Saleh et al. (2013) proposes that OC is non-absorbing, BC is required to have a high refractive index to compare well against observations of AAOD and SSA, as it currently does. Whilst increasing absorption from OC improves the model further, the value of the imaginary part of the refractive index is not appropriate for fossil fuel combustion. In contrast, in biomass burning regions, modern

literature strongly suggests that an absorbing OC should be accounted for in models (Feng et al., 2013; Wang et al., 2014), but are also aware that our efforts to implement this worsen the model. To resolve this dilemma, we run two simulations: One with the combined changes and an absorbing OC and one the combined changes without absorbing OC. We hope that the simulation with absorbing OC will be more representative of reality in biomass burning regions, and that the simulation without absorbing OC will be more representative of regions emitting fossil fuel combustion aerosols.

Table 6-1 shows the list of simulations run for the work in this chapter, listing the changes made in each compared to the control simulation and the reason why each change is included. Other than the described alterations, the setup for each simulation is identical to the control, with nudged horizontal winds and output simulated for 2006-2008 after a 4-month spin-up.

Simulation	Alterations included	Reason for inclusion
Combined Changes	BC and OC biomass burning emissions doubled.	Improves model to observation comparisons
	POM:OC biomass burning emission ratio increased from 1.4 to 2.8.	Improves model to observation comparisons
	BC density increased from 1.5 g cm^{-3} to 1.8 g cm^{-3}.	Required update
	OC density decreased from 1.5 g cm^{-3} to 1.2 g cm^{-3}.	Required update
	BC fossil and biofuel burning emissions increased by a factor of 1.7.	Improves model to observation comparisons
Combined Changes (inc OCabs)	As above, with additional change to imaginary part of OC refractive index, increasing from 0 to 0.03i.	Scientific justification for inclusion in biomass burning regions

Table 6-1 - List of simulations used in this chapter, details of the alterations included in each and the reason why the change was included.

6.2.2 Results of new simulations

In this section, we analyse the combined sensitivity simulations compared to the initial control simulation, and evaluate the ability of these combined sensitivity simulations to replicate observations, determining whether they represent an improvement on the original model.

Table 6-2 shows the percentage changes to CA mass and optical variables for both individual changes to the model, and combined simultaneous changes. The response to AOD, OC burden and surface OC concentrations are nearly double the addition of linear changes. Responses to surface BC concentrations and BC burden changes are only slightly larger than the linear increase expected, However, the AAOD percentage change between the combined changes simulation is lower than the linear addition of changes. When absorbing OC is added to the combined changes, AOD, surface OC concentration and OC burden are still changed by double the linear addition of each individual model change. AAOD is also increased by double the linear addition of each individual change in the model, despite the linear addition being greater than the model response without the absorbing OC.

The changes which show larger than expected responses in the initial combined changes simulation include all those for which OC is an important factor. Here, individual changes amplify the effects of others, increasing the response in the model beyond expectations. For example, increased amounts of OC will amplify the effects of lighter particles produced due to OC density decreases. This can be shown in the table by comparing the change between the combined changes simulation and combined changes with absorbing OC simulation, and comparing it to the change due to absorbing OC in the control simulation. The increase in OC emissions leads to an increase in the amount of OC absorption, meaning that both the optical depths and the secondary lifetime effects from increased absorption seen in Chapter 4 are increased. This highlights the sensitivity of how models respond to a given change depending on the initial setup of the model.

	FF BC x 1.7	BB x 2	BC + OC dens	POM to OC ratio	Combined Changes	OC abs	Combined Changes (with OC abs)
AOD	0.5	2.7	-0.1	2.2	**9.8** (5.3)	0.6	**11.2** (5.9)
AAOD	32.3	28.6	-10.6	-2.3	**41.7** (48.0)	51.6	**192.1** (99.6)
BC burden	51.0	23.0	3.8	-1.7	**80.0** (75.1)	-0.2	**79.5** (74.9)
OC burden	0.3	30.0	4.3	31.0	**110.1** (65.6)	0.1	**112.1** (65.7)
Surface BC Conc	47.9	23.5	4.9	-2.2	**80.6** (74.1)	-0.8	**78.0** (73.3)
Surface OC Conc	-0.6	24.6	5.1	25.9	**100.2** (55.0)	-0.7	**96.9** (54.3)

Table 6-2 - Globally averaged percentage changes from single perturbation changes, with comparisons to simultaneous changes in the model, averaged over 2006-2008. Bold numbers in the blue column show the percentage change seen when changes are made simultaneously Number in parentheses show linear additions of percentage changes in individual simulation changes.

6.2.2.1 AOD

Figure 6-3 shows the change in mean factor between the control and combined sensitivity simulations, and observations of AOD from AERONET. In all regions, the mean factor is increased by between 0.07 and 0.2, with the additional absorbing OC increasing the value by slightly more than the combined changes without absorbing OC. In Australia and at Oceanic sites, this increase leads to the model overestimating observed AOD, and worsens the comparison. In all other regions, the increase improves the comparison, but the model still underestimates AOD observations in most regions by around 25%.
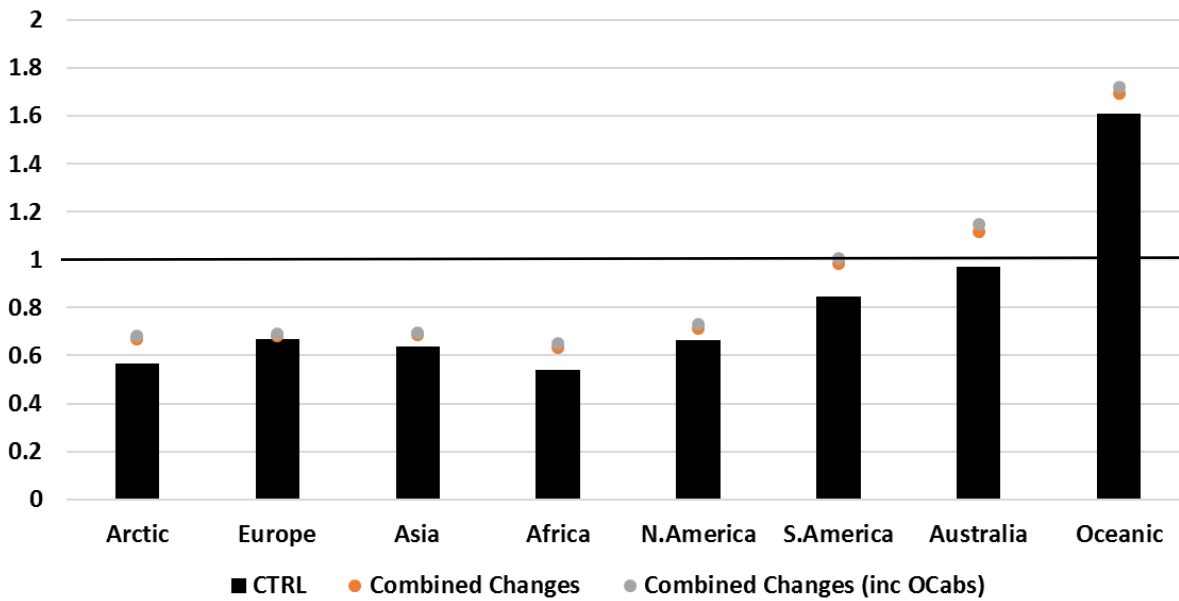
Figure 6-3 – Regional mean factor of aerosol optical depth, for control and combined sensitivity simulations, averaged over 3 years.

Figure 6-4 shows the correlation and normalised standard deviation change between the different modelled simulations and AERONET AOD. In all regions, adding absorbing OC to the combined changes simulation has little effect on the comparison to the observations. In South America and Australia, the combined changes increase the normalised standard deviation with no change in the correlation. This greatly improves the model comparison in those regions. The same effect is noted in the Arctic and North America, although the change and improvement is smaller. In Asia, the correlation is increased, improving the comparison to observations. However, in Asia and Oceanic regions, the normalised standard deviation is reduced by a small amount, worsening the comparison between model and observations. In Africa, where we see the highest percentage changes, the correlation of the model and observations is drastically worsened (0.73 in the control to 0.39 and 0.34 respectively), with no change in the normalised standard deviation.

The increase in mean factor when comparing the model and observations of AOD is expected due to the increased emissions added to both combined changes simulations. The effect still leaves underestimations of AOD however; one reason for this could be that there are

potentially other aerosol species which are underestimated in the model or missing entirely. HadGEM3-UKCA does not include nitrate for example, which would increase AOD. There is a variety of changes to the correlation between observations and model regions however. An increase in normalised standard deviation shows that the range of AOD is increased due to CA increasing high AOD. Decreases show that changes to CA have increased low AOD, reducing the range of AOD the model produces. Increased correlation and improved normalised standard deviation suggests that the temporal and spatial pattern of increases in aerosol burden caused by the changes more closely match observations. However, regions where only correlation or normalised standard deviation is improved, such as Africa, suggest deficiencies in AOD are due to other factors.

Figure 6-4 – Taylor Diagram of AOD showing normalised standard deviation and correlation between modelled and AERONET observed AOD at 550 nm.

Overall, the model shows good improvement to modelled AOD in most regions, and the amplification of the effects seen in individual sensitivity studies only further improves this.

However, the effect of increased CA in Africa appears to be an incorrect solution to discrepancies in AOD between model and observations there.

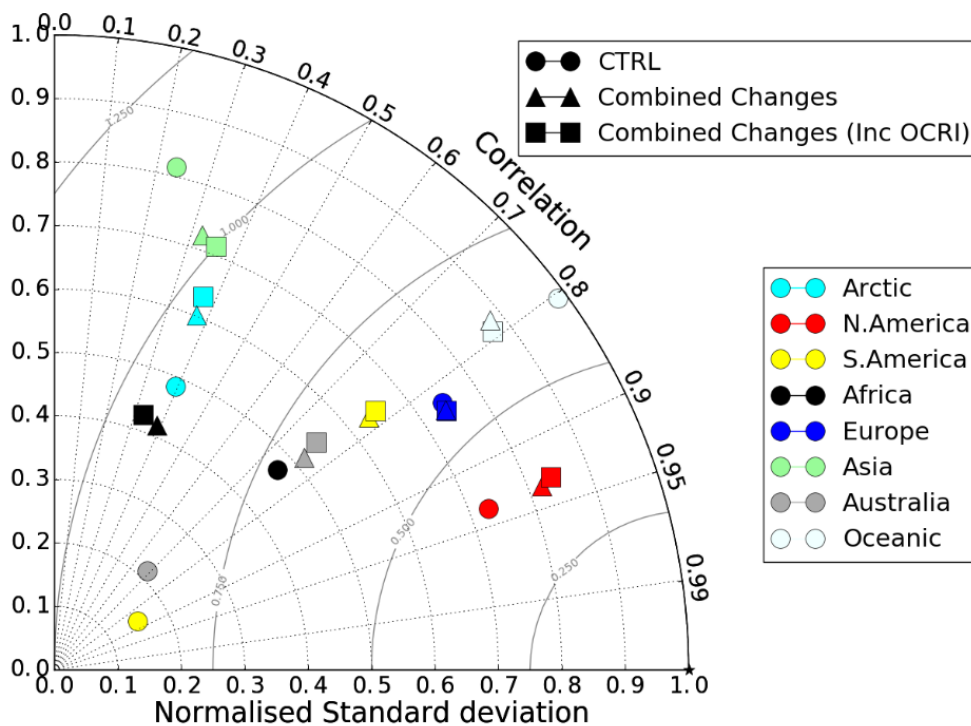### 6.2.2.2 AAOD

Figure 6-5 shows the change in mean factor for the control and combined sensitivity simulations compared to retrieved AAOD from AERONET. In all regions, the mean factor is increased for both the combined changes alone, and increased further when absorbing OC is also added to the model. Regionally, the effect of both sets of changes differs greatly depending on the location. The combined changes without absorbing OC improves the model comparison in all regions except Asia and the Arctic. In North and South America, Africa and Oceanic regions, the combined changes without absorbing OC give the best comparison with observations. In Europe and Australia, the best comparison with observations occurs when absorbing OC is added to the combined changes. However, in the Arctic, this leads to an overestimation of AAOD in the model by a factor of 6, and overestimations in South America and Asia by a factor of 2 compared with AERONET.

Figure 6-6 shows the correlation and normalised standard deviation of modelled AAOD and AERONET retrievals of AAOD on a 30-day time scale. When the initial combined changes are applied to the model, the normalised standard deviation is increased in all regions. In South America and Africa, the normalised standard deviation is doubled. There is little change in the correlation due to the combined changes in any region, although there is an improvement in the correlation between the model and observations in Oceanic regions from 0.41 to 0.56. When absorbing OC is also applied with the combined changes, the normalised standard deviation is further increased. In South America, Africa and Australia, the addition of absorbing OC doubles the normalised standard deviation again, meaning a 400% increase compared to the control simulation. Adding absorbing OC to the model also slightly increases the correlation in Oceanic and Africa regions, but decreases it in North America and Australia.

The increase in normalised standard deviation from the initial combined changes improves the model comparison in several regions. In Africa and the Arctic, the normalised standard deviation is nearly 1, showing the model standard deviation and observed standard deviation are similar. This is in line with improvements in the mean factor in Africa, suggesting that the new simulation is replicating the AAOD well, within AERONET sampling and with monthly

emissions. In Asia and South America, the normalised standard deviation values of 3.2 and 1.9 when combined changes are applied shows the model is much more variable than the observations. For South America, where the combined changes lead to an underestimation of mean AAOD but an overestimation of variability, this suggests that the background levels of absorption are too low. Increasing these would decrease variability, and increase mean AAOD. This could be due to the timing of emissions emitted, or missing emissions in the regions.

The addition of absorbing OC leads to the variability in the modelled AAOD in Africa and the Arctic also becoming overestimated. The normalised standard deviation in Oceanic, Australian, European and North American site comparisons is closer to 1 when absorbing OC is added to the model, showing large improvements over the other simulations. However, absorbing OC is unrealistic for Europe and North America, as fossil fuel burning produces much less absorbing OC than biomass burning regions, which is what we have based absorbing OC on for the simulation (Saleh et al., 2014). In North America and Europe, the correlation is still not significant to 99%, regardless of any changes applied. The lack of correlation suggests that although making OC absorbing improves the normalised standard deviation in North America and the normalised standard deviation and mean factor in Europe, the model is still failing to get the temporal and spatial pattern of absorption correct on these scales, and therefore making OC absorbing is not an answer for improving model performance in these areas.
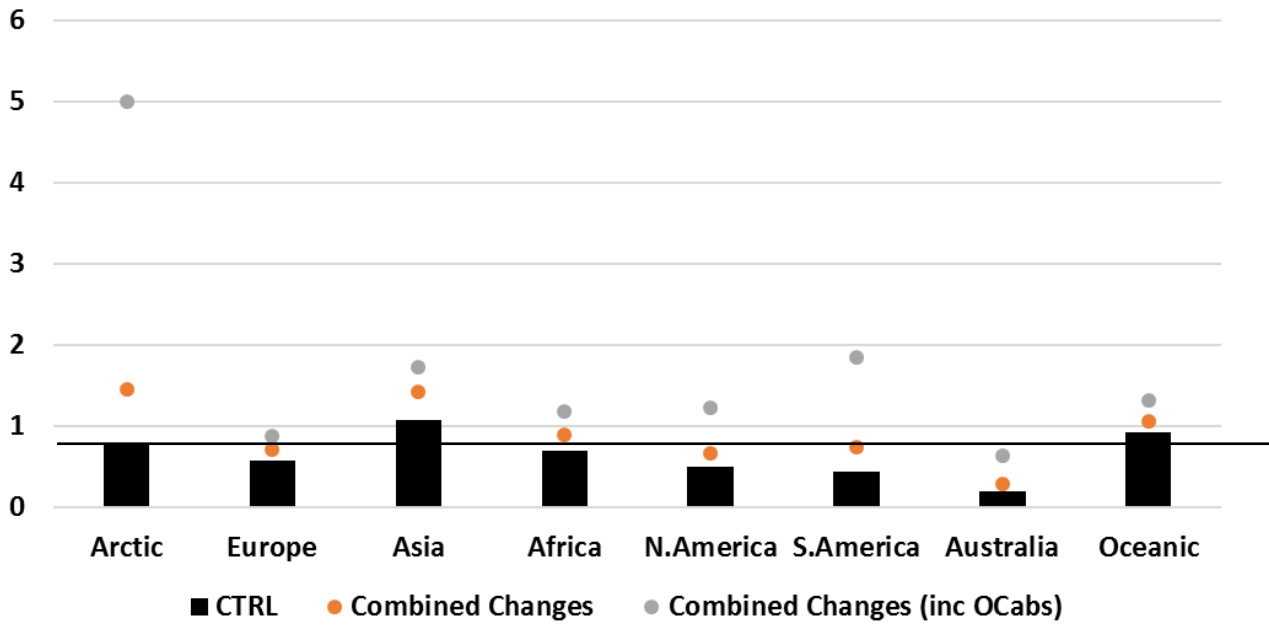
Figure 6-5 – Mean factor between modelled AAOD and AERONET observations of AAOD at 550 nm, split by region.
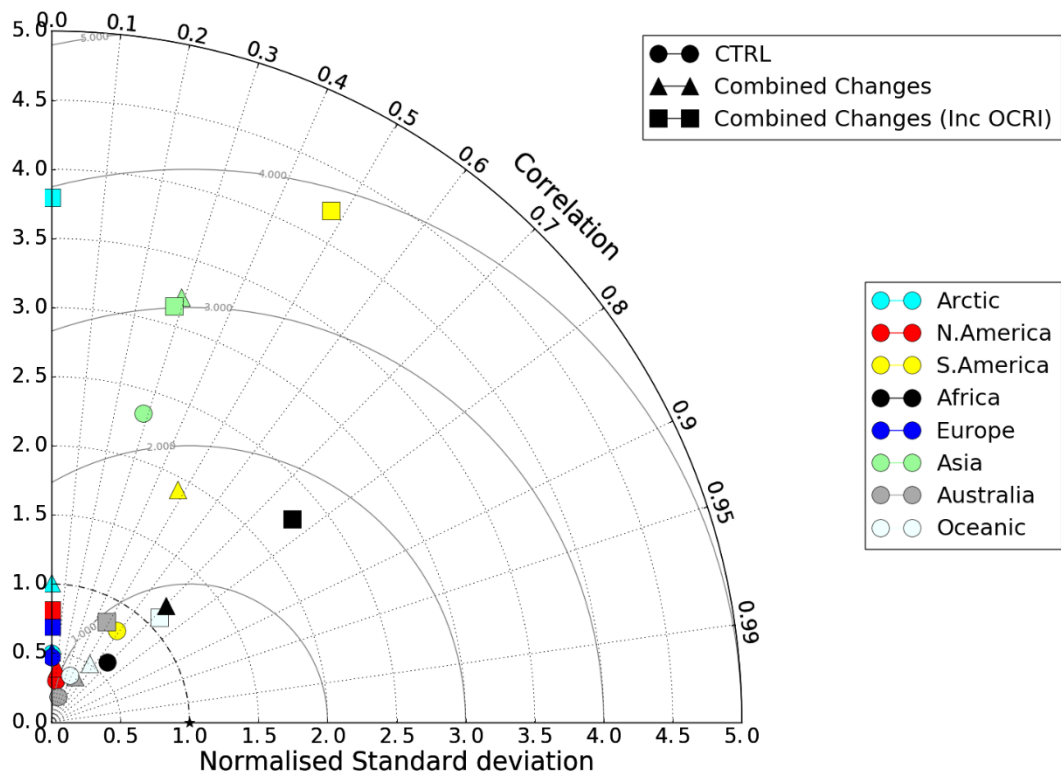
Figure 6-6 – Taylor Diagram of AAOD showing normalised standard deviation and correlation between modelled and AERONET observed AAOD at 550 nm.

6.2.2.3 Surface BC and OC Concentrations

Figure 6-7 shows the mean factor for surface BC concentration between the simulations and observations. The mean factor is increased for all regions when the combined changes are applied to the model. There is little visible difference in the mean factor when absorbing OC is also added, despite the increased sensitivity of the combined changes simulation. In all regions, the increase in mean factor improves the comparison between observations and the model. However, the new simulations still underestimate surface BC concentrations despite the changes, especially in remote regions such as sites in the Arctic and Oceanic regions.
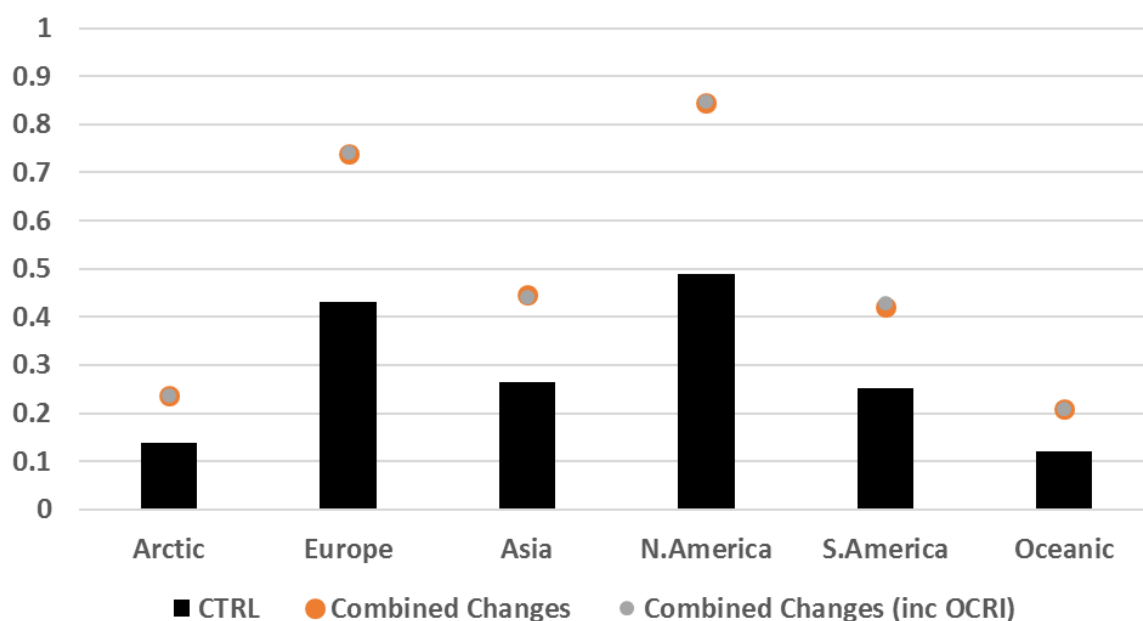
Figure 6-7 – Mean factor in comparison of the surface BC concentration between simulations and ground site observations, split by region.

In Chapter 2 we discussed the possible differences in definitions between modelled BC and observed BC concentrations, and the reasons why we expect that there may be continued discrepancies in the improved models because of those differences. Our analysis suggested that the absorption from BrC would lead to overestimated values of surface BC concentrations from observations, but unfortunately observing networks do not routinely distinguish between BC and BrC absorption. The regional differences in the model comparison suggest missing emission sources or misattribution of emissions to specific sectors, but this

section shows that the combined changes simulation is a better simulation than the previous control in respect to surface BC concentrations.

Figure 6-8 shows the mean factor of the comparison between the model and ground site observations of surface OC concentrations. The additional combined changes increase the mean factor in the model in all regions. Increases in areas of North America are larger than the increases in European regions. Surface OC concentrations in the combined changes simulation is overestimated in Desert and Coniferous forest regions of North America, although in the latter this is an improvement to the model comparison. Levels of surface OC concentrations are still underestimated by up to 18% in other North America regions. In Europe, surface OC concentration in the model is still under 30% of the concentration measured at observation sites. Adding absorbing OC to the combined changes in the model does not visibly influence the comparison of the model and observations of surface OC concentrations, despite the increased sensitivity shown to changes in mass by changing OC absorption. Overall, the comparison of surface OC concentration observations to the model shows a small improvement.
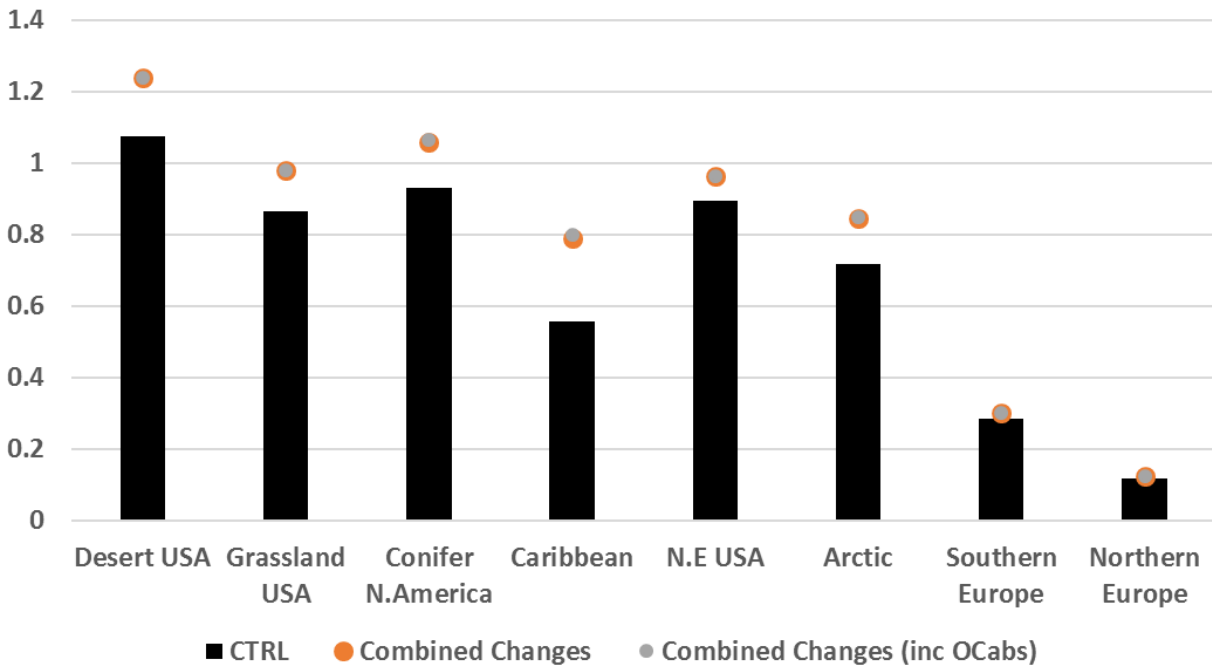
Figure 6-8 – Mean factor between modelled surface OC concentration and in-situ ground-based observations of surface OC concentration from IMPROVE and EMEP sites

6.2.2.4 BC and OC burden

Figure 6-9 shows the changes in BC burden between the combined sensitivity simulations and control simulation. The increase in BC burden is of the same magnitude as the change to surface BC concentration. This suggests that overall, there is little change to the proportional vertical distribution of BC in the model. Larger proportional increases in biomass burning emissions explain why these source regions show larger increases in BC burden than other regions. The cumulative effects of reduced dry deposition from reduced OC density and increased absorption increase lifetime in remote regions, leading to larger increases. The lessening of the impact of the combined changes on BC burden that occurs when the changes are applied simultaneously compared to individually in the model suggests that some of the changes make a similar adjustment to BC burden, and that the effect of these changes are limited. This would also explain why there is no global change in the BC burden when OC absorption is added to the combined changes simulation. However, the minor regional changes seen mimic those seen when OC absorption is increased in the control simulation, seen in Figure 4-13.

Figure 6-10 shows the percentage change in the OC burden in the altered model compared to the control. When the combined changes are included in the model, the OC burden is increased by 110%, nearly double the change seen when changes are applied individually. The largest regional changes occur in over the boreal forests of Canada, where OC burden is increased by up to 1000%. Further increases of up to 350% can be seen across most of the Arctic and Antarctic regions, with increases in the OC burden of up to 250% seen in other biomass burning source regions when the combined changes are applied to the model. When absorbing OC is also added with the combined changes to the model, the OC burden is increased globally by 112%, suggesting that the effect of OC absorption on OC burden is doubled in the combined changes simulation. The spatial pattern when OC absorption is added is almost identical to the initial combined changes simulation, though small increases can be seen in biomass burning plume regions.

Increases in OC burden of over 400% in Boreal Canada confirms that the OC lifetime is increased in this area, as OC emissions in pure biomass burning areas are only increased by

400% (doubled biomass burning and doubled POM:OC ratio). There are few other sources of OC emissions around the area, which partially explains why this area shows such a large increase in BC burden compared to other biomass burning areas. Previously, increases in lifetime were due to decreases in dry deposition (section 3.4.4), but the dry deposition rate of both BC and OC in the region is actually increased by a percentage greater than the burden change.

Figure 6-9 - Global distribution of percentage changes in BC burden between control simulation and combined changes simulations for the period 2006-2008

Figure 6-10 - Global distribution of percentage changes in OC burden between control simulation and combined changes simulations for the period 2006-2008

The cause for increased lifetime in boreal Canada is that the OC in the Aitken Insoluble bin is also increased. Figure 6-11 shows the global distribution of OC within the Aitken insoluble mode of GLOMAP-mode. The Aitken Insoluble OC increases in the combined changes simulation by up to 1000% over Northern Canada, significantly higher than the 400% increase in emissions. Aitken insoluble is where all primary OC is initially placed in the model after emission, and suggests that the increase in CA burdens are due to the model limiting the aging

of CA into a soluble state. Reduction in soluble CA means that wet deposition would be delayed, and so increases the lifetime. Why has Aitken insoluble mass increased? The production of soluble aerosols is unchanged in these simulations, so the increase of primary insoluble aerosols means that not all can become coated in enough soluble material to become soluble. This requires future work to fully confirm, but reiterates the conclusion that CA are sensitive to other aerosols in an internally-mixed aerosol model.

Figure 6-11- Global distribution of percentage changes to OC within the Aitken Insoluble mode between the control and combined changes simulation, averaged over 3 years.

6.2.2.5 SSA and Angstrom Exponent

Figure 6-12 shows the changes in SSA when changes are applied to the model compared with the control simulation. When the initial set of combined changes are applied, the SSA is decreased by 0.008 globally. However, regionally, the sign of change differs. In India and East Asia, the SSA is decreased by up to 0.04 when the combined changes are applied, whilst in Southern Africa, an increase in SSA of up to 0.04 in the model is observed. Further decreases of up to 0.025 occur over large urban areas, and increase of up to 0.01 occur in biomass

burning regions. When absorbing OC is also added to the list of changes, there is a global reduction in SSA by 0.021, with SSA reduced in all regions. In South America, Southern Africa and India, the SSA is reduced by over 0.06, whilst reductions of up to 0.03 occur in urbanised areas.

The increase of SSA with the combined changes over biomass burning regions can be explained through a combination of changes in OC and BC emissions. The effect of OC is quadrupled because of the doubling of both the emissions and POM:OC ratio, whereas BC absorption is only doubled with emissions. As there are few other emission sources nearby, especially in Africa, the effect of CA emission changes leads to an increase in SSA. In fossil fuel burning areas, where BC is increased by 1.7 and OC is not increased, the change in SSA is negative. Areas of higher fossil/biofuel burning emissions show larger decreases in SSA. The addition of absorbing OC dominates changes to SSA when applied. Areas of biomass burning, where OC is effectively quadrupled, see significantly higher decreases to SSA than fossil fuel burning areas because of the extra OC.

Figure 6-13 shows the correlation and normalised standard deviation of SSA in the model compared to AERONET retrievals of SSA. When the combined changes are applied to the model, the normalised standard deviation is decreased in biomass burning regions such as South America and Africa, but increased in fossil fuel burning regions such as North America, Europe and Asia. Correlation is decreased in Africa, reducing from 0.91 to 0.56, although the correlation is still significant at 99.9% confidence level. When absorbing OC is added to the combined changes in the model, the normalised standard deviation is increased in all regions except Africa, where it returns to the same level as the control. The correlation between model and retrievals is reduced in South America, but increased slightly in Europe with the absorbing OC.

The effect of the combined changes generally worsens the comparison of modelled SSA with AERONET in biomass burning regions, as the perturbed model vastly underestimates the AERONET variability. However, the increase in normalised standard deviation in fossil fuel regions is beneficial to the model in Europe and North America, as the variability in the model better matches AERONET. Increasing OC absorption brings the model variability nearer to that

of observations in all regions except Asia, suggesting that absorbing OC may be necessary to correctly model SSA variability in biomass burning regions.
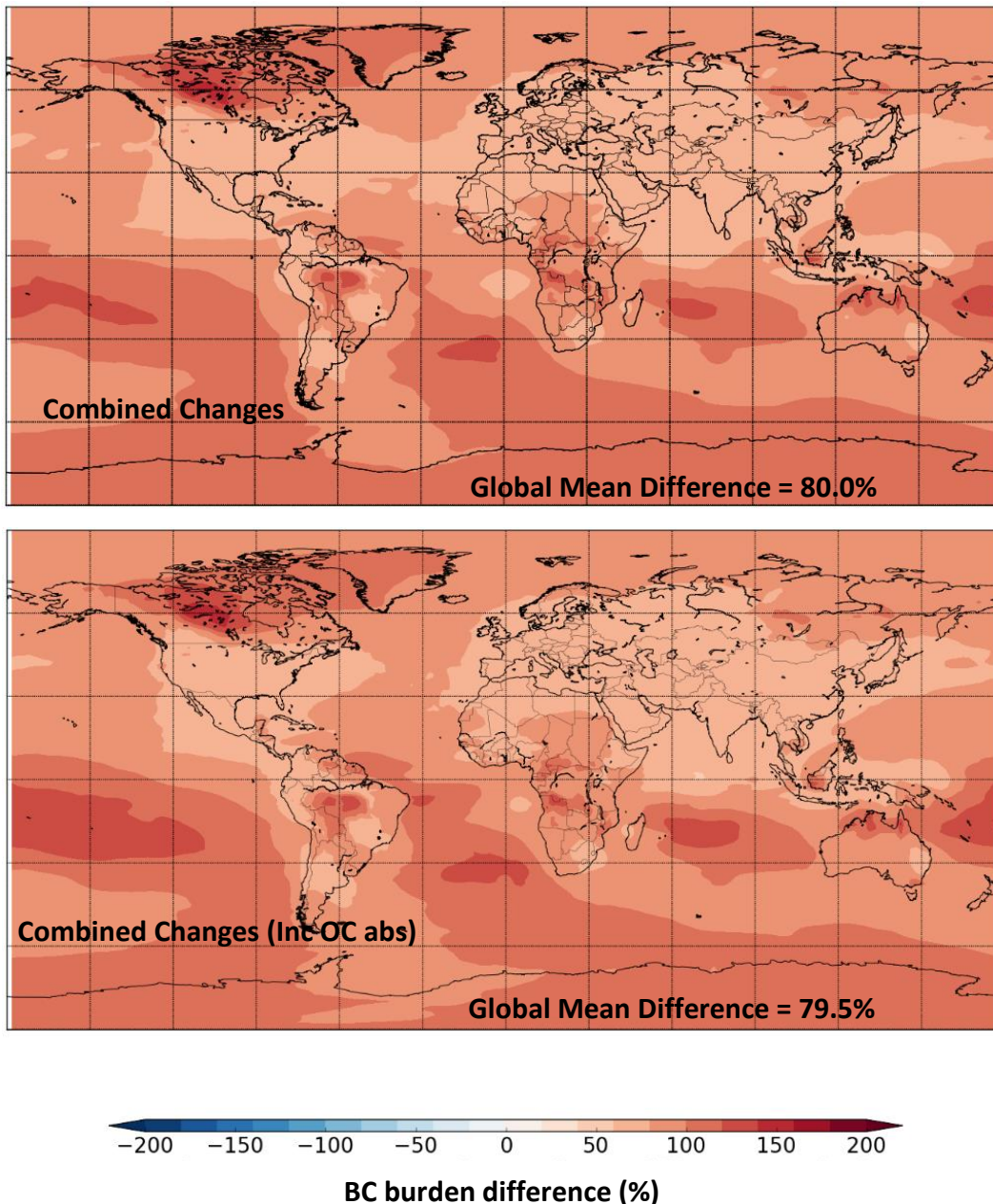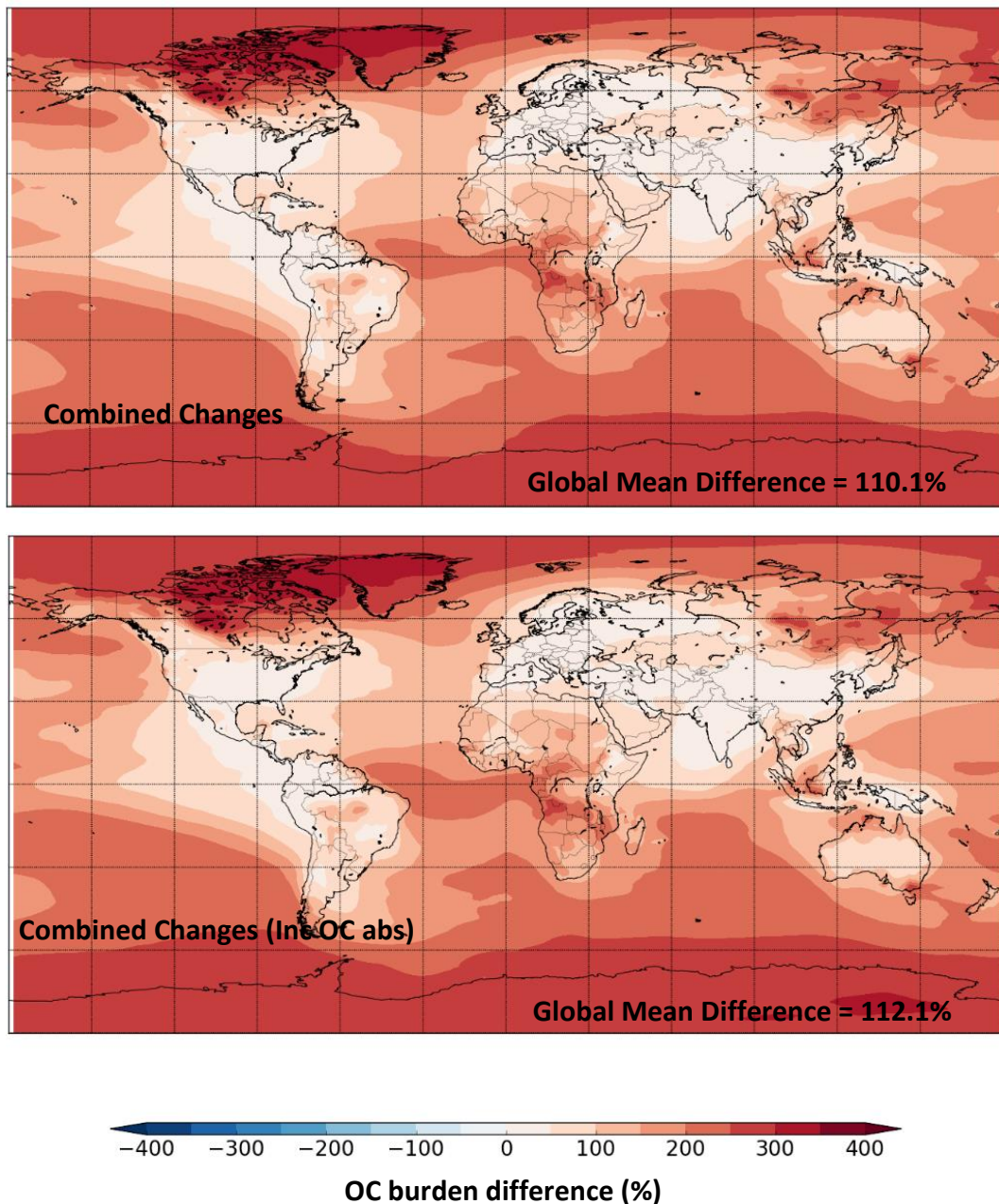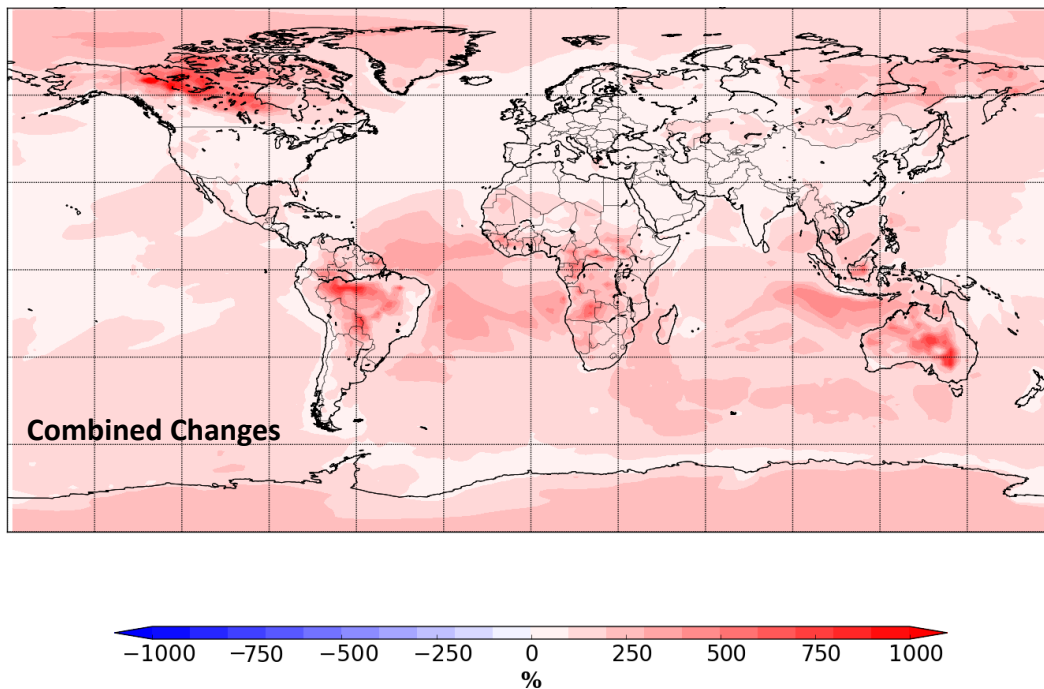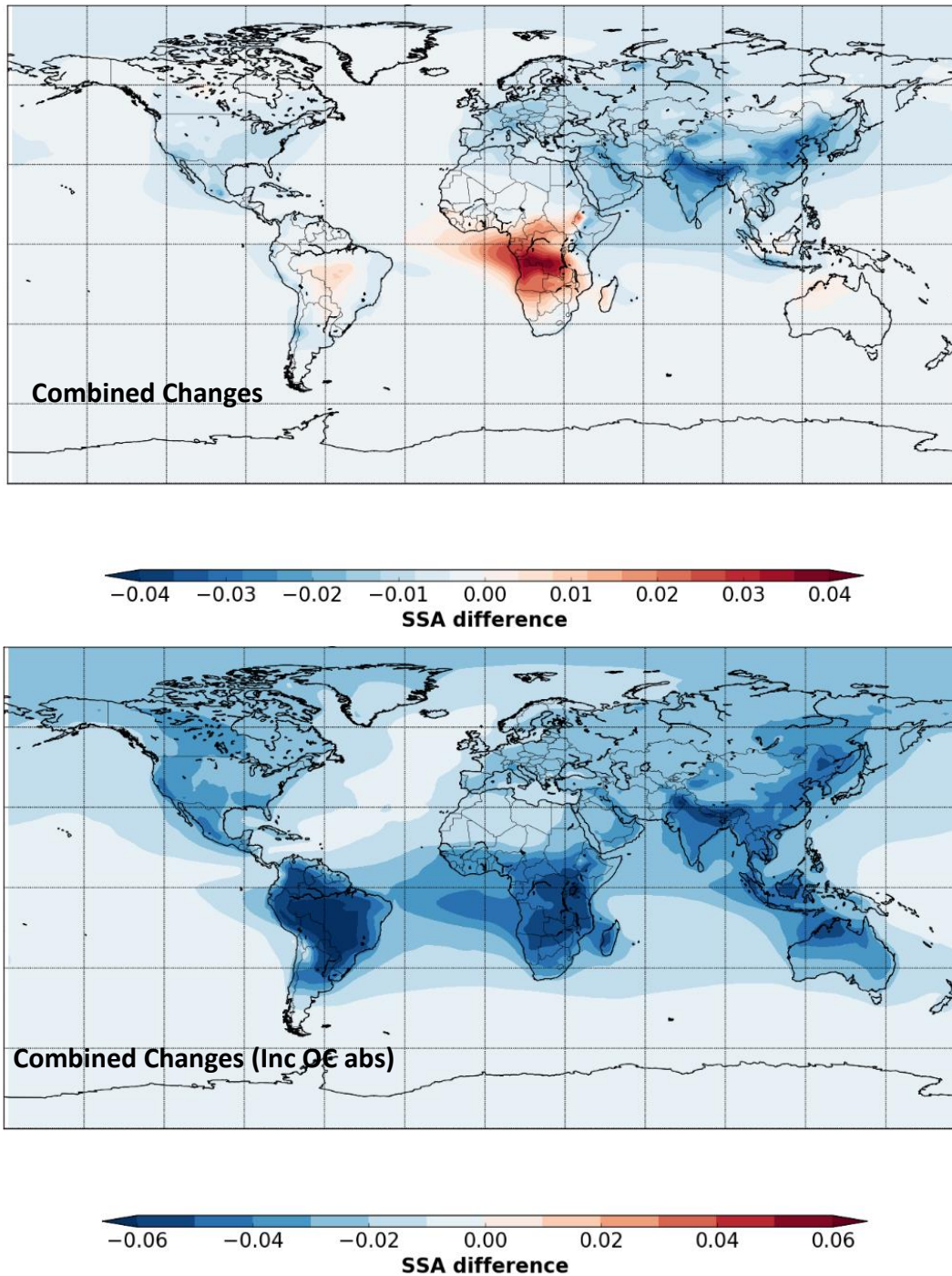

Figure 6-12 - Global distribution of percentage changes in single scattering albedo between control simulation and combined changes simulations for the period 2006-2008

Figure 6-14 shows the SSA as a function of AE across 3 regions for AERONET and modelled values. When the initial combined changes are applied to the model, there is a slight increase in SSA in the model in South East Asia. In South America, the model no longer calculates low SSAs with the same frequency, although these is no similar decreases in high SSAs. There is no significant change in AE in any region. In all regions, the model either improves or remains constant in its comparison to AERONET in these regions when the combined changes are applied.
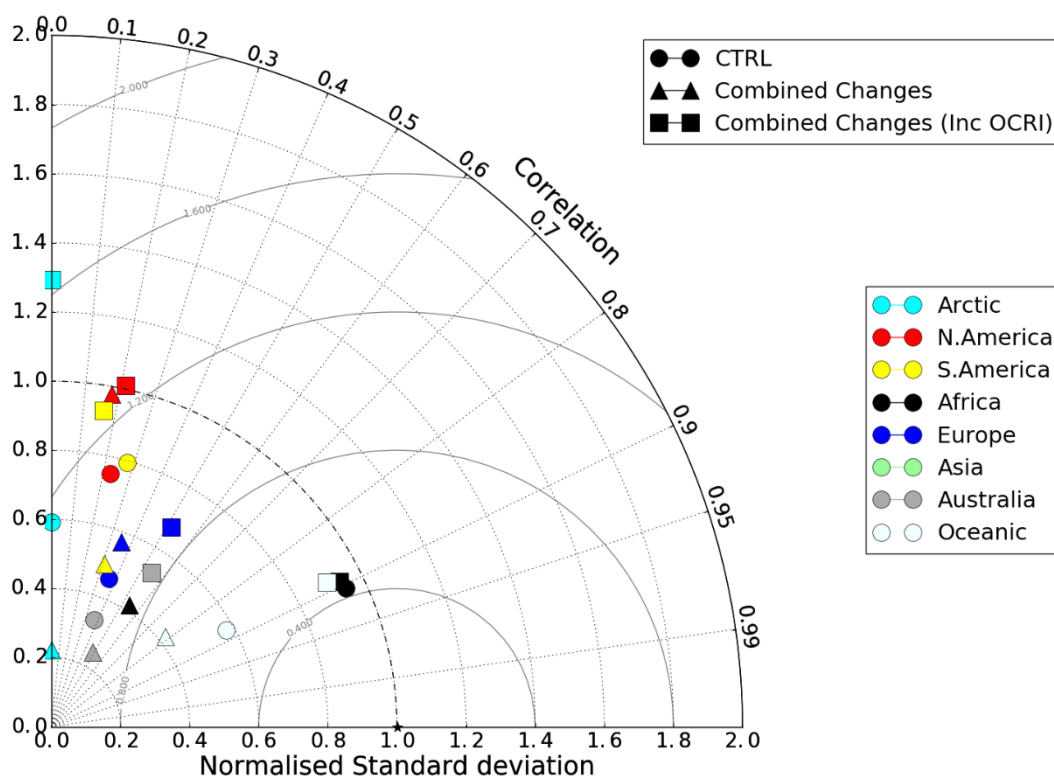
Figure 6-13 - Taylor Diagram of SSA showing normalised standard deviation and correlation between modelled and AERONET observed SSA at 550 nm. Not shown is Asia due to large values of normalised standard deviation.

When OC absorbing is added to the list of changes, the frequency of lower SSAs are increased and the frequency of high SSAs are reduced in all regions. In South America, the area the contour encircles when OC absorbing is added to the list of changes is only sampled by AERONET 8% of the time, compared to the contours for the control simulation and initial combined changes model simulations which encompass 93% and 84% of the AERONET retrievals.
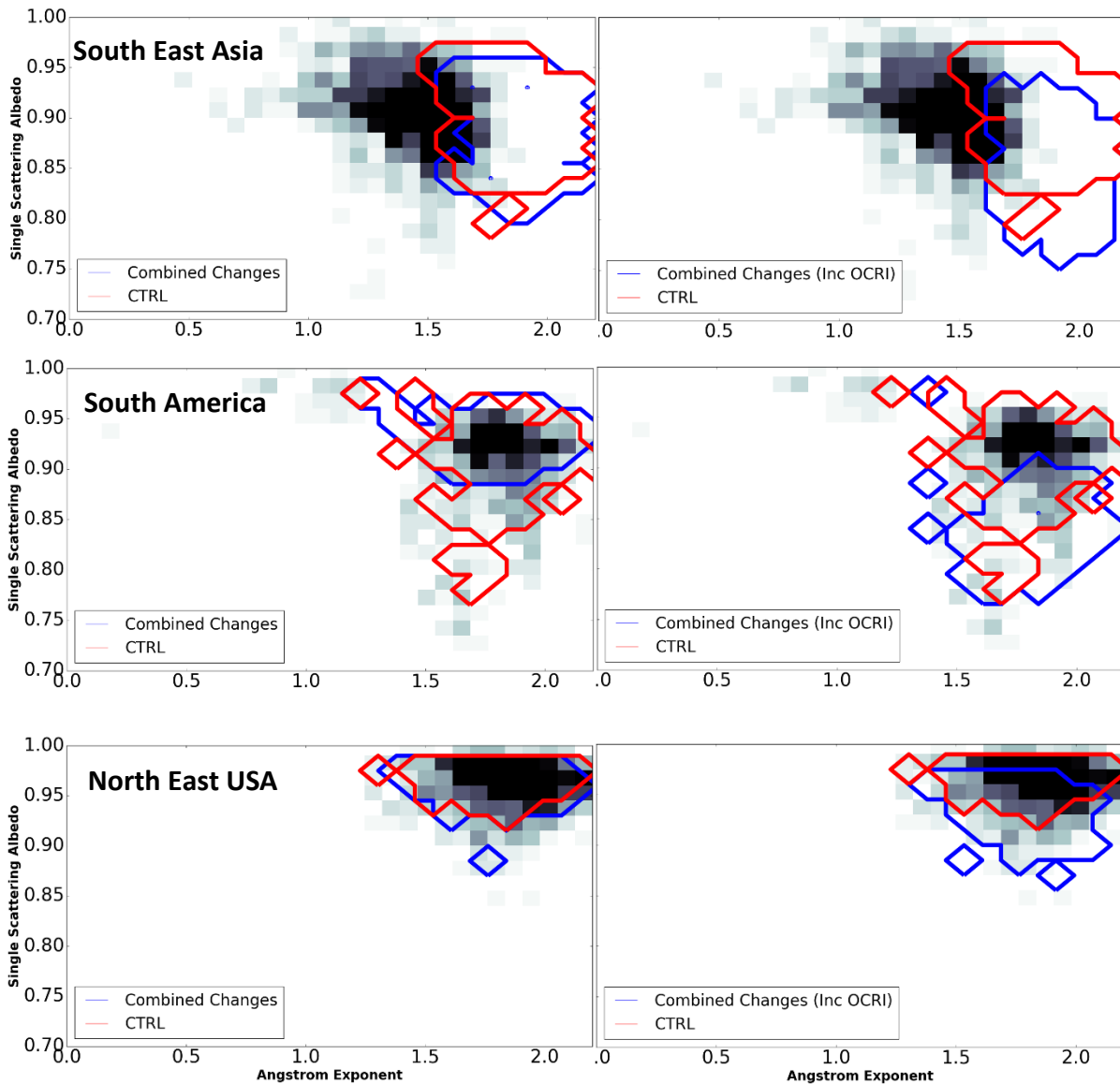
Figure 6-14 – Frequency plot of Single scattering albedo as a function of Angstrom exponent for AERONET retrievals (black density boxes) and model values.

The combined changes without OC absorbing show little change in the ability of the model to replicate AERONET SSA and AE patterns, although it does reduce the frequency of low SSAs seen in both AERONET and the control. Figure 6-13 showed that the change in normalised standard deviation does decrease the model ability, but that correlation is not compromised. This suggest that the combined changes model slightly underestimates absorption in South America during high AOD events. This suggests the brown carbon is necessary to improve the

model in this region, but the decrease in SSA from absorbing OC is too large. We therefore must conclude that a less absorbing OC may be required in biomass burning areas to avoid creating an SSA that is too low. The absorbing OC also overestimates low SSAs in South East Asia, where aerosols CA comes from a mixture of sources, and in North East USA, where CA aerosols come from fossil fuel burning. In these regions, OC should be less absorbing than the modelled value used, and so a correct regional implementation of absorbing OC would improve the comparison.

6.2.3 Conclusions on combined changes simulation

Throughout this section, we have considered two sets of changes to the model, and evaluated both alongside the original model. The initial set of combined changes, which does not include absorbing OC, either improves the comparison of observations and model compared to the control simulation, or has little effect. With the combined changes including an absorbing OC, comparisons to observations are worse, specifically comparisons in SSA and AAOD. This does not disprove the existence of BrC, or support the need for our absorbing OC change. But it shows that the model is currently set up to compensate for a lack of absorbing OC. This could be for several reasons, such as total carbonaceous absorption being used in previous work to constrain BC emissions, mass or refractive index. We showed in Chapter 3 that a high BC RI is necessary to simulate AAOD and SSA well in Europe and North America, but we also note that the model does not represent the different BC refractive indices that characterises biomass burning regions. In the next section, we compare only the combined changes simulation to the control simulation, as we have shown that this is an improvement on the control, whereas the simulation with absorbing OC is not. Despite this, there are some regions where the model does not improve all the comparison with all variables, and there are some areas of concern with the new setup we are proposing.

We show that the variability of both AAOD and SSA in biomass burning regions suffer slightly because of these changes, with AAOD becoming too variable and SSA not variable enough in the model. The introduction of an absorbing OC in these regions increases both variability, further worsening the AAOD comparison. The SSA in South America is also well constrained, and adding an absorbing OC worsens this. However, we show that the mean factor of AAOD in biomass burning regions is still slightly underestimated by around 20% with the new changes. This would allow for an increase in AAOD, assuming that the bias caused through

the AERONET sampling is less, but more work is clearly required to ensure that both SSA and AAOD compare well with AERONET if OC is to be made absorbing in the model in the future.

Our work also shows the sensitivity of the model to changes depends on the initial model setup. Comparing simulations where absorbing OC is the only change and where absorbing OC is added to the combined changes shows that the change in AAOD and SSA can differ globally by a factor of 2. Considering the diversity in how aerosols are characterised amongst different climate models, this result suggests that changes which improve one model may significantly worsen another.

Our work also highlights the effect of aerosol interactions within an internal mixture. The magnification of effects when combined simultaneously in the model, especially those relating to lifetime of aerosols, show that changes relating to one aerosol species are likely to change others. We show that the effect of changing the density of OC amplifies the effect of increasing BC emissions. Changes in emissions can also lead to large changes in regional lifetimes, especially when the increase in primary insoluble aerosols affects the aging processes. We cannot know for sure whether the response to doubling emissions in the real world would involve the same limiting factor. Further work should analyse those processes, as they could lead to non-linearity when increasing emissions for radiative forcing and future climate work.

Having shown that our combined changes improve the simulation of CA and optical variables, we now focus on how these changes affect aerosol radiative forcing.

6.3 Effect on Radiation and Effective Radiative Forcing

The effects of CA on radiation are explained in detail in Chapter 1. In this section, we look at the effect that the changes we have made to the model have had upon the radiative fluxes at the top of the atmosphere, and assess and quantify the sensitivity of the outgoing radiation to the range of parameters tested. We also look at the radiative effect of the combined changes simulation in comparison to the control simulation. We finally look at the effect that this new model simulation will have upon the current radiative forcing of aerosols by comparing both the control and combined changes simulation to pre-industrial simulations,

and discuss whether these changes have any impact on how CA could affect climate change in the future.

The results are based on the 3-year simulations from 2006-2008. We define the effective radiative forcing (ERF) as the difference between the top of atmosphere outgoing longwave and shortwave radiation between simulations with present day aerosol emissions and pre-industrial aerosol emissions. We further define the radiative effect as the same difference in top of atmosphere radiative fluxes, but between two present day simulations. For pre-industrial simulations, we use the CMIP5 standard emissions of sulphur dioxide, fossil fuel and biomass burning carbonaceous aerosol for the year 1850 (Lamarque et al., 2010; Taylor et al., 2012). Every other atmospheric component is kept the same, to guarantee that the radiative forcing is due to anthropogenic aerosols only. Low level horizontal winds are nudged to the same 2006-2008 ERA-interim reanalysis as the control simulation in order to reduce noise from dynamic differences. Figure 6-15 shows the all-sky ERF for the control simulation. The global ERF from the model is -2.43 W m^{-2}. Large local negative ERFs exist over Eastern Asia and off the coast of North and South America which exceed -10 W m^{-2}, showing an increase in outgoing radiation due to industrial era aerosols. Further negative ERFs of note occur over the Indian Ocean, Europe, North America and off the Western Coast of Africa. In India, and across deserted areas, the local ERF is positive.

The global mean value of -2.43 W m^{-2} is significantly higher than the IPCC expert judgement of aerosol ERF, which is given as -1.9 to -0.1 W m^{-2} (Myhre et al., 2013). This is a known problem with this version of HadGEM3-UKCA, and has been rectified for the UKESM1 model, as discussed in the conclusion. Areas of large negative forcing occur over both areas which have seen large increases in urbanisation and development, and areas of low marine stratocumulus clouds. In the former case, the increase in sulphates, which scatter incoming radiation, produced from large cities and industries have led to a negative forcing. Similarly, industries that did exist across Europe and America produced a much higher proportion of BC in 1850. This also leads to a negative forcing. In areas of low marine stratocumulus cloud, the increase in aerosols in the present day leads to brighter clouds, which have a higher albedo, creating a negative forcing. Over desert areas, where the surface albedo is already high, the increase in present day aerosols, particularly absorbing aerosols, reduces the planetary albedo, and leads to a positive ERF.

In the next section, we consider the radiative effect of the sensitivity studies used in Chapters 3, 4, and 5 compared to the control simulation.

Mean = -2.43 Wm^{-2}
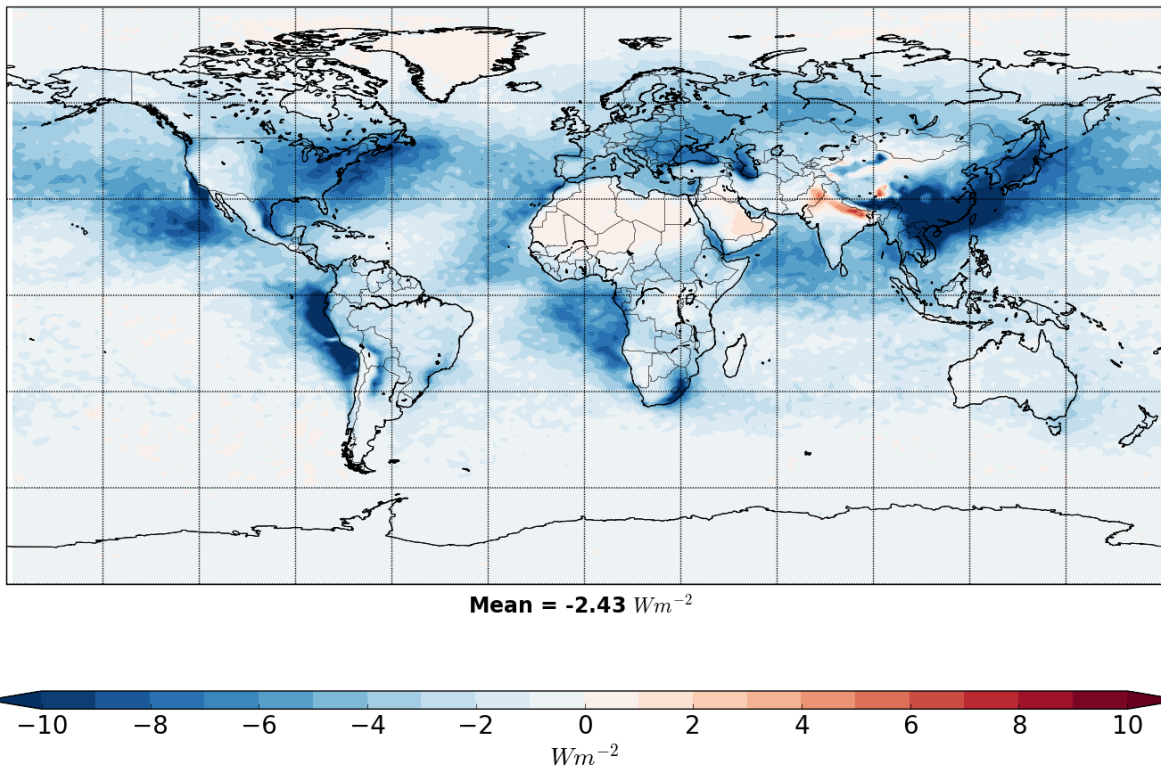
Figure 6-15 – Distribution of changes to the all-sky shortwave and longwave outgoing radiation at the top of atmosphere between present day control simulation and pre-industrial control simulation. Positive values indicate a warming effect in the combined changes simulation.

6.3.1 Clear sky effects of changes

Figure 6-16 shows the change in outgoing radiation at the top of the atmosphere in clear sky conditions. The largest changes occur when the refractive indices of BC and OC are altered, with an increase in radiative effect of 0.17 W m^{-2} when OC is made absorbing, and a reduction of 0.15 W m^{-2} when BC refractive index is lowered. Increasing emissions of CA and BC from fossil fuel and biofuel burning emissions also leads to increases in energy in the atmosphere of 0.10 and 0.15 W m^{-2}. However, increasing biomass burning emissions leads to a small negative forcing, whereas increasing only BC biomass burning leads to a small positive forcing. The largest regional effects on radiation occur mostly over Southern Asia and Africa, depending on the changes made.

The variability of changes to the radiative effects of CA parameters shown in Figure 6-16 explains why estimates of radiative forcing for BC and OC are so uncertain. Different combinations of the perturbations added linearly can lead anywhere from a negative direct forcing of −0.3 W m^{-2} to a positive direct forcing of +0.38 W m^{-2}, showing how sensitive ERF is to the representation of aerosols. The lack of observational constraints on CA makes it difficult to reduce this uncertainty. Considering the radiative forcing of BC in the IPCC report is +0.6 W m^{-2}, the level of uncertainty which exists within models explains why uncertainty ranges associated with the radiative forcing are so high. Areas of high CA aerosol loading, such as India and Southern Africa, correlate with areas which show the largest regional change in the direct radiative effects. Areas over surface with high albedos, such as desert areas, also show higher sensitivity to the modelled changes in CA, despite there being relatively less CA in these regions. This is due to the enhanced direct effect of aerosol over bright surface which reflect more shortwave radiation than darker surfaces. Therefore, a reduction in the initial downward shortwave radiation due to aerosol is enhanced.

6.3.2 Total Radiative Effects of Changes

In this section, we discuss the effect of each perturbed simulation on the total forcing, which includes the effects of aerosol-cloud interactions and other secondary effects.

Figure 6-17 shows the distribution of differences in combined longwave and shortwave radiative effect, averaged over 3 years. The largest global change in outgoing radiation is caused by doubling BC biomass burning emissions, which has a positive forcing of +0.28 W m^{-2}. The largest local increases in this comparison occur over India, Southern Asia and Northern Africa. This spatial pattern of positive forcing is similar replicated when fossil and biofuel burning emissions are increased as well. Reducing BC refractive indices shows the same spatial pattern, but the sign of the forcing is the opposite. Altering both BC and OC density leads to the largest global negative forcing of −0.27 W m^{-2}. However, the largest regional negative forcing is seen off the coast of Southern Africa and South America. The magnitude of the largest regional changes (up to −3 W m^{-2}) are smaller than the largest local changes seen when the BC refractive index is reduced (over 4 W m^{-2}), despite a lower global average.
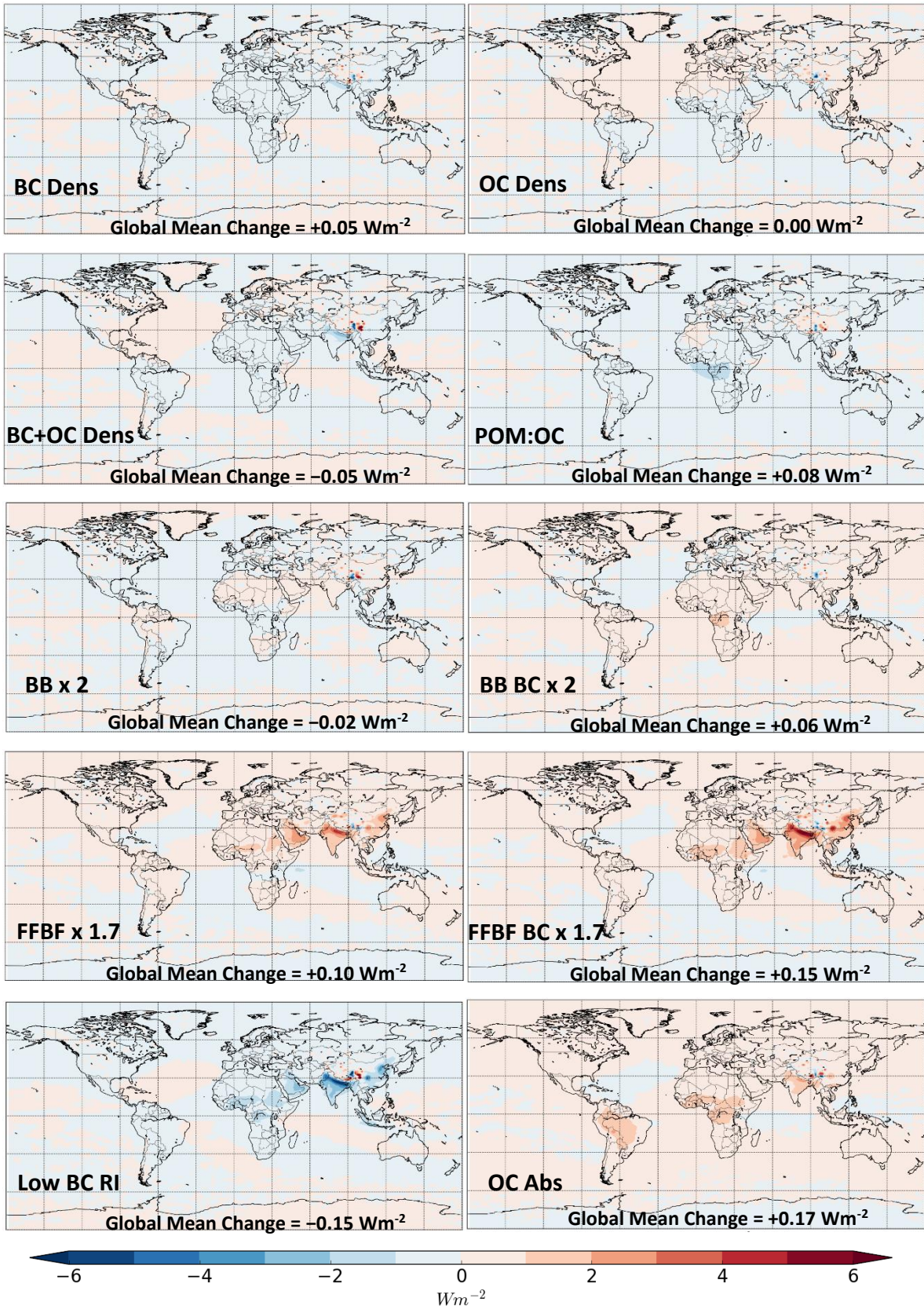
Figure 6-16 – Global distribution of changes in clear-sky shortwave and longwave radiation at the top of the atmosphere between control simulation and individual changes simulations

Different combinations of the perturbations suggest that combined, the radiative effect could be as high as +0.53 W m^{-2}, or as low as −0.63 W m^{-2}, although we have already shown that changes in the model are not necessarily linear. These changes are roughly the same as the value of the radiative forcing of BC, as specified by the IPCC report and shown in Figure 1-4. As we have taken extreme values for some of the sensitivity studies, we acknowledge that these combinations are likely overestimations to the uncertainty of the radiative effects of CA in climate models. However, they again show that differences in choices made when creating a climate model can have a large impact on the effects of CA on radiation, and so will have a large effect on any future or past predictions of radiative forcing.

The effects can be split into two distinct categories. The plots from individual perturbations to biomass burning emissions, fossil fuel emissions and BC refractive index show the same spatial pattern and similar magnitudes of change for both the all-sky and clear-sky radiative changes. This pattern suggests that the effects on radiation in these simulations are dominated by aerosol-radiation interactions. Aerosol-radiation interactions characterise the AOD and AAOD. Comparisons of the three sensitivity studies shows similar spatial patterns between the AOD/AAOD difference and the radiative effect. However, changes to OC density, POM:OC ratio and absorption of OC show a different spatial pattern, and, in the case of density changes, significantly larger negative forcing in the model. The location of the strongest changes coincide with areas which are consistently covered by layers of marine stratocumulus cloud, and are known areas of biomass burning CA transport (Johnson et al., 2004).
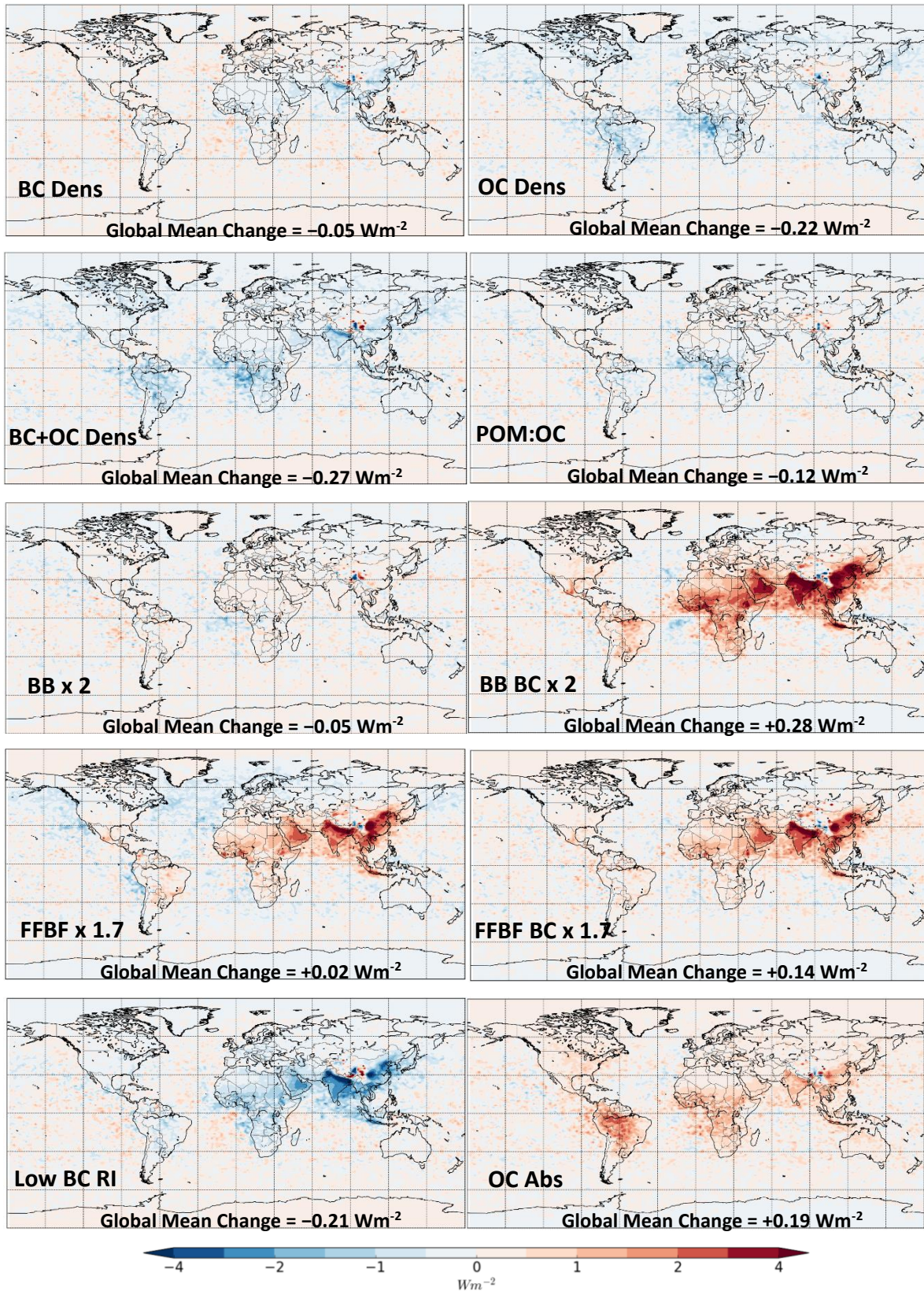
Figure 6-17 – Global distribution of changes in combined all-sky outgoing longwave and shortwave radiation between control simulation and individual changes simulations

Previous studies of climate models, including HadGEM3, have shown that the radiative effect of this type of cloud is very sensitive to changes in aerosol mass and aerosol properties (Mahajan et al., 2013; Stier et al., 2013). In our perturbed simulations, increased aerosol number can both increase the likelihood of clouds forming and greatly increase their brightness.

Figure 6-18 shows the change in outgoing longwave and shortwave radiation at the top of the atmosphere between the combined changes simulation and control simulation. The global radiative effect of the changes is -0.44 W m^{-2}. This is numerically greater than the combined radiative forcing of BC and OC since pre-industrial times. A positive forcing of up to 3 W m^{-2} occurs in India and Eastern Asia, with a smaller positive forcing in desert areas of Asia and Africa. The largest negative forcing occurs off the Western coast of Africa, with a regional forcing of -4 W m^{-2}. Further negative forcing of -1.5 W m^{-2} occur over coastal regions of Europe, North and South America and Asia.
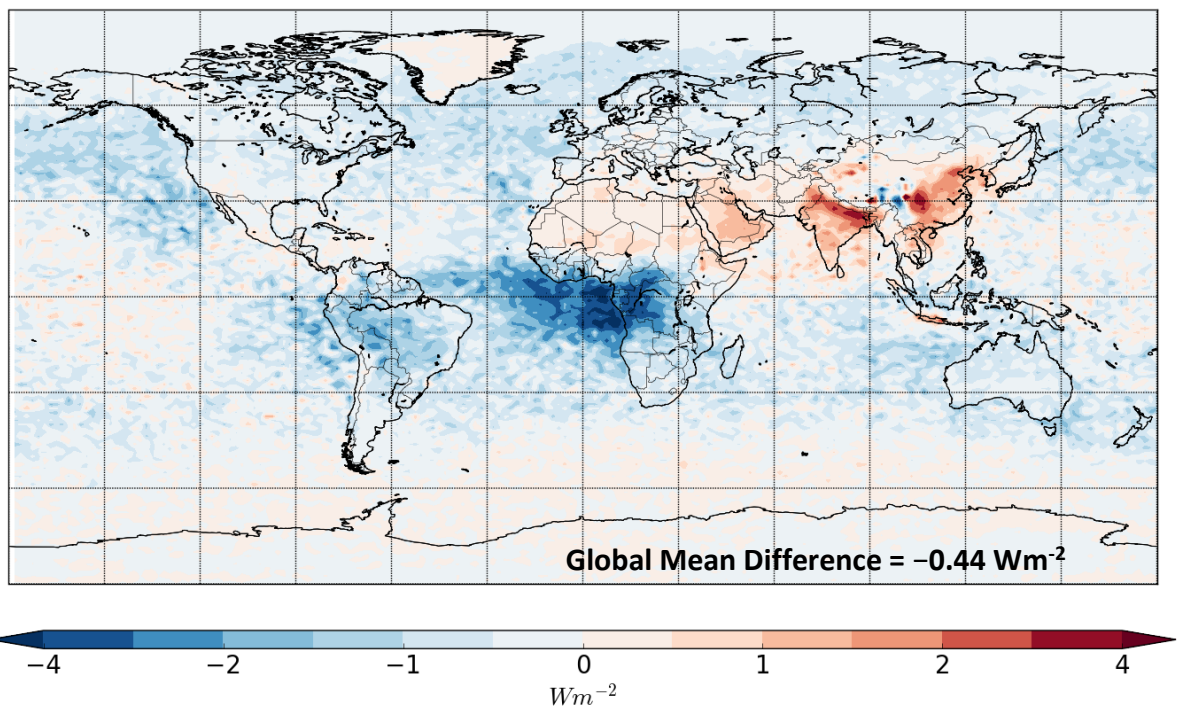
Figure 6-18 – Distribution of top of atmosphere changes in outgoing shortwave and longwave radiation between the combined changes and control simulations. Positive values indicate a warming effect in the combined changes simulation.

The comparison of radiation changes between the combined changes simulation and control shows a good likeness to the individual component changes. Increased positive forcing over Southern Asia and Desert areas are caused by the increased radiation interactions of absorbing aerosols over high albedo surfaces. The negative forcing over coastal regions is due to the aerosol cloud interactions from decreased OC density and extra aerosols in biomass burning regions.

These sensitivity studies give a good indication as to why there is so much inter-model variability in regards to the radiative effects of CA. We have suggested that the aerosol-cloud interaction effects are significant, and that the outgoing radiation is as sensitive to these effects as it is to the aerosol-radiation interactions when aerosol properties and mass are changed. We note from the previous section that merging changes simultaneously in the model does not necessarily give the same effect as linearly adding the individual effects. To determine this effect, we simulate a pre-industrial simulation with the combined changes setup.

6.3.3 Effect of Combined Changes on Aerosol Radiative Forcing

Figure 6-19 shows the ERF of aerosols between the pre-industrial and present day for both the original control simulation and the new set of combined changes used in the previous model. The ERF in the initial control simulation is described in Chapter 6.3.1. The simulation with the combined changes has an ERF of -2.4 W m^{-2}. This is not a significant change compared to the control simulation, as the inter-annual range for the 3 years is -0.12 W m^{-2} due to a mixture of reasons, such as internal variability, yearly differences in emissions and dynamics, and potential changes in dust and sea salt, which are emitted dynamically. On a regional scale, statistically significant differences between the two simulations do exist. The combined changes illicit a larger positive forcing in both India and the Middle East. This is balanced by an increased negative forcing over the North East of North America.

The increase in the magnitude in the regional forcing from the combined changes comparison compared to the original control comparison suggests that the ERF is more sensitive to changes in CA in this new configuration of the model. The enhanced changes in AOD and AAOD in the combined changes simulation described in the previous section also suggest the same conclusion. There is little sign of the increases of up to 3 W m^{-2} that occur over cloudy

areas in Africa and South America in the present-day difference between the two simulations shown in Figure 6-18. This suggests that the pre-industrial has a similar sensitivity to the changes in the model as the present day, despite having a much smaller loading of aerosol.

Figure 6-19 – All sky effective radiative forcing of aerosols between present day and pre-industrial, averaged over 3 years. Positive values reflect a positive forcing in present day.

Carslaw et al., (2013) shows that the sensitivity of the clean pre-industrial atmosphere to changes in aerosols is much higher than the sensitivity to changes in the present day. Increased CCN leads to lower sensitivity in albedo at higher cloud droplet concentrations which in turn means that the sensitivity of cloud albedo, and therefore forcing, is reduced as

emissions are increased. The range of emissions values used in pre-industrial simulations means that cloud albedo is much more sensitive in pre-industrial times than in modern day. Therefore, the increased sensitivity of the clouds compensates for the decreased aerosol amount in the pre-industrial simulation, meaning the forcing does not change significantly on a global scale when we added the combined changes to our model.

Whilst little difference can be seen in the all sky effective radiative forcing, we can examine the clear sky ERF, to determine whether the combined changes affect the ERF of aerosol-radiation interactions. Figure 6-20 shows the distribution of clear sky outgoing shortwave and longwave radiation differences between present day and pre-industrial for the two different model setups. The clear sky ERF of the original control is −0.62 W m^{-2}, which is approximately 25% of the total ERF seen in Figure 6-19. A large negative forcing, greater than 6 W m^{-2}, occurs over Eastern Asia, with a further negative forcing over Europe and North America up to −4 W m^{-2}. A positive forcing of up to 5 W m^{-2} occurs over India, and up to 3 W m^{-2} over the Middle East. With the combined changes, the clear sky ERF is −0.52 W m^{-2}, which is approximately 20% of the total ERF seen in Figure 6-19. The spatial spread of the negative forcing seen over East Asia is reduced, with the magnitude of reduced negative forcing over North America and Europe also reduced. The combined changes invoke a stronger negative forcing of up to −4 W m^{-2} over Western Africa, and increases the magnitude and spatial spread of the positive forcing over India, the Middle East and Saharan Africa compared to the original control setup.

The differences between the clear sky ERF with the control setup compared to the combined changes setup can be attributed to the individual changes seen in Figure 6-16. The increase in positive forcing over India and desert regions was seen when fossil fuel and biofuel emissions were increased in the model, as the increase in absorbing aerosol over high albedo surfaces magnifies the positive forcing so that it is clearly seen. Similarly, the decreases in the negative forcing over North America and Eastern Asia can both be attributed to the increase in absorbing aerosols with increased emissions of BC. The increase in the negative forcing off the coast of West Africa shows a similar spatial pattern to that seen when the POM:OC ratio is increased in the original control simulation, where scattering aerosol is increased.
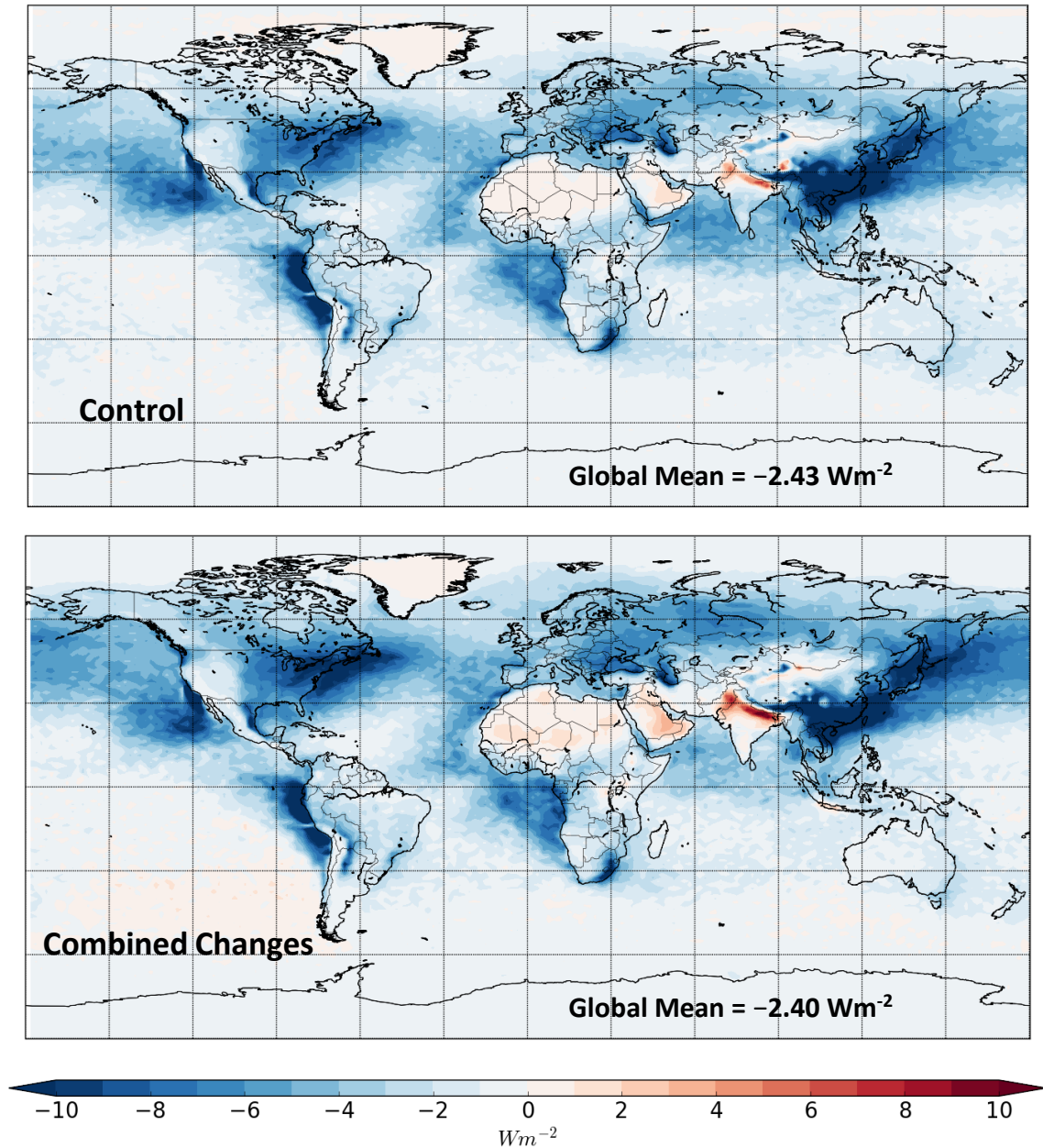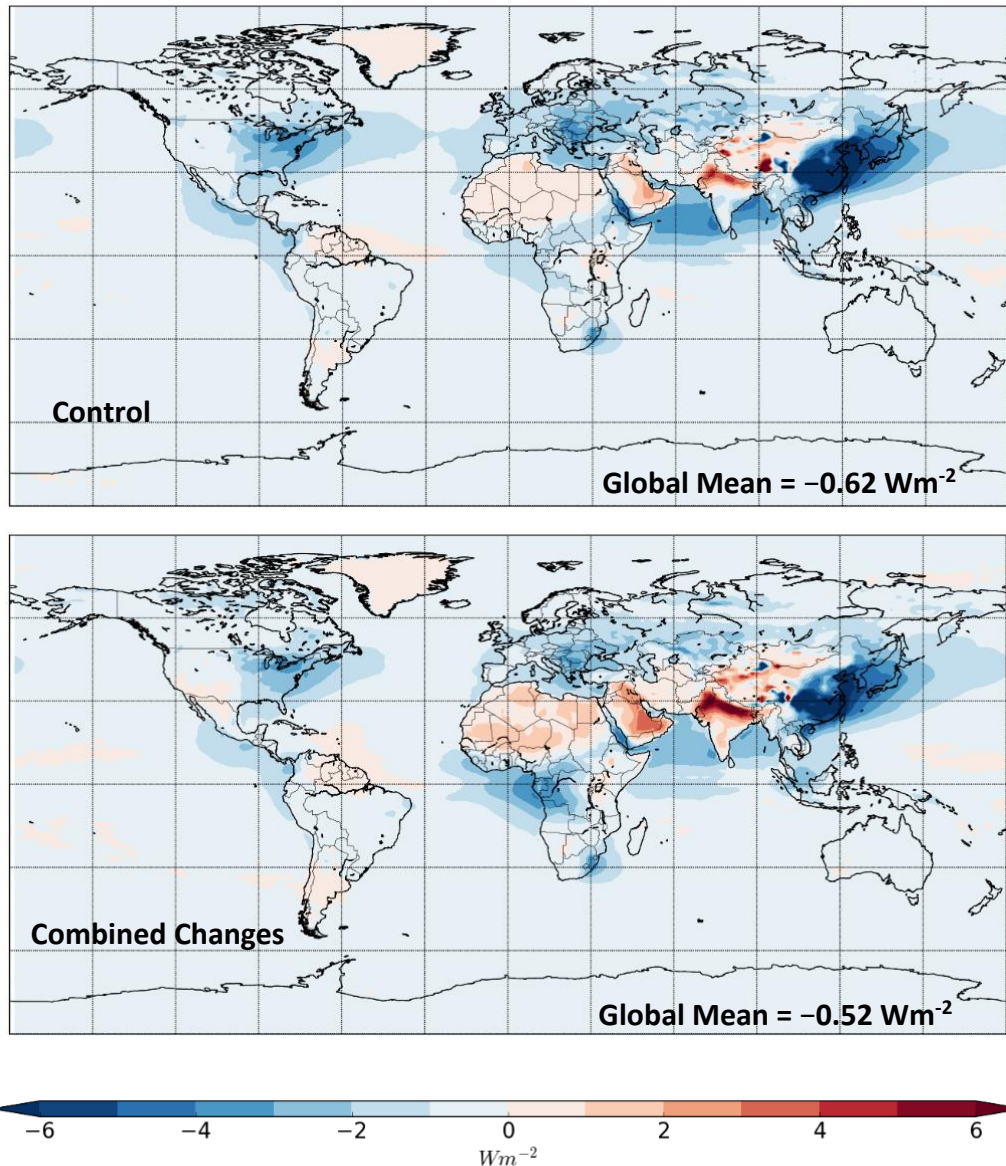
Figure 6-20 – Clear sky effective radiative forcing of aerosols between present day and pre-industrial, averaged over 3 years. Positive values reflect a positive forcing in present day.

The decrease in the negative forcing seen from the clear sky ERF suggests that the direct radiative effect of aerosols in the combined changes simulation is less negative than the previous version. However, it therefore suggests that the aerosol cloud interactions, which are already high in HadGEM3, are responsible for a larger fraction of the ERF than the previous control simulation. The changes of −0.52 W m^{-2} is similar to the direct forcing found by Bellouin et al. (2013), who found a radiative forcing of aerosol-radiation interactions in an earlier version of HadGEM with the GLOMAP modal scheme of −0.49 W m^{-2}. The authors note that GLOMAP had a lower first aerosol indirect effect radiative forcing than the previous

CLASSIC scheme. We note that the values considered in this report appears to be far larger, and are backed up by further analysis in Mulcahy et al. (2016) on this model. The values of aerosol-cloud radiation effects from the model exceed the recommended values in the IPCC report, and in this instance, lead to a net negative radiative forcing of all atmospheric constituents, suggesting that the world is cooling between 1850 and 2008. As we know this is not true, future changes should assess the sensitivity of clouds to determine whether this value is justifiable.

6.4 Summary and Conclusions

In this chapter, we devise two new simulations based around the sensitivity studies analysed in chapter 4, 5 and 6. Both simulations included altered CA densities, increased emissions and an increased biomass burning POM:OC ratio. In one of the two, the OC was made absorbing with a realistic biomass burning value that would encompass both brown carbon and non-absorbing organic carbon. Through comparison with mass observations and optical retrievals, we conclude that the altered simulation without absorbing OC was an improvement compared to the original control simulation. Whilst scientifically, an absorbing OC should exist within the model, the model worsens when it is included. This is an issue for future model development, and shows that further work needs to be done to correctly attribute absorption to both BC and BrC, and determine emissions for both. In the course of this work, we have assumed that BrC counts towards OC mass, whereas it may well be that BrC needs to be counted as a fraction of BC mass.

The improved simulation is, by no account, a perfect simulation. Whilst we have found improvements in comparisons with AERONET, the basis of several of our changes are from literature which uses other models. We show in this chapter than the internal setup of the model can lead to significant differences in how a model reacts to changes. Therefore, basing our changes on values and scaling factors required by other models to get a good observation to model comparison is not necessarily a guarantee of a correct improvement. In this study, we have not refined the parameters to fine tune the agreement between model and observations, although this could be done in the future.

We also study the effect of our new simulation on the radiative forcing. Our findings that the total effective radiative forcing of aerosol is virtually unchanged shows that the effect of changes in the model, where the difference in instantaneous forcing in the two model simulations is −0.44 W m^{-2} (Figure 6-18), can have amplified effects on the radiative changes in a clean atmosphere, as is seen in the pre-industrial. This explanation matches that of Carslaw et al. (2013), where changes in aerosol-cloud radiative effects in a cleaner atmosphere are larger than those in a polluted atmosphere, meaning that the radiative effect between the two model setups was similar in pre-industrial simulations. This has implications for potential studies which look at how changes in aerosols will affect cloud and radiation systems, and whether reducing aerosol emissions are likely to reduce their radiative forcing.

The difference in the setup leads to a difference in how the radiative forcing of aerosol is composed. The clear sky radiative forcing of aerosols is reduced from −0.62 W m^{-2} to −0.52 W m^{-2} with our new configuration. This decreases further if additional absorption from OC is included. This means that the new configuration exerts a larger negative aerosol-cloud radiative effect. HadGEM3-UKCA already simulates an indirect radiative effect of aerosols that is at the top of the range suggested by the IPCC report, and further increases push this outside the range. As discussed in this chapter, due to the overly large negative radiative forcing of aerosol, the effect of the aerosol-cloud interactions and their radiative effects are currently being studied. Given the increased sensitivity of our new simulation to aerosol, it would be of benefit to re-run these changes in any new configuration to determine whether the improvements seen here still hold, or whether the introduction of these changes requires further work to be done on these areas. To that effect, we have contributed to the Met Office Auto-Assess validation suite.

In the next chapter, we discuss the final results from this study, evaluate the understanding gained from this work and highlight areas where further improvement is available for future development of the model.

7   Chapter 7: Conclusion and Discussion

In this chapter, we detail the main conclusions from this work, and discuss what we bring to our current understanding. We also discuss whether the aims of the thesis, as outlined in Chapter 1, have been achieved.

7.1 Conclusions of this work

AERONET level 2 absorption products only constrain specific conditions, but this can be useful for determining the optical properties of the aerosol load.

In Chapter 2, we discuss how AERONET level 2 absorption products are sampled, and how the need for thick aerosol events to ensure low uncertainties in the dataset means that a true daily average would be much smaller than the daily average computed from just those retrievals. Our results show that the variability of both SSA and AE are small compared to all modelled values from each AERONET site, and that the values of SSA and AE are similar in sites near the same emission regions. The requirement of high AOD for AAOD retrievals means that the strict requirements can often only be satisfied by large-scale emission events, such as forest fires, or dust storms. Our method using the SSA and AE for a given emission-based region takes the constraint on AOD and co-locates the same modelled value in space and time, ensuring that the same emissions are being sampled. The spread of the SSA and AE can then be matched between the model and AERONET, without the need to worry about uncertainties in AOD and AAOD, as both SSA and AE are independent of them if aerosol constitution is the same. A similar method is used by Andrews et al., (2017), who compare the mean SSA at each AAOD between models and observations. The method described shows similar promise in being able to identify whether discrepancies in SSA occur during high or low optical depths events.

Whilst this method improves upon direct comparisons of AERONET and modelled output, which have been previous used in literature, we show that it constrains only a small amount of both the time and radiative effects of aerosols. We show that 85% of the aerosol radiative effect in HadGEM3-UKCA occurs when there is an AOD of less than 0.4, mirroring the results of Andrews et al. (2017) for AeroCom models. Our method needs to be used in conjunctions

with other observations to ensure that the comparisons are not overly dependent on high level AOD conditions.

The current HadGEM3-UKCA model underestimates both optical depth and CA mass compared to observations and retrievals.

Evaluation of the model in Chapter 2 highlights that the model underestimates both CA mass and aerosol optical depths in a large number of regions. This is consistent with work on both this model and a number of other climate models which share similar characteristics. Mann et al. (2010a) details the initial description of BC and POM mass in HadGEM3-UKCA with GLOMAP to be "biased low, but correlated well". Kinne et al. (2006) shows that most AeroCom-1 models, including HadGEM2, underestimate the AOD from both satellite and AERONET retrievals, whilst the AOD required emission scaling by 2 in HadGEM3-UKCA to agree with observations during the SAMBBA project (Johnson et al., 2016). We attribute some of the underestimation in AAOD to the sampling of AERONET noted above, but appreciate that the full difference is unlikely to be due to this.

The refractive index of BC from fossil fuel combustion needs to remain high to compare well with observations of AAOD and SSA. However, BC absorption must be reduced in biomass burning areas to leave room for BrC absorption.

Our results from Chapter 3 show that with a low value of BC refractive index, there is a significant decrease in the ability of the model to determine SSA and AAOD over areas dominated by fossil fuel combustion emissions. In these regions, where there is little dust and unlikely to be missing absorption from brown carbon, increasing BC emissions by a factor of 1.7 with a high BC refractive index was the only way to achieve low enough SSA to match both the variability and value of AERONET retrievals. This formed the basis of our reasoning to not include a lower BC refractive index in our final improved model.

This result compares well with results from Bond & Bergstrom (2006) and Moffet & Prather (2009) which both suggest high values of BC refractive index, with imaginary parts ranging from 0.6 to 0.8i. Our findings also agree with the recommendation from Bond et al. (2013), that BC refractive index must be at the higher end of the range. We also note that the value used, $1.83 - 0.71i$, is still in the middle value of that range suggested by Bond & Bergstrom

(2006), and that this could be increased further in future work. However, our comparisons with biomass burning regions suggest that whilst there is a singular value for BC refractive index in the model, increasing the BC refractive index further is not a viable option.

Emissions alone cannot be responsible for the discrepancies between observations and models.

We show in Chapter 4 that increasing emissions of BC or CA to increase absorption cannot be solely responsible for underestimations of absorption compared with observations. Differences in how the model compares to mass and optical retrievals within the same region after increasing emissions dictate that other changes must be required to achieve similar improvements in all regions. This means that solely attributing underestimations in AAOD to underestimations in emissions, as done in Bond et al. (2013) and Petrenko et al. (2012) is not a valid method. This suggests that the increases in emissions suggested in the Bond study are likely to be overestimated, as we prove that absorption can be gained from other sources and through other changes to aerosol properties.

This suggests that evidence for increases in emissions of BC or biomass burning aerosol derived from these techniques is likely overestimated, especially considering the missing absorption that comes from brown carbon, that is not yet implemented in several models. Again, we conclude that there is a need for mass-based measurements to also be a constraint when determining aerosol emissions.

Using an internally-mixed aerosol scheme means that changes in to one aerosol species can change the simulation of other aerosol types.

The influence of changes to one aerosol species due to changes in another species are exceptionally small, or do not occur in either an externally-mixed model or inert tracer transport model. However, in an internally mixed model, these changes can be significant. We note in Chapter 5 and 6 that due to the larger proportion of OC in the model compared to BC, changes in OC have a large influence on BC. The change in OC density not only changed the lifetime of BC by 4 hours, but also altered the vertical and regional distribution of BC. This is magnified further when we examine the improved simulation in Chapter 7.

This effect poses some important questions for aerosol modellers. We have shown that changes to OC influence BC concentrations and lifetime, but they will also have an effect on other aerosols as well. We have not tested to determine whether the changes made have improved or worsened the model simulation of these other aerosols. As such, we would question the wisdom of including the changes we propose in this work into the model until these outputs have been re-assessed to ensure that the gains in CA simulation ability do not come at the cost of diminishing the ability of the model to replicate other aerosols. However, changes to aerosols in general will also have knock on effects on cloud condensation nuclei, cloud formation, precipitation and convection, among other things. Although several of these variables are calculated outside of the UKCA-GLOMAP model, these too will be regularly compared to observations or other models. Our changes will inevitably affect all these other variables, which could undo previous work in that field. This effect within the aerosol scheme shows that future changes to the model may have to assess the impact on multiple variables within the model, not just those which are being changed. It also highlights the dilemma of including model changes which may be beneficial to your own modelling community at the possible expense of something else on the model. Projects such as the Met Office's Auto-Assess are designed specifically to avoid detrimental impacts on modelled climate.

The initial configuration of a model can make a large difference to how a given change will affect the model.

In Chapter 6, we compare two new setups to the original model. By doing so, we can see how the effect of the differences between them changed compared to the when the same differences had been applied to the control. We also compare the linear addition of changes to outputs from the individual alterations we made to the model against changes to output when the changes are made simultaneously.

The effect of implementing an absorbing OC into the model increased AAOD by a factor of 3 times as much with the improved model version, compared to the control simulation. Similar increases were noted for changes in AOD, SSA and OC burden. The changes also magnified the effect of absorbing OC on the BC burden. We also found that the changes were further magnified by one another, as simultaneously combining the alterations changed the OC burden by twice as much as the addition of changes seen from each individual alteration.

This highlights the previous conclusion, which is that changes added to a model can then influence the effectiveness of other changes. This means that some models will see lower changes in mass or optical depths when parameters are changed, whilst other models may see higher changes. Attempts to try to isolate specific effects of uncertainties or schemes within models which contribute to radiative forcing, as done by Carslaw et al. (2013), may differ depending on the model used, or even the setup of the model.

The effect of these magnified changes leads to a change in the present day outgoing combined radiation of -0.44 W m^{-2}. However, because the change is similar in the pre-industrial state, there is no significant change in radiative forcing. This has important implications in reducing uncertainties in aerosol radiative forcing, suggesting that changes in aerosol representation can affect the sensitivity of aerosol radiative effects to other future changes.

The implementation of brown carbon is necessary to correctly attribute absorption in CA, but it will need to be constrained by using multiple observed variables.

BrC is now widely accepted as a form of CA, which is not currently represented in climate models. Feng et al., (2013) researched the effect of adding a BrC tracer into a chemistry transport and radiative transfer models, and found the inclusion improved the comparison with AERONET Absorbing AE in most regions, but overpredicted the absorption in biomass burning regions. We show that there is potential to include a BrC tracer in HadGEM3-UKCA to increase the absorption in biomass burning regions. However, the SSA in these areas already compares well with SSA retrievals, meaning that the addition of extra absorption is likely to worsen the model with respect to AERONET SSA. Adding absorbing OC also leads to overestimations of both AAOD magnitude and AAOD variability. This means that simply increasing non-absorbing aerosols to offset the SSA is not a viable option. One possibility available would be to assume that the absorption of BrC has been wrongly attributed to BC, and reduce the absorption from BC via either removing mass or reducing the refractive index. The removal of mass would lead to a greater underestimation of surface BC concentration than already exists in these areas, but reducing the refractive index would worsen the model comparison in other regions. One possibility is that the BC refractive index from biomass burning emissions is lower than from fossil fuel emissions. Another is that BC mass has been wrongly estimated in biomass burning regions because of the presence of BrC. Observational

attribution of mass and absorption of BC and BrC separately is now needed to make further progress in aerosol modelling.

<u>Our combined changes simulation, based on multi-variable constraints, improves upon the current HadGEM3-UKCA model.</u>

Overall, our set of changes (increased BC density, decreased OC density, doubled CA biomass burning emissions, doubling the biomass burning POM:OC ratio, 1.7 x fossil and biofuel burning BC emission increase) improve the simulation of CA when applied to the model. These increases mean that emissions of BC are between 15 to 16 Tg yr^{-1} in total, with 75% of this coming from fossil and biofuel combustion sources. This is slightly lower than the 17 Tg yr^{-1} suggested by Bond et al. (2013). We find an improvement in comparisons of both mass based observations and optically retrieved observations from AERONET. We are confident that these changes are both scientifically robust, and in the case of CA density, more accurate than the previous values used in the model. Changes to the BC refractive index and the increase in biomass burning emission that are proposed in this work have already been added to the latest Earth system model from the Met Office, UKESM1, and further testing is taking place on our other proposals.

Our multi-variable technique is also shown to be a better method of constraining the model than just using a single variable, such as AAOD. We show that emissions alone are not responsible for differences between modelled and observation mass and optical depths. We show that differences in AAOD, SSA and BC and OC surface concentrations between models and observations imply that in some regions, changes in mass are required, but no change in AAOD is necessary, whilst in other regions, mass is well represented but absorption is not. Without using a multi-variable technique, we would not be able to assess the model as fully as we have.

7.2 Future Work

There are several areas where work is still required to make progress in improving how CA are modelled. We show that there is a potential need for separating BC and BrC, so that carbonaceous absorption can be correctly attributed. Observational methods of attributing absorption to BC and BrC are at an experimental stage. Bahadur et al. (2012) develops a

potential method for returning absorption from AAOD retrievals at multiple wavelengths, using the differences in the wavelength dependence of BrC and BC absorption. Such methods could be used in deriving mass of BrC using aethalometers with multiple wavelengths, giving modellers a constraint on BrC. This would make implementing a brown carbon tracer in HadGEM3-UKCA more scientifically robust. It could also help to identify what other changes to BC may have to be made in order to accommodate BrC in the model, preserving, and eventually improving the comparison with observations of AAOD and SSA.

In addition, this work highlights limitations in the spatial sampling of CA observations. There are currently limited observations of surface concentration of vertical profiles of mass in South East Asia, South America and Australia, with virtually no observations in Africa and Antarctica. In comparison, there are large numbers of sites in North America and Europe. To analyse CA, particularly from biomass burning, more surface concentration observations are required from Africa and South America. More accurate AERONET level 1.5 absorption products are soon to be published, which will increase the number of absorption retrievals available to use for model comparisons. Similarly, more advanced satellites are proposed, such as the 3MI imager which is planned for launch on the EPS-SG platform (Manolis et al., 2013). Further observations with better accuracies over large areas would lead to better understanding and allow climate models to be constrained more robustly.

We discuss how changes to CA aerosol has impacts on other aerosol species due to the internal mixture of aerosol in the model. This means that developers need to assess changes to all aerosol species, and not just the individual species that are modified. Future evolution of aerosol schemes and parameters should be only be added to the model after a full analysis has been carried out. In the UK Met Office, the Auto-Assess suite allows developers to see how all model variables respond when changes are made. This implementation should prevent changes being added to future versions of the model with unknown consequences on other areas, and encourages more co-operation between developers of different modelling areas when such changes occur. As the complexity of models grows to include more interactive feedbacks, this process becomes more vital to ensuring continuous model improvements.

Chapter 7: Conclusion and Discussion

Our work has not focused on improving the AE, but our initial assessment in Chapter 2 identifies regions where AE is overestimated in the model. Such discrepancies could be explained by coated dust particles, a process that is not modelled in HadGEM3-UKCA currently. Further improvements on the dust scheme within GLOMAP-mode could lead to this interaction being included, which could change the modelled AE in areas where dust mixed with SOA is found in observations.

References

Abdul-Razzak, H., & Ghan, S. J. (2000). A parameterization of aerosol activation: 2. Multiple aerosol types. *Journal of Geophysical Research*, *105*, 6837. https://doi.org/10.1029/1999JD901161

Akagi, S. K., Yokelson, R. J., Wiedinmyer, C., Alvarado, M. J., Reid, J. S., Karl, T., … Wennberg, P. O. (2011). Emission factors for open and domestic biomass burning for use in atmospheric models. *Atmospheric Chemistry and Physics*, *11*(9), 4039–4072. https://doi.org/10.5194/acp-11-4039-2011

Alexander, D. T. L., Crozier, P. A., & Anderson, J. R. (2008). Brown carbon spheres in East Asian outflow and their optical properties. *Science (New York, N.Y.)*, *321*(5890), 833–6. https://doi.org/10.1126/science.1155296

Amiridis, V., Giannakaki, E., Balis, D. S., Gerasopoulos, E., Pytharoulis, I., Zanis, P., … Zerefos, C. (2010). Smoke injection heights from agricultural burning in Eastern Europe as seen by CALIPSO. *Atmospheric Chemistry and Physics*, *10*(23), 11567–11576. https://doi.org/10.5194/acp-10-11567-2010

Andreae, M. O., & Gelencsér, a. (2006). Black carbon or brown carbon? The nature of light-absorbing carbonaceous aerosols. *Atmospheric Chemistry and Physics Discussions*, *6*(3), 3419–3463. https://doi.org/10.5194/acpd-6-3419-2006

Andrews, E., Ogren, J. A., Kinne, S., & Samset, B. (2017). Comparison of AOD, AAOD and column single scattering albedo from AERONET retrievals and in situ profiling measurements. *Atmospheric Chemistry and Physics*, *17*(9), 6041–6072. https://doi.org/10.5194/acp-17-6041-2017

Aquila, V., Hendricks, J., Lauer, A., Riemer, N., Vogel, H., Baumgardner, D., … Dall'Amico, M. (2011). MADE-in: A new aerosol microphysics submodel for global simulation of insoluble particles and their mixing state. *Geoscientific Model Development*, *4*(2), 325–355. https://doi.org/10.5194/gmd-4-325-2011

Arrhenius, S. (1896). On the influence of carbonic acid in the air upon the temperature of the ground. *Philosophical Magazine and Journal of Science*, *41*, 239–276. https://doi.org/10.1080/14786449608620846

Bahadur, R., Praveen, P. S., Xu, Y., & Ramanathan, V. (2012). Solar absorption by elemental and brown carbon determined from spectral observations. *Proceedings of the National Academy of Sciences*, *109*(43), 17366–17371. https://doi.org/10.1073/pnas.1205910109

Barnard, J. C., Kassianov, E. I., Ackerman, T. P., Johnson, K., Zuberi, B., Molina, L. T., & Molina, M. J. (2007). Estimation of a "radiatively correct" black carbon specific absorption during the Mexico City Metropolitan Area (MCMA) 2003 field campaign. *Atmospheric Chemistry and Physics*, *7*(6), 1645–1655. https://doi.org/10.5194/acp-7-1645-2007

Batten, C. E. (1985). Spectral optical constants of soots from polarized angular reflectance measurements. *Applied Optics*, *24*(8), 1193. https://doi.org/10.1364/AO.24.001193

Bauer, S. E., Mishchenko, M. I., Lacis, A. A., Zhang, S., Perlwitz, J., & Metzger, S. M. (2007). Do sulfate and nitrate coatings on mineral dust have important effects on radiative properties and climate modeling? *Journal of Geophysical Research Atmospheres*, *112*(6). https://doi.org/10.1029/2005JD006977

Beegum, S. N., Moorthy, K. K., Babu, S. S., Satheesh, S. K., Vinoj, V., Badarinath, K. V. S., … Pant, P. (2009). Spatial distribution of aerosol black carbon over India during pre-monsoon season. *Atmospheric Environment*, *43*(5), 1071–1078. https://doi.org/10.1016/j.atmosenv.2008.11.042

References

Bellouin, N., Boucher, O., Haywood, J., Johnson, C., Jones, A., Rae, J., & Woodward, S. (2007). *Improved representation of aerosols for HadGEM2. Hadley Centre technical note 73.*

Bellouin, N., Mann, G. W., Woodhouse, M. T., Johnson, C., Carslaw, K. S., & Dalvi, M. (2013). Impact of the modal aerosol scheme GLOMAP-mode on aerosol forcing in the hadley centre global environmental model. *Atmospheric Chemistry and Physics*, *13*(6), 3027–3044. https://doi.org/10.5194/acp-13-3027-2013

Bentsen, M., Bethke, I., Debernard, J. B., Iversen, T., Kirkevåg, a., Seland, Ø., … Kristjánsson, J. E. (2012). The Norwegian Earth System Model, NorESM1-M – Part 1: Description and basic evaluation. *Geoscientific Model Development Discussions*, *5*, 2843–2931. https://doi.org/10.5194/gmdd-5-2843-2012

Bhattachan, A., D'Odorico, P., & Okin, G. S. (2015). Biogeochemistry of dust sources in Southern Africa. *Journal of Arid Environments*, *117*, 18–27. https://doi.org/10.1016/j.jaridenv.2015.02.013

Bond, T. C., Anderson, T. L., & Campbell, D. (1999). Calibration and Intercomparison of Filter-Based Measurements of Visible Light Absorption by Aerosols. *Aerosol Science and Technology*, *30*(6), 582–600. https://doi.org/10.1080/027868299304435

Bond, T. C., & Bergstrom, R. W. (2006). Light Absorption by Carbonaceous Particles: An Investigative Review. *Aerosol Science and Technology*, *40*(1), 27–67. https://doi.org/10.1080/02786820500421521

Bond, T. C., Doherty, S. J., Fahey, D. W., Forster, P. M., Berntsen, T., Deangelo, B. J., … Zender, C. S. (2013). Bounding the role of black carbon in the climate system: A scientific assessment. *Journal of Geophysical Research Atmospheres*, *118*(11), 5380–5552. https://doi.org/10.1002/jgrd.50171

Bond, T. C., Streets, D. G., Yarber, K. F., Nelson, S. M., Woo, J. H., & Klimont, Z. (2004). A technology-based global inventory of black and organic carbon emissions from combustion. *Journal of Geophysical Research D: Atmospheres*, *109*(14). https://doi.org/10.1029/2003JD003697

Boucher, O., Randall, D., Artaxo, P., Bretherton, C., Feingold, G., Forster, P., … Zhan, X. Y. (2013). Clouds and Aerosols. *Climate Change 2013: The Physical Science Basis. Contribution of Working Group I to the Fifth Assessment Report of the Intergovernmental Panel on Climate Change*, 571–657. https://doi.org/10.1017/CBO9781107415324.016

Brito, J., Rizzo, L. V., Morgan, W. T., Coe, H., Johnson, B., Haywood, J., … Artaxo, P. (2014). Ground-based aerosol characterization during the South American Biomass Burning Analysis (SAMBBA) field experiment. *Atmospheric Chemistry and Physics*. https://doi.org/10.5194/acp-14-12069-2014

Brunekreef, B., & Forsberg, B. (2005). Epidemiological evidence of effects of coarse airborne particles on health. *European Respiratory Journal*. https://doi.org/10.1183/09031936.05.00001805

Bush, S. J., Turner, A. G., Woolnough, S. J., Martin, G. M., & Klingaman, N. P. (2015). The effect of increased convective entrainment on Asian monsoon biases in the MetUM general circulation model. *Quarterly Journal of the Royal Meteorological Society*, *141*(686), 311–326. https://doi.org/10.1002/qj.2371

Cape, J. N., Coyle, M., & Dumitrean, P. (2012). The atmospheric lifetime of black carbon. *Atmospheric Environment*, *59*, 256–263. https://doi.org/10.1016/j.atmosenv.2012.05.030

Capes, G., Johnson, B., McFiggans, G., Williams, P. I., Haywood, J., & Coe, H. (2008). Aging of biomass burning aerosols over West Africa: Aircraft measurements of chemical

composition, microphysical properties, and emission ratios. *Journal of Geophysical Research Atmospheres*, *113*(23). https://doi.org/10.1029/2008JD009845

Cappa, C. D., Onasch, T. B., Massoli, P., Worsnop, D. R., Bates, T. S., Cross, E. S., … Zaveri, R. A. (2012). Radiative Absorption Enhancements Due to the Mixing State of Atmospheric Black Carbon. *Science*, *337*(6098), 1078–1081. https://doi.org/10.1126/science.1223447

Carslaw, K. S., Lee, L. a, Reddington, C. L., Mann, G. W., & Pringle, K. J. (2013). The magnitude and sources of uncertainty in global aerosol. *Faraday Discussions*, *165*, 495–512. https://doi.org/10.1039/c3fd00043e

Carslaw, K. S., Lee, L. a, Reddington, C. L., Pringle, K. J., Rap, a, Forster, P. M., … Pierce, J. R. (2013). Large contribution of natural aerosols to uncertainty in indirect forcing. *Nature*, *503*(7474), 67–71. https://doi.org/10.1038/nature12674

Chakrabarty, R. K., Moosmüller, H., Chen, L. W. A., Lewis, K., Arnott, W. P., Mazzoleni, C., … Kreidenweis, S. M. (2010). Brown carbon in tar balls from smoldering biomass combustion. *Atmospheric Chemistry and Physics*, *10*(13), 6363–6370. https://doi.org/10.5194/acp-10-6363-2010

Chan, T. W., Brook, J. R., Smallwood, G. J., & Lu, G. (2011). Time-resolved measurements of black carbon light absorption enhancement in urban and near-urban locations of southern Ontario, Canada. *Atmospheric Chemistry and Physics*, *11*(20), 10407–10432. https://doi.org/10.5194/acp-11-10407-2011

Chen, L. W. A., Chow, J. C., Watson, J. G., Moosmüller, H., & Arnott, W. P. (2004). Modeling reflectance and transmittance of quartz-fiber filter samples containing elemental carbon particles: Implications for thermal/optical analysis. *Journal of Aerosol Science*, *35*(6), 765–780. https://doi.org/10.1016/j.jaerosci.2003.12.005

Chen, Y., & Bond, T. C. (2009). Light absorption by organic carbon from wood combustion. *Atmospheric Chemistry and Physics Discussions*, *9*(2001), 20471–20513. https://doi.org/10.5194/acpd-9-20471-2009

Chow, J. C., Watson, J. G., Chen, L. W. A., Arnott, W. P., Moosmüller, H., & Fung, K. (2004). Equivalence of elemental carbon by thermal/optical reflectance and transmittance with different temperature protocols. *Environmental Science and Technology*, *38*(16), 4414–4422. https://doi.org/10.1021/es034936u

Chow, J. C., Watson, J. G., Lowenthal, D. H., Chen, L.-W. A., & Motallebi, N. (2010). Black and Organic Carbon Emission Inventories: Review and Application to California. *Journal of the Air & Waste Management Association*, *60*(4), 497–507. https://doi.org/10.3155/1047-3289.60.4.497

Chow, J. C., Watson, J. G., Pritchett, L. C., Pierson, W. R., Frazier, C. A., & Purcell, R. G. (1993). The dri thermal/optical reflectance carbon analysis system: description, evaluation and applications in U.S. Air quality studies. *Atmospheric Environment Part A, General Topics*, *27*(8), 1185–1201. https://doi.org/10.1016/0960-1686(93)90245-T

Cohan, D. S., Xu, J., Greenwald, R., Bergin, M. H., & Chameides, W. L. (2002). Impact of atmospheric aerosol light scattering and absorption on terrestrial net primary productivity. *Global Biogeochemical Cycles*, *16*(4).

Collins, W. J., Bellouin, N., Doutriaux-Boucher, M., Gedney, N., Halloran, P., Hinton, T., … Woodward, S. (2011). Development and evaluation of an Earth-system model – HadGEM2. *Geoscientific Model Development*, *4*, 1051–1075. https://doi.org/10.5194/gmd-4-1051-2011

Collins, W. J., Bellouin, N., Doutriaux-Boucher, M., Gedney, N., Hinton, T., Jones, C. D., … Kim, J. (2008). Evaluation of HadGEM2 model. *Meteorological Office Hadley Centre, Technical*

References

Note 74, 47 pp.

Conant, W. C., Nenes, A., & Seinfeld, J. H. (2002). Black carbon radiative heating effects on cloud microphysics and implications for the aerosol indirect effect. 1. Extended K??hler theory. *Journal of Geophysical Research Atmospheres*, *107*(21). https://doi.org/10.1029/2002JD002094

Crosbie, E., Youn, J.-S., Balch, B., Wonaschütz, a., Shingler, T., Wang, Z., … Sorooshian, a. (2015). On the competition among aerosol number, size and composition in predicting CCN variability: a multi-annual field study in an urbanized desert. *Atmospheric Chemistry and Physics*, *15*(12), 6943–6958. https://doi.org/10.5194/acp-15-6943-2015

Cross, E. S., Onasch, T. B., Ahern, A., Wrobel, W., Slowik, J. G., Olfert, J., … Davidovits, P. (2010). Soot Particle Studies—Instrument Inter-Comparison—Project Overview. *Aerosol Science and Technology*, *44*(8), 592–611. https://doi.org/10.1080/02786826.2010.482113

Cui, X., Wang, X., Yang, L., Chen, B., Chen, J., Andersson, A., & Gustafsson, Ö. (2016). Radiative absorption enhancement from coatings on black carbon aerosols. *Science of the Total Environment*, *551–552*, 51–56. https://doi.org/10.1016/j.scitotenv.2016.02.026

De Graaf, M., Tilstra, L. G., Wang, P., & Stammes, P. (2012). Retrieval of the aerosol direct radiative effect over clouds from spaceborne spectrometry. *Journal of Geophysical Research Atmospheres*, *117*(7). https://doi.org/10.1029/2011JD017160

Dentener, F. J., Kinne, S., Bond, T., Boucher, O., Cofala, J., Generoso, S., … Wilson, J. (2006). Emissions of primary aerosol and precursor gases in the years 2000 and 1750, prescribed data-sets for AeroCom. *Atmospheric Chemistry and Physics*, *6*(2), 2703–2763. https://doi.org/10.5194/acpd-6-2703-2006

Deshler, T. (2008). A review of global stratospheric aerosol: Measurements, importance, life cycle, and local stratospheric aerosol. *Atmospheric Research*, *90*(2–4), 223–232. https://doi.org/10.1016/j.atmosres.2008.03.016

Diehl, T., Heil, A., Chin, M., Pan, X., Streets, D., Schultz, M., & Kinne, S. (2012). Anthropogenic, biomass burning, and volcanic emissions of black carbon, organic carbon, and SO2 from 1980 to 2010 for hindcast model experiments. *Atmospheric Chemistry and Physics Discussions*, *12*, 24895–24954. https://doi.org/10.5194/acpd-12-24895-2012

Dietz, S., Bowen, A., Dixon, C., & Gradwell, P. (2016). "Climate value at risk" of global financial assets. *Nature Climate Change*, (April), 1–5. https://doi.org/10.1038/nclimate2972

Donnell, E. a., Fish, D. J., Dicks, E. M., & Thorpe, A. J. (2001). Mechanisms for pollutant transport between the boundary layer and the free troposphere. *Journal of Geophysical Research*, *106*(D8), 7847. https://doi.org/10.1029/2000JD900730

Dubovik, O., Holben, B., Eck, T. F., Smirnov, A., Kaufman, Y. J., King, M. D., … Slutsker, I. (2002). Variability of Absorption and Optical Properties of Key Aerosol Types Observed in Worldwide Locations. *Journal of the Atmospheric Sciences*, *59*(3), 590–608. https://doi.org/10.1175/1520-0469(2002)059<0590:VOAAOP>2.0.CO;2

Dubovik, O., & King, M. D. (2000). A flexible inversion algorithm for retrieval of aerosol optical properties from Sun and sky radiance measurements. *Journal of Geophysical Research*, *105*(D16), 20673. https://doi.org/10.1029/2000JD900282

Dubovik, O., Sinyuk, A., Lapyonok, T., Holben, B. N., Mishchenko, M., Yang, P., … Slutsker, I. (2006). Application of spheroid models to account for aerosol particle nonsphericity in remote sensing of desert dust. *Journal of Geophysical Research Atmospheres*, *111*(11), 1–34. https://doi.org/10.1029/2005JD006619

Dubovik, O., Smirnov, a., Holben, B. N., King, M. D., Kaufman, Y. J., Eck, T. F., & Slutsker, I. (2000). Accuracy assessments of aerosol optical properties retrieved from Aerosol

References

Robotic Network (AERONET) Sun and sky radiance measurements. *Journal of Geophysical Research*, *105*(D8), 9791. https://doi.org/10.1029/2000JD900040

Dufresne, J. L., Foujols, M. A., Denvil, S., Caubel, A., Marti, O., Aumont, O., … Vuichard, N. (2013). Climate change projections using the IPSL-CM5 Earth System Model: From CMIP3 to CMIP5. *Climate Dynamics*, *40*(9–10), 2123–2165. https://doi.org/10.1007/s00382-012-1636-1

Edwards, J. M., & Slingo, A. (1996). Studies with a flexible new radiation code. I: Choosing a configuration for a large-scale model. *Quarterly Journal of the Royal Meteorological Society*, *122*(531), 689–719. https://doi.org/10.1002/qj.49712253107

Emmons, L. K., Deeter, M. N., Gille, J. C., Edwards, D. P., Attié, J.-L., Warner, J., … Ziereis, H. (2004). Validation of Measurements of Pollution in the Troposphere (MOPITT) CO retrievals with aircraft in situ profiles. *Journal of Geophysical Research: Atmospheres*, *109*(D3), n/a-n/a. https://doi.org/10.1029/2003JD004101

Engelhart, G. J., Moore, R. H., Nenes, A., & Pandis, S. N. (2011). Cloud condensation nuclei activity of isoprene secondary organic aerosol. *J. Geophys. Res.*, *116*(D2), D02207. https://doi.org/10.1029/2010jd014706

Feng, Y., Ramanathan, V., & Kotamarthi, V. R. (2013). Brown carbon: A significant atmospheric absorber of solar radiation. *Atmospheric Chemistry and Physics*, *13*(17), 8607–8621. https://doi.org/10.5194/acp-13-8607-2013

Formenti, P. (2003). Inorganic and carbonaceous aerosols during the Southern African Regional Science Initiative (SAFARI 2000) experiment: Chemical characteristics, physical properties, and emission data for smoke from African biomass burning. *Journal of Geophysical Research*, *108*(D13), 1–16. https://doi.org/10.1029/2002JD002408

Gadhavi, H. S., Renuka, K., Ravi Kiran, V., Jayaraman, A., Stohl, A., Klimont, Z., & Beig, G. (2015). Evaluation of black carbon emission inventories using a Lagrangian dispersion model - A case study over southern India. *Atmospheric Chemistry and Physics*, *15*(3), 1447–1461. https://doi.org/10.5194/acp-15-1447-2015

Ghan, S., Wang, M., Zhang, S., Ferrachat, S., Gettelman, A., Griesfeller, J., … Zhang, K. (2016). Challenges in constraining anthropogenic aerosol effects on cloud radiative forcing using present-day spatiotemporal variability. *Proceedings of the National Academy of Sciences*, *113*(21), 5804–5811. https://doi.org/10.1073/pnas.1514036113

Gupta, I., & Kumar, R. (2006). Trends of particulate matter in four cities in India. *Atmospheric Environment*, *40*(14), 2552–2566. https://doi.org/10.1016/j.atmosenv.2005.12.021

Hansen, A. D. A., Rosen, H., & Novakov, T. (1984). The aethalometer — An instrument for the real-time measurement of optical absorption by aerosol particles. *Science of The Total Environment*, *36*, 191–196. https://doi.org/10.1016/0048-9697(84)90265-1

Hansen, J., Johnson, D., Lacis, a, Lebedeff, S., Lee, P., Rind, D., & Russell, G. (1981). Climate impact of increasing atmospheric carbon dioxide. *Science (New York, N.Y.)*, *213*(4511), 957–966. https://doi.org/10.1126/science.213.4511.957

Hansen, J., Sato, M., & Ruedy, R. (1997). Radiative forcing and climate response. *Journal of Geophysical Research*, *102*(D6), 6831–6864. https://doi.org/10.1029/96JD03436

Hantson, S., Arneth, A., Harrison, S. P., Kelley, D. I., Colin Prentice, I., Rabin, S. S., … Yue, C. (2016). The status and challenge of global fire modelling. *Biogeosciences*, *13*(11), 3359–3375. https://doi.org/10.5194/bg-13-3359-2016

Hawkins, E., & Sutton, R. (2009). The potential to narrow uncertainty in regional climate predictions. *Bulletin of the American Meteorological Society*, *90*(8), 1095–1107. https://doi.org/10.1175/2009BAMS2607.1

References

Hess, M., Koepke, P., & Schult, I. (1998). Optical Properties of Aerosols and Clouds: The Software Package OPAC. *Bulletin of the American Meteorological Society*, *79*(5), 831–844. https://doi.org/10.1175/1520-0477(1998)079<0831:OPOAAC>2.0.CO;2

Hewitt, H. T., Copsey, D., Culverwell, I. D., Harris, C. M., Hill, R. S. R., Keen, A. B., … Hunke, E. C. (2011). Design and implementation of the infrastructure of HadGEM3: The next-generation Met Office climate modelling system. *Geoscientific Model Development*, *4*(2), 223–253. https://doi.org/10.5194/gmd-4-223-2011

Hodgson, A. K., Morgan, W. T., Darbyshire, E., Allan, J. D., & Coe, H. (2013). Case study analysis of biomass burning plumes observed over Brazil during SAMBBA, September 2012. In *AIP Conference Proceedings* (Vol. 1527, pp. 598–601). https://doi.org/10.1063/1.4803342

Hodnebrog, Ø., Myhre, G., & Samset, B. H. (2014). How shorter black carbon lifetime alters its climate effect. *Nature Communications*, *5*(May), 5065. https://doi.org/10.1038/ncomms6065

Hoegh-Guldberg, O., & Bruno, J. F. (2010). The impact of climate change on the world's marine ecosystems. *Science*, *328*(5985), 1523–1528. https://doi.org/10.1126/science.1189930

Holben, B., Eck, T., Slutsker, I., Smirnov, a, Sinyuk, a, Schafer, J., … Dubovik, O. (2006). AERONET ' s Version 2.0 quality assurance criteria. *Remote Sensing of Atmosphere and Clouds*. https://doi.org/10.1117/12.706524

Holben, B. N. (2006). AERONET Inversion Products. *Weather*, 1–6.

Holben, B. N., Eck, T. F., Slutsker, I., Tanré, D., Buis, J. P., Setzer, A., … Smirnov, A. (1998). AERONET—A Federated Instrument Network and Data Archive for Aerosol Characterization. *Remote Sensing of Environment*, *66*(1), 1–16. https://doi.org/10.1016/S0034-4257(98)00031-5

Hungershöfer, K., Zeromskiene, K., Iinuma, Y., Helas, G., Trentmann, J., Trautmann, T., … Schmid, O. (2007). Modelling the optical properties of fresh biomass burning aerosol produced in a smoke chamber: results from the EFEU campaign. *Atmospheric Chemistry and Physics Discussions*, *7*(4), 12657–12686. https://doi.org/10.5194/acpd-7-12657-2007

Inoue, M., Morino, I., Uchino, O., Miyamoto, Y., Saeki, T., Yoshida, Y., … Matsueda, H. (2014). Validation of XCH4derived from SWIR spectra of GOSAT TANSO-FTS with aircraft measurement data. *Atmospheric Measurement Techniques*, *7*(9), 2987–3005. https://doi.org/10.5194/amt-7-2987-2014

Jacob, D. J., Crawford, J. H., Maring, H., Clarke, A. D., Dibb, J. E., Emmons, L. K., … Fisher, J. A. (2010). The arctic research of the composition of the troposphere from aircraft and satellites (ARCTAS) mission: Design, execution, and first results. *Atmospheric Chemistry and Physics*, *10*(11), 5191–5212. https://doi.org/10.5194/acp-10-5191-2010

Jacobson, M. Z., Cappa, C. D., Jacobson, M. Z., Mikhailov, E. F., Vlasenko, S. S., Podgorny, I. A., … Jacobson, M. Z. (2013). Comment on "Radiative absorption enhancements due to the mixing state of atmospheric black carbon". *Science (New York, N.Y.)*, *339*(6118), 393. https://doi.org/10.1126/science.1229920

Jickells, T. D. (2005). Global Iron Connections Between Desert Dust, Ocean Biogeochemistry, and Climate. *Science*, *308*(5718), 67–71. https://doi.org/10.1126/science.1105959

Jo, D. S., Park, R. J., Lee, S., Kim, S. W., & Zhang, X. (2016). A global simulation of brown carbon: Implications for photochemistry and direct radiative effect. *Atmospheric Chemistry and Physics*, *16*(5), 3413–3432. https://doi.org/10.5194/acp-16-3413-2016

Johnson, B. T., Haywood, J. M., Langridge, J. M., Darbyshire, E., Morgan, W. T., Szpek, K., … Bellouin, N. (2016). Evaluation of biomass burning aerosols in the HadGEM3 climate

References

model with observations from the SAMBBA field campaign. *Atmospheric Chemistry and Physics*, *16*(22), 14657–14685. https://doi.org/10.5194/acp-16-14657-2016

Johnson, B. T., Shine, K. P., & Forster, P. M. (2004). The semi-direct aerosol effect: Impact of absorbing aerosols on marine stratocumulus. *Quarterly Journal of the Royal Meteorological Society*, *130*(599), 1407–1422. https://doi.org/10.1256/qj.03.61

Jones, A., Thomson, D., Hort, M., & Devenish, B. (2007). The U . K . Met Officve ' s next generation atmospheric dispersion model, NAME III. *UK Met Office*, 1–8.

Junker, C., & Liousse, C. (2006). A global emission inventory of carbonaceous aerosol from historic records of fossil fuel and biofuel consumption for the period 1860–1997. *Atmospheric Chemistry and Physics Discussions*, *6*(3), 4897–4927. https://doi.org/10.5194/acpd-6-4897-2006

Kaiser, J. W., Heil, A., Andreae, M. O., Benedetti, A., Chubarova, N., Jones, L., … Van Der Werf, G. R. (2012). Biomass burning emissions estimated with a global fire assimilation system based on observed fire radiative power. *Biogeosciences*, *9*(1), 527–554. https://doi.org/10.5194/bg-9-527-2012

Kaskaoutis, D. G., Singh, R. P., Gautam, R., Sharma, M., Kosmopoulos, P. G., & Tripathi, S. N. (2012). Variability and trends of aerosol properties over Kanpur, northern India using AERONET data (2001–10). *Environmental Research Letters*, *7*(2), 24003. https://doi.org/10.1088/1748-9326/7/2/024003

Kaufman, Y. J., Tanré, D., & Boucher, O. (2002). A satellite view of aerosols in the climate system. *Nature*, *419*(6903), 215–223. https://doi.org/10.1038/nature01091

Kim, M., Zhang, X., Holt, J. B., Liu, Y., Branch, S., Disease, C., & Promotion, P. H. (2015). Spatio-Temporal Variations in the Associations between Hourly PM2.5 and Aerosol Optical Depth (AOD) from MODIS Sensors on Terra and Aqua. *Health (Irvine Calif).*, *5*, 8–13. https://doi.org/10.4236/health.2013.510A2002.Spatio-Temporal

Kinne, S., Schulz, M., Textor, C., Guibert, S., Balkanski, Y., Bauer, S. E., … Tie, X. (2006). An AeroCom initial assessment – optical properties in aerosol component modules of global models. *Atmospheric Chemistry and Physics*, *6*, 1815–1834. https://doi.org/10.5194/acpd-5-8285-2005

Kipling, Z., Stier, P., Schwarz, J. P., Perring, A. E., Spackman, J. R., Mann, G. W., … Telford, P. J. (2013). Constraints on aerosol processes in climate models from vertically-resolved aircraft observations of black carbon. *Atmospheric Chemistry and Physics*, *13*(12), 5969–5986. https://doi.org/10.5194/acp-13-5969-2013

Kirchstetter, T. W., Novakov, T., & Hobbs, P. V. (2004). Evidence that the spectral dependence of light absorption by aerosols is affected by organic carbon. *Journal of Geophysical Research D: Atmospheres*, *109*(21), 1–12. https://doi.org/10.1029/2004JD004999

Koch, D., & Del Genio, A. D. (2010). Black carbon semi-direct effects on cloud cover: Review and synthesis. *Atmospheric Chemistry and Physics*, *10*(16), 7685–7696. https://doi.org/10.5194/acp-10-7685-2010

Kondo, Y., Sahu, L., Moteki, N., Khan, F., Takegawa, N., Liu, X., … Miyakawa, T. (2011). Consistency and Traceability of Black Carbon Measurements Made by Laser-Induced Incandescence, Thermal-Optical Transmittance, and Filter-Based Photo-Absorption Techniques. *Aerosol Science and Technology*, *45*(2), 295–312. https://doi.org/10.1080/02786826.2010.533215

Kristiansen, N. I., Stohl, A., Olivi??, D. J. L., Croft, B., S??vde, O. A., Klein, H., … Zhang, H. (2016). Evaluation of observed and modelled aerosol lifetimes using radioactive tracers of opportunity and an ensemble of 19 global models. *Atmospheric Chemistry and Physics*,

References

16(5), 3525–3561. https://doi.org/10.5194/acp-16-3525-2016

Kulmala, M., Asmi, A., Lappalainen, H. K., Baltensperger, U., Brenguier, J. L., Facchini, M. C., … Pandis, S. N. (2011). General overview: European Integrated project on Aerosol Cloud Climate and Air Quality interactions (EUCAARI)-integrating aerosol research from nano to global scales. *Atmospheric Chemistry and Physics*, *11*(24), 13061–130143. https://doi.org/10.5194/acp-11-13061-2011

Kuwata, M., Zorn, S. R., & Martin, S. T. (2012). Using elemental ratios to predict the density of organic material composed of carbon, hydrogen, and oxygen. *Environmental Science and Technology*, *46*(2), 787–794. https://doi.org/10.1021/es202525q

Labonne, M., Bréon, F. M., & Chevallier, F. (2007). Injection height of biomass burning aerosols as seen from a spaceborne lidar. *Geophysical Research Letters*, *34*(11). https://doi.org/10.1029/2007GL029311

Laborde, M., Mertes, P., Zieger, P., Dommen, J., Baltensperger, U., & Gysel, M. (2012). Sensitivity of the Single Particle Soot Photometer to different black carbon types. *Atmospheric Measurement Techniques*, *5*(5), 1031–1043. https://doi.org/10.5194/amt-5-1031-2012

Lack, D. A., & Cappa, C. D. (2010). Impact of brown and clear carbon on light absorption enhancement, single scatter albedo and absorption wavelength dependence of black carbon. *Atmospheric Chemistry and Physics*, *10*(9), 4207–4220. https://doi.org/10.5194/acp-10-4207-2010

Lack, D. A., Cappa, C. D., Covert, D. S., Baynard, T., Massoli, P., Sierau, B., … Ravishankara, A. R. (2008). Bias in Filter-Based Aerosol Light Absorption Measurements Due to Organic Aerosol Loading: Evidence from Ambient Measurements. *Aerosol Science and Technology*, *42*(12), 1033–1041. https://doi.org/10.1080/02786820802389277

Lack, D. a., Langridge, J. M., Bahreini, R., Cappa, C. D., Middlebrook, a. M., & Schwarz, J. P. (2012). Brown carbon and internal mixing in biomass burning particles. *Proceedings of the National Academy of Sciences*, *109*(37), 14802–14807. https://doi.org/10.1073/pnas.1206575109

Lack, D. A., Moosmüller, H., McMeeking, G. R., Chakrabarty, R. K., & Baumgardner, D. (2014). Characterizing elemental, equivalent black, and refractory black carbon aerosol particles: A review of techniques, their limitations and uncertainties. *Analytical and Bioanalytical Chemistry*. https://doi.org/10.1007/s00216-013-7402-3

Lamarque, J. F., Bond, T. C., Eyring, V., Granier, C., Heil, A., Klimont, Z., … Van Vuuren, D. P. (2010). Historical (1850-2000) gridded anthropogenic and biomass burning emissions of reactive gases and aerosols: Methodology and application. *Atmospheric Chemistry and Physics*, *10*(15), 7017–7039. https://doi.org/10.5194/acp-10-7017-2010

Lee, S. (2002). Chemical components of single particles measured with Particle Analysis by Laser Mass Spectrometry (PALMS) during the Atlanta SuperSite Project: Focus on organic/sulfate, lead, soot, and mineral particles. *Journal of Geophysical Research*. https://doi.org/10.1029/2000JD000011

Lee, S. K., Park, W., Van Sebille, E., Baringer, M. O., Wang, C., Enfield, D. B., … Kirtman, B. P. (2011). What caused the significant increase in Atlantic Ocean heat content since the mid-20th century? *Geophysical Research Letters*, *38*(17). https://doi.org/10.1029/2011GL048856

Lelieveld, J., Evans, J., Fnais, M., Giannadaki, D., & Pozzer, A. (2015). The contribution of outdoor air pollution sources to premature mortality on a global scale. *Nature*, *525*(7569), 367–371. https://doi.org/10.1038/nature15371

References

Lesins, G., Chylek, P., & Lohmann, U. (2002). A study of internal and external mixing scenarios and its effect on aerosol optical properties and direct radiative forcing. *Journal of Geophysical Research-Atmospheres*, *107*(D10), art. no.-4094. https://doi.org/Artn 4094\rDoi 10.1029/2001jd000973

Levy, R. C., Remer, L. A., & Dubovik, O. (2007). Global aerosol optical properties and application to Moderate Resolution Imaging Spectroradiometer aerosol retrieval over land. *Journal of Geophysical Research Atmospheres*, *112*(13). https://doi.org/10.1029/2006JD007815

Li, J., Carlson, B. E., Dubovik, O., & Lacis, A. A. (2014). Recent trends in aerosol optical properties derived from AERONET measurements. *Atmos. Chem. Phys.*, *14*(22), 12271–12289. https://doi.org/10.5194/acp-14-12271-2014

Li, J., Han, Z., & Zhang, R. (2014). Influence of aerosol hygroscopic growth parameterization on aerosol optical depth and direct radiative forcing over East Asia. *Atmospheric Research*, *140–141*, 14–27. https://doi.org/10.1016/j.atmosres.2014.01.013

Liousse, C., Guillaume, B., Grégoire, J. M., Mallet, M., Galy, C., Pont, V., … Van Velthoven, P. (2010). Updated African biomass burning emission inventories in the framework of the AMMA-IDAF program, with an evaluation of combustion aerosols. *Atmospheric Chemistry and Physics*, *10*(19), 9631–9646. https://doi.org/10.5194/acp-10-9631-2010

Liousse, C., Penner, J. E., Chuang, C., Walton, J. J., Eddleman, H., & Cachier, H. (1996). A global three-dimensional model study of carbonaceous aerosols. *Journal of Geophysical Research*, *101*(D14), 19411. https://doi.org/10.1029/95JD03426

Lu, Z., Streets, D. G., Winijkul, E., Yan, F., Chen, Y., Bond, T. C., … Carmichael, G. R. (2015). Light Absorption Properties and Radiative Effects of Primary Organic Aerosol Emissions. *Environmental Science & Technology*, 150409080054009. https://doi.org/10.1021/acs.est.5b00211

Mahajan, S., Evans, K. J., Hack, J. J., & Truesdale, J. E. (2013). Linearity of climate response to increases in black carbon aerosols. *Journal of Climate*, *26*(20), 8223–8237. https://doi.org/10.1175/JCLI-D-12-00715.1

Mann, G. W., Carslaw, K. S., Reddington, C. L., Pringle, K. J., Schulz, M., Asmi, A., … Henzing, J. S. (2014). Intercomparison and evaluation of global aerosol microphysical properties among AeroCom models of a range of complexity. *Atmospheric Chemistry and Physics*, *14*(9), 4679–4713. https://doi.org/10.5194/acp-14-4679-2014

Mann, G. W., Carslaw, K. S., Spracklen, D. V., Ridley, D. a., Manktelow, P. T., Chipperfield, M. P., … Johnson, C. E. (2010a). Description and evaluation of GLOMAP-mode: a modal global aerosol microphysics model for the UKCA composition-climate model. *Geoscientific Model Development Discussions*, *3*, 519–551. https://doi.org/10.5194/gmd-3-519-2010

Mann, G. W., Carslaw, K. S., Spracklen, D. V., Ridley, D. A., Manktelow, P. T., Chipperfield, M. P., … Johnson, C. E. (2010b). Description and evaluation of GLOMAP-mode: a modal global aerosol microphysics model for the UKCA composition-climate model. *Geoscientific Model Development*, *3*(2), 519–551. https://doi.org/10.5194/gmd-3-519-2010

Mann, M. (2009). Do Global Warming and Climate Change Represent a Serious Threat to our Welfare and Environment? *Social Philosophy and Policy*, 193–230. https://doi.org/10.1017/S0265052509090220

Manolis, I., Grabarnik, S., Caron, J., Bézy, J.-L., Loiselet, M., Betto, M., … Meynart, R. (2013). The MetOp second generation 3MI instrument. *Proc SPIE*, *5*(Ici), 88890J.

References

https://doi.org/10.1117/12.2028662

Matsui, T., Beltrán-Przekurat, A., Niyogi, D., Pielke Sr., R. A., & Coughenour, M. (2008). Aerosol light scattering effect on terrestrial plant productivity and energy fluxes over the eastern United States. *J. Geophys. Res.*, *113*(D14), D14S14. https://doi.org/10.1029/2007jd009658

Maxwell Garnett, J. C. (1906). Colours in Metal Glasses, in Metallic Films, and in Metallic Solutions. II. *Philosophical Transactions of the Royal Society A: Mathematical, Physical and Engineering Sciences*, *205*(387–401), 237–288. https://doi.org/10.1098/rsta.1906.0007

McMeeking, G. R., Morgan, W. T., Flynn, M., Highwood, E. J., Turnbull, K., Haywood, J., & Coe, H. (2011). Black carbon aerosol mixing state, organic aerosols and aerosol optical properties over the United Kingdom. *Atmospheric Chemistry and Physics*, *11*(17), 9037–9052. https://doi.org/10.5194/acp-11-9037-2011

McMichael, A. J., Woodruff, R. E., & Hales, S. (2006). Climate change and human health: Present and future risks. *Lancet*. https://doi.org/10.1016/S0140-6736(06)68079-3

Meehl, G. A., Washington, W. M., Arblaster, J. M., Hu, A., Teng, H., Kay, J. E., … Strand, W. G. (2013). Climate change projections in CESM1(CAM5) compared to CCSM4. *Journal of Climate*, *26*(17), 6287–6308. https://doi.org/10.1175/JCLI-D-12-00572.1

Mie, G. (1908). Contributions to the optics of turbid media, particularly of colloidal metal solutions. *Ann. Phys.* https://doi.org/10.1002/andp.19083300302

Mishchenko, M. I., Travis, L. D., & Mackowski, D. W. (2010). T-matrix method and its applications to electromagnetic scattering by particles: A current perspective. *Journal of Quantitative Spectroscopy and Radiative Transfer*, *111*(11), 1700–1703. https://doi.org/10.1016/j.jqsrt.2010.01.030

Moffet, R. C., & Prather, K. a. (2009). In-situ measurements of the mixing state and optical properties of soot with implications for radiative forcing estimates. *Proceedings of the National Academy of Sciences of the United States of America*, *106*(29), 11872–11877. https://doi.org/10.1073/pnas.0900040106

Morgan, W. T., Allan, J. D., Flynn, M., Darbyshire, E., Hodgson, A., Johnson, B. T., … Coe, H. (2013). Overview of the South American biomass burning analysis (SAMBBA) field experiment. *AIP Conference Proceedings*, *1527*, 587–590. https://doi.org/10.1063/1.4803339

Morgenstern, O., Braesicke, P., Hurwitz, M. M., O'Connor, F. M., Bushell, A. C., Johnson, C. E., & Pyle, J. A. (2008). The world avoided by the Montreal Protocol. *Geophysical Research Letters*, *35*(16). https://doi.org/10.1029/2008GL034590

Morgenstern, O., Braesicke, P., O'Connor, F. M., Bushell, a. C., Johnson, C. E., Osprey, S. M., & Pyle, J. a. (2009). Evaluation of the new UKCA climate-composition model – Part 1: The stratosphere. *Geoscientific Model Development*, *2*, 43–57. https://doi.org/10.5194/gmd-2-43-2009

Morton, J. F. (2007). The impact of climate change on smallholder and subsistence agriculture. *Proceedings of the National Academy of Sciences of the United States of America*, *104*(50), 19680–5. https://doi.org/10.1073/pnas.0701855104

Moteki, N., & Kondo, Y. (2010). Dependence of Laser-Induced Incandescence on Physical Properties of Black Carbon Aerosols: Measurements and Theoretical Interpretation. *Aerosol Science and Technology*, *44*(8), 663–675. https://doi.org/10.1080/02786826.2010.484450

Mulcahy, J. P., Walters, D. N., Bellouin, N., & Milton, S. F. (2014). Impacts of increasing the

References

aerosol complexity in the Met Office global numerical weather prediction model. *Atmospheric Chemistry and Physics*, *14*(9), 4749–4778. https://doi.org/10.5194/acp-14-4749-2014

Mulcahy, J., Sellar, A., Office, M., Centre, H., Boutle, I., Johnson, B., … Jones, C. (2016). Improving aerosol processes and radiative forcing in preparation for UKESM1, 7–9.

Myhre, G., Samset, B. H., Schulz, M., Balkanski, Y., Bauer, S., Berntsen, T. K., … Zhou, C. (2013). Radiative forcing of the direct aerosol effect from AeroCom Phase II simulations. *Atmospheric Chemistry and Physics*, *13*(4), 1853–1877. https://doi.org/10.5194/acp-13-1853-2013

Myhre, G., Shindell, D., Bréon, F.-M., Collins, W., Fuglestvedt, J., Huang, J., … Zhang, H. (2013). 8: Anthropogenic and Natural Radiative Forcing. *Climate Change 2013: The Physical Science Basis*, (8), 1–141. Retrieved from papers3://publication/uuid/3FE291E6-1236-4CF0-9EC2-83D39F6664FF

NOAA; CCMI working group. (2017). Global Model Evaluation Home Page. Retrieved from https://www.esrl.noaa.gov/csd/globalmodeleval/

Novakov, T., Menon, S., Kirchstetter, T. W., Koch, D., & Hansen, J. E. (2005). Aerosol organic carbon to black carbon ratios: Analysis of published data and implications for climate forcing. *Journal of Geophysical Research*, *110*(D21), 1–13. https://doi.org/10.1029/2005JD005977

O'Connor, F. M., Johnson, C. E., Morgenstern, O., Abraham, N. L., Braesicke, P., Dalvi, M., … Pyle, J. A. (2014). Evaluation of the new UKCA climate-composition model-Part 2: The troposphere. *Geoscientific Model Development*, *7*(1), 41–91. https://doi.org/10.5194/gmd-7-41-2014

Ogren, J., & Andrews, E. (2014). Is there bias in the estimated climate forcing by black carbon aerosols? In *Global Monitoring Annual Conference*. Boulder. Retrieved from https://www.esrl.noaa.gov/gmd/publications/annual_meetings/2014/slides/3-140317-A.pdf

Pacifico, F., Harrison, S. P., Jones, C. D., Arneth, A., Sitch, S., Weedon, G. P., … Schurgers, G. (2011). Evaluation of a photosynthesis-based biogenic isoprene emission scheme in JULES and simulation of isoprene emissions under present-day climate conditions. *Atmospheric Chemistry and Physics*, *11*(9), 4371–4389. https://doi.org/10.5194/acp-11-4371-2011

Pan, X., Chin, M., Gautam, R., Bian, H., Kim, D., Colarco, P. R., … Bellouin, N. (2015). A multi-model evaluation of aerosols over South Asia: Common problems and possible causes. *Atmospheric Chemistry and Physics*, *15*(10), 5903–5928. https://doi.org/10.5194/acp-15-5903-2015

Peers, F., Bellouin, N., Waquet, F., Ducos, F., Goloub, P., Mollard, J., … Zhang, K. (2016). Comparison of aerosol optical properties above clouds between POLDER and AeroCom models over the South East Atlantic Ocean during the fire season. *Geophysical Research Letters*, *43*(8), 3991–4000. https://doi.org/10.1002/2016GL068222

Peng, J., Hu, M., Guo, S., Du, Z., Zheng, J., Shang, D., … Zhang, R. (2016). Markedly enhanced absorption and direct radiative forcing of black carbon under polluted urban environments. *Proceedings of the National Academy of Sciences of the United States of America*, 1602310113-. https://doi.org/10.1073/pnas.1602310113

Péré, J. C., Mallet, M., Bessagnet, B., & Pont, V. (2009). Evidence of the aerosol core-shell mixing state over Europe during the heat wave of summer 2003 by using CHIMERE simulations and AERONET inversions. *Geophysical Research Letters*, *36*(9).

References

https://doi.org/10.1029/2009GL037334

Petit, R. J., Raynaud, D., Basile, I., Chappellaz, J., Ritz, C., Delmotte, M., … Pe, L. (1999). Climate and atmospheric history of the past 420,000 years from the Vostok ice core, Antarctica. *Nature*, *399*, 429–413. https://doi.org/10.1038/20859

Petrenko, M., Kahn, R., Chin, M., Soja, A., Kucsera, T., & Harshvardhan. (2012). The use of satellite-measured aerosol optical depth to constrain biomass burning emissions source strength in the global model GOCART. *Journal of Geophysical Research Atmospheres*, *117*(17). https://doi.org/10.1029/2012JD017870

Pierce, J. R., Chen, K., & Adams, P. J. (2007). Contribution of carbonaceous aerosol to cloud condensation nuclei: processes and uncertainties evaluated with a global aerosol microphysics model. *Atmospheric Chemistry and Physics Discussions*, *7*(3), 7723–7765. https://doi.org/10.5194/acpd-7-7723-2007

Pósfai, M., Anderson, J. R., Buseck, P. R., & Sievering, H. (1999). Soot and sulfate aerosol particles in the remote marine troposphere. *Journal of Geophysical Research*, *104*(D17), 21685. https://doi.org/10.1029/1999JD900208

Prather, M., McElroy, M., Wofsy, S., Russell, G., & Rind, D. (1987). Chemistry of the global troposphere: Fluorocarbons as tracers of air motion. *Journal of Geophysical Research*, *92*(D6), 6579. https://doi.org/10.1029/JD092iD06p06579

Prospero, J. M., Ginoux, P., Torres, O., Nicholson, S. E., & Gill, T. E. (2002). Environmental characterization of global sources of atmospheric soil dust identified with the NIMBUS 7 Total Ozone Mapping Spectrometer (TOMS) absorbing aerosol product. *Reviews of Geophysics*, *40*(1), 1–31. https://doi.org/10.1029/2000RG000095

Putaud, J. P., Cavalli, F., Dos Santos, M., & Dell'Acqua, A. (2014). Long-term trends in aerosol optical characteristics in the Po Valley, Italy. *Atmospheric Chemistry and Physics*, *14*(17), 9129–9136. https://doi.org/10.5194/acp-14-9129-2014

Raffuse, S. M., Craig, K. J., Larkin, N. K., Strand, T. T., Sullivan, D. C., Wheeler, N. J. M., & Solomon, R. (2012). An evaluation of modeled plume injection height with satellite-derived observed plume height. *Atmosphere*, *3*(1), 103–123. https://doi.org/10.3390/atmos3010103

Ramachandran, G., & Reist, P. C. (1995). CHARACTERIZATION OF MORPHOLOGICAL-CHANGES IN AGGLOMERATES SUBJECT TO CONDENSATION AND EVAPORATION USING MULTIPLE FRACTAL DIMENSIONS. *Aerosol Science and Technology*, *23*, 431–442.

Randerson, J. T., Chen, Y., Van Der Werf, G. R., Rogers, B. M., & Morton, D. C. (2012). Global burned area and biomass burning emissions from small fires. *Journal of Geophysical Research: Biogeosciences*, *117*(4). https://doi.org/10.1029/2012JG002128

Randerson, J. T., Van Der Werf, G. R., Giglio, L., Collatz, G. J., & Kasibhatla, P. S. (2013). Global Fire Emissions Database, Version 3 (GFEDv3.1). ORNL Distributed Active Archive Center. Retrieved from http://dx.doi.org/10.3334/ORNLDAAC/1191

Reddington, C. L., Butt, E. W., Ridley, D. A., Artaxo, P., Morgan, W. T., Coe, H., & Spracklen, D. V. (2015). Air quality and human health improvements from reductions in deforestation-related fire in Brazil. *Nature Geoscience*, *8*(10), 768–771. https://doi.org/10.1038/ngeo2535

Riemer, N., West, M., Zaveri, R., & Easter, R. (2010). Estimating black carbon aging time-scales with a particle-resolved aerosol model. *Journal of Aerosol Science*, *41*(1), 143–158. https://doi.org/10.1016/j.jaerosci.2009.08.009

Riipinen, I., Pierce, J. R., Yli-Juuti, T., Nieminen, T., Häkkinen, S., Ehn, M., … Kulmala, M. (2011). Organic condensation: A vital link connecting aerosol formation to cloud condensation

References

nuclei (CCN) concentrations. *Atmospheric Chemistry and Physics*, *11*(8), 3865–3878. https://doi.org/10.5194/acp-11-3865-2011

Rohr, J. R., Dobson, A. P., Johnson, P. T. J., Kilpatrick, A. M., Paull, S. H., Raffel, T. R., … Thomas, M. B. (2011). Frontiers in climate change-disease research. *Trends in Ecology and Evolution*. https://doi.org/10.1016/j.tree.2011.03.002

Russell, P. B., Kacenelenbogen, M., Livingston, J. M., Hasekamp, O. P., Burton, S. P., Schuster, G. L., … Holben, B. (2014). A multiparameter aerosol classification method and its application to retrievals from spaceborne polarimetry. *Journal of Geophysical Research: Atmospheres*, *119*(16), 9838–9863. https://doi.org/10.1002/2013JD021411

Ryder, C. L., Highwood, E. J., Lai, T. M., Sodemann, H., & Marsham, J. H. (2013). Impact of atmospheric transport on the evolution of microphysical and optical properties of Saharan dust. *Geophysical Research Letters*, *40*(10), 2433–2438. https://doi.org/10.1002/grl.50482

Saleh, R., Hennigan, C. J., McMeeking, G. R., Chuang, W. K., Robinson, E. S., Coe, H., … Robinson, A. L. (2013). Absorptivity of brown carbon in fresh and photo-chemically aged biomass-burning emissions. *Atmospheric Chemistry and Physics*, *13*(15), 7683–7693. https://doi.org/10.5194/acp-13-7683-2013

Saleh, R., Robinson, E. S., Tkacik, D. S., Ahern, A. T., Liu, S., Aiken, A. C., … Robinson, A. L. (2014). Brownness of organics in aerosols from biomass burning linked to their black carbon content. *Nature Geoscience*, *7*(September), 1–4. https://doi.org/10.1038/ngeo2220

Samset, B. H., Myhre, G., Herber, A., Kondo, Y., Li, S. M., Moteki, N., … Zhang, K. (2014). Modelled black carbon radiative forcing and atmospheric lifetime in AeroCom Phase II constrained by aircraft observations. *Atmospheric Chemistry and Physics*, *14*(22), 12465–12477. https://doi.org/10.5194/acp-14-12465-2014

Scarnato, B. V., Vahidinia, S., Richard, D. T., & Kirchstetter, T. W. (2013). Effects of internal mixing and aggregate morphology on optical properties of black carbon using a discrete dipole approximation model. *Atmospheric Chemistry and Physics*, *13*(10), 5089–5101. https://doi.org/10.5194/acp-13-5089-2013

Schauer, C., Niessner, R., & Pöschl, U. (2003). Polycyclic aromatic hydrocarbons in urban air particulate matter: decadal and seasonal trends, chemical degradation, and sampling artifacts. *Environmental Science & Technology*, *37*(13), 2861–2868. https://doi.org/10.1021/es034059s

Schkolnik, G., Chand, D., Hoffer, A., Andreae, M. O., Erlick, C., Swietlicki, E., & Rudich, Y. (2007). Constraining the density and complex refractive index of elemental and organic carbon in biomass burning aerosol using optical and chemical measurements. *Atmospheric Environment*, *41*(5), 1107–1118. https://doi.org/10.1016/j.atmosenv.2006.09.035

Schmid, H., Laskus, L., Jürgen Abraham, H., Baltensperger, U., Lavanchy, V., Bizjak, M., … Puxbaum, H. (2001). Results of the "carbon conference" international aerosol carbon round robin test stage I. *Atmospheric Environment*, *35*(12), 2111–2121. https://doi.org/10.1016/S1352-2310(00)00493-3

Schuster, G. L., Dubovik, O., Holben, B. N., & Clothiaux, E. E. (2005). Inferring black carbon content and specific absorption from Aerosol Robotic Network (AERONET) aerosol retrievals. *Journal of Geophysical Research D: Atmospheres*, *110*(10), 1–19. https://doi.org/10.1029/2004JD004548

Schutgens, N. A. J., Gryspeerdt, E., Weigum, N., Tsyro, S., Goto, D., Schulz, M., & Stier, P.

References

(2016). Will a perfect model agree with perfect observations? The impact of spatial sampling. *Atmospheric Chemistry and Physics*, *16*(10), 6335–6353. https://doi.org/10.5194/acp-16-6335-2016

Schutgens, N. a. J., Partridge, D. G., & Stier, P. (2015). The importance of temporal collocation for the evaluation of aerosol models with observations. *Atmospheric Chemistry and Physics Discussions*, *15*(18), 26191–26230. https://doi.org/10.5194/acpd-15-26191-2015

Schwarz, J. P., Gao, R. S., Fahey, D. W., Thomson, D. S., Watts, L. A., Wilson, J. C., … Aikin, K. C. (2006). Single-particle measurements of midlatitude black carbon and light-scattering aerosols from the boundary layer to the lower stratosphere. *Journal of Geophysical Research Atmospheres*, *111*(16). https://doi.org/10.1029/2006JD007076

Schwarz, J. P., Gao, R. S., Spackman, J. R., Watts, L. A., Thomson, D. S., Fahey, D. W., … Del Negro, L. A. (2008). Measurement of the mixing state, mass, and optical size of individual black carbon particles in urban and biomass burning emissions. *Geophysical Research Letters*, *35*(13). https://doi.org/10.1029/2008GL033968

Schwarz, J. P., Samset, B. H., Perring, A. E., Spackman, J. R., Gao, R. S., Stier, P., … Fahey, D. W. (2013). Global-scale seasonally resolved black carbon vertical profiles over the Pacific. *Geophysical Research Letters*, *40*(20), 5542–5547. https://doi.org/10.1002/2013GL057775

Schwarz, J. P., Spackman, J. R., Gao, R. S., Watts, L. A., Stier, P., Schulz, M., … Fahey, D. W. (2010). Global-scale black carbon profiles observed in the remote atmosphere and compared to models. *Geophysical Research Letters*, *37*(18). https://doi.org/10.1029/2010GL044372

Sekhon, R. S., & Srivastava, R. C. (1971). Doppler Radar Observations of Drop-Size Distributions in a Thunderstorm. *Journal of the Atmospheric Sciences*. https://doi.org/10.1175/1520-0469(1971)028<0983:DROODS>2.0.CO;2

Shi, L., Zanobetti, A., Kloog, I., Coull, B. A., Koutrakis, P., Melly, S. J., & Schwartz, J. D. (2016). Low-concentration PM2.5 and mortality: Estimating acute and chronic effects in a population-based study. *Environmental Health Perspectives*, *124*(1), 46–52. https://doi.org/10.1289/ehp.1409111

Simpson, D., Yttri, K. E., Klimont, Z., Kupiainen, K., Caseiro, A., Gelencs??r, A., … Legrand, M. (2007). Modeling carbonaceous aerosol over Europe: Analysis of the CARBOSOL and EMEP EC/OC campaigns. *Journal of Geophysical Research Atmospheres*, *112*(23). https://doi.org/10.1029/2006JD008158

Slinn, W. G. N. (1982). Predictions for particle deposition to vegetative canopies. *Atmospheric Environment (1967)*, *16*(7), 1785–1794. https://doi.org/10.1016/0004-6981(82)90271-2

Slowik, J. G., Cross, E. S., Han, J. H., Davidovits, P., Onasch, T. B., Jayne, J. T., … Petzold, A. (2007). An inter-comparison of instruments measuring black carbon content of soot particles. *Aerosol Science and Technology*, *41*(3), 295–314. https://doi.org/Doi 10.1080/02786820701197078

Spracklen, D. V., Carslaw, K. S., P??schl, U., Rap, A., & Forster, P. M. (2011). Global cloud condensation nuclei influenced by carbonaceous combustion aerosol. *Atmospheric Chemistry and Physics*. https://doi.org/10.5194/acp-11-9067-2011

Spracklen, D. V., Pringle, K. J., Carslaw, K. S., Mann, G. W., Manktelow, P., & Heintzenberg, J. (2007). Evaluation of a global aerosol microphysics model against size-resolved particle statistics in the marine atmosphere. *Atmospheric Chemistry and Physics*, *7*, 2073–2090. https://doi.org/10.5194/acp-7-2073-2007

References

Spracklen, S. T. T. and E. W. B. and T. B. R. and G. W. M. and C. L. R. and P. M. F. and J. H. and M. C. and G. J.-M. and C. E. J. and N. B. and K. S. C. and D. V. (2016). The impact of European legislative and technology measures to reduce air pollutants on air quality, human health and climate. *Environmental Research Letters*, *11*(2), 24010. https://doi.org/10.1088/1748-9326/11/2/024010

Stier, P., Feichter, J., Kinne, S., Kloster, S., Vignati, E., Wilson, J., … Boucher, O. (2004). The aerosol-climate model ECHAM5-HAM. *Atmospheric Chemistry and Physics Discussions*, *4*(5), 5551–5623. https://doi.org/10.5194/acpd-4-5551-2004

Stier, P., Schutgens, N. A. J., Bellouin, N., Bian, H., Boucher, O., Chin, M., … Zhou, C. (2013). Host model uncertainties in aerosol radiative forcing estimates: Results from the AeroCom Prescribed intercomparison study. *Atmospheric Chemistry and Physics*, *13*(6), 3245–3270. https://doi.org/10.5194/acp-13-3245-2013

Stocker, T. F., Qin, D., Plattner, G.-K., Tignor, M. M. B., Allen, S. K., Boschung, J., … Midgley, P. M. (2013). *Climate Change 2013 - The Physical Science Basis. Contribution of Working Group I to the Fifth Assessment Report of the Intergovernmental Panel on Climate Change*. *IPCC*. https://doi.org/10.1038/446727a

Stohl, A., Klimont, Z., Eckhardt, S., Kupiainen, K., Shevchenko, V. P., Kopeikin, V. M., & Novigatsky, A. N. (2013). Black carbon in the Arctic: The underestimated role of gas flaring and residential combustion emissions. *Atmospheric Chemistry and Physics*, *13*(17), 8833–8855. https://doi.org/10.5194/acp-13-8833-2013

Stohl, A, Forster, C., Frank, a, Seibert, P., & Wotawa, G. (2005). Technical note : The Lagrangian particle dispersion model FLEXPART v6.2. *Atmospheric Chemistry and Physics*, *2005*, 2461–2474. https://doi.org/10.5194/acp-5-2461-2005

Streets, D. G., Bond, T. C., Lee, T., & Jang, C. (2004). On the future of carbonaceous aerosol emissions. *Journal of Geophysical Research D: Atmospheres*, *109*(24), 1–19. https://doi.org/10.1029/2004JD004902

Syktus, J., Jeffrey, S., Rotstayn, L., Wong, K., Toombs, N., Dravitzki, S., … Moeseneder, C. (2011). The CSIRO-QCCCE contribution to CMIP5 using the CSIRO Mk3.6 climate model. In *MODSIM 2011 - 19th International Congress on Modelling and Simulation - Sustaining Our Future: Understanding and Living with Uncertainty* (pp. 2782–2788).

Takemura, T. (2008). Aerosol effects on climate system : past , present , and future.

Taylor, K. E., Stouffer, R. J., & Meehl, G. A. (2012). An overview of CMIP5 and the experiment design. *Bulletin of the American Meteorological Society*. https://doi.org/10.1175/BAMS-D-11-00094.1

Telford, P. J., Braesicke, P., Morgenstern, O., & Pyle, J. a. (2007). Technical Note: Description and assessment of a nudged version of the new dynamics Unified Model. *Atmospheric Chemistry and Physics Discussions*, *7*(6), 17261–17297. https://doi.org/10.5194/acpd-7-17261-2007

Textor, C., Schulz, M., Guibert, S., Kinne, S., Balkanski, Y., Bauer, S., … Tie, X. (2006). Analysis and quantification of the diversities of aerosol life cycles within AeroCom. *Atmospheric Chemistry and Physics*, *6*, 1777–1813. https://doi.org/10.5194/acpd-5-8331-2005

Thompson, D. W. J., Kennedy, J. J., Wallace, J. M., & Jones, P. D. (2008). A large discontinuity in the mid-twentieth century in observed global-mean surface temperature. *Nature*, *453*(7195), 646–649. https://doi.org/10.1038/nature06982

Tiitta, P., Vakkari, V., Croteau, P., Beukes, J. P., Van Zyl, P. G., Josipovic, M., … Laakso, L. (2014). Chemical composition, main sources and temporal variability of PM1 aerosols in southern African grassland. *Atmospheric Chemistry and Physics*, *14*(4), 1909–1927.

References

https://doi.org/10.5194/acp-14-1909-2014

Timonen, H., Jaffe, D. A., Wigder, N., Hee, J., Gao, H., Pitzman, L., & Cary, R. A. (2014). Sources of carbonaceous aerosol in the free troposphere. *Atmospheric Environment*, *92*, 146–153. https://doi.org/10.1016/j.atmosenv.2014.04.014

Torres, O., Bhartia, P. K., Herman, J. R., Ahmad, Z., & Gleason, J. (1998). Derivation of aerosol properties from satellite measurements of backscattered ultraviolet radiation: Theoretical basis. *Journal of Geophysical Research: Atmospheres*, *103*(D14), 17099–17110. https://doi.org/10.1029/98JD00900

Torres, O., Tanskanen, A., Veihelmann, B., Ahn, C., Braak, R., Bhartia, P. K., … Levelt, P. (2007). Aerosols and surface UV products form Ozone Monitoring Instrument observations: An overview. *Journal of Geophysical Research Atmospheres*, *112*(24), 1–14. https://doi.org/10.1029/2007JD008809

Trenberth, K. E. (2011). Changes in precipitation with climate change. *Climate Research*, *47*(1–2), 123–138. https://doi.org/10.3354/cr00953

Tsigaridis, K., Daskalakis, N., Kanakidou, M., Adams, P. J., Artaxo, P., Bahadur, R., … Zhang, X. (2014). The AeroCom evaluation and intercomparison of organic aerosol in global models. *Atmospheric Chemistry and Physics*, *14*(19), 10845–10895. https://doi.org/10.5194/acp-14-10845-2014

Twomey, S. (1977). The Influence of Pollution on the Shortwave Albedo of Clouds. *Journal of the Atmospheric Sciences*, *34*(7), 1149–1152. https://doi.org/10.1175/1520-0469(1977)034<1149:TIOPOT>2.0.CO;2

Van Dingenen, R., Dentener, F. J., Raes, F., Krol, M. C., Emberson, L., & Cofala, J. (2009). The global impact of ozone on agricultural crop yields under current and future air quality legislation. *Atmospheric Environment*, *43*(3), 604–618. https://doi.org/10.1016/j.atmosenv.2008.10.033

Veira, A., Kloster, S., Wilkenskjeld, S., & Remy, S. (2015). Fire emission heights in the climate system - Part 1: Global plume height patterns simulated by ECHAM6-HAM2. *Atmospheric Chemistry and Physics*, *15*(13), 7155–7171. https://doi.org/10.5194/acp-15-7155-2015

Venkataraman, C., Habib, G., Kadamba, D., Shrivastava, M., Leon, J. F., Crouzille, B., … Streets, D. G. (2006). Emissions from open biomass burning in India: Integrating the inventory approach with high-resolution Moderate Resolution Imaging Spectroradiometer (MODIS) active-fire and land cover data. *Global Biogeochemical Cycles*, *20*(2). https://doi.org/10.1029/2005GB002547

Verma, R. L., Kondo, Y., Oshima, N., Matsui, H., Kita, K., Sahu, L. K., … Miyakawa, T. (2011). Seasonal variations of the transport of black carbon and carbon monoxide from the Asian continent to the western Pacific in the boundary layer. *Journal of Geophysical Research Atmospheres*, *116*(21). https://doi.org/10.1029/2011JD015830

Vignati, E., Karl, M., Krol, M., Wilson, J., Stier, P., & Cavalli, F. (2009). Sources of uncertainties in modelling Black Carbon at the global scale. *Atmospheric Chemistry and Physics Discussions*, *9*, 24317–24360. https://doi.org/10.5194/acpd-9-24317-2009

Walters, D. N., Best, M. J., Bushell, A. C., Copsey, D., Edwards, J. M., Falloon, P. D., … Williams, K. D. (2011). The Met Office Unified Model Global Atmosphere 3.0/3.1 and JULES Global Land 3.0/3.1 configurations. *Geoscientific Model Development*, *4*(4), 919–941. https://doi.org/DOI 10.5194/gmd-4-919-2011

Walther, G.-R., Post, E., Convey, P., Menzel, A., Parmesan, C., Beebee, T. J. C., … Bairlein, F. (2002). Ecological responses to recent climate change. *Nature*, *416*(6879), 389–95. https://doi.org/10.1038/416389a

References

Wang, C. (2004). A modeling study on the climate impacts of black carbon aerosols. *Journal of Geophysical Research*, *109*(D3), 1–28. https://doi.org/10.1029/2003JD004084

Wang, C. (2013). Impact of anthropogenic absorbing aerosols on clouds and precipitation: A review of recent progresses. *Atmospheric Research*. https://doi.org/10.1016/j.atmosres.2012.11.005

Wang, G., Cheng, C., Meng, J., Huang, Y., Li, J., & Ren, Y. (2015). Field observation on secondary organic aerosols during Asian dust storm periods: Formation mechanism of oxalic acid and related compounds on dust surface. *Atmospheric Environment*, *113*, 169–176. https://doi.org/10.1016/j.atmosenv.2015.05.013

Wang, X., Heald, C. L., Ridley, D. A., Schwarz, J. P., Spackman, J. R., Perring, A. E., … Clarke, A. D. (2014). Exploiting simultaneous observational constraints on mass and absorption to estimate the global direct radiative forcing of black carbon and brown carbon. *Atmospheric Chemistry and Physics*, *14*(20), 10989–11010. https://doi.org/10.5194/acp-14-10989-2014

West, R. E. L., Stier, P., Jones, A., Johnson, C. E., Mann, G. W., Bellouin, N., … Kipling, Z. (2014). The importance of vertical velocity variability for estimates of the indirect aerosol effects. *Atmospheric Chemistry and Physics*, *14*(12), 6369–6393. https://doi.org/10.5194/acp-14-6369-2014

Wexler, A. S., & Clegg, S. L. (2002). Atmospheric aerosol models for systems including the ions H+, NH4+, Na+, SO42−, NO3−, Cl−, Br−, and H2O. *Journal of Geophysical Research: Atmospheres*, *107*(D14), art. no. 4207. https://doi.org/10.1029/2001JD000451

Wilcox, L. J., Highwood, E. J., Booth, B. B. B., & Carslaw, K. S. (2015). Quantifying sources of inter-model diversity in the cloud albedo effect. *Geophysical Research Letters*, *42*(5), 1568–1575. https://doi.org/10.1002/2015GL063301

Willis, K. J., & Bhagwat, S. A. (2009). Biodiversity and Climate Change. *Science*, *326*, 806–807. https://doi.org/10.1126/science.1178838

Wilson, D. R., Bushell, A. C., Kerr-Munslow, A. M., Price, J. D., Morcrette, C. J., & Bodas-Salcedo, A. (2008). PC2: A prognostic cloud fraction and condensation scheme. II: Climate model simulations. *Quarterly Journal of the Royal Meteorological Society*, *134*(637), 2109–2125. https://doi.org/10.1002/qj.332

Wiscombe, W. J. (1980). Improved Mie scattering algorithms. *Applied Optics*, *19*(9), 1505–9. https://doi.org/10.1364/AO.19.001505

Wolff, H., & Perry, L. (2010). Trends in clean air legislation in Europe: Particulate matter and low emission zones. *Review of Environmental Economics and Policy*, *4*(2), 293–308. https://doi.org/10.1093/reep/req008

Woodward, S. (2001). Modeling the atmospheric life cycle and radiative impact of mineral dust in the Hadley Centre climate model. *Journal of Geophysical Research*, *106*(D16), 18155. https://doi.org/10.1029/2000JD900795

Woollings, T., & Blackburn, M. (2012). The north Atlantic jet stream under climate change and its relation to the NAO and EA patterns. *Journal of Climate*, *25*(3), 886–902. https://doi.org/10.1175/JCLI-D-11-00087.1

Xin, J., Wang, Y., Pan, Y., Ji, D., Liu, Z., Wen, T., … Wang, L. (2015). The campaign on atmospheric aerosol research network of China: CARE-China. *Bulletin of the American Meteorological Society*, *96*(7), 1137–1155. https://doi.org/10.1175/BAMS-D-14-00039.1

Yuan, J. F., Huang, X. F., Cao, L. M., Cui, J., Zhu, Q., Huang, C. N., … He, L. Y. (2016). Light absorption of brown carbon aerosol in the PRD region of China. *Atmospheric Chemistry and Physics*, *16*(3), 1433–1443. https://doi.org/10.5194/acp-16-1433-2016

References

Zerefos, C. S., Tetsis, P., Kazantzidis, A., Amiridis, V., Zerefos, S. C., Luterbacher, J., … Papayannis, A. (2014). Further evidence of important environmental information content in red-to-green ratios as depicted in paintings by great masters. *Atmospheric Chemistry and Physics*, *14*(6), 2987–3015. https://doi.org/10.5194/acp-14-2987-2014

Zhang, Q., Jiang, X., Tong, D., Davis, S. J., Zhao, H., Geng, G., … Guan, D. (2017). Transboundary health impacts of transported global air pollution and international trade. *Nature*, *543*(7647), 705–709. https://doi.org/10.1038/nature21712

Zhang, R., Khalizov, A. F., Pagels, J., Zhang, D., Xue, H., & McMurry, P. H. (2008). Variability in morphology, hygroscopicity, and optical properties of soot aerosols during atmospheric processing. *Proceedings of the National Academy of Sciences of the United States of America*, *105*(30), 10291–6. https://doi.org/10.1073/pnas.0804860105

Zhang, X. Y., Wang, Y. Q., Zhang, X. C., Guo, W., & Gong, S. L. (2008). Carbonaceous aerosol composition over various regions of China during 2006. *Journal of Geophysical Research Atmospheres*, *113*(14). https://doi.org/10.1029/2007JD009525

Zhao, D. F., Buchholz, A., Kortner, B., Schlag, P., Rubach, F., Fuchs, H., … Mentel, T. F. (2016). Cloud condensation nuclei activity, droplet growth kinetics, and hygroscopicity of biogenic and anthropogenic secondary organic aerosol (SOA). *Atmospheric Chemistry and Physics*, *16*(2), 1105–1121. https://doi.org/10.5194/acp-16-1105-2016

References

Appendix

Abu_Al_Bukhoosh (25N,53E)   Adelaide_Site_7 (34S,138E)   Agoufou (15N,1W)
Al_Ain (24N,55E)   Alta_Floresta (9S,56W)   Ames (42N,93W)
Anmyon (36N,126E)   Ascension_Island (7S,14W)   Avignon (43N,4E)
Bac_Giang (21N,106E)   BackGarden_GZ (23N,113E)   Bac_Lieu (9N,105E)
Bahrain (26N,50E)   Banizoumbou (13N,2E)   Barcelona (41N,2E)
Barrow (71N,156W)   Beijing (39N,116E)   Belsk (51N,20E)
Billerica (42N,71W)   Birdsville (25S,139E)   Blida (36N,2E)
Bonanza_Creek (64N,148W)   BONDVILLE (40N,88W)   Bratts_Lake (50N,104W)
Brussels (50N,4E)   BSRN_BAO_Boulder (40N,105W)   Cabauw (51N,4E)
Cabo_da_Roca (38N,9W)   Caceres (39N,6W)   Cairo_EMA (30N,31E)
Campo_Grande_SONDA (20S,54W)   Canberra (35S,149E)   Cape_San_Juan (18N,65W)
Capo_Verde (16N,22W)   Carpentras (44N,5E)   CARTEL (45N,71W)
Cart_Site (36N,97W)   CCNY (40N,73W)   CEILAP-BA (34S,58W)
CEILAP-RG (51S,69W)   Chapais (49N,74W)   Chen-Kung_Univ (23N,120E)
Chiang_Mai_Met_Sta (18N,98E)   Chilbolton (51N,1W)   City_GZ (23N,113E)
Cordoba-CETT (31S,64W)   COVE (36N,75W)   COVE_SEAPRISM (36N,75W)
Crozet_Island (46S,51E)   CUIABA-MIRANDA (15S,56W)   Dakar (14N,16W)
Dalanzadgad (43N,104E)   Davos (46N,9E)   Dhabi (24N,54E)
Dhadnah (25N,56E)   Djougou (9N,1E)   DMN_Maine_Soroa (13N,12E)
Dunedin (45S,170E)   Dunkerque (51N,2E)   Egbert (44N,79W)
Egbert_X (44N,79W)   El_Arenosillo (37N,6W)   EPA-NCU (24N,121E)
Epanomi (40N,22E)   ETNA (37N,15E)   EVK2-CNR (27N,86E)
Evora (38N,7W)   Fontainebleau (48N,2E)   FORTH_CRETE (35N,25E)
Frenchman_Flat (36N,115W)   Fresno (36N,119W)   Gandhi_College (25N,84E)
Gosan_SNU (33N,126E)   Granada (37N,3W)   GSFC (38N,76W)
Guadeloup (16N,61W)   Guam (13N,144E)   Gustav_Dalen_Tower (58N,17E)
Gwangju_GIST (35N,126E)   Halifax (44N,63W)   Hamburg (53N,9E)
Hamim (22N,54E)   Hefei (31N,117E)   Helgoland (54N,7E)
Helsinki_Lighthouse (59N,24E)   HJAndrews (44N,122W)   Hong_Kong_PolyU (22N,114E)
Hornsund (77N,15E)   Howland (45N,68W)   ICIPE-Mbita (0S,34E)
IER_Cinzana (13N,5W)   Ilorin (8N,4E)   IMAA_Potenza (40N,15E)
IMS-METU-ERDEMLI (36N,34E)   Irkutsk (51N,103E)   ISDGM_CNR (45N,12E)
Ispra (45N,8E)   Izana (28N,16W)   Jabiru (12S,132E)
Ji_Parana_SE (10S,61W)   Kanpur (26N,80E)   Karachi (24N,67E)
Karlsruhe (49N,8E)   Kellogg_LTER (42N,85W)   Kelowna (49N,119W)
Kibale (0N,30E)   KONZA_EDC (39N,96W)   Kuujjuarapik (55N,77W)
La_Crau (43N,4E)   Laegeren (47N,8E)   Lahore (31N,74E)
La_Jolla (32N,117W)   Lake_Argyle (16S,128E)   La_Laguna (28N,16W)
Lampedusa (35N,12E)   La_Parguera (17N,67W)   La_Paz (16S,68W)
Lecce_University (40N,18E)   Le_Fauga (43N,1E)   Leipzig (51N,12E)
Lille (50N,3E)   Lulin (23N,120E)   Mainz (49N,8E)
Maricopa (33N,111W)   Mauna_Loa (19N,155W)   MCO-Hanimaadhoo (6N,73E)
MD_Science_Center (39N,76W)   Merredin (31S,118E)   Messina (38N,15E)
Mexico_City (19N,99W)   Midway_Island (28N,177W)   Milyering (22S,113E)
Minsk (53N,27E)   MISR-JPL (34N,118W)   Missoula (46N,114W)
Modena (44N,10E)   Moldova (47N,28E)   Mongu (15S,23E)
Moscow_MSU_MO (55N,37E)   Moss_Landing (36N,121W)   Mount_Chacaltaya (16S,68W)
Mukdahan (16N,104E)   Muscat (23N,58E)   Mussafa (24N,54E)
Nairobi (1S,36E)   NAM_CO (30N,90E)   Nauru (0S,166E)
NCU_Taiwan (24N,121E)   Nes_Ziona (31N,34E)   Niamey (13N,2E)
Ny_Alesund (78N,11E)   OHP_OBSERVATOIRE (43N,5E)   Oostende (51N,2E)
Osaka (34N,135E)   Ouagadougou (12N,1W)   Palaiseau (48N,2E)

References

Palencia (41N,4W)
Paris (48N,2E)
Pickle_Lake (51N,90W)
Pimai (15N,102E)
PKU_PEK (39N,116E)
Prospect_Hill (32N,64W)
Quarzazate (30N,6W)
Railroad_Valley (38N,115W)
Ras_El_Ain (31N,7W)
Red_Mountain_Pass (37N,107W)
Resolute_Bay (74N,94W)
Richland (46N,119W)
Rimrock (46N,116W)
Rome_Tor_Vergata (41N,12E)
Saada (31N,8W)
SACOL (35N,104E)
San_Nicolas (33N,119W)
SANTA_CRUZ (17S,63W)
Santa_Cruz_Tenerife (28N,16W)
SANTA_CRUZ_UTEPSA (17S,63W)
Sao_Paulo (23S,46W)
Saturn_Island (48N,123W)
SEDE_BOKER (30N,34E)
SERC (38N,76W)
Sevastopol (44N,33E)
Sevilleta (34N,106W)
Shirahama (33N,135E)
Silpakorn_Univ (13N,100E)
Singapore (1N,103E)
Sioux_Falls (43N,96W)
Skukuza (24S,31E)
SMHI (58N,16E)
Solar_Village (24N,46E)
TABLE_MOUNTAIN_CA (34N,117W)
Tahiti (17S,149W)
Taihu (31N,120E)
Taipei_CWB (25N,121E)
Tamanrasset_INM (22N,5E)
Tamanrasset_TMP (22N,5E)
Tamihua (21N,97W)
Tampico_MAX_MEX (22N,97W)
The_Hague (52N,4E)
Thessaloniki (40N,22E)
Thompson (55N,97W)
Tinga_Tingana (28S,139E)
T0_MAX_MEX (19N,99W)
T1_MAX_MEX (19N,98W)
Tomsk (56N,85E)
Toravere (58N,26E)
Toronto (43N,79W)
Toulon (43N,6E)
Trelew (43S,65W)
Trinidad_Head (41N,124W)
Tucson (32N,110W)
Tuxtla_Gutierrez (16N,93W)
UCLA (34N,118W)
UCSB (34N,119W)
Univ_of_Houston (29N,95W)
USDA-BARC (39N,76W)
USDA-Howard (39N,76W)
Ussuriysk (43N,132E)
Venise (45N,12E)
Villefranche (43N,7E)
Walker_Branch (35N,84W)
Wallops (37N,75W)
Waskesiu (53N,106W)
White_Sands_HELSTF (32N,106W)
Wits_University (26S,28E)
XiangHe (39N,116E)
Xinglong (40N,117E)
Yakutsk (61N,129E)
Yekaterinburg (57N,59E)
Yufa_PEK (39N,116E)
Zvenigorod (55N,36E)

Full list of AERONET sites used in this study, with latitude and longitudes. This list corresponds to Figure 2-8, which maps the locations of these sites.